NASA TECHNICAL MEMORANDUM

NASA TM X-53770

August 21, 1968

NASA TM X-53770

RESULTS OF SEVERAL EXPERIMENTAL INVESTIGATIONS OF THE STATIC AERODYNAMIC CHARACTERISTICS FOR THE APOLLO/SATURN V LAUNCH VEHICLE

By Clyde E. Walker
Aero-Astrodynamics Laboratory

NASA

George C. Marshall Space Flight Center
Marshall Space Flight Center, Alabama

TECHNICAL MEMORANDUM X-53770

RESULTS OF SEVERAL EXPERIMENTAL INVESTIGATIONS OF THE STATIC AERODYNAMIC CHARACTERISTICS FOR THE APOLLO/SATURN V LAUNCH VEHICLE

By

Clyde E. Walker

George C. Marshall Space Flight Center
Huntsville, Alabama

ABSTRACT

Experimental static aerodynamic data for six configurations of the Apollo/Saturn V launch vehicle are presented. Tests were conducted at six different facilities on 0.3366, 0.9, and/or 4 percent scale models at Mach numbers ranging from 0.5 through 7.81, at angles of attack ranging from -4 through +20 degrees, and for Reynolds numbers ranging from 0.5×10^6 through 8.0×10^6 based on vehicle reference diameter. All configurations were tested at a roll angle of zero degrees, and some were also tested at +45 and +90 degrees roll angle. Correlation of data from the different tests was reasonably good except where the force balance was not properly matched to the configuration and, in one case, where protuberance effects were not correctly simulated with the smallest model.

NASA - GEORGE C. MARSHALL SPACE FLIGHT CENTER

NASA - GEORGE C. MARSHALL SPACE FLIGHT CENTER

Technical Memorandum X-53770

August 21, 1968

RESULTS OF SEVERAL EXPERIMENTAL INVESTIGATIONS OF THE STATIC AERODYNAMIC CHARACTERISTICS FOR THE APOLLO/SATURN V LAUNCH VEHICLE

By

Clyde E. Walker

EXPERIMENTAL AERODYNAMICS SECTION
AERODYNAMIC DESIGN BRANCH
AEROPHYSICS DIVISION
AERO-ASTRODYNAMICS LABORATORY
RESEARCH AND DEVELOPMENT OPERATIONS

TABLE OF CONTENTS

LIST OF ILLUSTRATIONS

LIST OF ILLUSTRATIONS (Continued)

LIST OF ILLUSTRATIONS (Continued)

LIST OF ILLUSTRATIONS (Continued)

DEFINITION OF SYMBOLS

Symbol	Definition
C_{A_b}	base axial force coefficient; $(P - P_b) A_b/qS$
C_{A_f}	forebody axial force coefficient; $C_{A_T} - C_{A_b}$
C_{A_T}	total axial force coefficient; (Axial Force)/qS
C_ℓ	rolling moment coefficient; (Rolling Moment)/qSD
C_{m_g}	pitching moment coefficient about S-IC gimbal station (vehicle station 100); (Pitching Moment)/qSD
C_N	normal force coefficient; (Normal Force)/qS
C_{N_α}	normal force coefficient gradient with angle of attack at $\alpha \approx 0°$; $dC_N/d\alpha$ (deg^{-1})
C_n	yawing moment coefficient; (Yawing Moment)/qSD
C_y	yawing force coefficient; (Yawing Force)/qS
CP/D	center of pressure (in calibers) forward of vehicle station 100 (S-IC gimbal station)
D	Saturn V reference diameter (S-IC stage), 33 feet, full scale
M	free stream Mach number
P	free stream static pressure
P_p	base pressure
P_t	total (stagnation) pressure
q	free stream dynamic pressure $\frac{\gamma}{2} PM^2$
R_N/FT	free stream Reynolds number per foot; $\frac{\rho V}{\mu}$ ft^{-1}
R_{N_D}	free stream Reynolds number based on reference diameter; $\rho VD/\mu$
S	reference area based on diameter; $\frac{\pi}{4} D^2$ (ft^2)
V	free stream velocity (ft/sec)

DEFINITION OF SYMBOLS (Continued)

Symbol	Definition
α	angle of attack (degrees)
μ	free stream absolute viscosity
ρ	free stream density

NONSTANDARD ABBREVIATIONS

CM	command module
LES	launch escape system
SM	service module
LEM	lunar excursion module
S-IC	first stage for the Saturn V launch vehicle
LTV	Ling-Temco-Vought
CAL	Cornell Aeronautical Laboratory
AEDC	Arnold Engineering Development Center
MSFC	Marshall Space Flight Center

TECHNICAL MEMORANDUM X-53770

RESULTS OF SEVERAL EXPERIMENTAL INVESTIGATIONS OF THE STATIC AERODYNAMIC CHARACTERISTICS FOR THE APOLLO/SATURN V LAUNCH VEHICLE

SUMMARY

Experimental static aerodynamic data for six configurations of the Apollo-Saturn V Launch Vehicle at roll angles of 0, +45, and/or +90 degrees are presented. These data, which were needed to complement preliminary small-scale model data, were obtained from six wind tunnel tests on 0.3366, 0.9, and/or 4.0 percent scale models. Although six-component force data were obtained during each test, only longitudinal stability and axial force coefficients are presented, because other coefficients are small and are thus of secondary interest. Test conditions span a Mach number range from 0.5 through 7.81, an angle-of-attack range from -4 through +20 degrees, and a Reynolds number range from 0.5×10^6 through 8.0×10^6 based on reference diameter.

Results show that the small scale model data from MSFC agree well with data from the larger models and tunnels except for one case on the smallest size model where the effects of base flow deflectors on forebody axial force coefficient was not correctly simulated, thus indicating the need for caution in using this scale model to determine the effects of small external protuberances.

The correlation of data from all the tests -- even gradients near zero degrees for the high angle-of-attack tests -- is within acceptable limits for most purposes except when the force balance was not properly matched to the configurations without fins and shrouds.

I. INTRODUCTION

The Saturn V, the largest U. S. launch vehicle under development, is, with the Apollo capsule mounted, over 363 feet long, weighs approximately six million pounds with fuel, and generates 8.7 million pounds of thrust in its first three stages. In Project Apollo, the Saturn V will launch 280,000 pounds into an earth orbit. Then from the earth parking orbit, the 95,000-pound spacecraft, including the LEM, SM, and CM, will be injected into the proper trajectory to proceed with its mission of lunar exploration.

This report presents experimental, static aerodynamic data for the flight configuration of the Apollo-Saturn V launch vehicle. These data were obtained to complement previous experimental data which had been obtained primarily on smaller scale models, without protuberances, and in many cases on preliminary configurations. (A bibliography of previous Saturn V static aerodynamic reports is included.) Six-component force data obtained in each of the six wind tunnel tests were reduced to coefficient form including C_N, C_{m_g}, C_A, C_y, C_n and C_ℓ. However, the latter three, which for the Apollo-Saturn V vehicle are quite small compared to the first three, are of secondary interest, and are not included in this report. They can be found -- at least in tabulated form -- in references 11, 13, 15, 16, and 22. Data were obtained on the six different test configurations presented in figure 1.

The first test was conducted during June 1966 in the Cornell Aeronautical Laboratory 8-foot Transonic Wind Tunnel. Data were obtained on a 0.9 percent scale model over a Mach number range from 0.5 through 1.3 and over an α range from -4 through +10 degrees. The α range was limited so that balance sensitivity would provide more accurate data resolution near zero degrees.

In the second test, conducted during July 1966, in the Arnold Engineering Development Center 40-inch Supersonic Tunnel "A", the same 0.9 percent scale model was tested over a Mach number range from 1.5 through 5.9, and over an α range from -4 through +10 degrees. The primary objective was, again, accurate data resolution near zero degrees angle of attack. In the third test conducted during August 1966, in the Ling-Temco-Vought 4-foot High Speed Wind Tunnel, the same 0.9 percent scale model was tested over a Mach number range from -4 through +22 degrees. Its purpose was to extend the angle of attack range and to run limited checks on the effect of Reynolds number variations.

Concurrently with the above test, a fourth test using a 0.3366 percent scale model was conducted in the Marshall Space Flight Center 14-inch Trisonic Wind Tunnel over a Mach number range from 0.5 through 4.96, and over an α range from -4 through +16 degrees. This test was conducted to check for tunnel interference and model scale effects in the MSFC 14-inch TWT which has been used extensively for preliminary Saturn V testing. Another objective was to obtain data on some special configurations to aid in the analysis of protuberance effects. Those data may be found in reference 16.

The fifth test was conducted during October 1966 in the Arnold Engineering Development Center 12-inch Hypersonic Tunnel "E", using the same 0.3366 percent scale model tested at MSFC over a Mach number range from 5.0 through 7.8, and over an α range from -4 through +12 degrees. These data were obtained to extend the Mach range of available data.

The sixth and final test was conducted during November 1967 in the Arnold Engineering Development Center Transonic 16-foot Propulsion Wind Tunnel (16T). A 4.0 percent scale model was tested over a Mach number range from .6 through 1.3 and over an α range from -3 through +16 degrees to determine Reynolds number effect on the aerodynamic characteristics, particularly at high angles of attack, and to obtain pressure data in the tailbarrel region, particularly on the fins and shrouds. Only the force data from this test are presented in this report.

Data are first presented by facility. Then they are combined into summary plots for comparison. The principal objectives of this report are as follows: (1) To present an accurate, complete set of Apollo-Saturn V experimental static aerodynamic force data -- including the effects of major protuberances -- which will complement previous experimental data obtained primarily on smaller scale models without protuberances; (2) to point out problems encountered during each test which may be reflected in the data and misunderstood by those not familiar with test details; (3) to compare data obtained at various facilities with different scale models or, in two cases, with the same scale model; and (4) to show the effect of Reynolds number variation on the aerodynamic characteristics in the transonic Mach number range.

Because questions have arisen concerning the magnitude of the accuracy band required for the aerodynamic design curves (which were derived from these and other experimental data), a secondary objective of this report is to compare the design curves and current accuracy bands with the several representative sets of data presented in this report and thereby to indicate their validity in regard to experimental data variations.

II. TESTS

A. Model Descriptions

A sting-mounted 0.3366 percent scale model with all major protuberances was tested in the MSFC 14-inch wind tunnel and the AEDC/VKF 12-inch tunnel "E". Two separate aft bodies were available so that data could be obtained with and without fins and shrouds. The model was also segmented and had extra noses so that the LES abort and CM abort configurations could be tested if desired. The model was mounted on a removable sleeve which was attached to the sting-balance combination. Different sleeves were provided for testing at MSFC and AEDC Tunnel "E" because the sleeve for the latter test had to adapt to an AEDC water jacket. A model installation photograph is shown as Figure 4.

A sting-mounted 0.9 percent scale model with all major protuberances was tested in the CAL 8-foot, AEDC "A" 40-inch, and the LTV 4-foot wind tunnels. All protuberances, fins, and shrouds were removable. The body was segmented so that various configurations, including the S-IC alone, SM abort, CM abort, and LES abort could be tested if desired. S-IC engine bells were also available if needed. A model installation photograph is presented as Figure 3.

A sting-mounted 4.0 percent scale model with all major protuberances was tested in the AEDC/PWT 16T tunnel. All protuberances, fins, and shrouds were removable. The model was a combination force and pressure model. The tailbarrel, fins, and shrouds were instrumented with 720 pressure orifices. The model cavity and base were instrumented with 38 pressure orifices [18]. A model installation photograph is presented in Figure 5.

B. Test Facilities

1. Cornell Aeronautical Laboratory (CAL) 8-Foot Transonic Wind Tunnel

This facility was selected for the principal transonic test because a statistical analysis of data on similar models from several facilities showed that the data from the CAL Tunnel had the smallest accuracy band. This facility is a continuous flow, closed-circuit tunnel. The test section, a removable cart, has a perforated throat, walls constructed of perforated plate, and an auxiliary pumping system for plenum pumping. An operating range from one-sixth to two and one-half atmospheres in total pressure provides a wide range of test Mach numbers and Reynolds numbers. During model changes, two gate valves isolate the test section from the tunnel proper, making it necessary to bring only the test sphere to atmospheric conditions. The angle-of-attack sector operates in the pitch-pause mode. A most accurate method was used for determining the model angle of attack by installing electrolytic bubbles inside the model, thereby eliminating the necessity to correct for sting-balance deflections and sting-joint hysteresis. Accuracies of ±0.02 degrees are possible with this system. Other methods of determining α are available if needed. A remote roll mechanism is also available.

2. AEDC/VKF 40-Inch Supersonic Tunnel "A"

This facility is a continuous, closed-circuit, variable density tunnel with Mach number range from 1.5 to 6.0. Mach number can be varied from 1.5 to 4.0 in increments of 0.25 and from 4.0 to 6.0 in increments of 0.50. The nozzle control system allows setting interpolated contours for intermediate Mach numbers. Models are generally mounted on a sector which rotates in the horizontal plane, providing angular displacements from -5 to +15 degrees with a straight sting. Maximum tunnel stagnation pressures from 29 to 200 psia are available at Mach numbers 1.5 and 6.0, respectively. Minimum operating pressures are less than one-tenth of maximum. Below Mach 5, the tunnel is normally operated with a stagnation temperature of 100°F. This temperature can be raised to a maximum of 300°F. The absolute humidity of the tunnel can be maintained below 0.0001 pounds of water per pound of air by large capacity silica gel driers [3, 6].

3. LTV 4-Foot High Speed Wind Tunnel

This facility is an atmospheric exhaust, blowdown wind tunnel with a Mach number range from 0.20 to 4.0. The angle-of-attack sector can be operated over a range from -13 to +23 degrees in either a continuous pitch mode or a pitch-pause mode. The tunnel circuit uses both supersonic and transonic test sections. For supersonic operations, a single peak variable diffuser is placed downstream of the supersonic test section. For transonic operation, the variable diffuser is removed from the circuit and replaced with a porous wall (22.5 percent porosity), transonic test section. The model is located approximately 11 feet farther downstream for transonic testing than for supersonic testing. The transonic plenum is pumped by ejector action of the main tunnel airstream acting on controllable ejector flaps located downstream of the test section [22].

4. MSFC 14-Inch Trisonic Wind Tunnel

This facility is an intermittent, trisonic, blowdown tunnel operated from pressure storage to vacuum or atmospheric exhaust. There are two interchangeable test sections. The transonic section permits testing at Mach numbers from 0.20 through 2.50, and the supersonic section permits testing at Mach numbers from 2.74 through 5.84. A hydraulically controlled vertical pitch sector downstream of the test section provides a total angle-of-attack range of ±10 degrees with a straight sting. Air temperature can be controlled from ambient to approximately 180°F [15].

5. AEDC/VKF 12-Inch Hypersonic Tunnel E

This facility is an intermittent, blowdown (exhaust to vacuum) wind tunnel with a Mach number range from 5 to 8. Models are usually supported from the rear by stings attached to a vertical sector. The angle-of-attack sector can be varied over a range of ±13 degrees. An automatic angle-of-attack programming control system is provided. Within a core 7.5 inches in diameter and 20 inches long, the flow distribution is uniform within about ±1 percent in Mach number at each of the four nominal Mach numbers [5, 6, 7 and 8]. On the centerline over the same 20-inch length, the flow distribution is uniform within ±0.2 to ±0.5 percent depending on Mach number and pressure levels. Air temperatures up to 940°F, adequate to prevent mainstream liquefaction, are obtained from the electric heater which forms a part of the tunnel [3].

6. AEDC/PWT 16-Foot Transonic Wind Tunnel

This facility is a continuous flow, closed-circuit wind tunnel capable of operation at Mach numbers from .5 to 1.6 and stagnation pressures from approximately 100 to 4000 psf. Stagnation temperatures are automatically controlled within ±1°F of the set temperature through the normal range from 90° to 120°F. The angle-of-attack sector operates in a pitch-pause mode. The removable test section is 40 feet long and 16 feet square with 6 percent porosity walls. Plenum suction is used for removing air through the test section wall to prevent choking in the transonic range [9].

C. Test Conditions and Procedures

1. General

Nominal test conditions at each facility are presented in Table 1. R_{N_D} versus M are presented in Figure 6 and compared to a typical Apollo-Saturn V full scale trajectory curve. Model aerodynamic forces were measured with a six-component, internal strain gage balance at each facility. Data at each facility were corrected, where necessary, for model weight tare and for sting-balance-strut deflections. Roll angle variations were made by holding the balance stationary and rolling the model relative to the balance for each different roll angle. All data are presented in this non-rolling body axis system, and are referenced to the S-IC gimbal station which was approximated to be 10 inches (full scale) aft of the base of the vehicle.

2. CAL 8-Foot TWT

Configurations 1, 2, 3 and 4 were tested at ϕ = 0° and +45°. Configurations 1 and 4 were tested at ϕ = +90° also. The model was pitched in the vertical plane, and the α sector was operated in a pitch-pause mode. Model α was determined with an electrolytic potentiometer bubble pack located inside the model so that no corrections for sting-balance-strut deflections or for sting-joint hysteresis were necessary. Four base pressures measured just aft of the balance, in the model cavity, were used to determine C_{A_b}. Several runs were made with two boundary layer total pressure rakes located in the fin-shroud region to determine the boundary layer profile in that area; and schlieren photographs were also made of the aft portion of the model at α = 0 and +10 degrees for most Mach numbers. These data may be found in reference 17.

3. AEDC 40-Inch Tunnel A

Configurations 1 and 4 were tested at ϕ = 0 degrees. The model was pitched in the horizontal plane, and the α sector was operated in the pitch-pause mode. Base pressure measurements made in the model cavity were used to compute C_{A_b}. Trajectory Reynolds numbers could not be simulated at all Mach numbers, but boundary layer trips were placed on the nose of the LES to prevent possible laminar separation on the LES at the higher Mach numbers. The model flow field was observed with a schlieren system,and photographs were taken at several Mach numbers. As expected before the test, a reflected shock impinged on a small section of the tailbarrel at Mach number 1.53. However, the data were only slightly affected (see section III). More information on this and other aspects of this test may be found in reference 11.

4. LTV 4-Foot HSWT

Configuration 1 was tested at ϕ = 0, +45 and +90 degrees; and configurations 5 and 6 were tested only at ϕ = 0 degrees. The model was pitched in the vertical plane, and the α sector was operated in the continuous pitch mode. The pitch rate was approximately 1.75 degrees per second, and data were sampled at 5 samples per second. The large center of pressure shift and reduced load range caused by removing the fins and shrouds from the model produced some unfavorable model dynamic and load resolution problems for configurations 4 and 5, which resulted in increased data scatter near α = 0 degrees. The balance was moved 5.5 inches forward in the model for most of configuration 5 runs and this seemed to alleviate the problem somewhat. Two base pressures were measured in the model cavity and used to compute C_{A_b}. Two other pressure measurements were made on the sting at the base of the model, but were used for monitoring purposes only. Further information on this test can be found in reference 23.

5. MSFC 14-Inch TWT

Configurations 1 and 4 were tested at ϕ = 0, +45 and 90 degrees. The model was pitched in the vertical plane and the α sector was operated in the pitch-pause mode. C_{A_b} was computed from base pressures measured on the sting at the base of the model.

At Mach numbers from 3 to 5, boundary layer trips are normally used, in this facility, on the nose of the LES to induce boundary layer transition and thereby prevent laminar flow separation. Experience has shown that this technique is required to simulate expected conditions for the full-scale vehicle since tunnel limitations make it impossible to simulate Saturn V trajectory Reynolds numbers. However, during this test the trips were inadvertently omitted. Resulting effects are discussed in section III.

Data obtained on some special configurations to aid in analysis of protuberance effects may be found in reference 16.

6. AEDC 12-Inch Tunnel E

Configurations 1 and 4 were tested at ϕ = 0 degrees. Configuration 1 was tested also at ϕ = 0, +45 and +90 degrees. The model was pitched in the vertical plane and the α sector was operated in the pitch-pause mode. Trajectory Reynolds numbers were simulated at all Mach numbers except Mach 5, where the model was run with boundary layer trips on the nose of the LES to prevent possible laminar separation on the LES. C_{A_b} was determined from base pressures measured on the sting just inside the base of the model. The balance was cooled with a water jacket which extended over the length of the balance, and the forward end of the sting was water-cooled internally. Balance temperatures were monitored during the test. Some difficulty was experienced in shielding the water lines from flow impingement when the fins and shrouds were removed. These effects are described in section III. Other details of this test may be found in reference 11.

7. AEDC 16-Foot Transonic Wind Tunnel

Configuration 1 was tested at ϕ = 45 degrees. The model was pitched in the vertical plane, and the α sector was operated in the pitch-pause mode. The angle of attack was measured with an alpha meter located inside the model so that no corrections for sting-balance-strut deflection were necessary. Reynolds number variations (see Table 1) were made by varying P_t. Thirty-eight base pressure measurements in the model cavity and on the base of the model were used to compute C_{A_b}.

Although not included in this report, 720 pressure measurements were made on the tailbarrel, fins, and shrouds at all of the even angles of attack. Those data, along with more detailed information on this test, can be found in references 14, 19, and 20.

III. RESULT OF TESTS

A. Variation of Normal Force Coefficient with Angle of Attack and with Pitching Moment Coefficient

1. General

Figures 7 through 21 presents the C_N vs α and Cm_g vs C_N curves for each configuration tested. The following comments can generally be applied to all configurations tested except as stated.

2. C_N versus α

These curves show that C_N increases smoothly with increasing α. Because of tunnel flow angularity, fin-shroud misalignment, and protuberance asymmetry, the curves do not usually pass through zero. Data are generally linear over $\pm$ 2 to 4 degrees. However, at Mach numbers 7.12 and 7.81, the linear region decreases to approximately $\pm 1/2$ degree. This effect results from a forward movement of the laminar separation point on the LES, and is discussed in some detail in reference 3.

At angles from approximately 3 to 12 degrees, C_N varies nonlinearly with α for all configurations. For configurations with fins and shrouds, and to a lesser extent, those with shrouds, but without fins, an "underlinear" trend is seen at $3 \leqq \alpha \leqq 12$ degrees from Mach numbers 0.8 through 1.2 This trend is attributed to a reduction in fin-shroud lift efficiency with increasing angle of attack which is gradually offset by increased normal force from the S-IC system tunnels and viscous cross forces. The effect is seen in total vehicle aerodynamics by causing the total vehicle normal force coefficient to be underlinear and by moving the center of pressure forward as the angle of attack is increased [18]. The pressure data discussed in references 14, 19, and 20 provides more detailed information on the causes of this trend.

At angles of attack greater than 10 to 12 degrees, the viscous cross forces become more significant and the gradients increase notably. Gradients over this α range tend to vary less with Mach number than do the gradients near zero degrees α. It may be noted that the gradients over this region do tend to increase very slightly up to Mach number 1.6 and then to decrease slightly with increasing Mach number.

Notable problem areas include the -1 and -1/2 degree data points in the data from the CAL facility, which, for all configurations tested at CAL, deviate from the expected linear trend. Since all configurations were similarly affected, including those without protuberances, without fins, and without fins and shrouds, model asymmetry does not seem to be the cause. A possible cause common to all configurations is the bubble pack used to measure the angle of attack. Each angle is measured by a different bubble unit so that any malfunctioning unit would be in error for all configurations; therefore, the bubble pack is considered to be the most likely cause of erratic data at the angles in question.

Careful examination of the data from the AEDC tunnel at Mach number 1.53, presented in Figure 11(a), reveals a slight "hump" from $\alpha = 3$ to 5 degrees which results from the reflected shock mentioned in section II. Erratic data at Mach numbers 2.99 and 5.91 on Figure 11(a) and at Mach number 5.91 on Figure 12(a) are caused by data resolution problems resulting from very low loads at these Mach numbers.

As explained in section II, data resolution problems near zero degrees α were also experienced at LTV, particularly for the configurations without fins and shrouds, because of the reduced loads and the large shift in the center of pressure. Therefore, an undesirable amount of scatter was present in these data. This was also true to a lesser extent for the data obtained at MSFC.

3. C_{m_g} versus C_N

These curves are linear through zero over a region corresponding with approximately ±4 degrees angle of attack. Above this linear region, C_m increases nonlinearly with increasing C_N. For configurations with fins and shrouds, gradients over the region corresponding with $4 \leqq \alpha \leqq 10$ degrees increase, compared with those near zero, from Mach number .5 through 1.6, remain almost the same at Mach 2.0, and decrease slightly from Mach 2.4 through 7.8. For configurations without fins and shrouds, gradients over the same region decrease, compared with those near zero, over the entire Mach range from 0.5 through 7.8. This would be the expected trend, considering the body shape and fin-shroud efficiency as a function of angle of attack.

B. Variation of Static Longitudinal Stability with Mach Number at Angles of Attack near Zero Degrees

1. Configuration 1

Figure 22 presents the variation of C_{N_α} and CP/D with M near zero degrees α for the Apollo-Saturn V launch vehicle. The gradients were derived from the previously presented C_N versus α and C_{m_g} versus C_N

curves for a range corresponding with $-2 \leq \alpha \leq +2$ degrees. Parts (a), (b), and (c) of this figure present static longitudinal stability characteristics for the vehicle at ϕ = 0, +45, and +90 degrees, respectively. Detailed analysis of roll angle trends are presented in references 7, 10, and 13 and are therefore not included here. However, comments pertinent to these particular tests are included in the following paragraphs.

Figure 22(a) presents data, from five different facilities, for the vehicle at zero degrees ϕ over a Mach number range from 0.50 through 7.81. As explained in section II, the CP/D data from MSFC at Mach numbers 4.00 and 4.96 disagree with the other data because of laminar flow separation. Disregarding those data, it can be seen that where the data overlaps there is reasonably good agreement between data from the various facilities. The greatest differences occur over the Mach number range from 0.7 through 1.2. The maximum variation over this range (using the CAL data as a baseline for comparison because test conditions there were optimized for accurate gradient determination near zero degrees α) is -6.5 percent in C_{N_α} at Mach 1.1 and +.16 caliber in CP/D at Mach 1.2. The average variation of the LTV data over this range is 3.6 percent in C_{N_α} and +.035 calibers in CP/D. The average variation of the MSFC data is -1.9 percent in C_{N_α} and +.055 calibers in CP/D.

Figure 22(b) presents data for the vehicle at +45 degrees over a Mach number range from 0.50 through 4.0. Again using the CAL data as a baseline, the maximum variations over the transonic Mach number range from 0.7 through 1.2 are -7.46 percent in C_{N_α} at Mach number 1.1 and +.36 caliber in CP/D at Mach number 1.2. Then limiting the range of comparison to Mach numbers from 0.8 through 1.1 so that data points from each facility are available at each Mach number, we see an average variation of the LTV data of -3.45 percent in C_{N_α} and +.068 calibers in CP/D. The average variation of the MSFC data is -2.44 percent in C_{N_α} and +.15 calibers in CP/D. The average variation of the AEDC 16T data is -4.5 percent in C_{N_α} at +.15 calibers in CP/D.

Figure 22(c) presents data from the vehicle at +90 degrees ϕ over a Mach number range from 0.50 through 4.0. Comparison with the CAL data over the Mach number range from 0.7 through 1.2 shows a maximum variation of -6.41 percent in C_{N_α} at Mach 1.2 and +.21 calibers in CP/D at Mach 1.1. Further comparison shows that the average variation of the LTV data over this range is -2.34 percent in C_{N_α} and +.03 calibers in CP/D. The average variation of the MSFC data is -1.95 percent in C_{N_α} and +.167 calibers in CP/D.

It is notable that the above average variations are biased instead of being random. The most probable reason for this phenomenon seems to be decreased C_N resolution resulting from use of the less sensitive balances required to obtain data over the high α ranges tested at MSFC and LTV. A check of balance design load ranges and sensitivities in the test data reports [11, 16, 17 and 23] substantiates this conjecture. However, that this is not the entire reason is indicated by the C_{N_α} trends over the Mach number range from 1.0 through 1.3. The LTV data are considerably lower than the CAL data over this Mach number range for all three roll angles; but the MSFC data agree closely with the CAL data at ϕ = 0 degrees, not quite so well at ϕ = 90 degrees, and, at ϕ = +45 degrees, they agree more closely with the LTV and AEDC 16T data. Since the trend at MSFC is somewhat roll-dependent, it may indicate that the difference is related to protuberance effects; or since the blockage at MSFC, LTV, and AEDC 16T was higher than at CAL, we might suspect tunnel interference effects. In any event, the existing data have not yet yielded a conclusive explanation. It is also notable that the MSFC small-scale model data generally compare as well with the CAL data as do the data of the larger scale models. The C_{N_α} data agree a little better and the CP/D not quite so well, indicating that in general the $C_{m_{g\alpha}}$ of the MSFC data is a little higher over this Mach number range.

The dashed line fairing on figure 22(a) is from the Apollo-Saturn V aerodynamic design criteria [18], which was derived from these and other experimental and analytical data. This curve is presented for comparison purposes because interest has been expressed in the magnitude required for the design accuracy band, and experimental inaccuracies are certainly one factor to be considered. To avoid cluttering, the current design accuracy band of ±6 percent for C_{N_α} and ±.2 caliber for CP/D is omitted. However, examination of the data will show that with few exceptions all of the data from the various tests would lie within this band. Even the AEDC Tunnel E data, which were obtained after reference 18 was published, fall outside the accuracy band only slightly at Mach 6.08.

2. Configuration 2

Figure 23 presents C_{N_α} and CP/D as a function of Mach number for the Apollo-Saturn V launch vehicle without protuberances. Data are presented for ϕ = 0 and +45 degrees. Maximum C_{N_α} and the most rearward CP/D location occur at Mach 0.9 for both roll orientations. C_{N_α} at ϕ = +45 degrees is an average of 2.3 percent higher over the included Mach range from 0.5 through 1.3 than it is at ϕ = 0 degrees. CP/D is practically the same at both roll angles.

The increase in C_{N_α} is attributed to increased efficiency of the fins and shrouds which receive full upwash effects at ϕ = 45 degrees [18]. The close proximity of the fins and shrouds to the reference center would explain the lack of a corresponding change in CP/D.

3. Configuration 3

Figure 24 presents C_{N_α} and CP/D as a function of Mach number for the Apollo-Saturn V launch vehicle without fins at ϕ = 0 and +45 degrees. Again, the maximum C_{N_α} and the most rearward CP/D location occur at Mach number 0.9 for both roll orientations. C_{N_α} at ϕ = +45 degrees is an average of 3.8 percent higher over the included Mach range from 0.5 through 1.3 than it is at ϕ = 0 degrees. The fact that the difference is greater than it was for configuration 2 is attributed to increased upwash effects caused by the addition of protuberances. Again, as would be expected, only slight differences are noted in the CP/D curves.

4. Configuration 4

Figure 25 presents C_{N_α} and CP/D as a function of Mach number for the Apollo-Saturn V launch vehicle without fins and shrouds at ϕ = 0, +45, and +90 degrees.

Figure 25(a) presents data for configuration 4 at ϕ = 0 degrees. It should again be noted that the MSFC CP/D data points are invalid because of LES sepatation (see section II). Other problem areas in these data which require comment can be categorically described as resulting from data resolution problems.

The load range of the balance was selected at each facility, and the location of the balance in each model was determined to insure optimum data resolution for configuration 1. A comparison of figure 25(a) with figure 22(a) shows that a considerable reduction in C_{N_α} and a sizeable forward shift in CP/D (see figure 35 also) result when the fins and shrouds are removed from configuration 1. The magnitude of the effect this had on the data resolution is a function of the test conditions at each facility, particularly the range of q and α.

The deviation of the AEDC Tunnel "A" data points from the faired curve at Mach 5.91 is attributed to the load reduction caused by removing the fins and shroud and to the large reduction (78 percent) between maximum q conditions at Mach 1.53 and the minimum q conditions of Mach 5.91. The variation of the LTV data from the faired curve, which is based on the CAL and AEDC Tunnel "A" data, is attributed in part to the stiff balance that had to be used to measure the high normal force loads accompanying the α range which exceeded 20 degrees. This made accurate load resolution near zero degrees α subject to question even for configuration 1, and particularly questionable for configurations without fins and shrouds. This problem could have been worsened somewhat by increased model dynamics resulting from the combination of a heavy model, and a CP/D considerably forward of the balance. The same problems were experienced at MSFC except the model was not proportionately as heavy and the α range was slightly less (16 degrees).

It is readily apparent that the agreement of data between facilities where there is overlapping data is not so good as for configuration 1. Again using the CAL data as a base line, comparison of data over the Mach number range from 0.7 through 1.2 shows maximum variations of -9.81 percent in C_{N_α} at Mach 0.7 and +.41 calibers in CP/D at Mach 0.7. The average variation of the LTV data over this Mach number range is -4.2 percent in C_{N_α} and +.12 calibers in CP/D. The average variation of the MSFC data is -6.26 percent in C_{N_α} and +.28 calibers in CP/D. As it was for configuration 1 the variation is biased rather than random.

Figures 25(b) and (c) present configuration 4 at ϕ = +45 and +90 degrees, respectively. Significant scatter and some rather unusual trends are attributed to the data resolution problems. Because of these problems, analysis of roll angle trends and further comparison of data for configuration 4 from the various facilities are not considered worthwhile.

5. Configuration 5

Figure 26 presents C_{N_α} and CP/D as a function of Mach number for the Apollo-Saturn V launch vehicle without fins, shrouds, and protuberances. Most of the data for this configuration were obtained with the balance moved 5.5 inches forward of the position it occupied when data on configuration 4 were obtained. This brought the balance gage center closer to the CP/D location, and the total pressure was increased; thus, data trends are somewhat smoother than they were for configuration 4.

6. Configuration 6

Figure 27 presents C_{N_α} and CP/D as a function of Mach number for the Apollo-Saturn V launch vehicle without the LES and CM. The dashed line fairing is taken from reference 8, which is the current static aerodynamic design criterion for the aborted Apollo-Saturn V launch vehicle, and which was derived from these and other pressure and force data. The dashed line fairing of reference 8 is presented in support of the fairing described here since only a few data points were obtained during these tests.

C. Variation of Axial Force Coefficient with Mach Number at Angles of Attack near Zero Degrees

General

At $\alpha = 0°$ there should be no significant variation of axial force with ϕ for these configurations. Therefore, data in this section are presented only for the $\phi = 0$ degree case except for the AEDC 16T configuration 1 which was tested only at $\phi = +45$ degrees.

1. Configuration 1

The axial force coefficient is shown in figure 28 as a function of Mach number for the Apollo-Saturn V launch vehicle. Except for the MSFC data, the agreement of data from the various facilities is within reasonable limits. The AEDC 16T data are considered to be the most accurate because of the more accurate determination of C_{A_b}, as discussed in section II. Only the nominal Reynolds number data from AEDC 16T are presented on this figure. Data at all three Reynolds numbers are presented in figure 38 for C_{A_f}.

The greatest variation in C_{A_f} between facilities occurs from Mach 0.5 through 2.0. Using the CAL data as a base line for comparison -- to be consistent with the stability analysis -- we can see that, over the Mach number range from 0.8 through 1.2, where there are overlapping data, the average variation of C_{A_f} is -4.2 percent for the LTV data, -3.8 percent for AEDC 16T data, and -23.2 percent for the MSFC data.

None of the average variations are considered to be excessive except that for the MSFC data. The fact that the MSFC data are considerably lower than the other data is attributed to smaller protuberance effects -- particularly from the base flow deflectors -- than were obtained on the larger scale models. This conclusion is based on data from references 4 and 17 which showed that removing the base flow deflectors from the small scale model tested at MSFC had no effect on C_{A_f}, while removing them from the model tested at CAL caused a reduction in C_{A_f} varying from 51 percent at Mach 0.5 to 11 percent at Mach 1.3.

The dashed line fairing on figure 28 is from the static aerodynamic design criteria [18].

2. Configurations 2 and 3

Figures 29 and 30 present the variation of axial force coefficient with Mach number for the Apollo-Saturn V launch vehicle without protuberances and without fins, respectively. These data, obtained only at CAL, are believed to be valid in both magnitude and trend.

3. Configuration 4

Figure 31 presents the variation of axial force coefficient with Mach number for the Apollo-Saturn V launch vehicle without fins, shrouds, and base flow deflectors.

The agreement of the MSFC data with those from the other facilities is better than it was for configuration 1. This improvement is attributed to the absence of the base flow deflectors.

The AEDC Tunnel "E" data point at Mach number 5.04 is erroneous because of flow impingement on the balance-cooling water lines which, after the fins and shrouds were removed, were not very well shielded from the airstream [11].

The AEDC Tunnel "A" C_{A_T} and C_{A_b} data points at Mach 1.53 were affected by the shock reflection previously discussed in section II.

Over the Mach number range from .7 through 1.2, where there are overlapping data, the average variation of the LTV data from the CAL data is -9.0 percent.

4. Configuration 5

Figure 32 presents the variation of axial force coefficient with Mach number for the Apollo-Saturn V launch vehicle without fins, shrouds, and protuberances. These data were obtained at higher Reynolds numbers than the data for configuration 4. The magnitude and trends of the data presented are believed to be valid.

5. Configuration 6

Figure 33 presents the variation of axial force coefficient with Mach number for the Apollo-Saturn V launch vehicle without the LES and CM. The dashed line fairing for C_{A_T} is from the current static aerodynamic data for the aborted Apollo-Saturn V launch vehicle [8]. This fairing was derived from these and previous force and pressure data. It is presented to support the solid-line fairing since the relatively few data points obtained during this test required a good deal of judicious interpolation to arrive at the presented curve.

D. Variation of Static Longitudinal Stability with Mach Number at Angles of Attack from +2 to +20 Degrees

1. C_N versus M

Figure 34(a) presents C_N as a function of Mach number for $2 \leqq \alpha \leqq 20$ degrees. The C_N variation with Mach number is small at low angles of attack. The transonic peak is primarily a function of fin, shroud, and protuberance influence as indicated by figure 36. At angles of attack greater than 10 degrees, body lift becomes significant and produces a peak which increases in magnitude with increasing α. The location of this peak varies with α between Mach number 2.5 and 3.5.

Evidence is presented in reference 25 that the dip seen at Mach 1.10 is caused by local shocks in the tailbarrel region. Shadowgraphs obtained during the test reported in reference 12 verify the fact that local shocks in the tailbarrel region are much stronger at Mach 1.10.

The dashed lines indicate the ±6 percent error band for the static aerodynamic design curves presented in reference 18. The curves themselves are not presented because their close proximity to the fairing of these data would create confusion. With few exceptions, all data presented from the different facilities lie within this error band even though, in some instances, the fairing is obviously conservative. A notable exception is the fairing at $\alpha = 8$ degrees which should obviously be lower above Mach 2.75.

The average variation from the arithmetic mean of the data from CAL, LTV, and MSFC over the Mach number regime from .7 to 1.2 ranges from 5 percent at $\alpha = 2$ degrees to 2 percent at $\alpha = 10$ degrees. From 10 to 16 degrees, the MSFC and LTV data generally agree within ±1 percent of their arithmetic mean. Variations would be only slightly greater if the CAL data were used as a base line as done for the gradients near zero.

2. CP/D versus M

Figure 34(b) presents CP/D as a function of Mach number for $2 \leqq \alpha \leqq 20$ degrees. As before, the dashed line represents the accuracy band (±.2 calibers) of the design curves presented in reference 18. As can be seen, most of the data lie within this band.

The agreement of the CAL, LTV, and MSFC data over the Mach range from .7 to 1.2 is generally very good. The variation from the arithmetic mean is less than .1 calibers at all angles with the exception of a few points at Mach numbers 1.1 and 1.2. As was true near zero degrees, the CP/D data from MSFC are always greater (more forward) than the CP/D data from the other facilities over the transonic Mach number range.

E. Effects of Fins, Shrouds, and/or Protuberances on the Variation of Static Longitudinal Stability with Mach Number at Angles of Attack near Zero Degrees

Figure 35 presents the effects of fins, engine shrouds, and protuberances on the static longitudinal stability characteristics of the Apollo-Saturn V launch vehicle at ϕ = 0 degrees. The symbols on this figure do not represent discrete experimental data points, but they rather represent a difference in the faired data of the various configurations indicated on the legend.

These components have a significant effect on the total launch vehicle throughout the Mach number range from 0.5 through 7.8, but are the most effective in the transonic range where the combined effects of removing the fins, shrouds, and protuberances from the total vehicle (configuration 1) cause a maximum forward shift in CP/D of 3.3 calibers at Mach 1.1 and a maximum decrease in C_{N_α} of -57 percent at Mach 0.7.

The fin-shroud curve also includes base flow deflectors, but according to reference 5, these have no effect on the static longitudinal stability.

F. Effects of Reynolds Number on the Static Longitudinal Stability Variation with Mach Number of Angles of Attack Near Zero Degrees

Figure 36 presents the variation of C_{N_α} and CP/D with M near zero degrees α for the Apollo-Saturn V at ϕ = +45 degrees. These gradients were derived from the previously presented basic data for an angle-of-attack range of ±2 degrees. Although only data from the AEDC 16T test are presented, the results of Reynolds number variations at the other facilities are in agreement with the data presented.

As seen in Table 1, three different Reynolds numbers were run at each Mach number. The Reynolds numbers run were the highest and lowest possible as determined by facility limitations, and a nominal value was run to supplement these two values. The Reynolds numbers obtained are compared in figure 6 with the Reynolds numbers for the other tests presented herein and with the trajectory Reynolds numbers for the full-scale flight vehicle.

The faired curve is based on the arithmetic mean of the three sets of data. The variation of both C_{N_α} and CP/D is slight. A maximum variation from the arithmetic mean of ±1.9 percent in C_{N_α} at Mach 1.2 and ±.07 calibers in CP/D at Mach 1.2. The average variation across the Mach range from .6 through 1.3 is ±1.35 percent for C_{N_α} and ±.06 calibers for CP/D. Actually, for most Mach numbers, these variations are within the accuracy range which might be expected of experimental data, and no consistent trends as a function of Reynolds number are apparent.

G. Effect of Reynolds Number on the Forebody Axial Force Coefficient Variation with Mach Number at Angles of Attack near Zero Degrees

Figure 37 presents the variation of C_{A_f} with Mach number near zero degrees α for the Apollo-Saturn V launch vehicle at $\phi = 45$ degrees.

The faired curve is based on the arithmetic mean of the three sets of data. A variation from the arithmetic mean of 14.3 percent at Mach 0.60 and of ±6.4 percent at Mach 0.80 is observed. At the higher Mach numbers, the variation decreases to approximately ±3 percent or less. The average variation over the Mach number range from 0.6 through 1.3 is ±5 percent.

The large variation at Mach numbers 0.6 and 0.8 is attributed in part [20] to a trend of decreasing C_{A_f} with increasing Reynolds number which is caused by the influence of Reynolds number on the skin friction component of C_{A_f}.

H. Effects of Reynolds Number on the Static Longitudinal Stability Variation with Mach Number at Angles of Attack from 2 to 16 Degrees

Figure 38 presents the variation of C_N and CP/D with M for the Apollo-Saturn V launch vehicle at $2 \leqq \alpha \leqq 16$ degrees and $\phi = +45$ degrees. Three Reynolds numbers were tested at each Mach number. The faired curve is based on the arithmetic mean of the three sets of data. The average variation of the data from this mean over the Mach number range from .6 through 1.3 is less than ±2 percent for C_N at all angles and less than ±.1 calibers for CP/D at all angles except 4 degrees, where it went to ±.18 calibers.

As previously explained, the dip in the C_N curve and the corresponding forward movement of CP/D near Mach 1.1 is attributed to local shocks in the tailbarrel region. Even though the range of Reynolds number at which this model was tested overlapped the Reynolds numbers at which the smaller models were tested, this trend is much more evident for all Reynolds numbers at which this model was tested than it was for the smaller models. However, the C_N dip is less prominent for the low Reynolds number case. There also seems to be a slight tendency for C_N to decrease and CP/D to increase with increasing Reynolds number, but the trend is not consistent at all Mach numbers and the differences are so small that a conclusive statement is not possible.

IV. CONCLUSIONS

It is shown that the agreement of small-scale model data from the MSFC 14-inch wind tunnel with data from the larger models and tunnels is good with one exception. The C_{A_f} data were significantly lower in the transonic Mach number regime for the MSFC model because the effect of the base flow deflectors was not correctly simulated. This indicates that caution should be exercised when seeking to simulate protuberance effects on this size model.

Correlation of data from the different tests -- even gradients near zero for the high α tests -- is adequate except for configurations without fins and shrouds. It is evident that a more sensitive balance should have been used for these configurations.

A reduction in C_N and corresponding increase in CP/D at Mach number 1.1 is attributed to local shocks in the tailbarrel region. However, this trend is not seen over the range to α = 10 degrees and Mach number = 1.3 when the external protuberances forward of the engine shrouds are removed; apparently because of changes in the boundary layer. The trend is most prominent for the largest model tested and seemed to increase slightly with increasing Reynolds number. It is therefore considered a valid trend for the full scale vehicle.

The accuracy band presented in the current static aerodynamic design criteria is shown to adequately contain experimental inaccuracies over a wide range of test conditions if proper experimental procedures are followed.

TABLE I

TABLE OF TEST CONDITIONS

Facility	Nominal Mach No.	Nominal $R_N/Ft \times 10^{-6}$	Nominal P_t (psia)	Nominal Tt (°R)	Nominal α (deg)	Model Scale
MSFC 14" TWT	0.50	4.2	22	560	-4 to +16	.3366%
	0.70	5.3	22	560		
	0.80	5.8 & 9.2	22 & 34	560		
	0.90	6.1	22	560		
	1.00	6.3 & 9.1	22 & 31	560		
	1.10	6.4	22	560		
	1.20	6.5 & 9.1	22 & 30	560		
	1.30	6.5	22	560		
	1.46	6.2	22	560		
	1.96	6.7	28	560		
	2.99	4.3	30	560		
	4.00	6.4	75	560		
	4.96	5.0	90	560		
LTV 4' HSWT	0.70	7.2	28	548	-4 to +21	.9%
	0.80	7.6	28	570		
	0.90	7.4 & 9.5	27 & 29	574		
	1.00	7.0	24	572		
	1.10	7.1	25	583		
	1.20	7.4 & 10.5	25 & 37	576		
	1.41	6.7	24	598		
	1.61	7.2 & 11.0	25 & 41	558 - 583		
	2.00	6.3	29	609		
	2.41	6.5 & 13.9	38 & 76	623 - 590		
	2.99	7.9	61	600		
CAL 8' TWT	0.50	3.0	16	578	-4 to -10	.9%
	0.70	3.5	15	586		
	0.80	1.9 & 3.5	7 & 14	596		
	0.90	1.9 & 3.5	7 & 13	596		
	1.00	1.7 & 3.5	6 & 13	602		
	1.10	3.5	15	605		
	1.20	3.5	15	613		
	1.30	3.5	13	620		
AEDC 40" TUNNEL A	1.53	3.7	14	560	-4 to +10	.9%
	2.00	2.3 & 3.9	10 & 16	560		
	2.49	3.6	18	560		
	3.00	1.6 & 4.9	11 & 33	560		
	3.50	5.1	45	560		
	4.00	5.2	60	560		
	5.00	5.1	115	625		
	5.91	2.4	80	625		
AEDC 12" TUNNEL E	5.04	14.9	310	675	-3 to +12	.3366%
	6.08	8.8	273	855		
	7.12	4.6	350	1050		
	7.81	2.8	410	1285		

TABLE I (Concluded)

Facility	Nominal Mach No.	Nominal $R_N/Ft \times 10^{-6}$	Nominal P_t (psia)	Nominal Tt (°R)	Nominal α (deg)	Model Scale
AEDC 16' TWT	0.60	0.7,2.8 & 5.7	3, 13 & 26	572	-3 to +16	4%
	0.80	0.8,3.3 & 6.4	3, 13 & 25	572		
	0.90	0.9,3.4 & 6.2	3, 13 & 22	572		
	1.00	0.9,3.6 & 6.0	3, 13 & 21	572		
	1.05	3.6	13	572		
	1.10	0.9,3.6 & 5.7	3, 13 & 20	572		
	1.15	3.6	13	572		
	1.20	0.9,3.6 & 5.3	3, 13 & 18	572		
	1.30	0.9,3.0 & 4.9	3, 10 & 17	572		
	1.40	2.4 & 4.2	8 & 15	572		

Configuration Nomenclature

Configuration 1	APOLLO - SATURN V Launch Vehicle
Configuration 2	APOLLO - SATURN V Launch Vehicle without Protuberances
Configuration 3	APOLLO - SATURN V Launch Vehicle without Fins
Configuration 4	APOLLO - SATURN V Launch Vehicle without Fins, Shrouds, and Base Flow Deflectors
Configuration 5	APOLLO - SATURN V Launch Vehicle without Fins, Shrouds and Protuberances
Configuration 6	APOLLO - SATURN V Launch Vehicle without Launch Escape System and Command Module

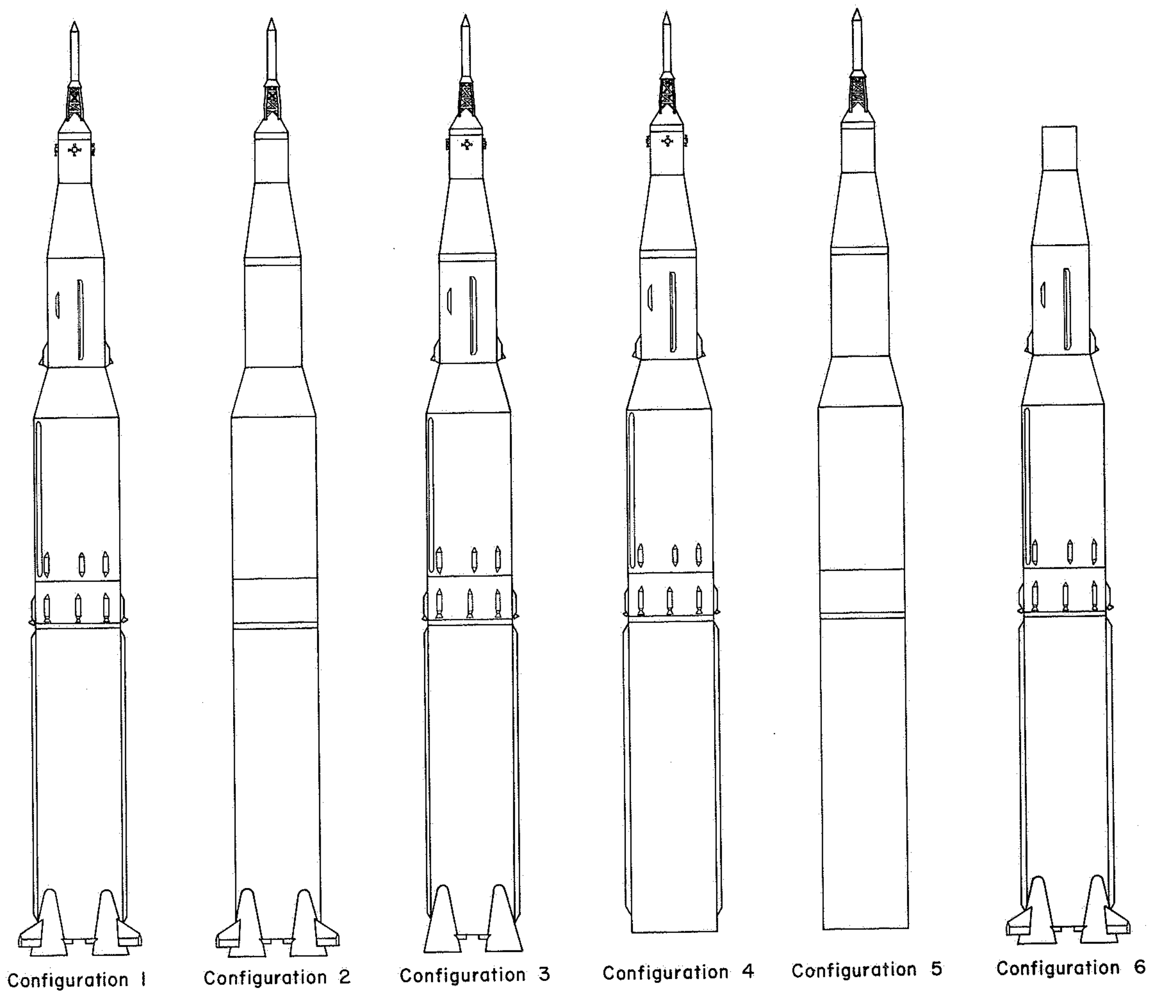

Figure 1 TEST CONFIGURATIONS

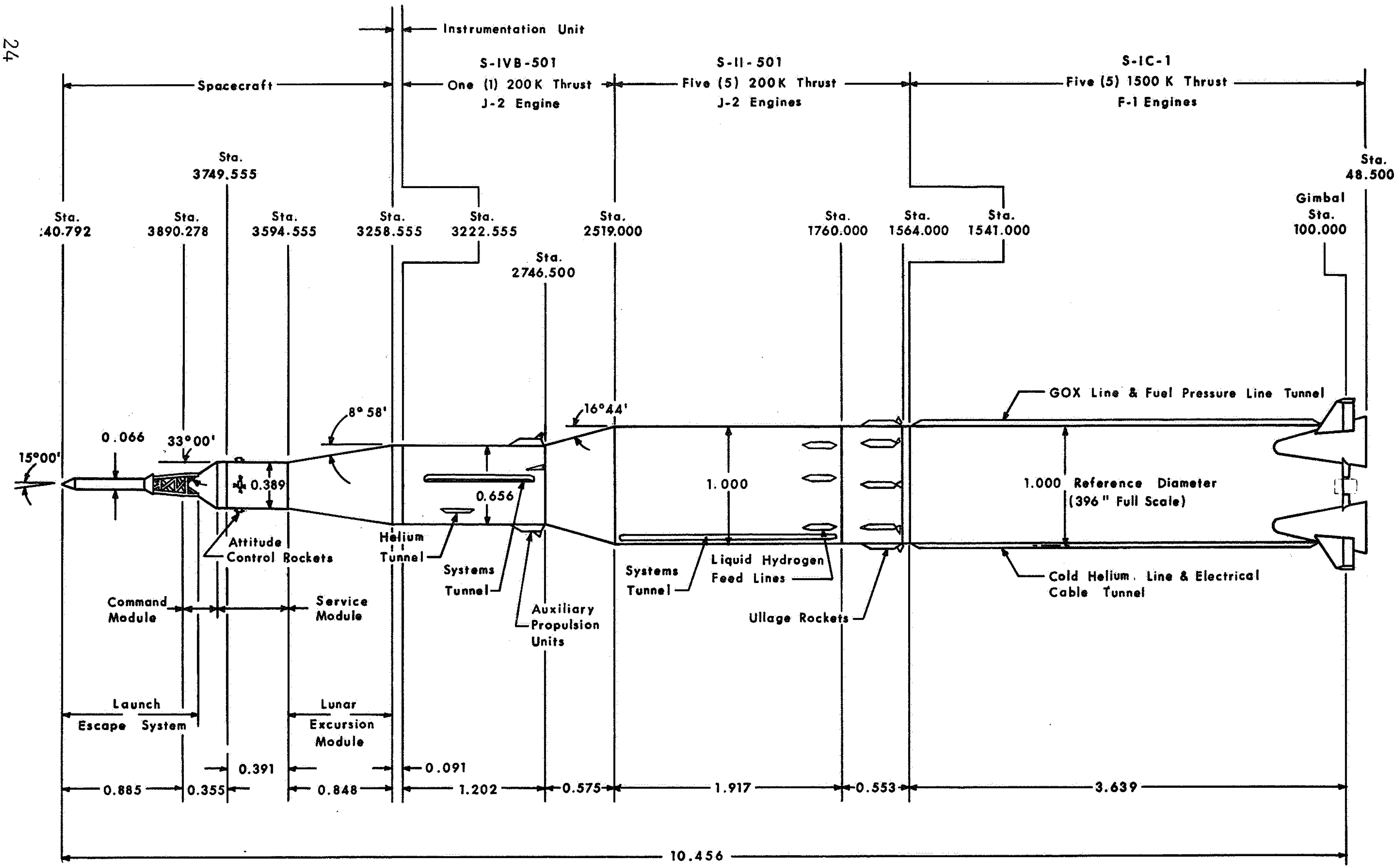

NOTES:

1. All vehicle stations in inches.
2. All linear dimensions in calibers.

Figure 2 Model Geometry – APOLLO-SATURN V Launch Vehicle

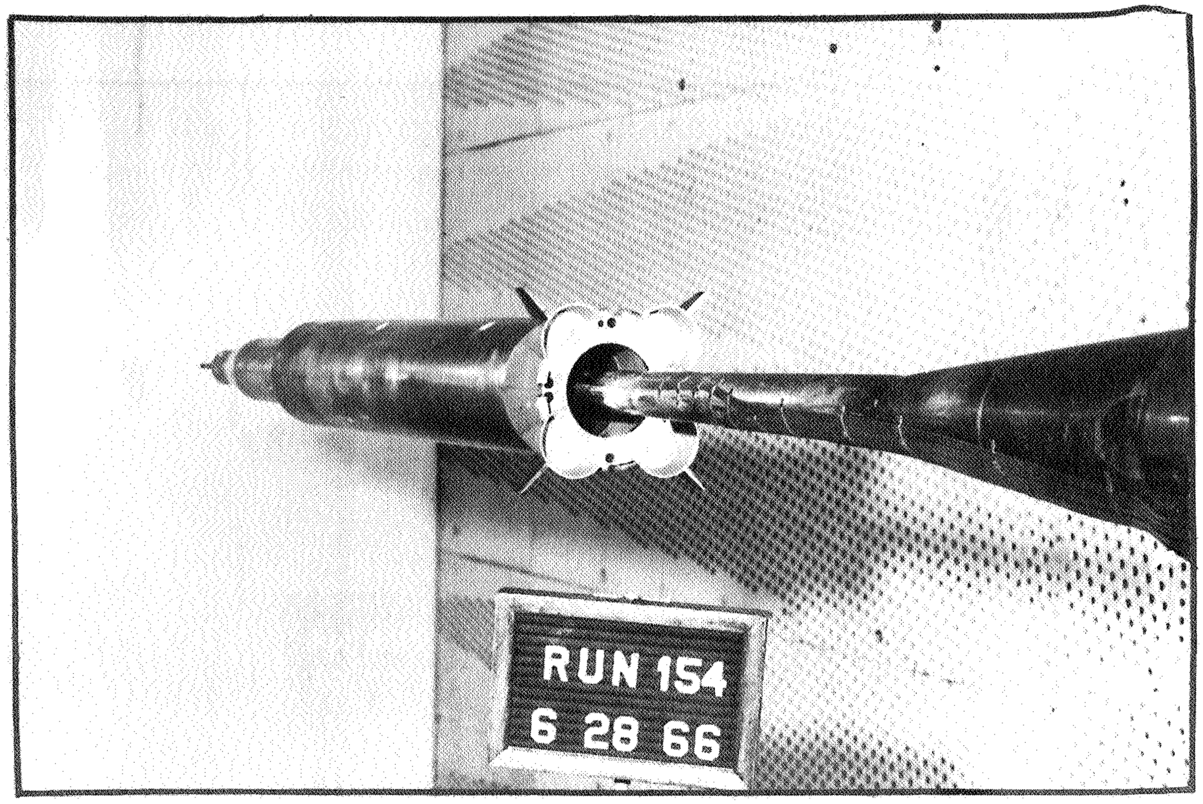

Configuration 2 ; $\phi = 0°$

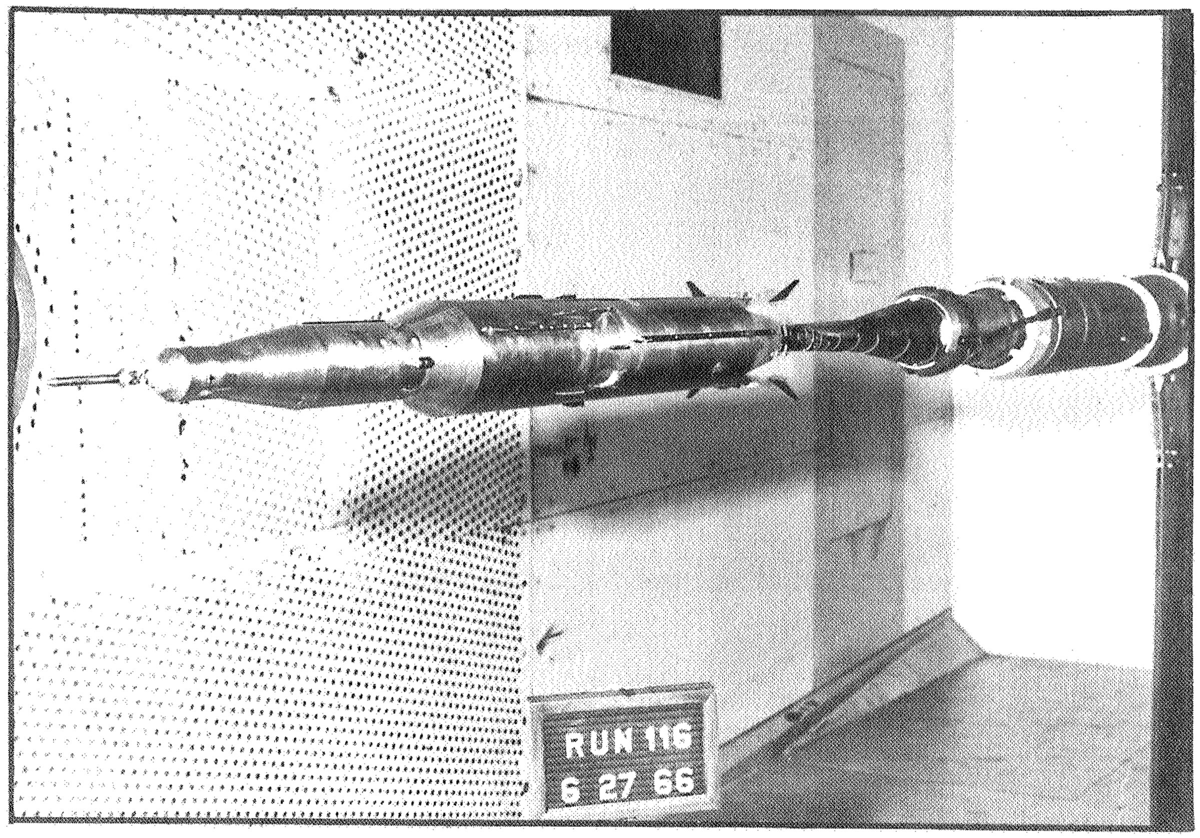

Configuration 1 ; $\phi = 90°$

Figure 3 Photographs from CAL 8-Foot T.W.T. of Typical Model Installations of .9% APOLLO-SATURN V Launch Vehicle

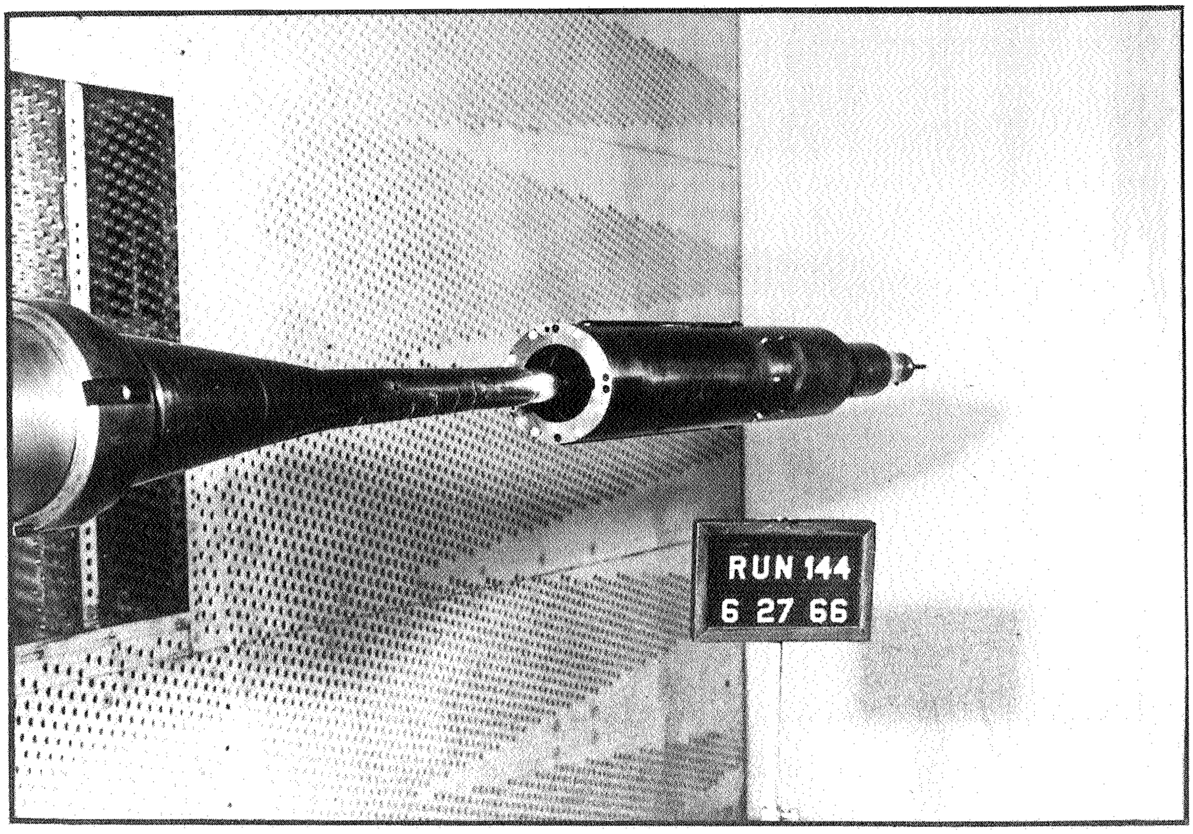

Configuration 4 ; $\phi = 0°$

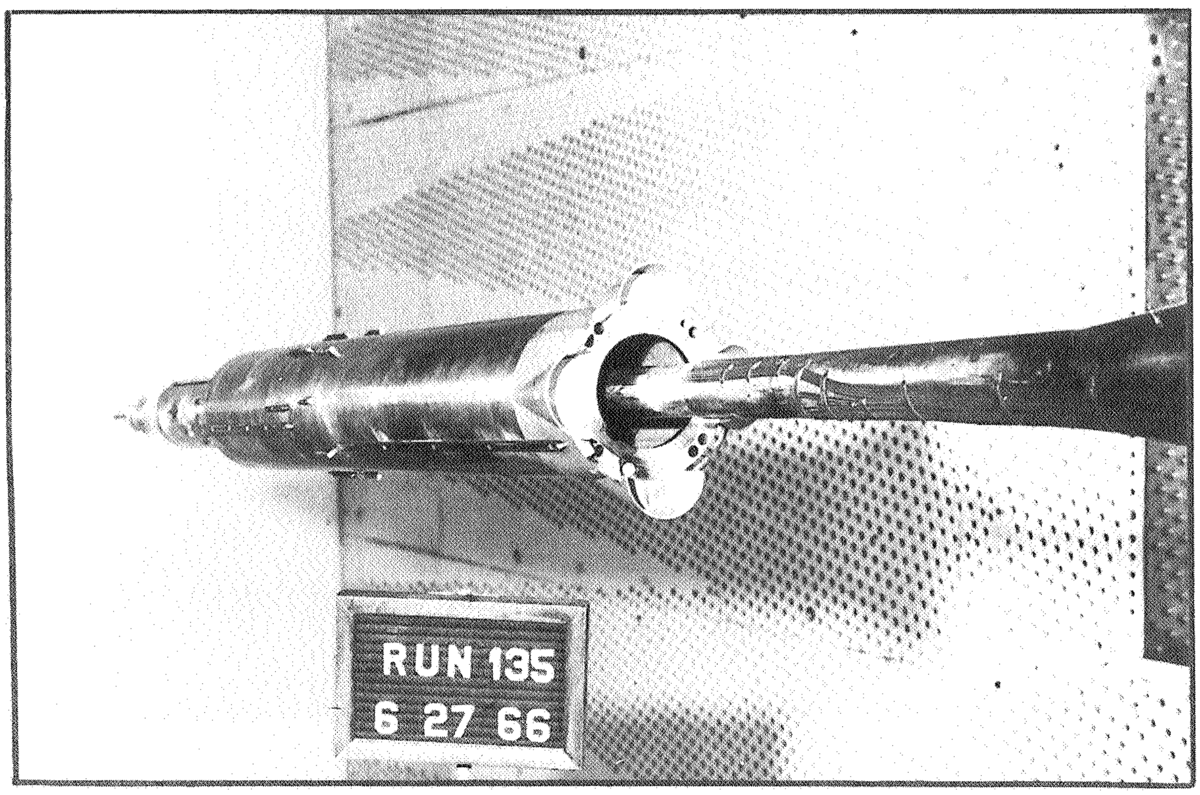

Configuration 3 ; $\phi = 45°$

Figure 3 Concluded

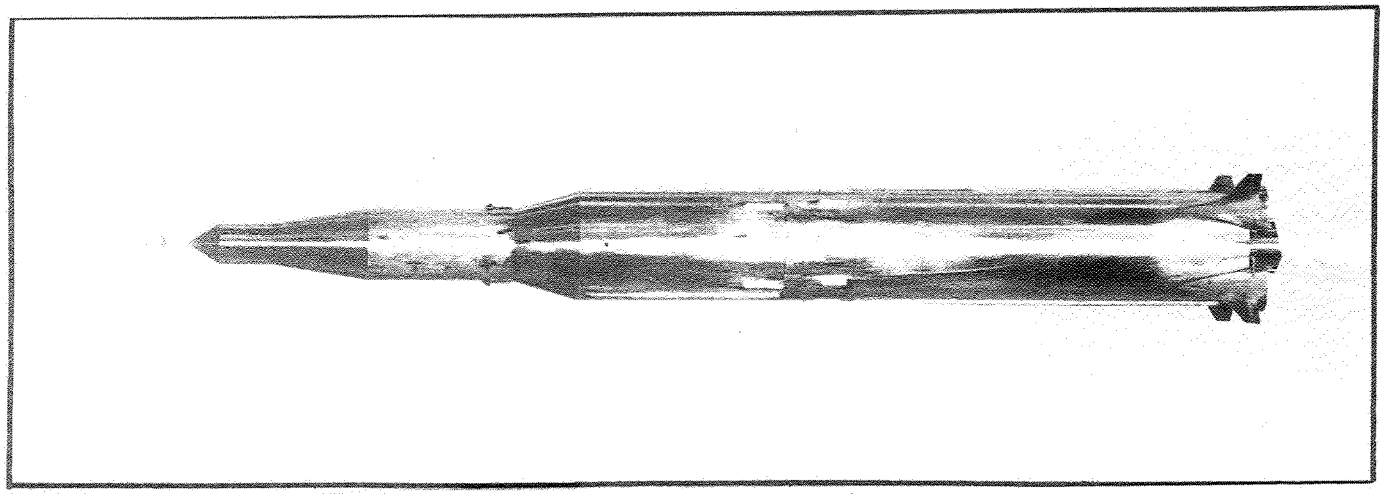

Configuration 1 ; $\phi = 0^\circ$

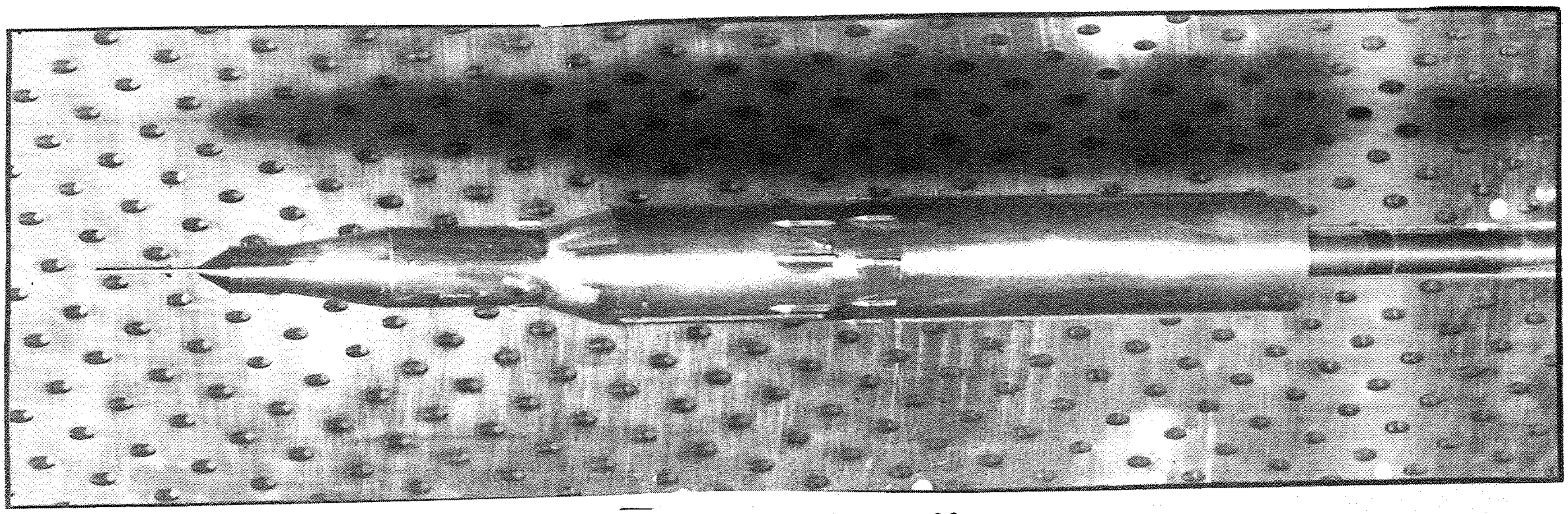

Configuration 4 ; $\phi = 0^\circ$

Figure 4 Photographs from MSFC 14 - Inch T.W.T of Typical Model Installations of .3366% APOLLO-SATURN V Launch Vehicle

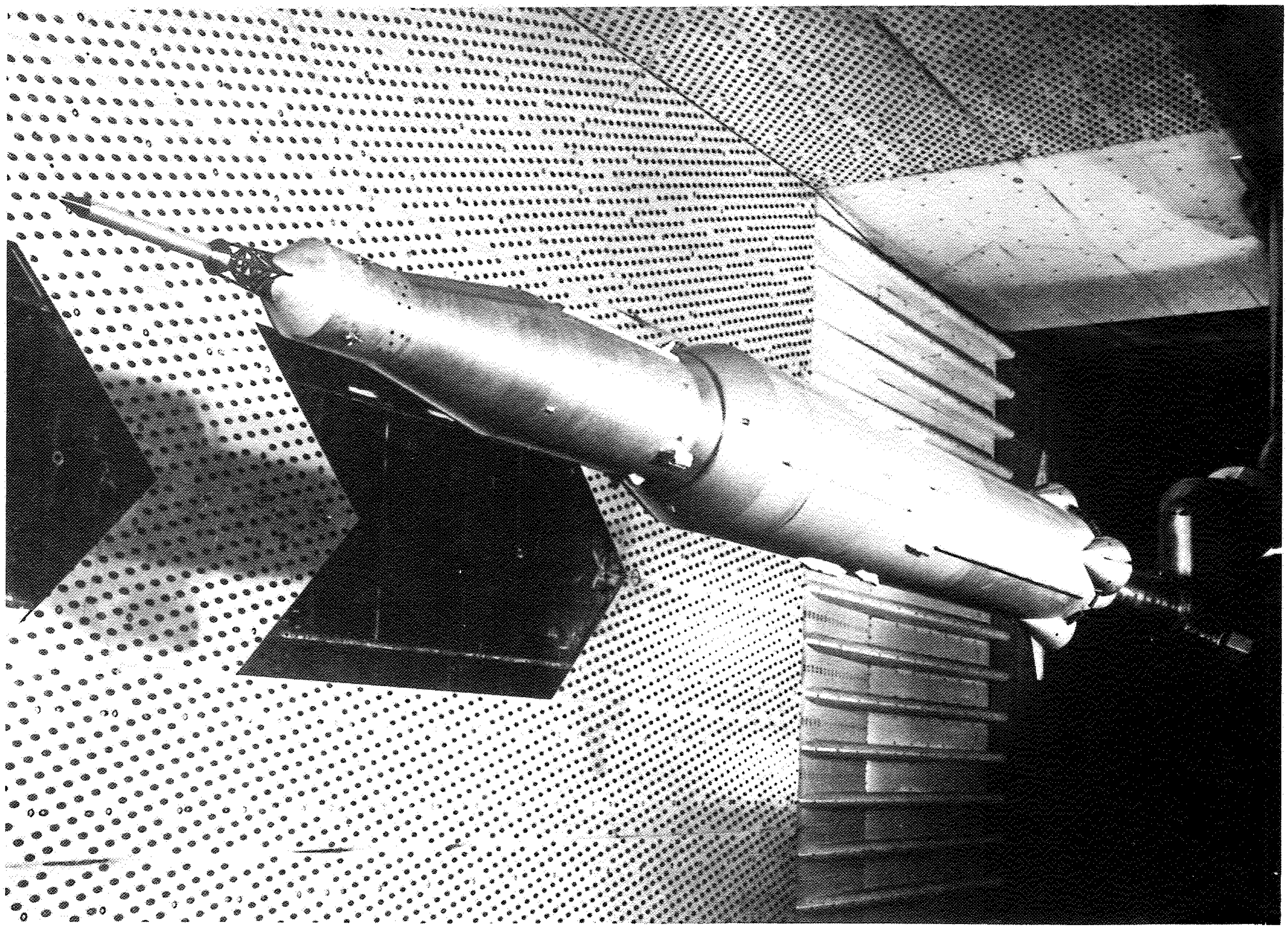

Configuration I; $\phi = 45°$

Figure 5 Photograph from AEDC 16-Foot T.W.T. of Typical Model Installation of 4% APOLLO-SATURN V Launch Vehicle

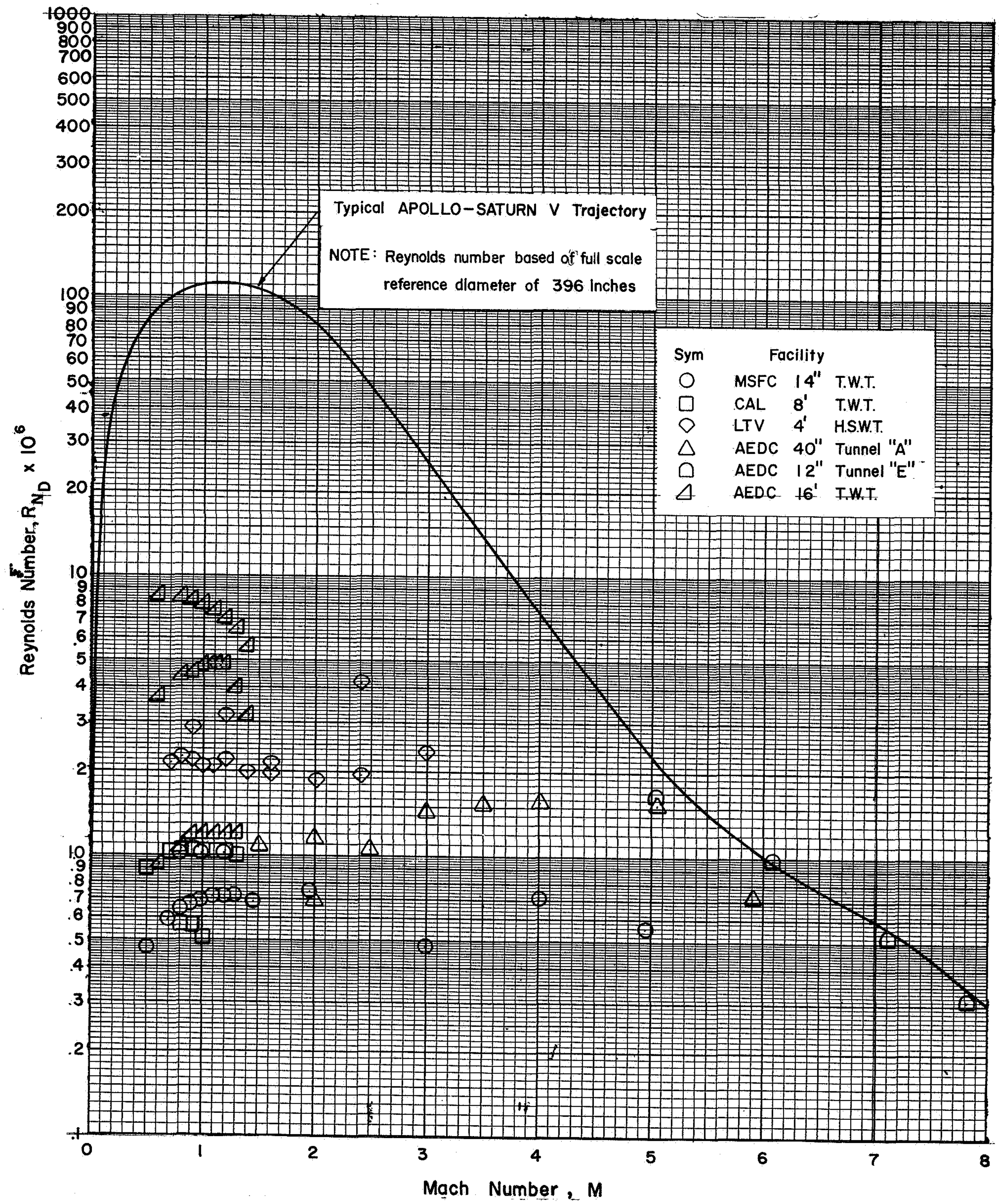

Figure 6 Variation of Reynolds Number with Mach Number for the APOLLO-SATURN V Launch Vehicle - Experimental Test Conditions Compared to Data for Typical Trajectory

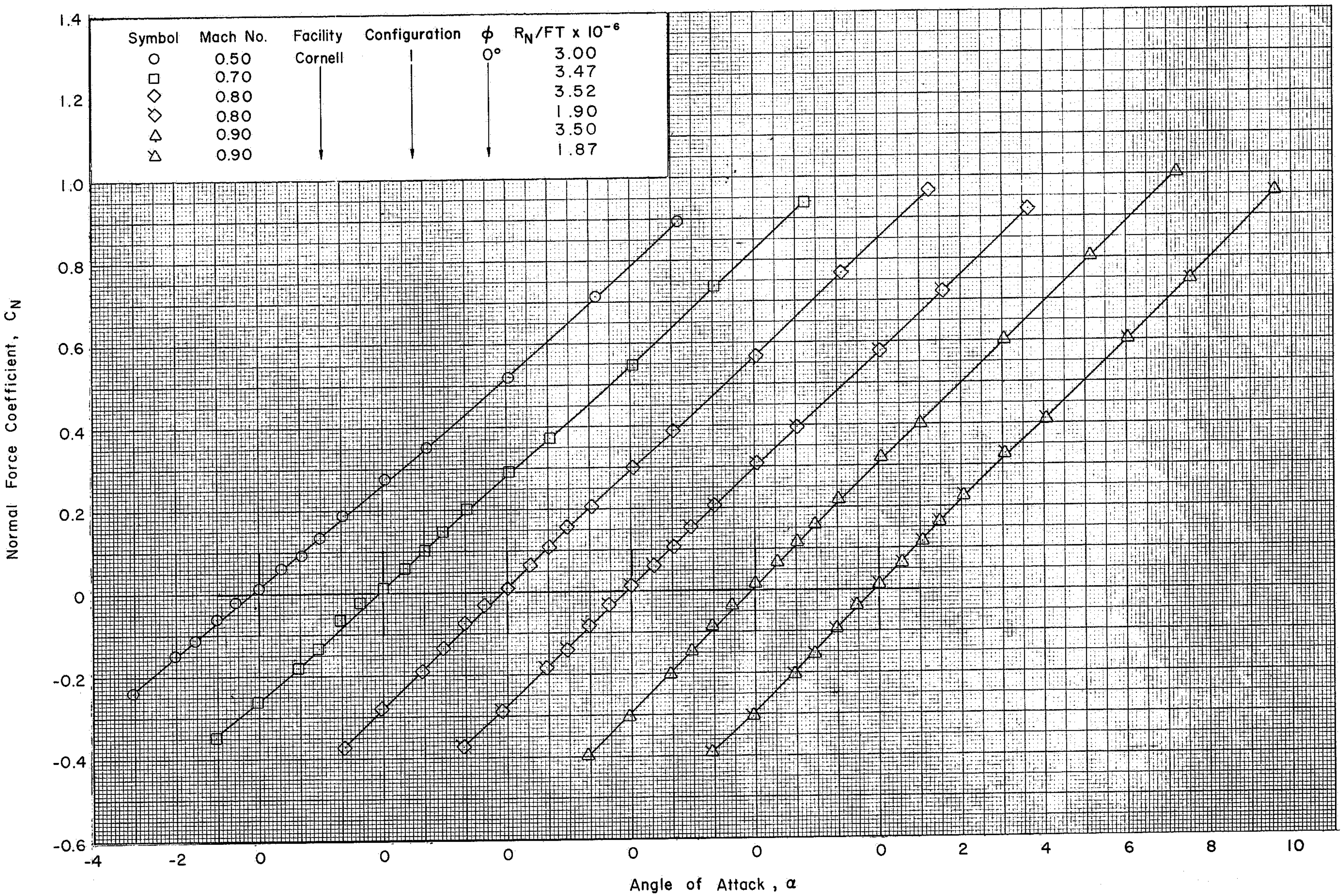

(a) C_N vs. α : ϕ=0° (M=0.50-0.90)

Figure 7 Static Aerodynamic Characteristics of the APOLLO-SATURN V Launch Vehicle in the CAL 8-Foot Transonic Wind Tunnel

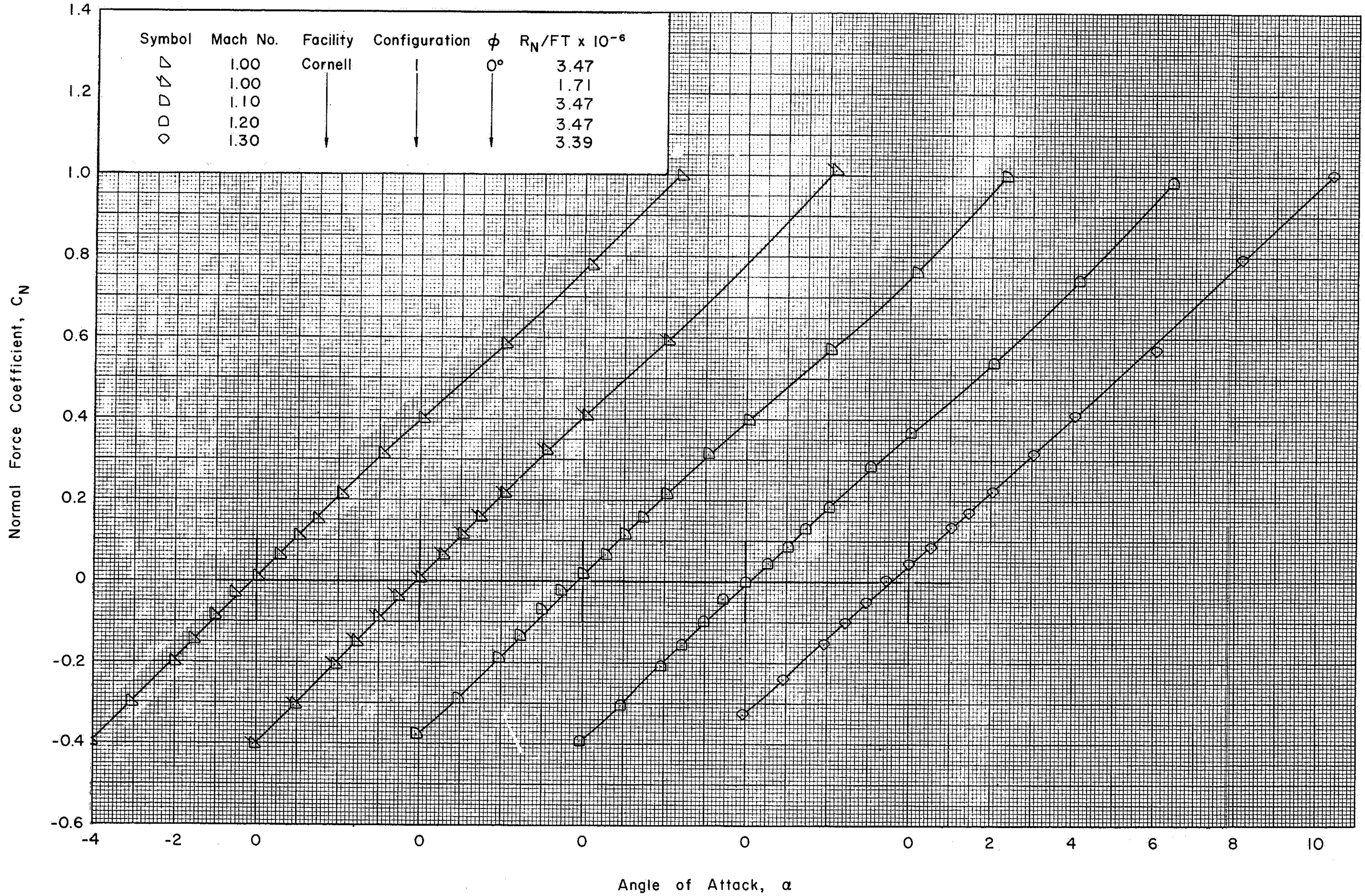

(a) Concluded : $\phi=0°$ (M=1.00–1.30)

Figure 7 Continued

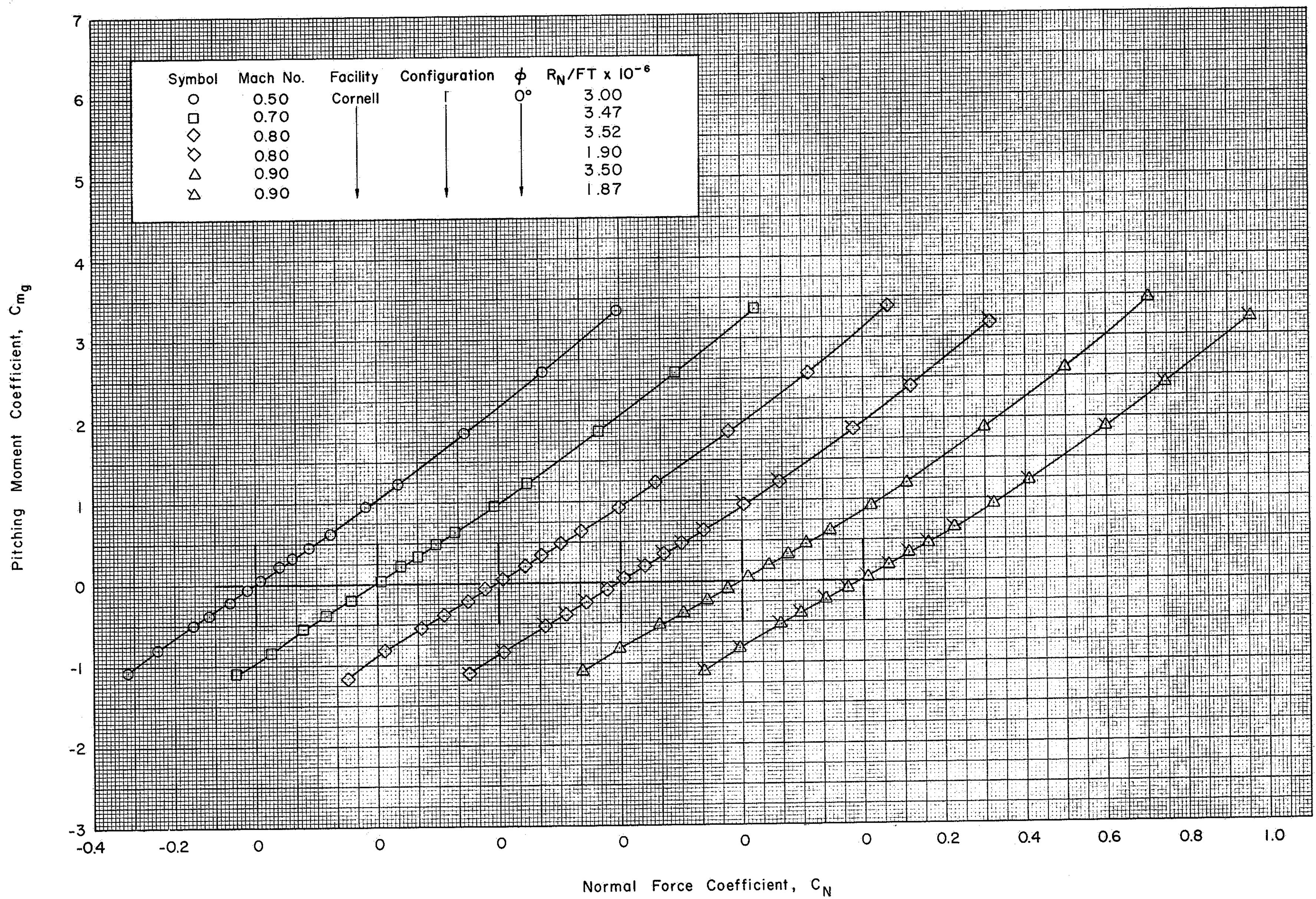

(b) C_{m_g} vs. C_N : ϕ=0° (M=0.50–0.90)

Figure 7 Continued

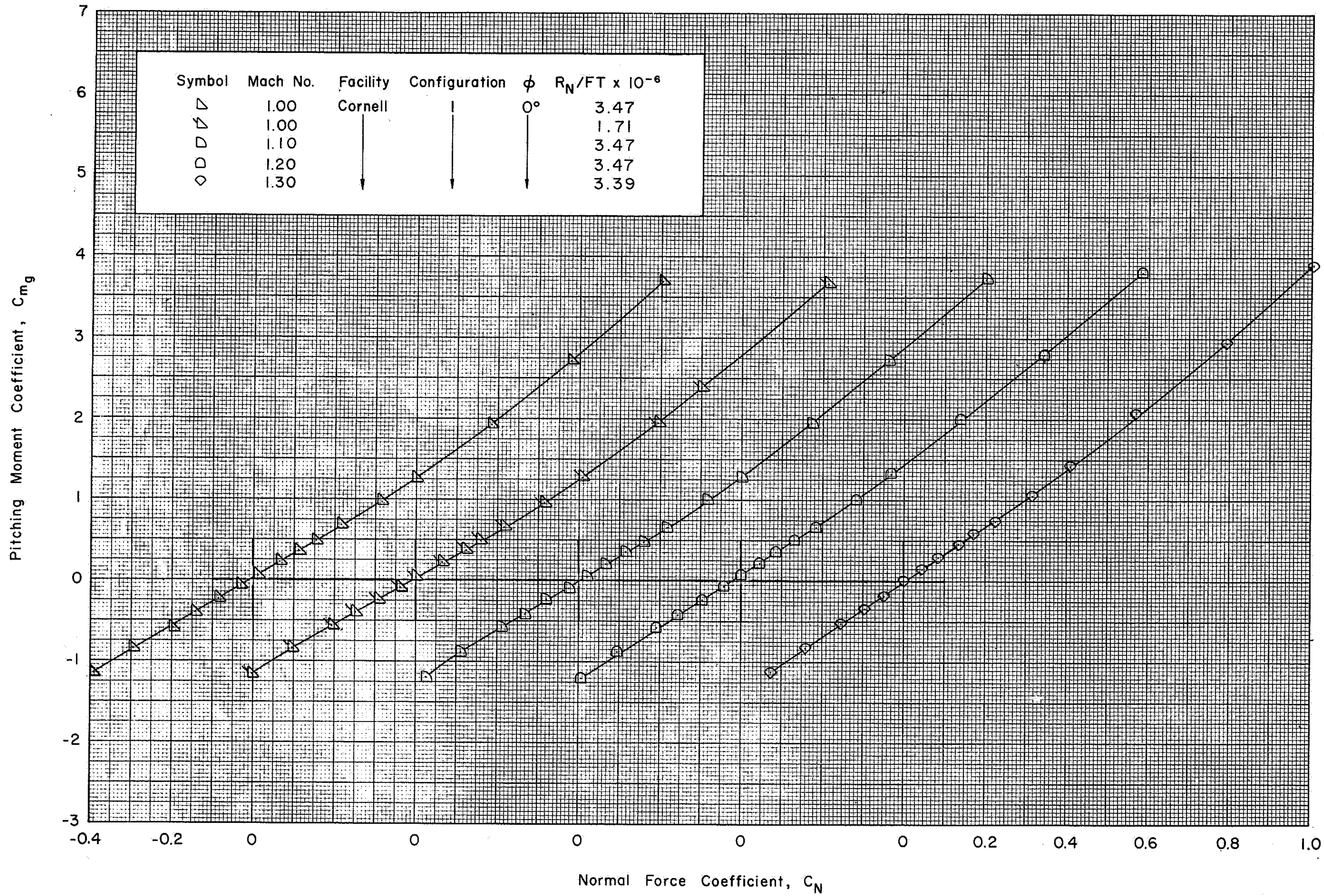

(b) Concluded : ϕ=0° (M=1.00–1.30)

Figure 7 Continued

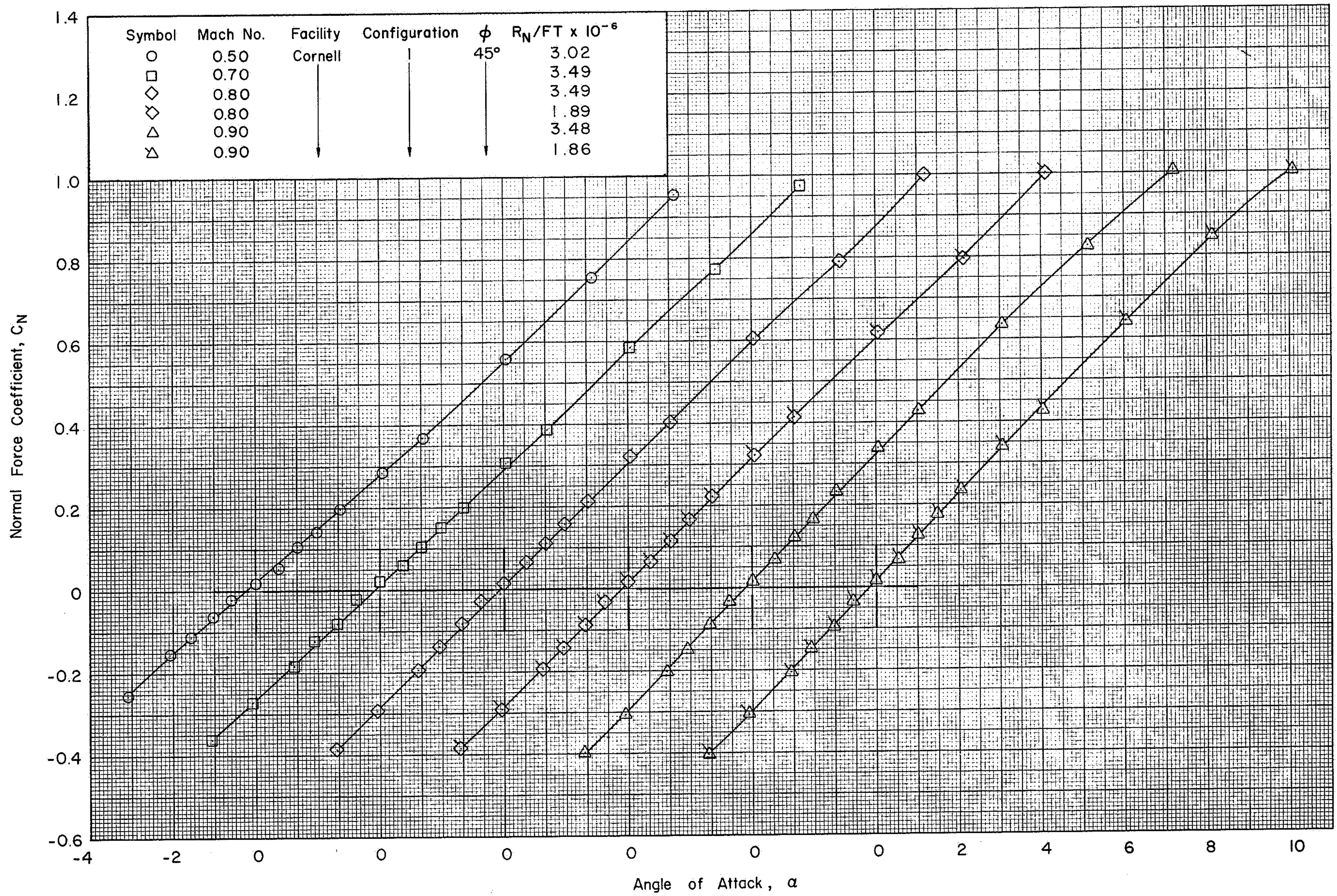

(c) C_N vs. α : $\phi = 45°$ (M=0.50–0.90)

Figure 7 Continued

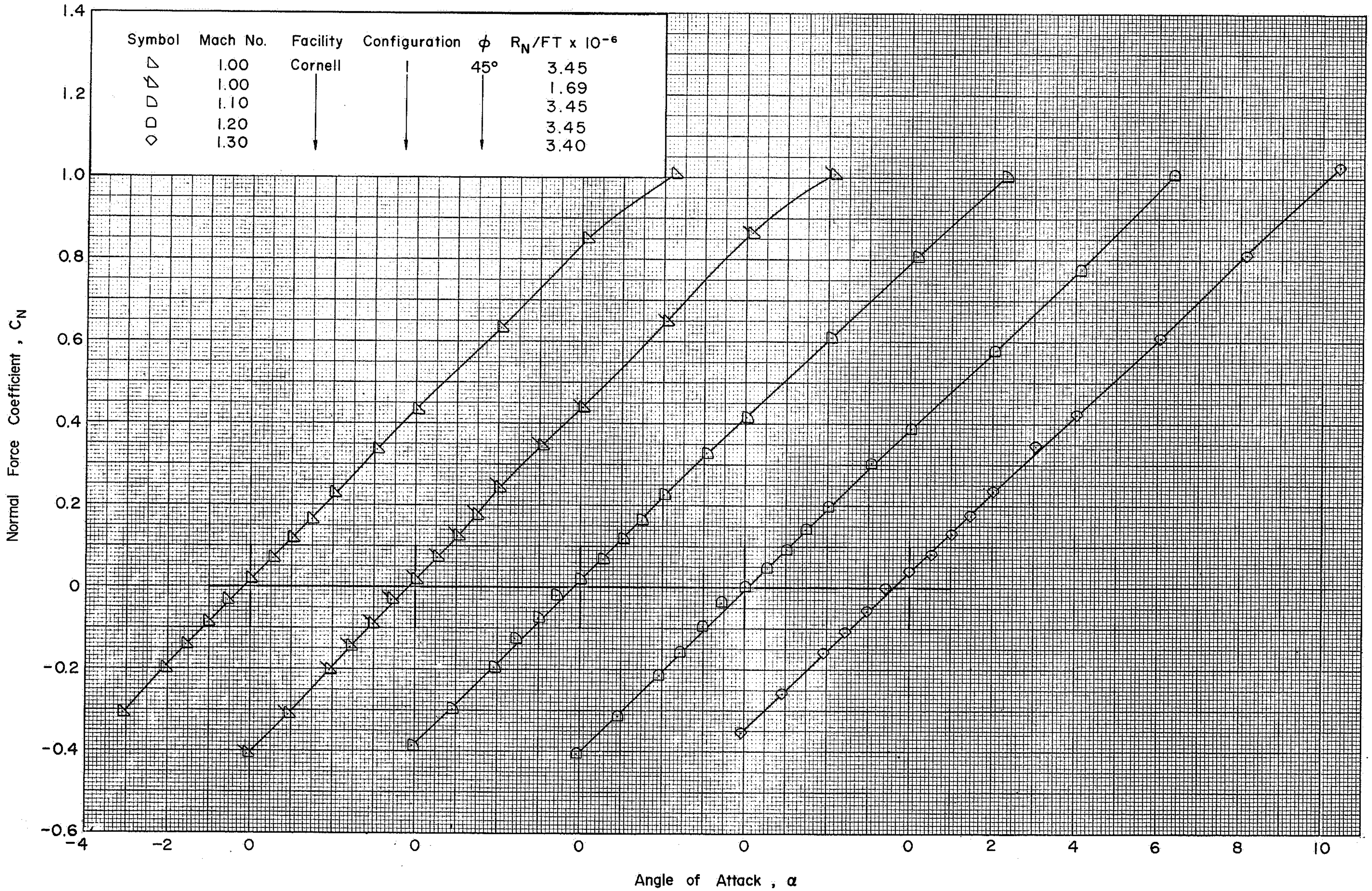

(c) Concluded : $\phi = 45°$ (M=1.00–1.30)

Figure 7 Continued

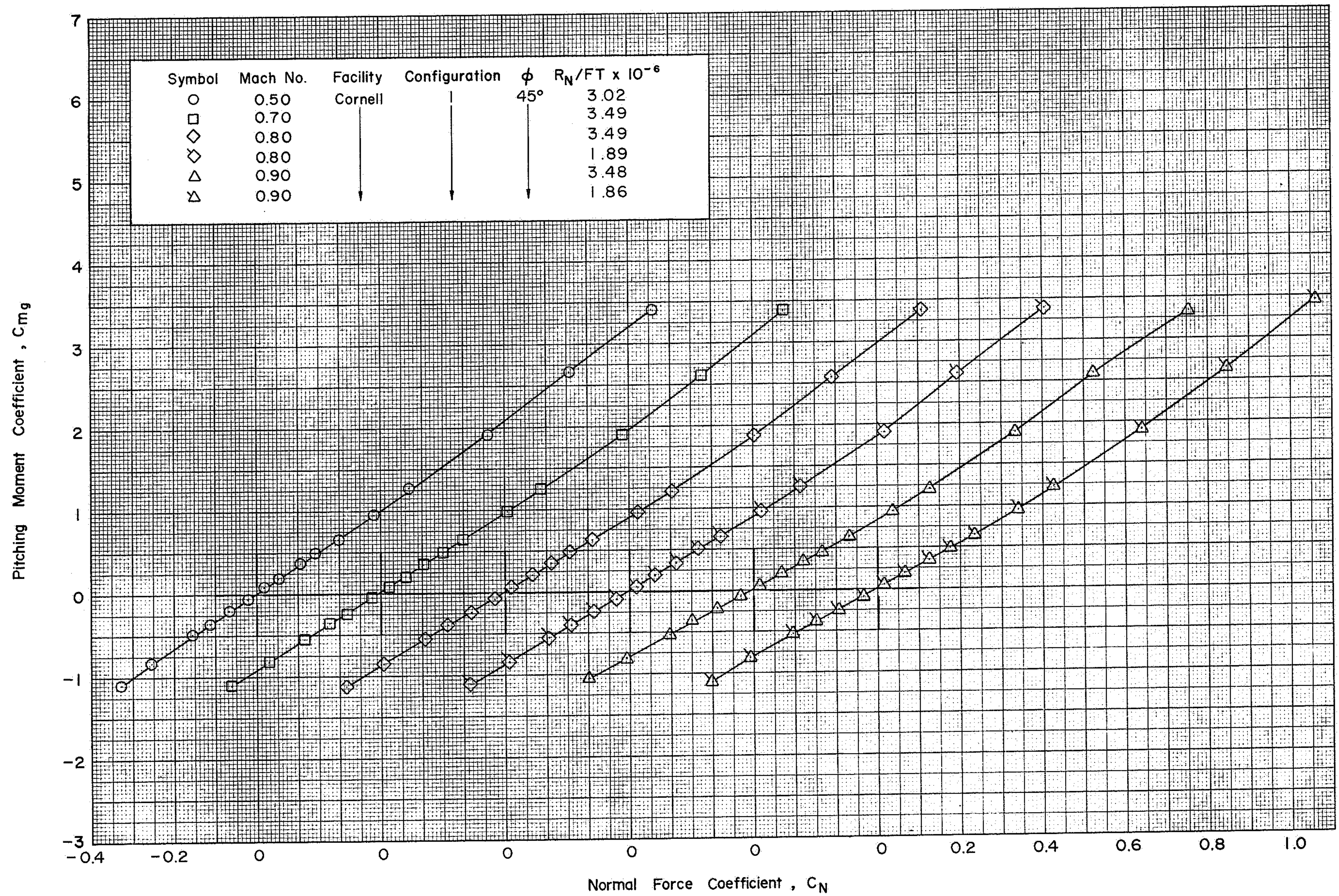

(d) C_{m_g} vs. C_N : ϕ= 45° (M=0.50–0.90)

Figure 7 Continued

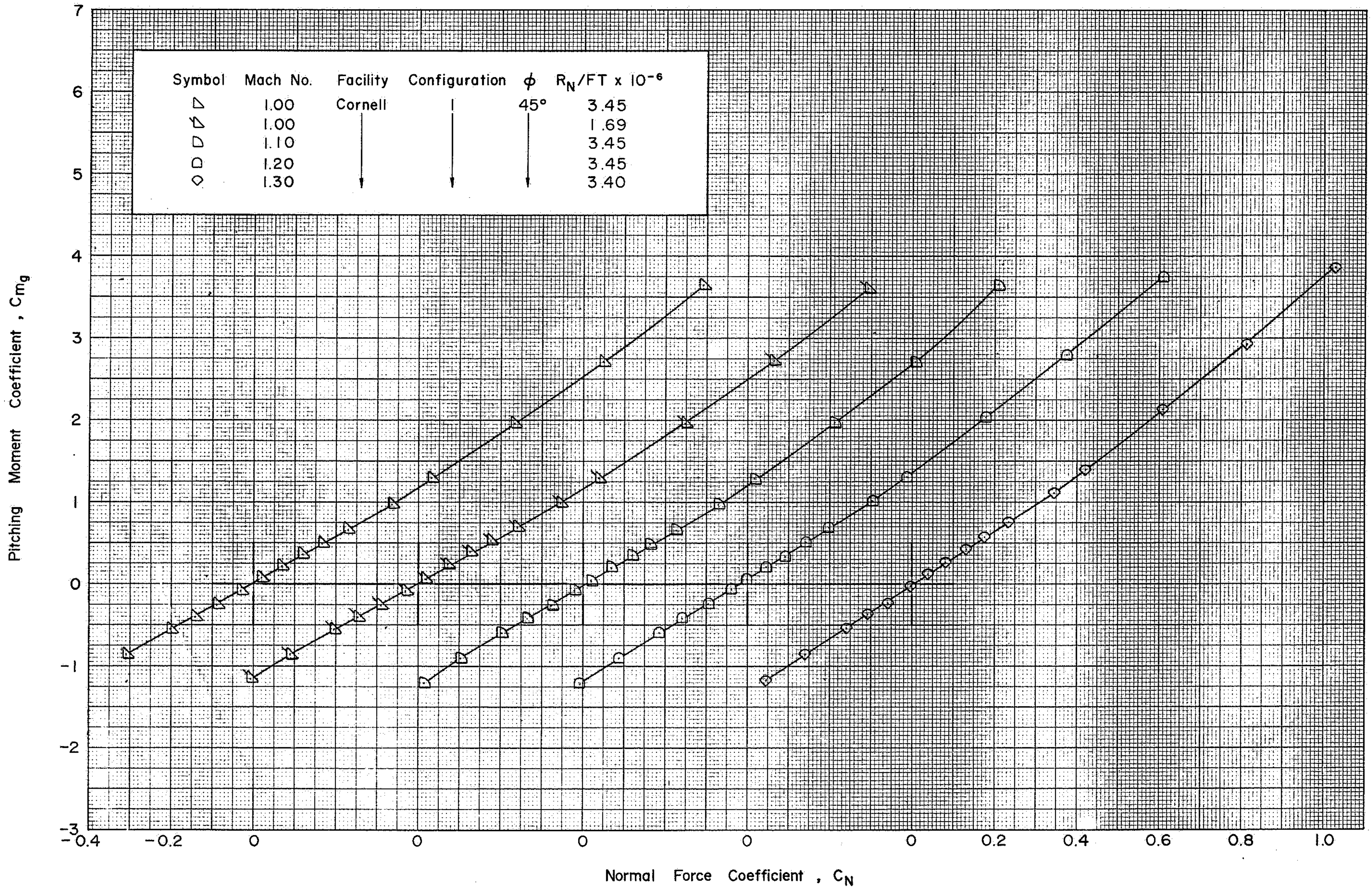

(d) Concluded : ϕ = 45° (M=1.00-1.30)

Figure 7 Continued

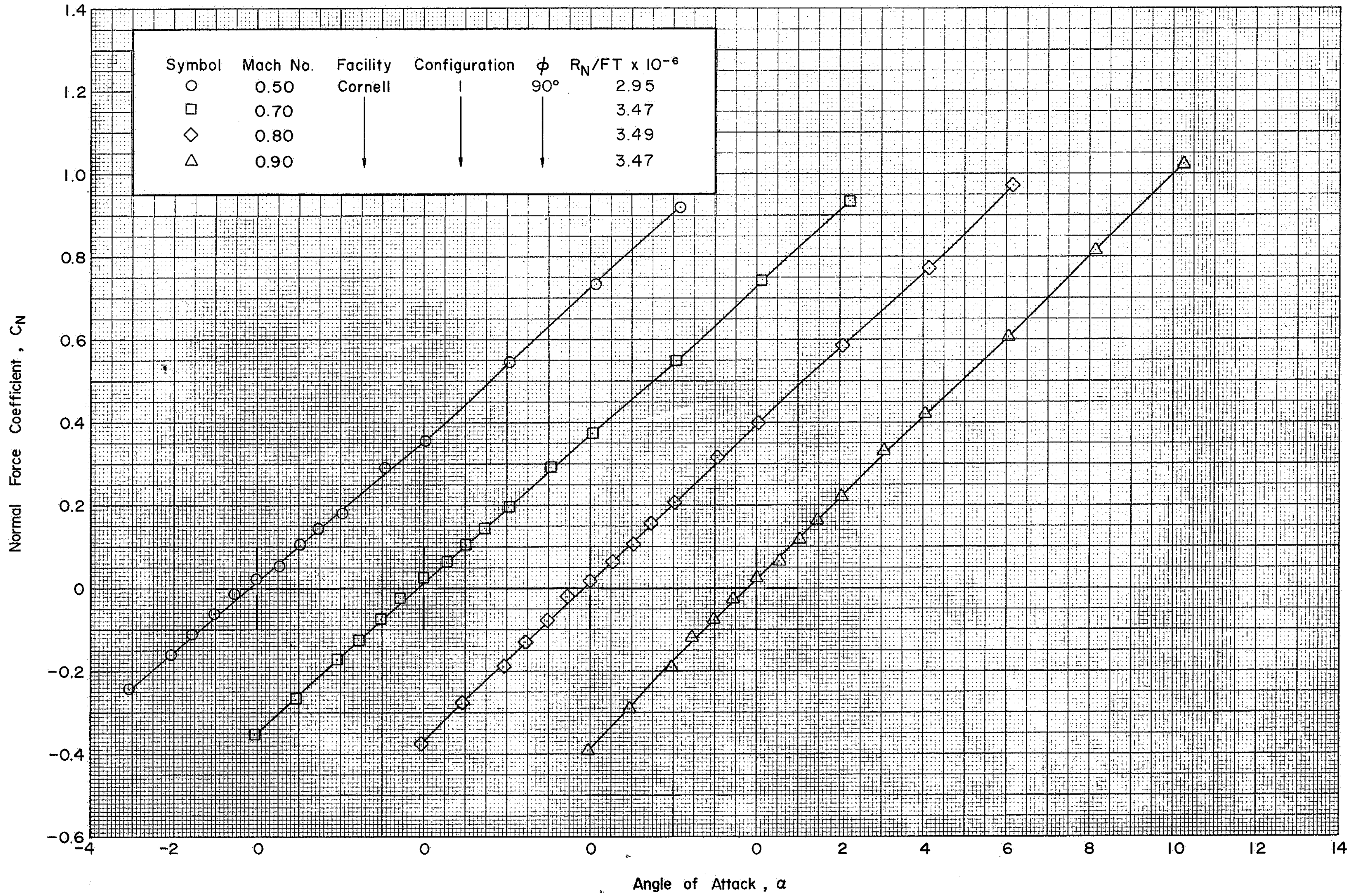

(e) C_N vs. α : ϕ=90° (M=0.50–0.90)

Figure 7 Continued

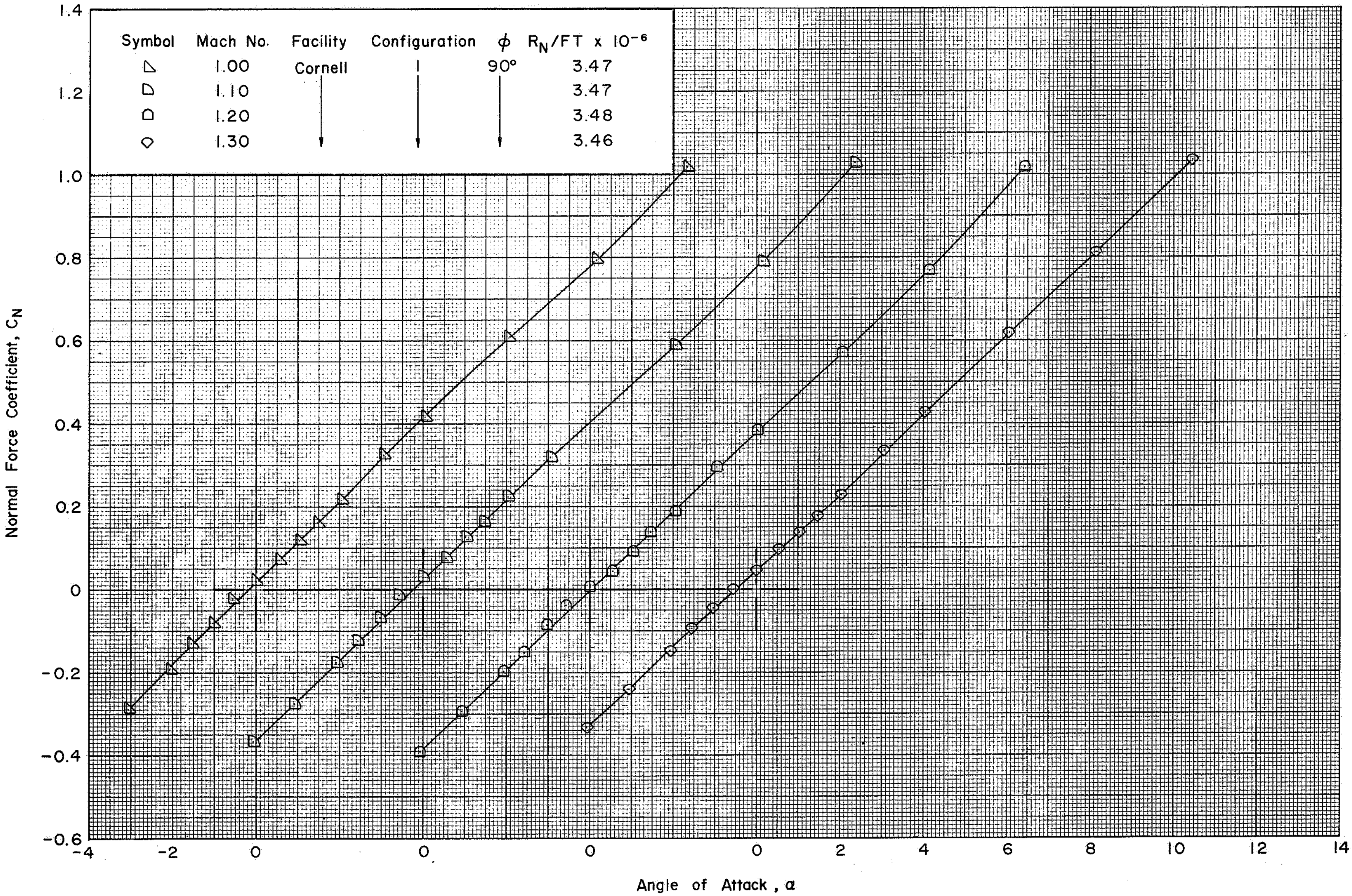

(e) Concluded : ϕ= 90° (M=1.00–1.30)

Figure 7 Continued

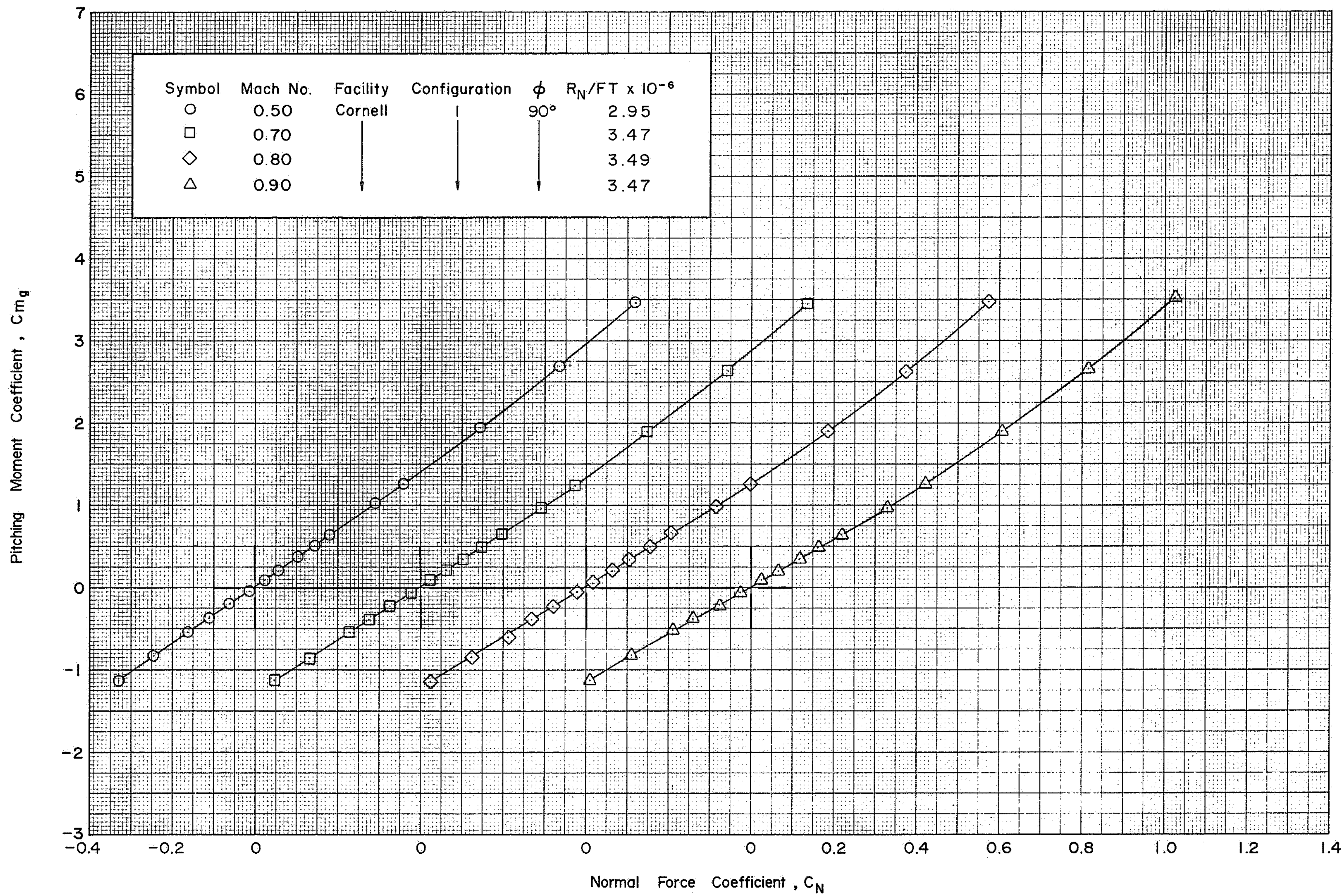

(f) C_{m_g} vs. C_N : ϕ=90° (M=0.50-0.90)

Figure 7 Continued

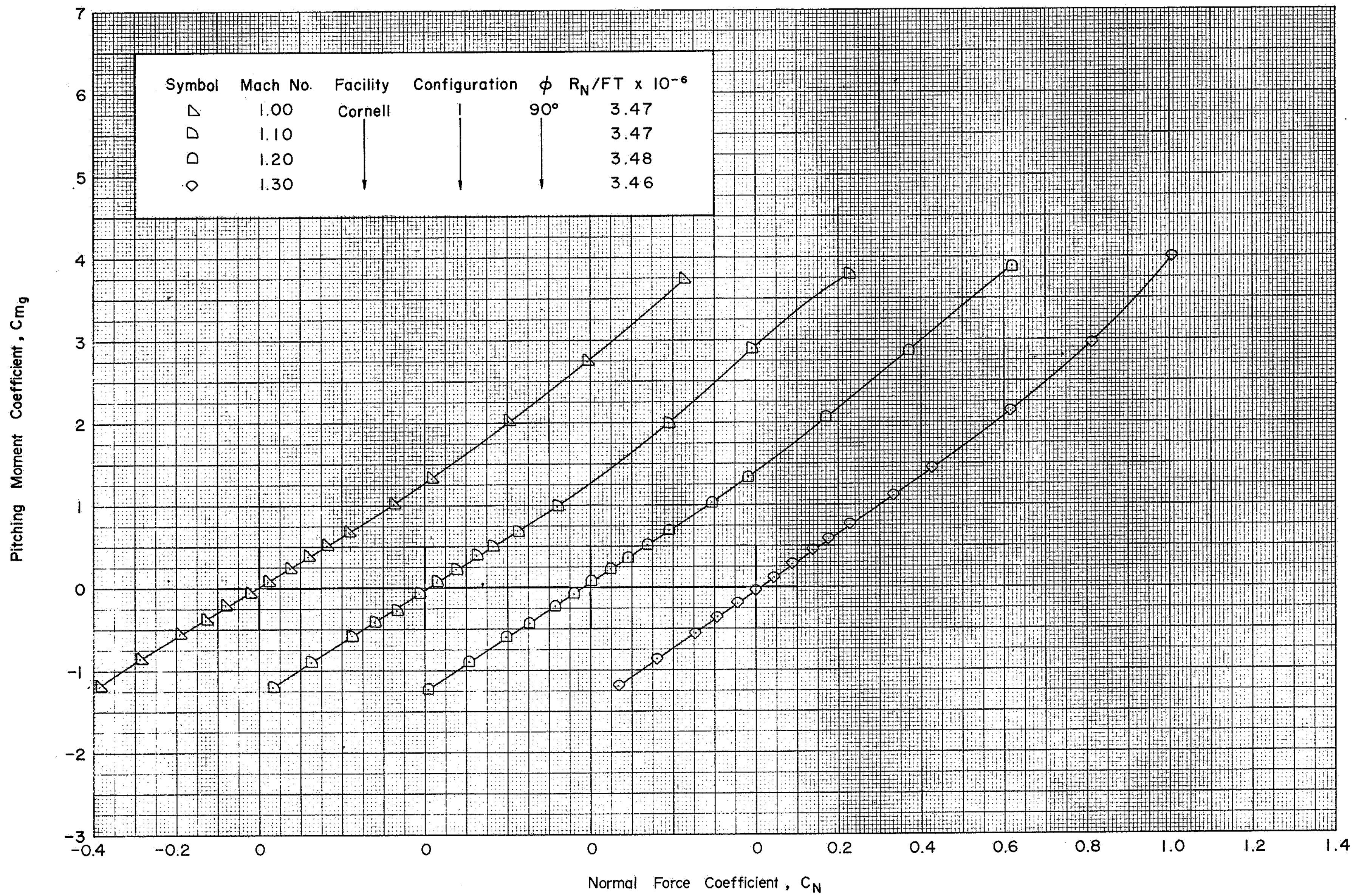

(f) Concluded : ϕ = 90° (M=1.00 – 1.30)

Figure 7 Concluded

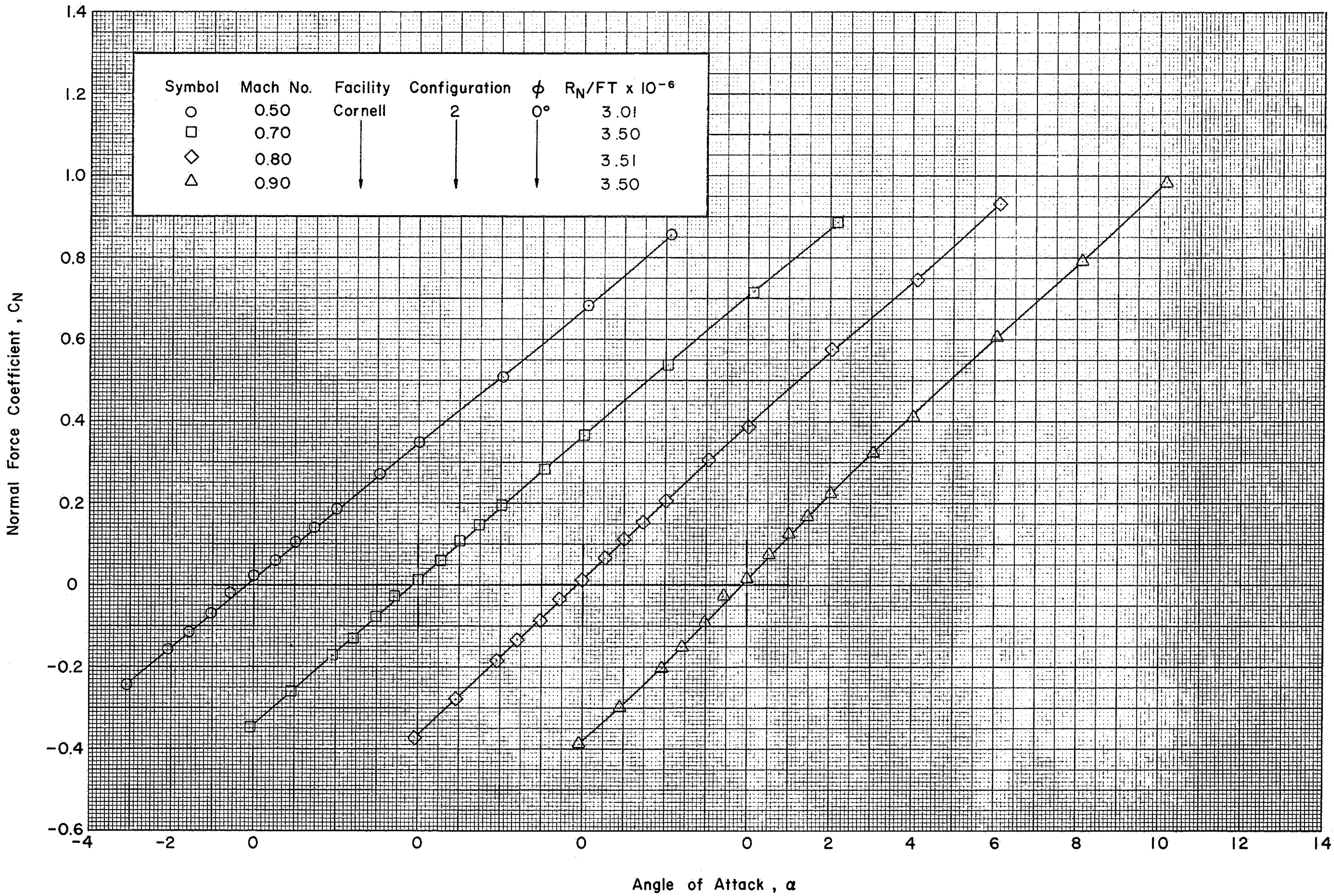

(a) C_N vs. α : ϕ=0° (M=0.50-0.90)

Figure 8 Static Aerodynamic Characteristics of the APOLLO-SATURN V Launch Vehicle without Protuberances in the CAL 8-Foot Transonic Wind Tunnel

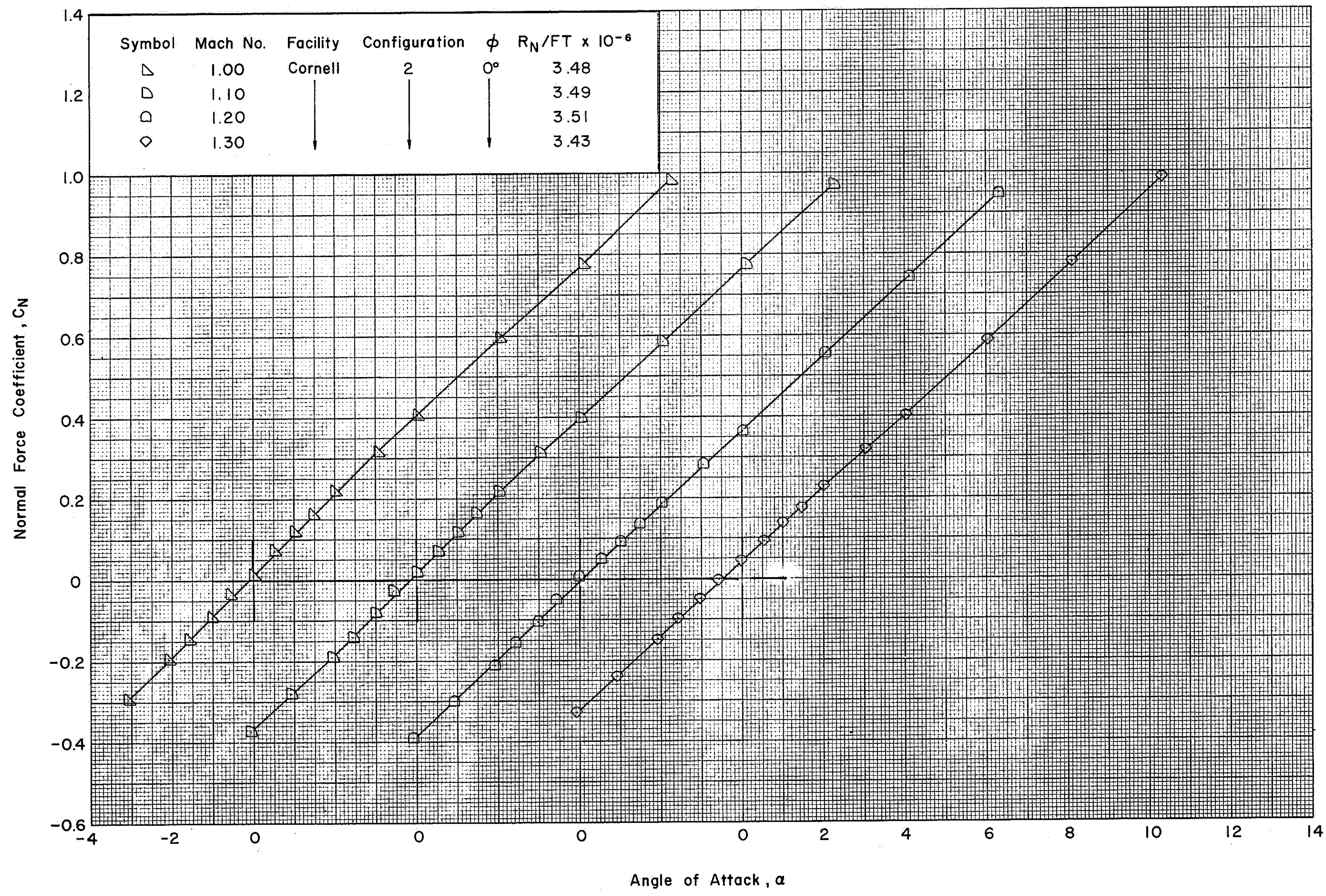

(a) Concluded : ϕ = 0° (M=1.00-1.30)

Figure 8 Continued

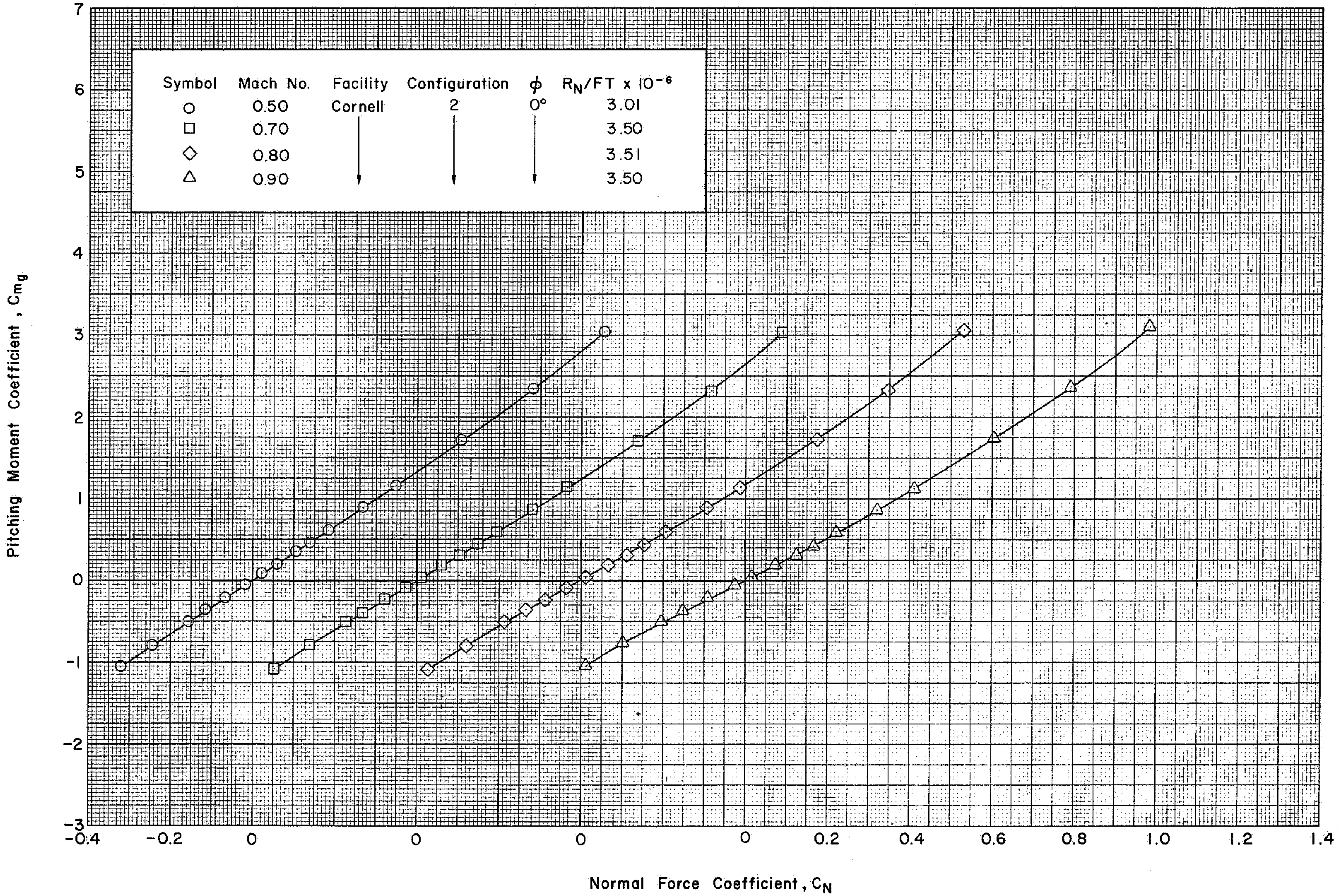

(b) C_{m_g} vs. C_N : ϕ=0° (M=0.50-0.90)

Figure 8 Continued

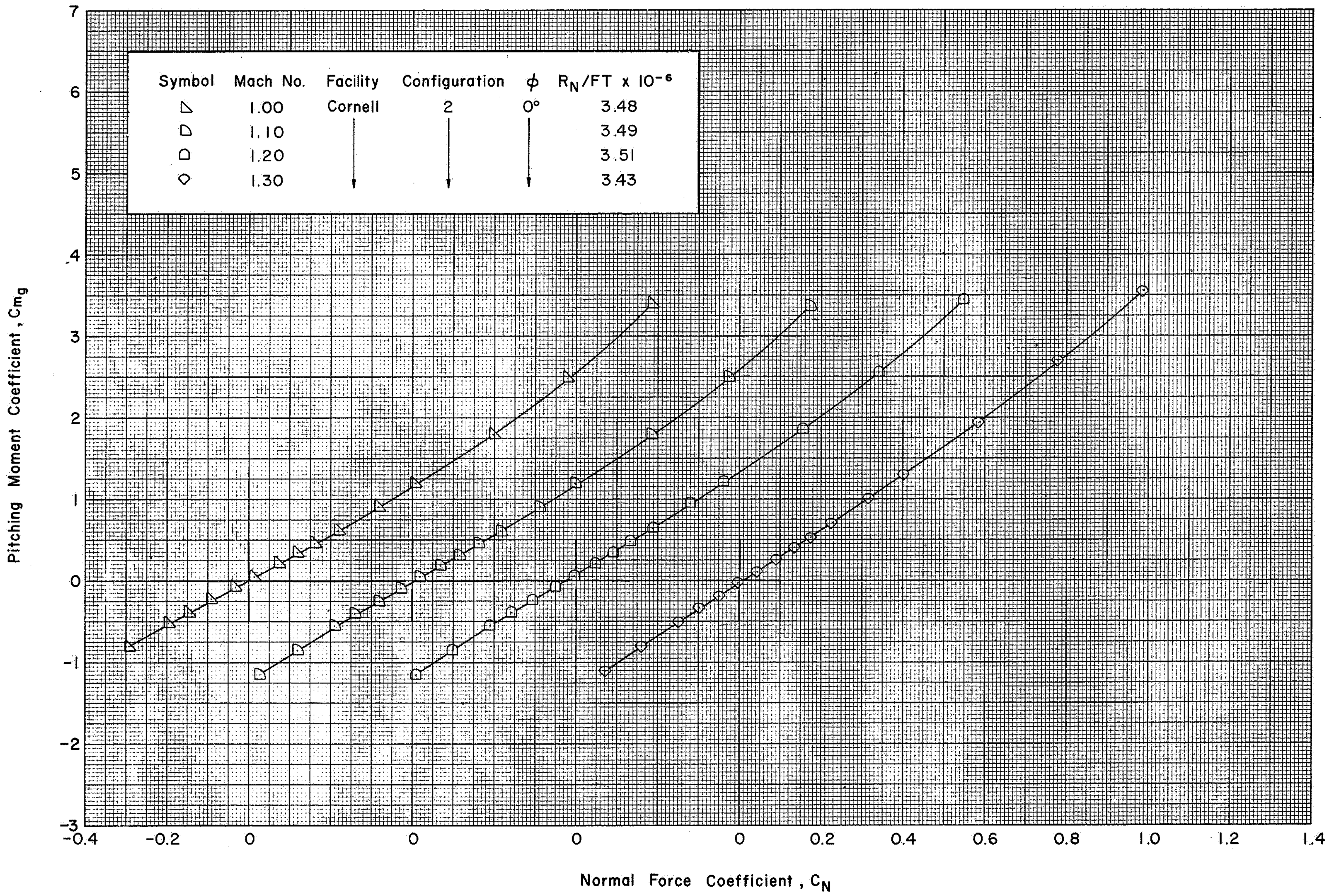

(b) Concluded : ϕ=0° (M=1.00–1.30)

Figure 8 Continued

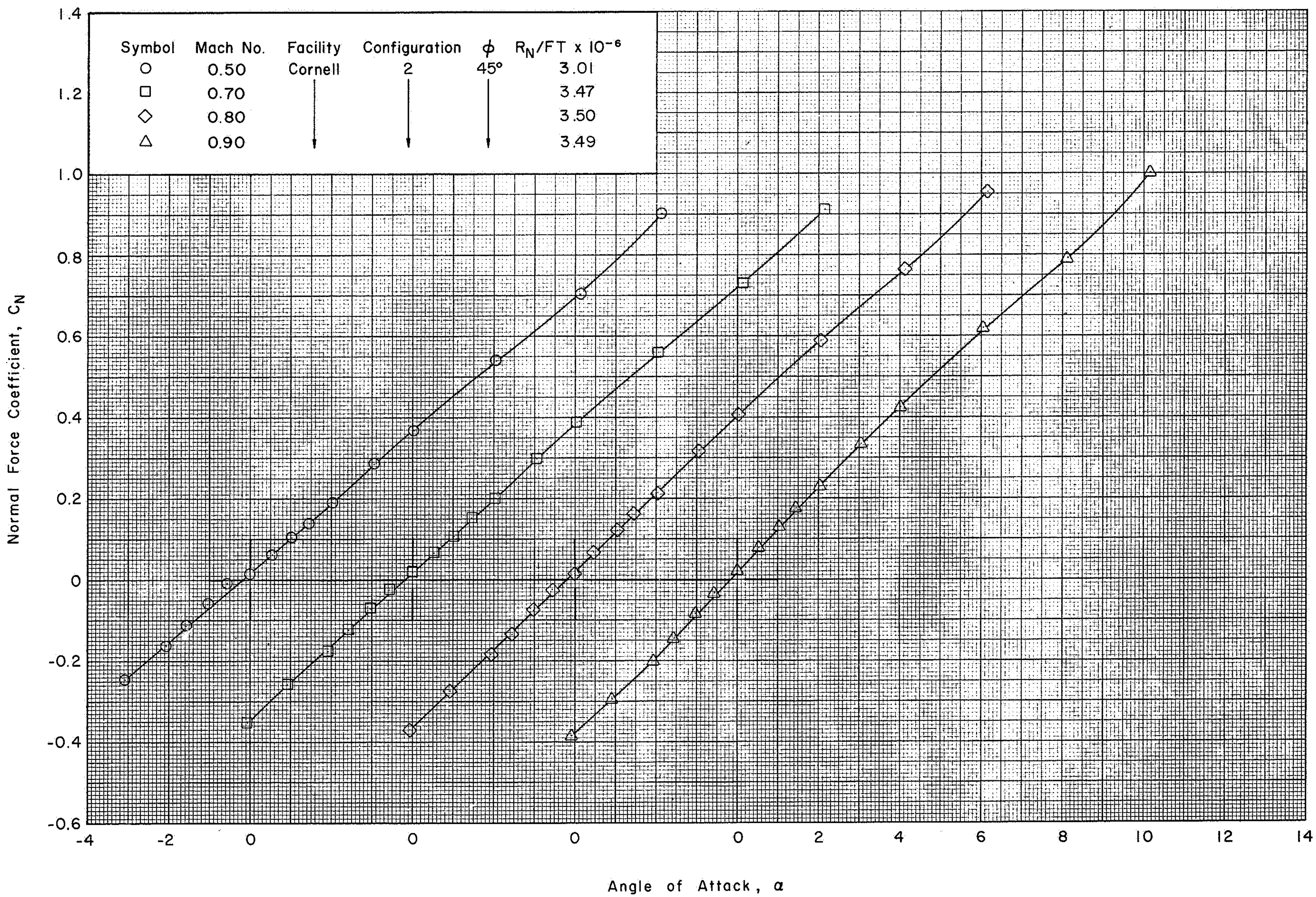

(c) C_N vs. α : ϕ=45° (M=0.50–0.90)

Figure 8 Continued

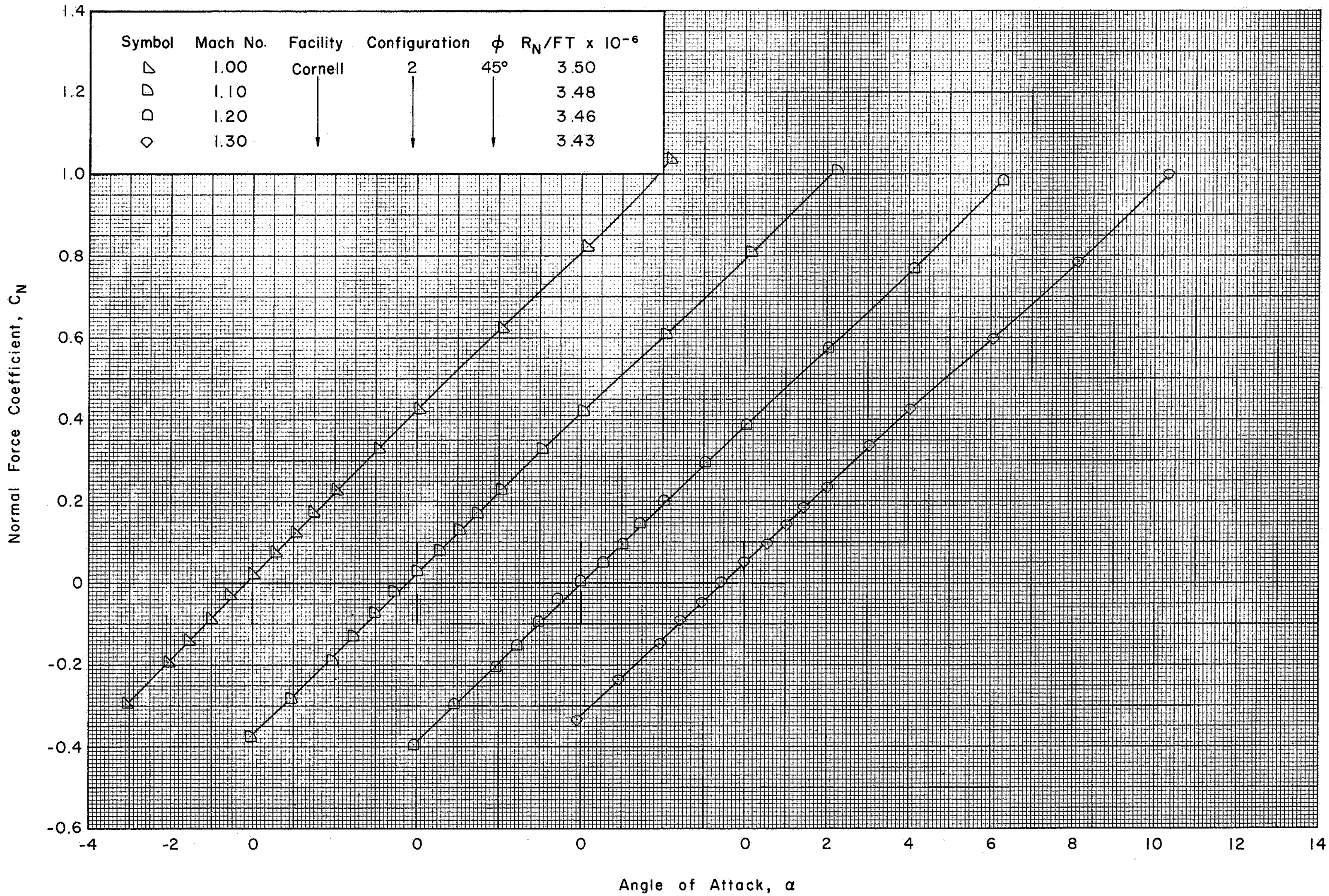

(c) Concluded : ϕ=45° (M=1.00-1.30)

Figure 8 Continued

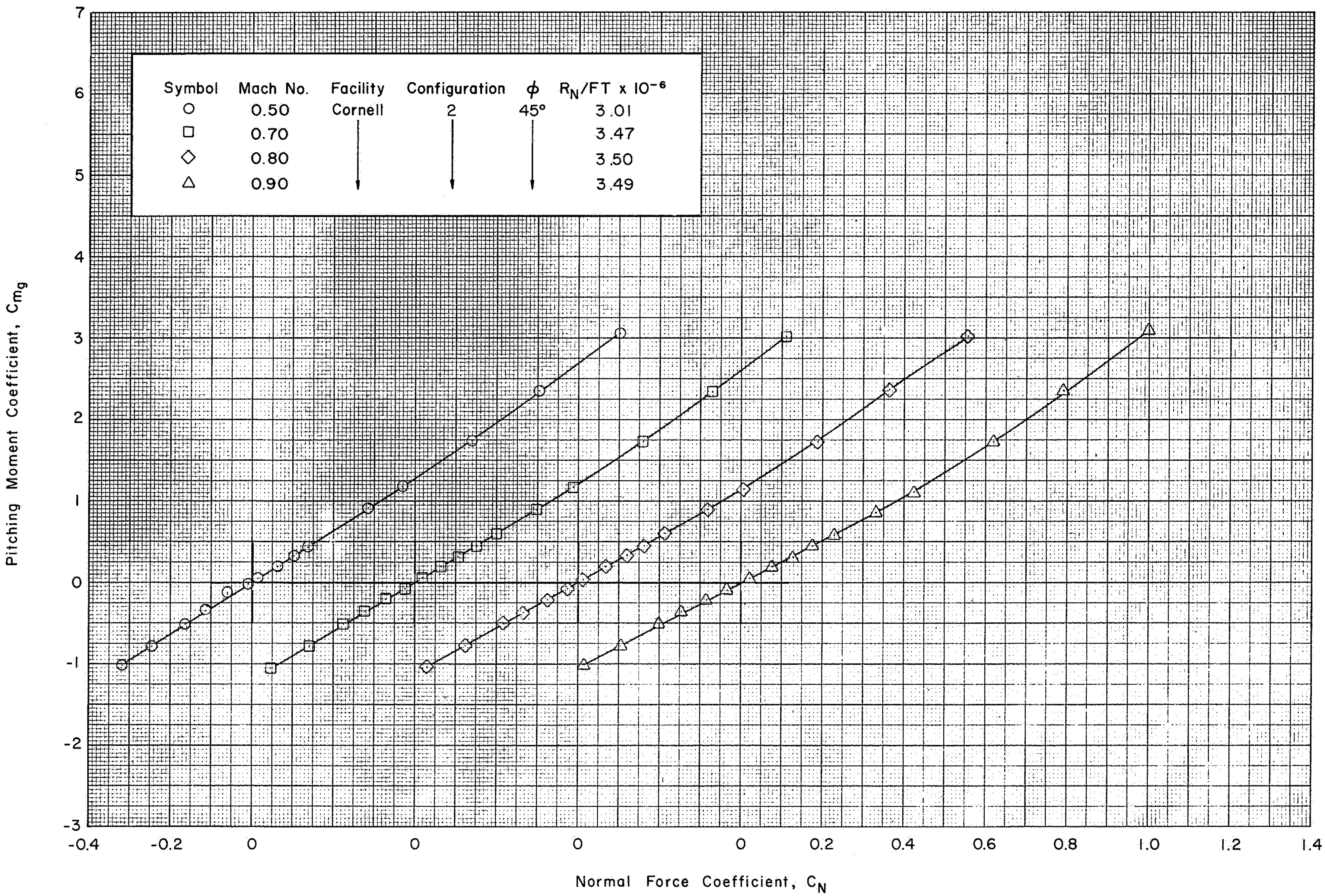

(d) C_{m_g} vs. C_N : ϕ=45° (M=0.50–0.90)

Figure 8 Continued

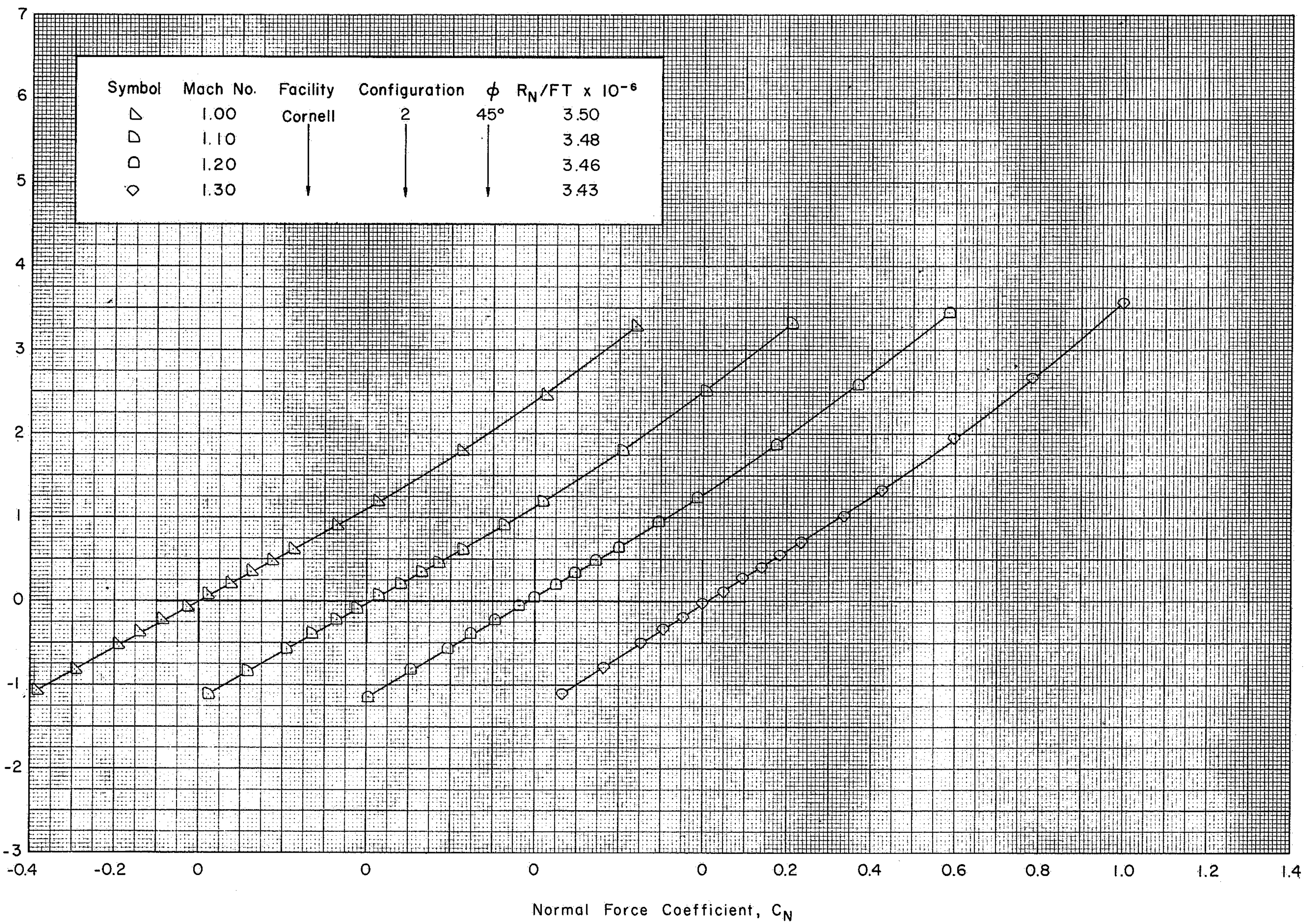

(d) Concluded : ϕ=45° (M=1.00–1.30)

Figure 8 Concluded

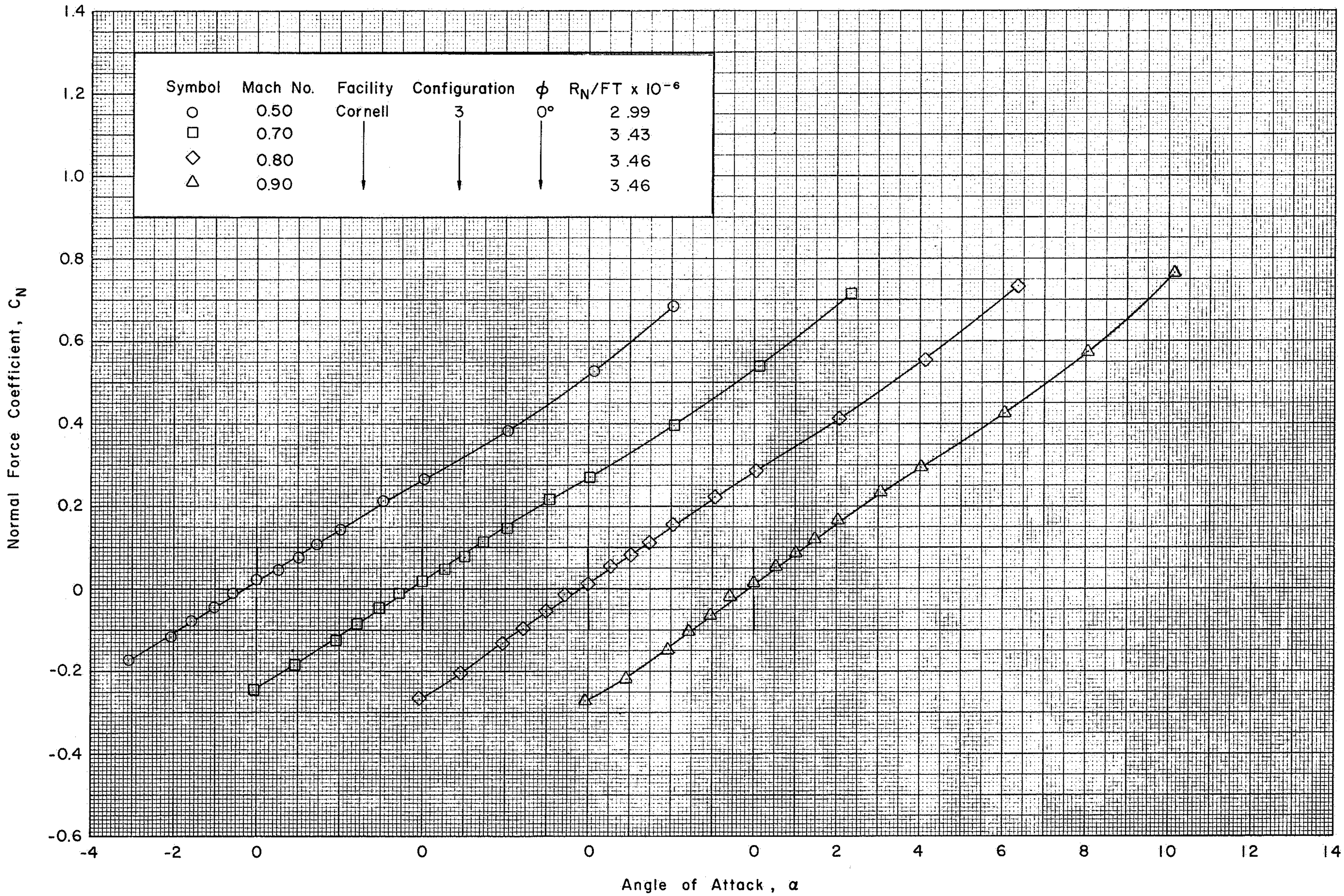

(a) C_N vs. α : ϕ=0° (M=0.50–0.90)

Figure 9 Static Aerodynamic Characteristics of the APOLLO-SATURN V Launch Vehicle without Fins in the CAL 8-Foot Transonic Wind Tunnel

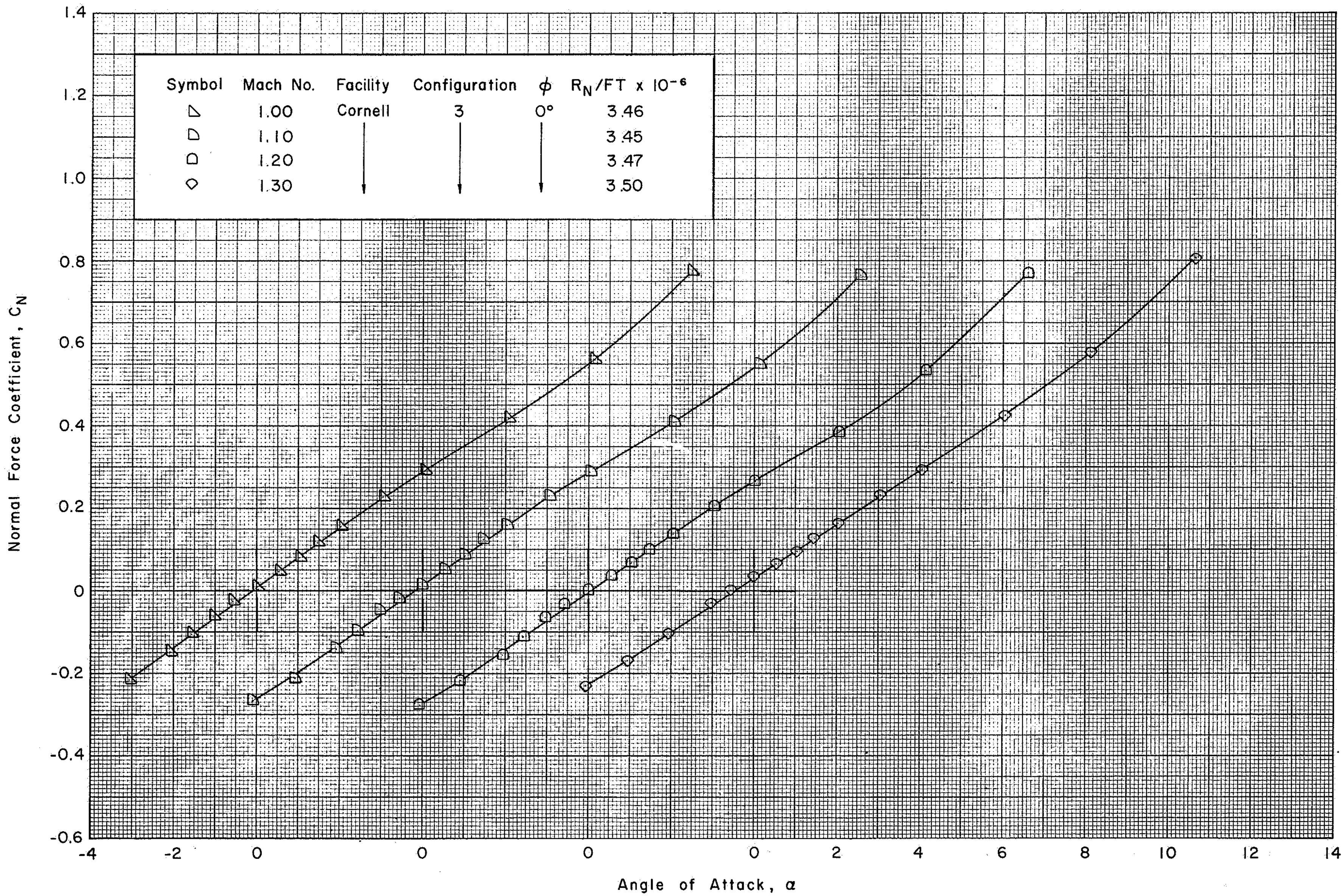

(a) Concluded : ϕ=0° (M=1.00–1.30)

Figure 9 Continued

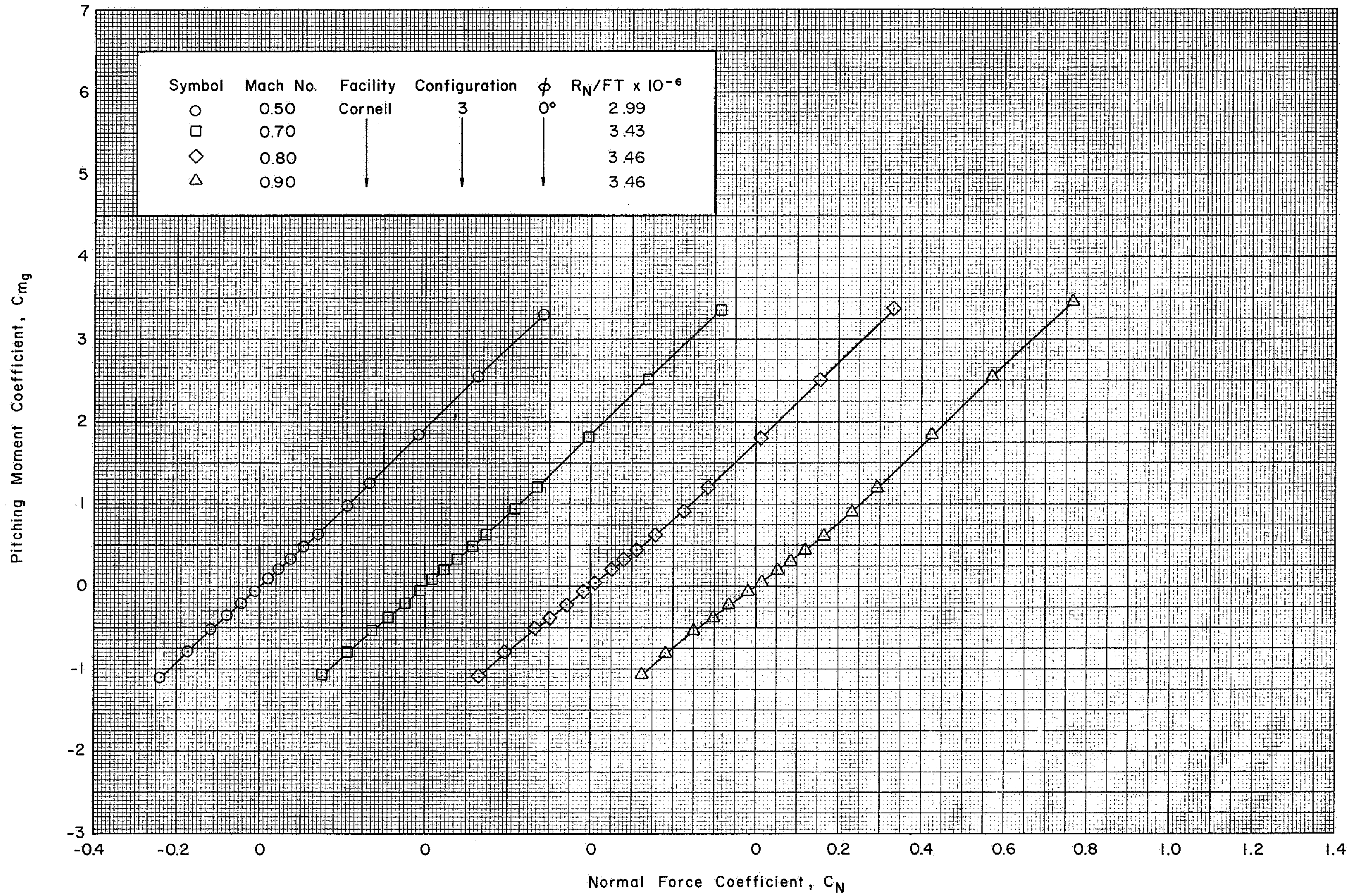

(b) C_{m_g} vs. C_N : ϕ=0° (M=0.50–0.90)

Figure 9 Continued

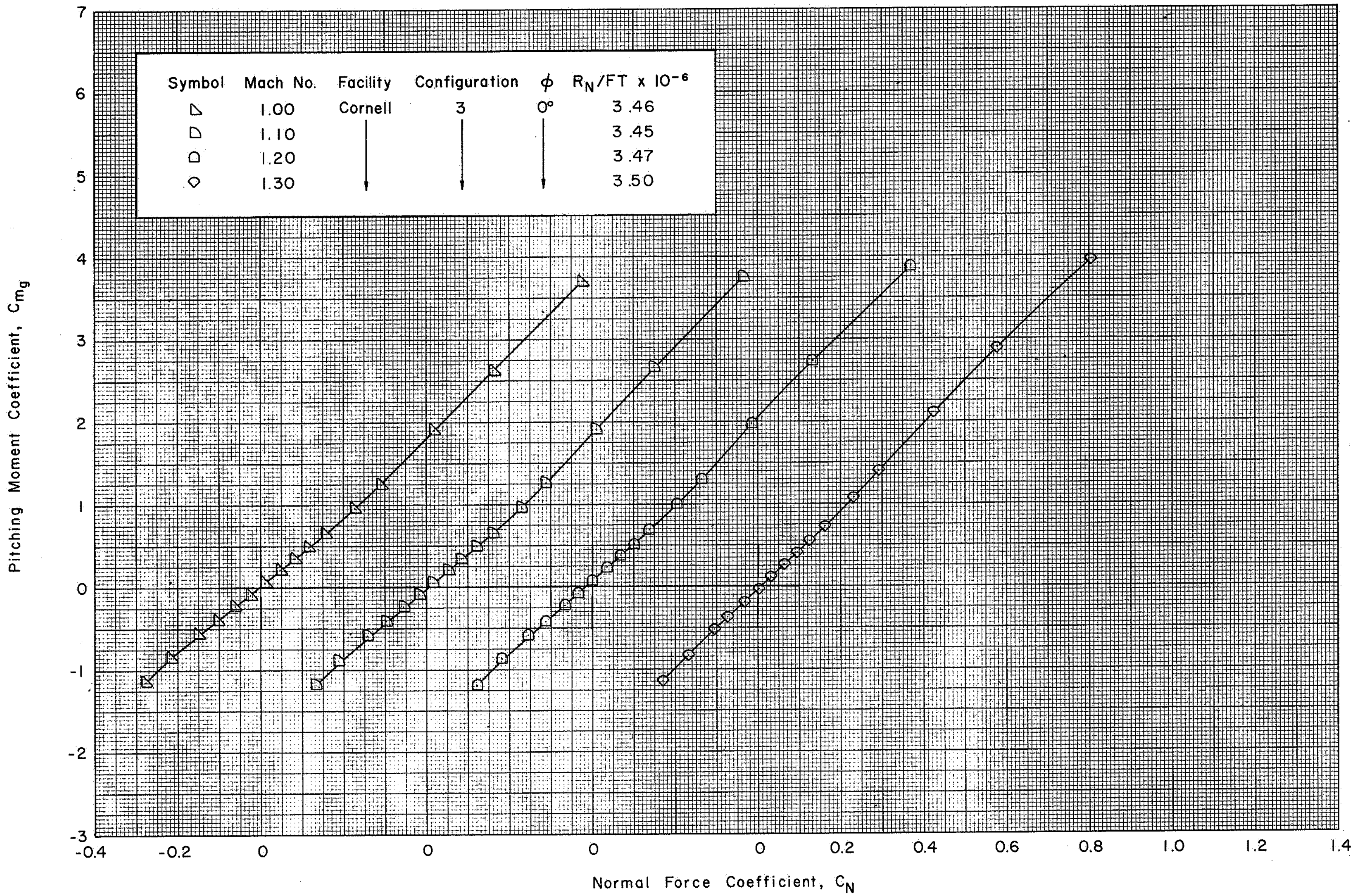

(b) Concluded : ϕ=0° (M=1.00–1.30)

Figure 9 Continued

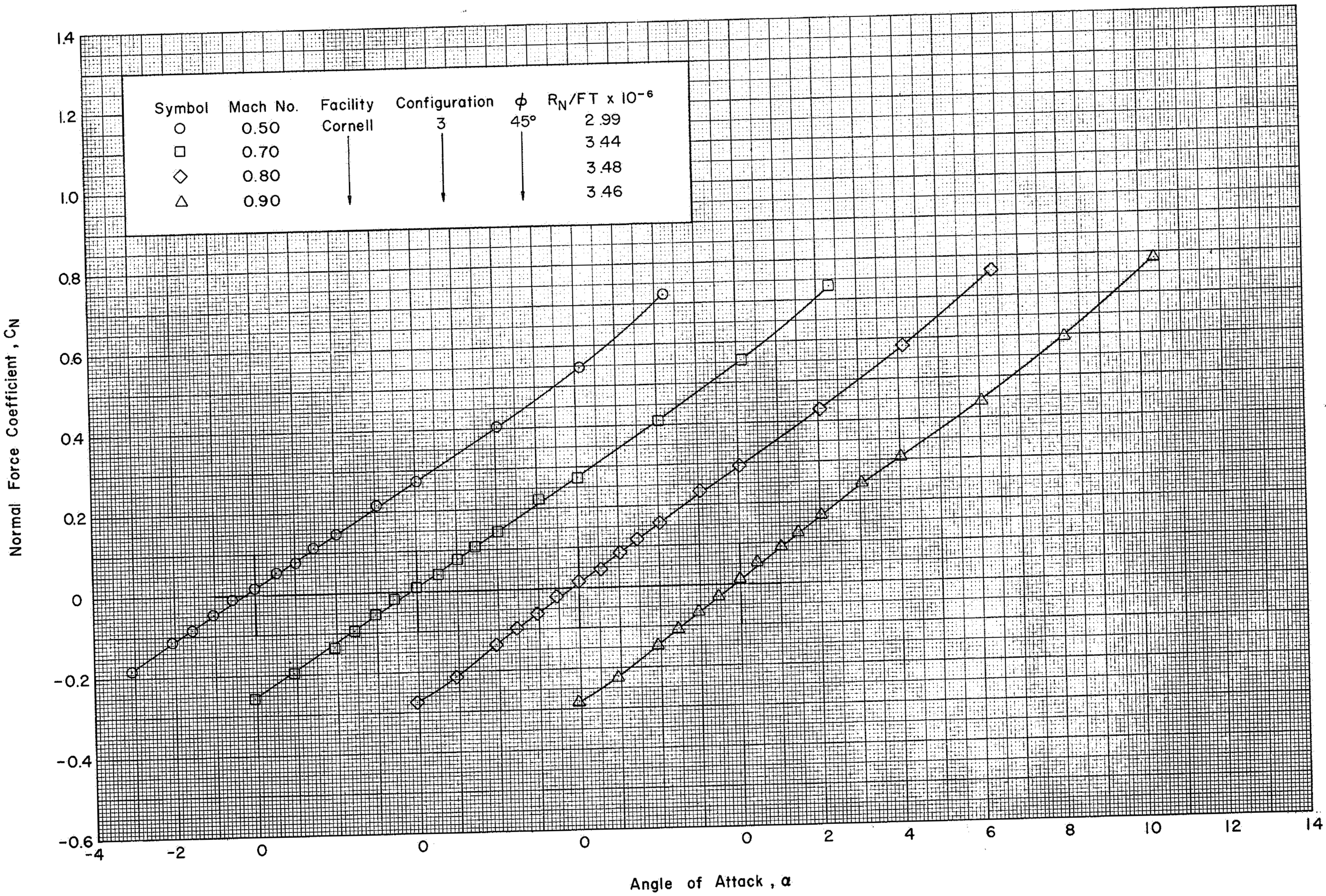

(c) C_N vs. α : ϕ=45° (M=0.50–0.90)

Figure 9 Continued

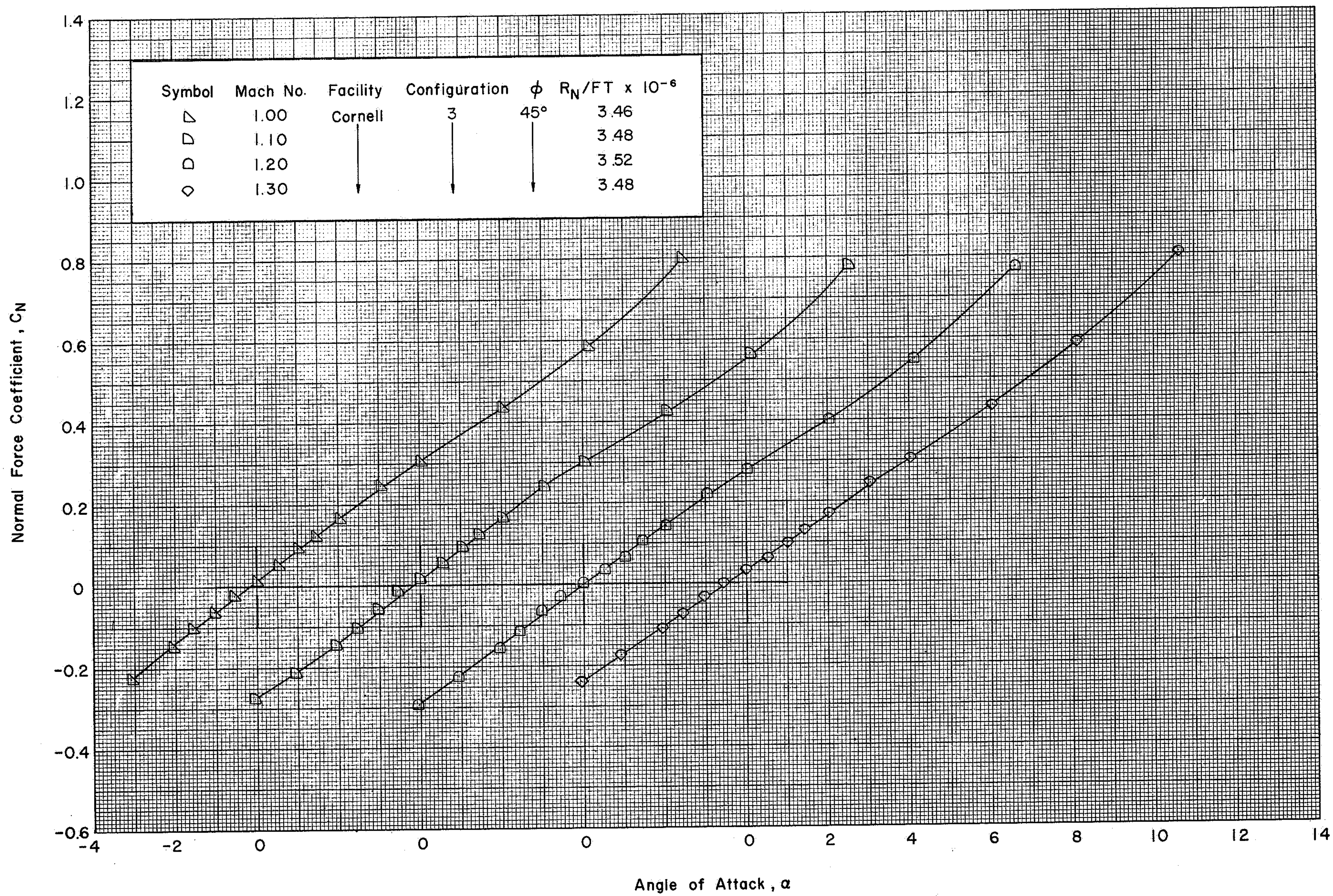

(c) Concluded : ϕ=45° (M=1.00–1.30)

Figure 9 Continued

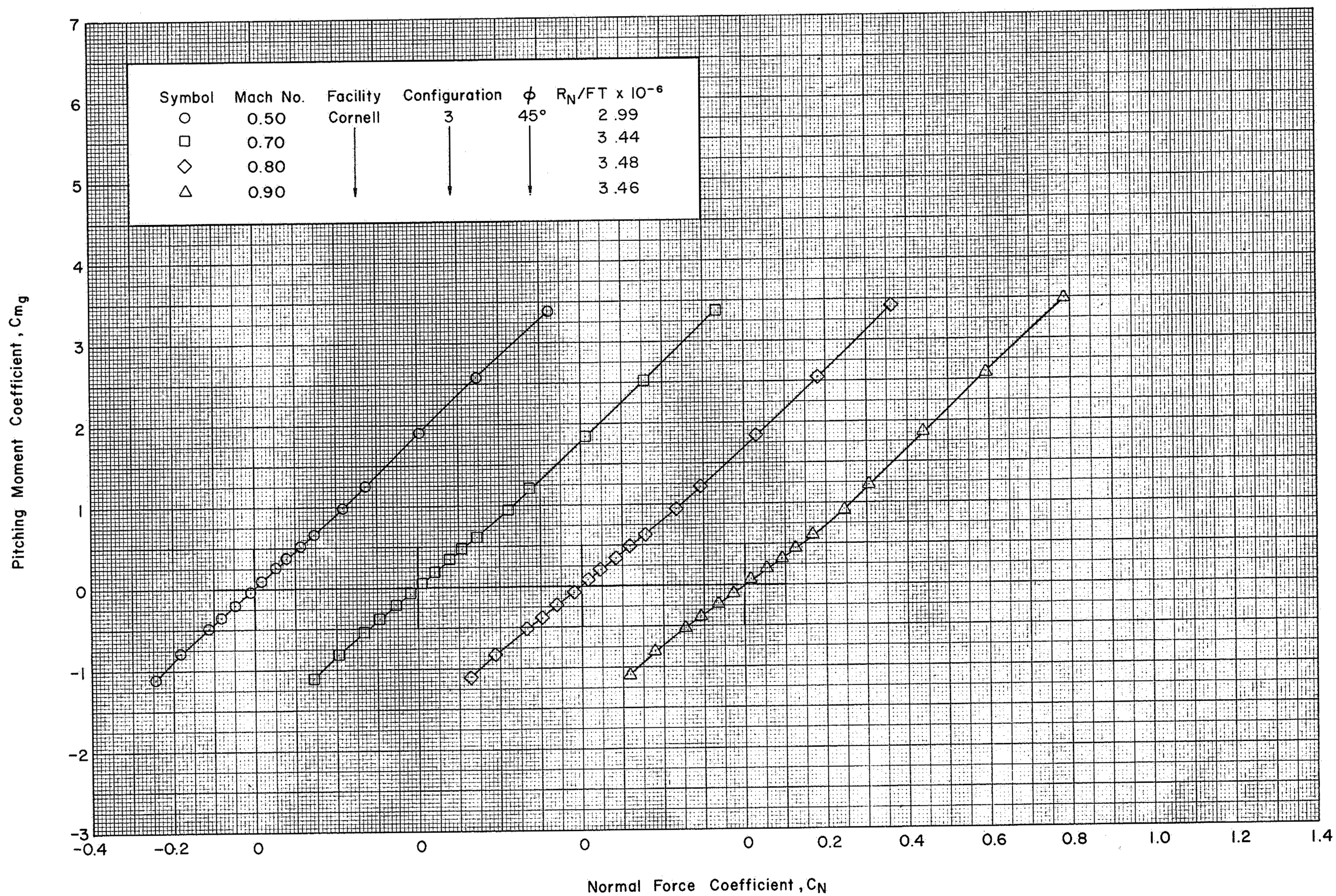

(d) C_{m_g} vs. C_N : ϕ=45° (M=0.50-0.90)

Figure 9 Continued

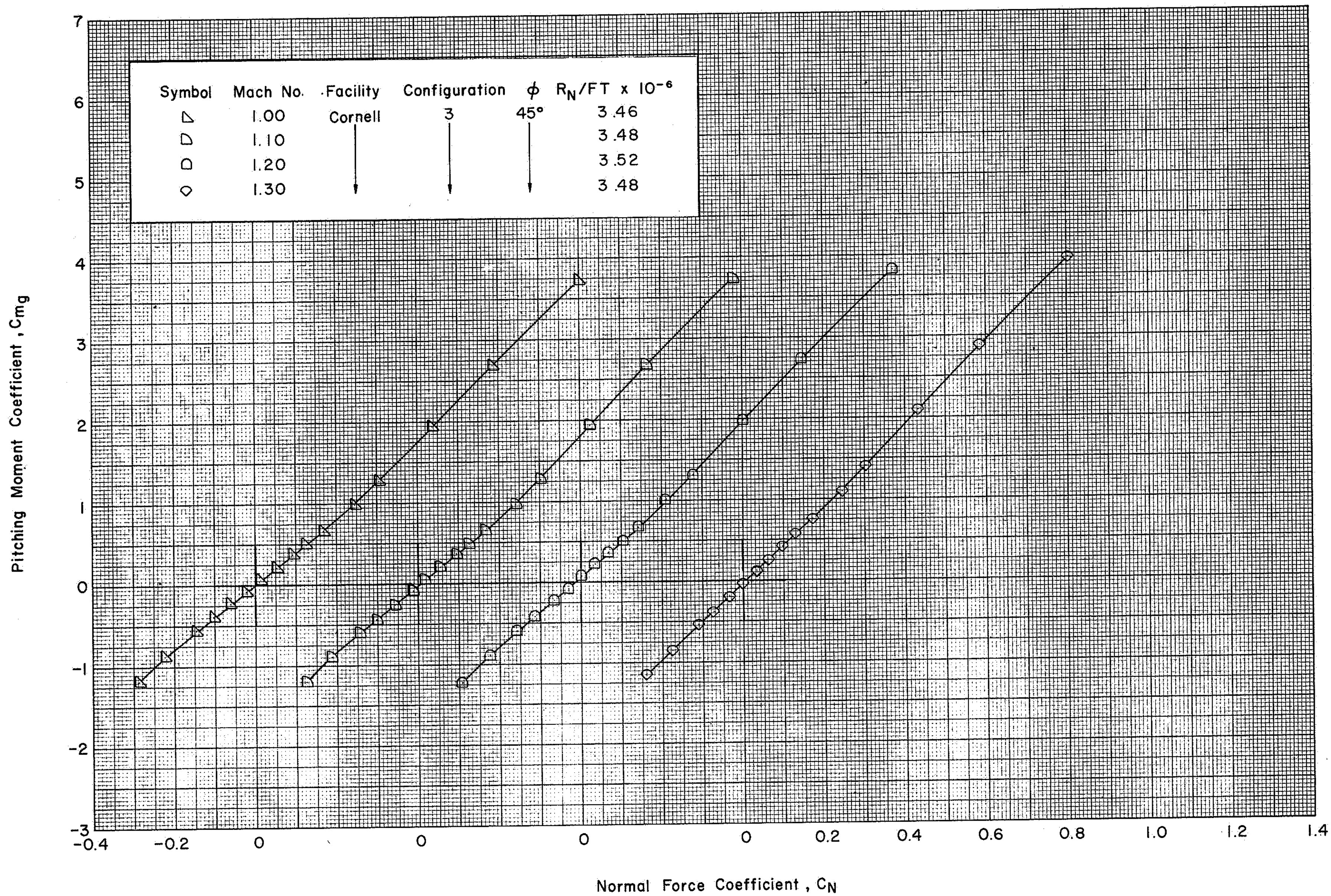

(d) Concluded : ϕ=45° (M=1.00-1.30)

Figure 9 Concluded

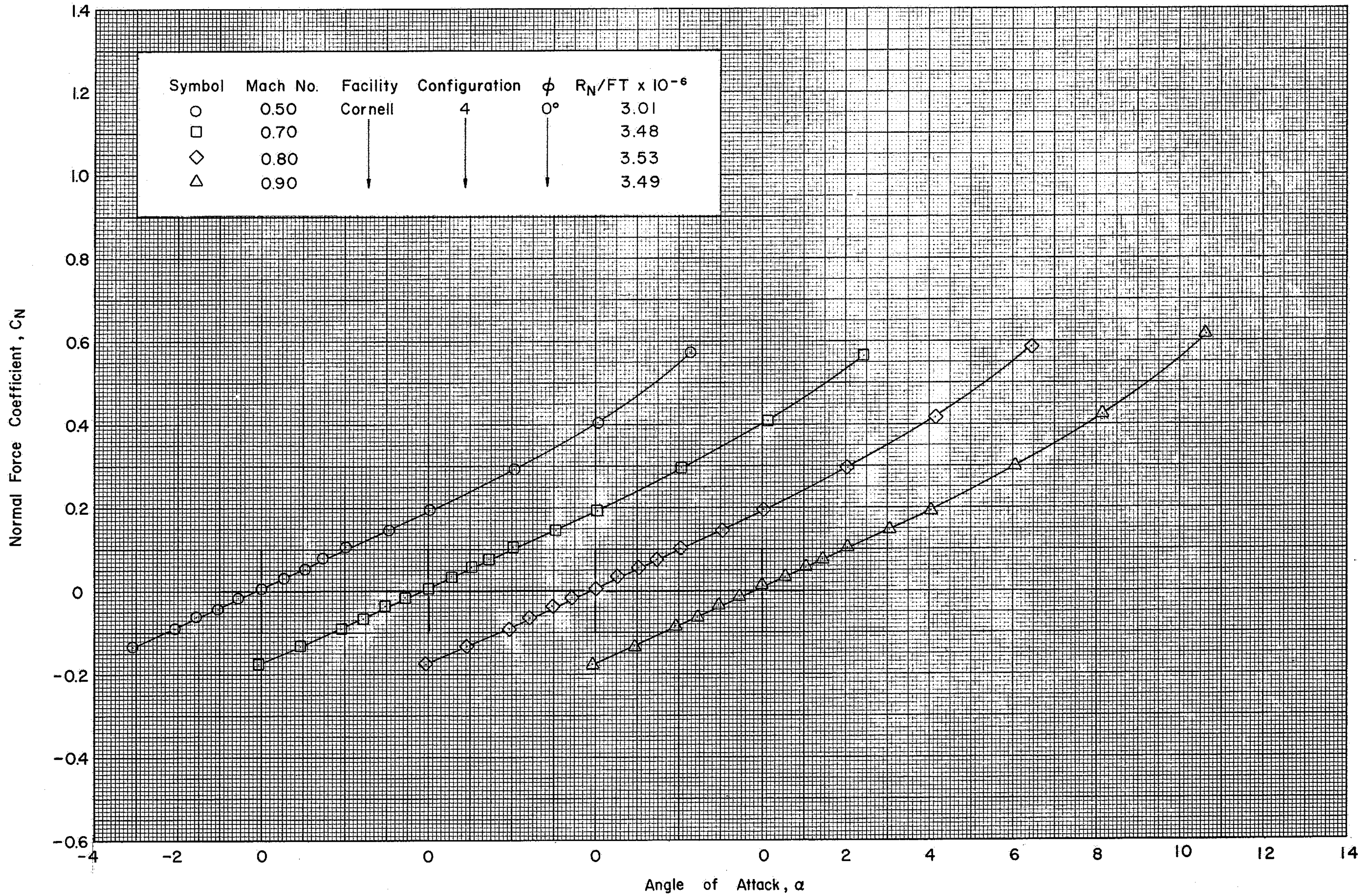

(a) C_N vs. α : ϕ=0° (M=0.50–0.90)

Figure 10 Static Aerodynamic Characteristics of the APOLLO-SATURN V Launch Vehicle without Fins, Shrouds, and Base Flow Deflectors in the CAL 8-Foot Transonic Wind Tunnel

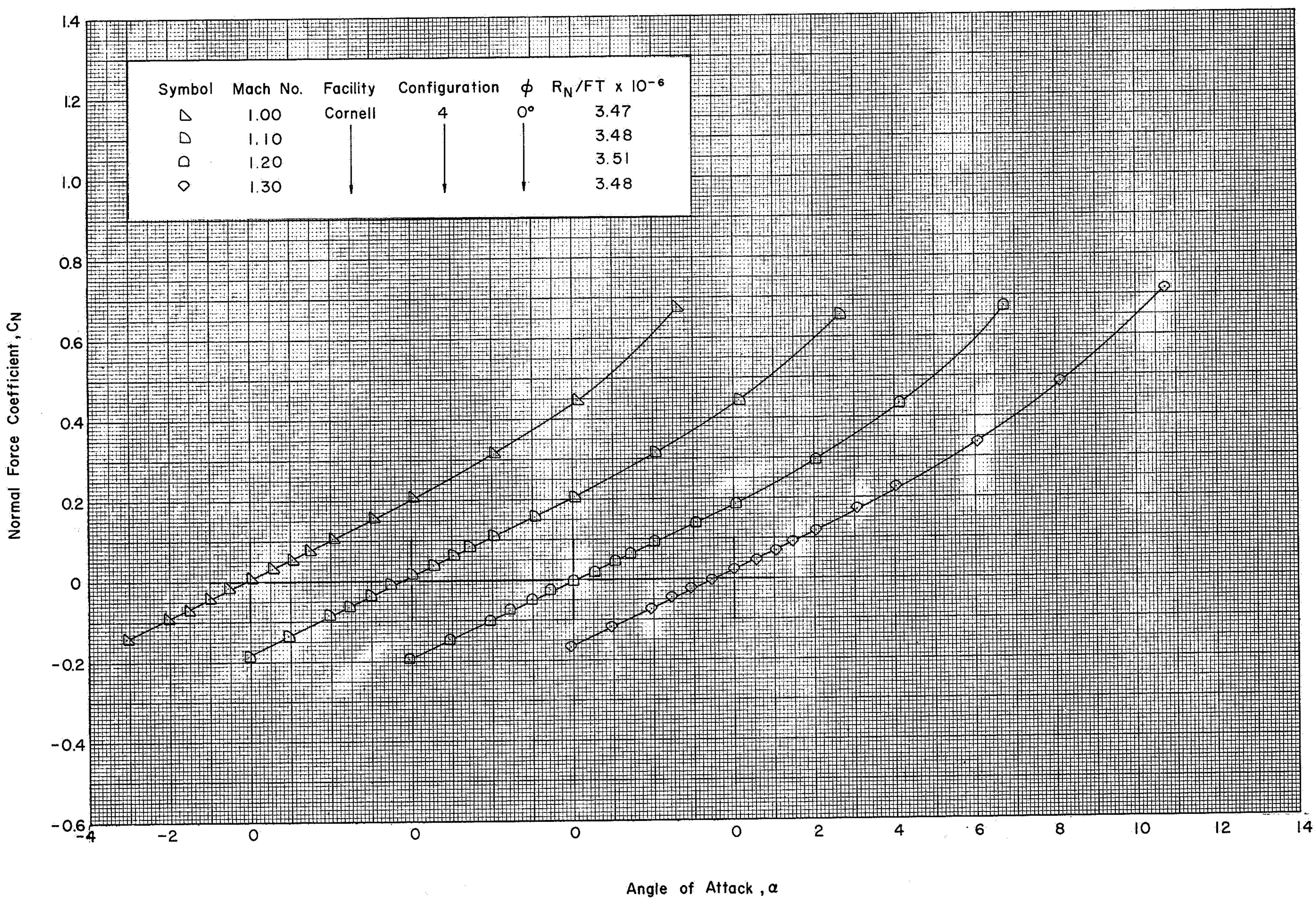

(a) Concluded : ϕ=0° (M=1.00-1.30)

Figure 10 Continued

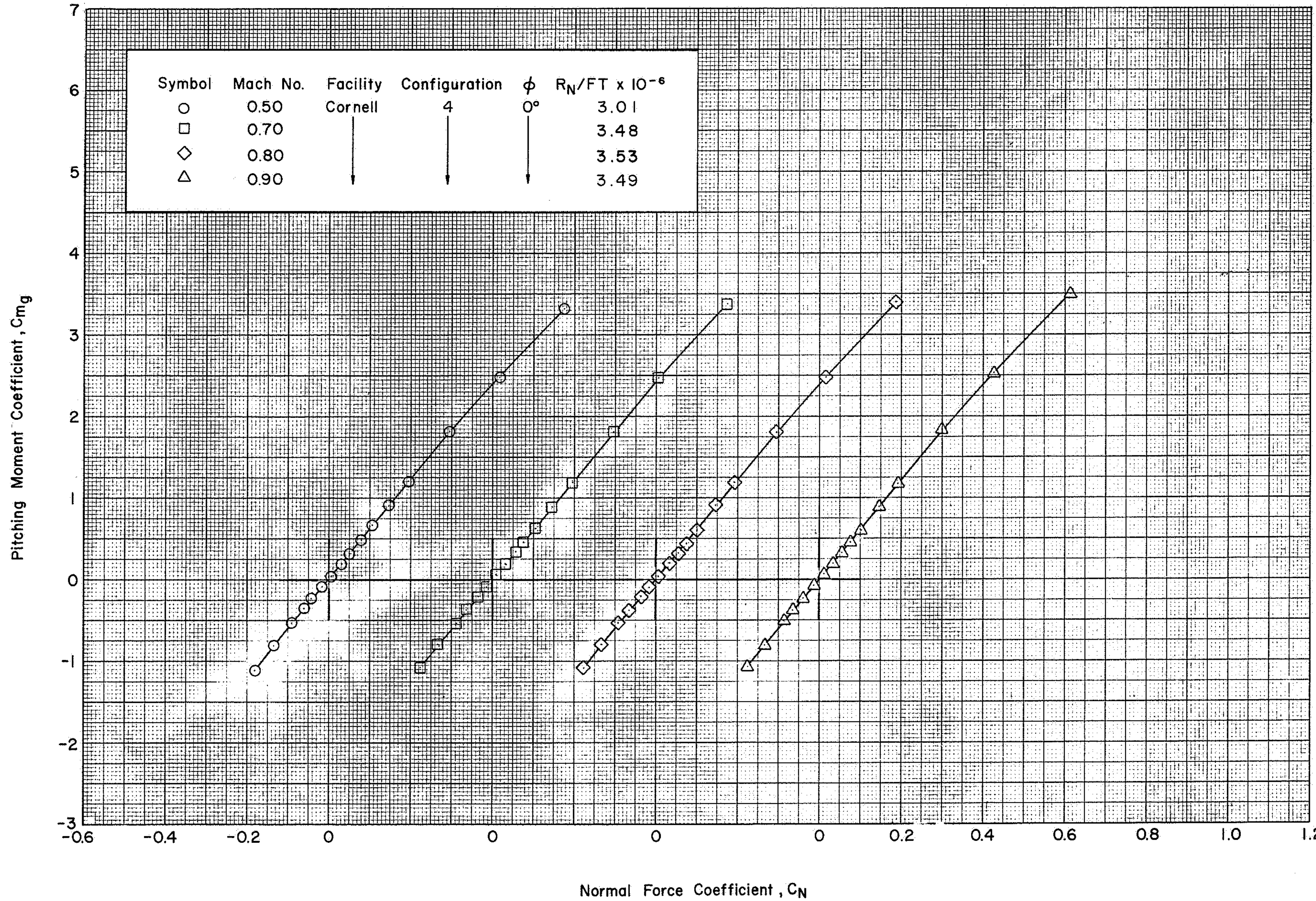

(b) C_{m_g} vs. C_N : $\phi=0°$ (M=0.50-0.90)

Figure 10 Continued

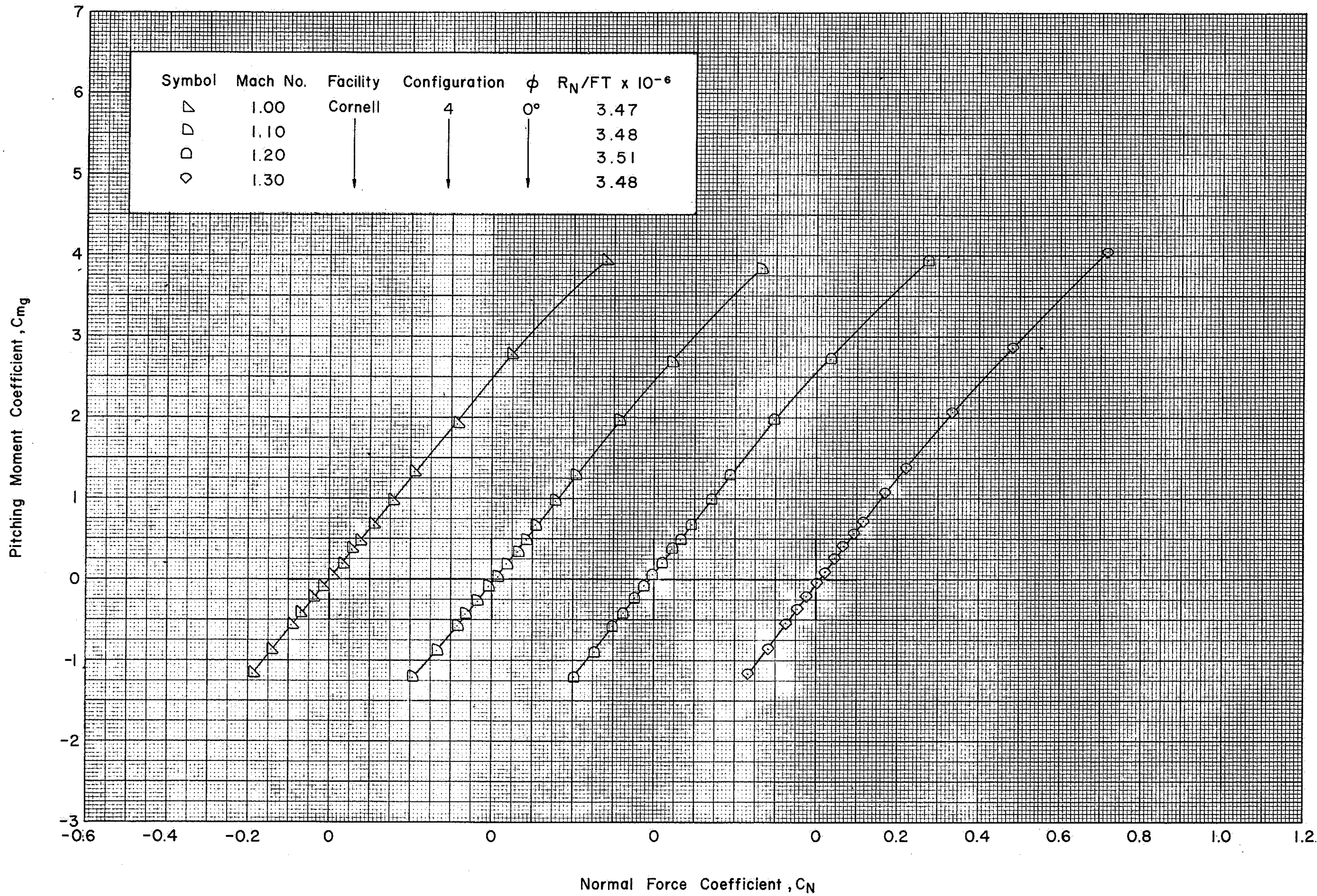

(b) Concluded : ϕ=0° (M=1.00–1.30)

Figure 10 Concluded

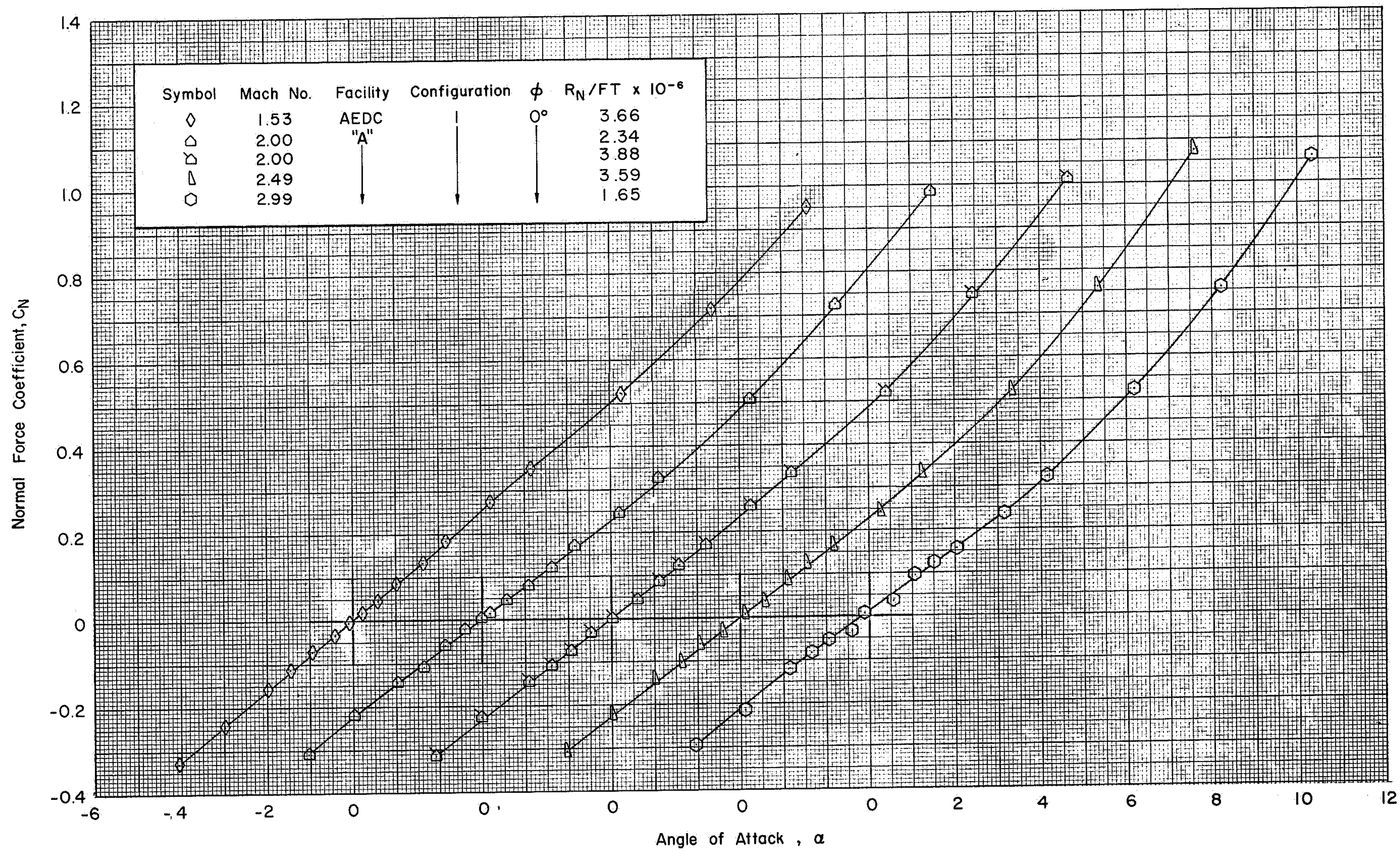

(a) C_N vs. α : ϕ=0° (M=1.53-2.99)

Figure 11 Static Aerodynamic Characteristics of the APOLLO-SATURN V Launch Vehicle in the AEDC/VKF 40-Inch Supersonic Tunnel "A"

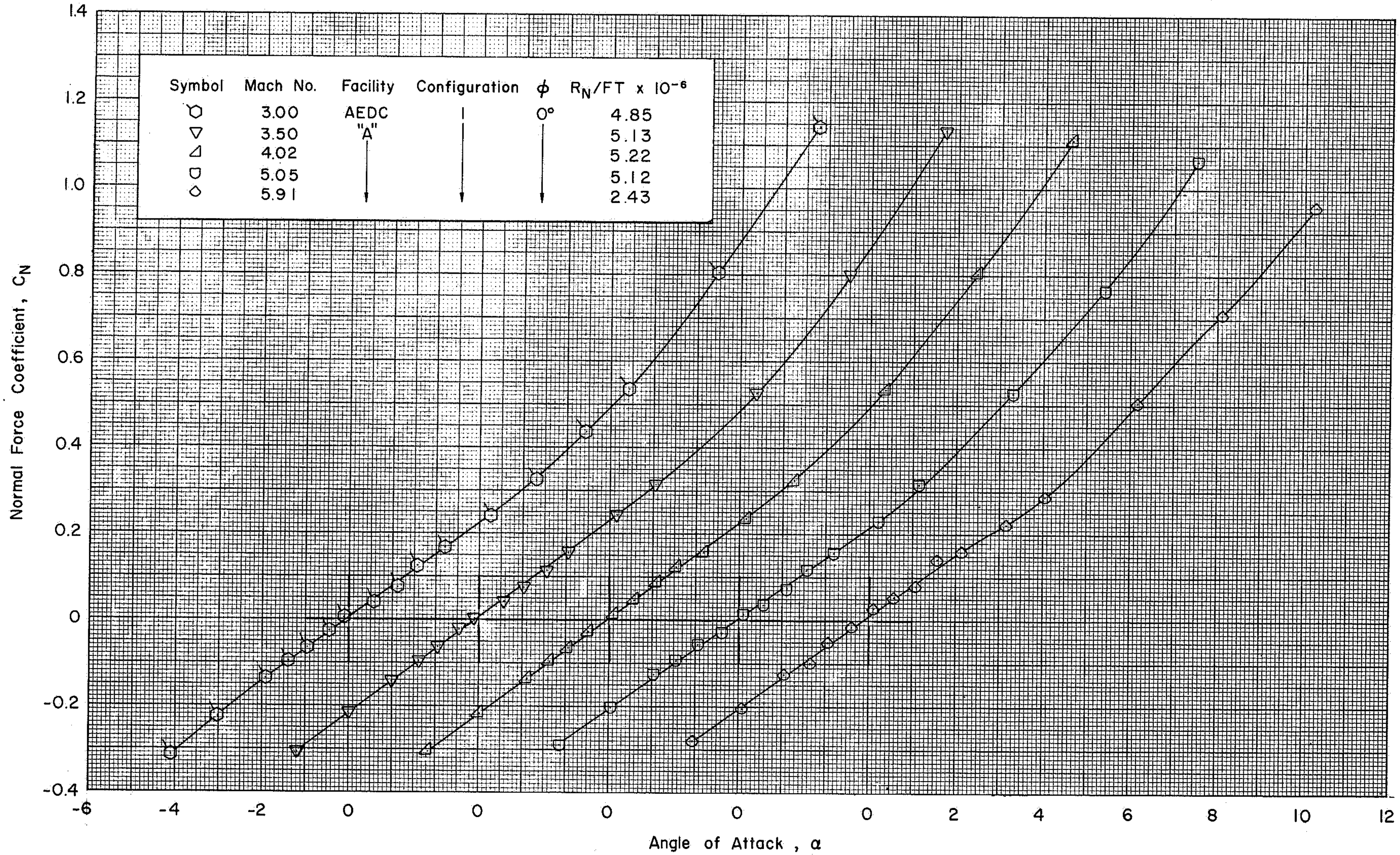

(a) Concluded : $\phi=0°$ (M=3.00–5.91)

Figure 11 Continued

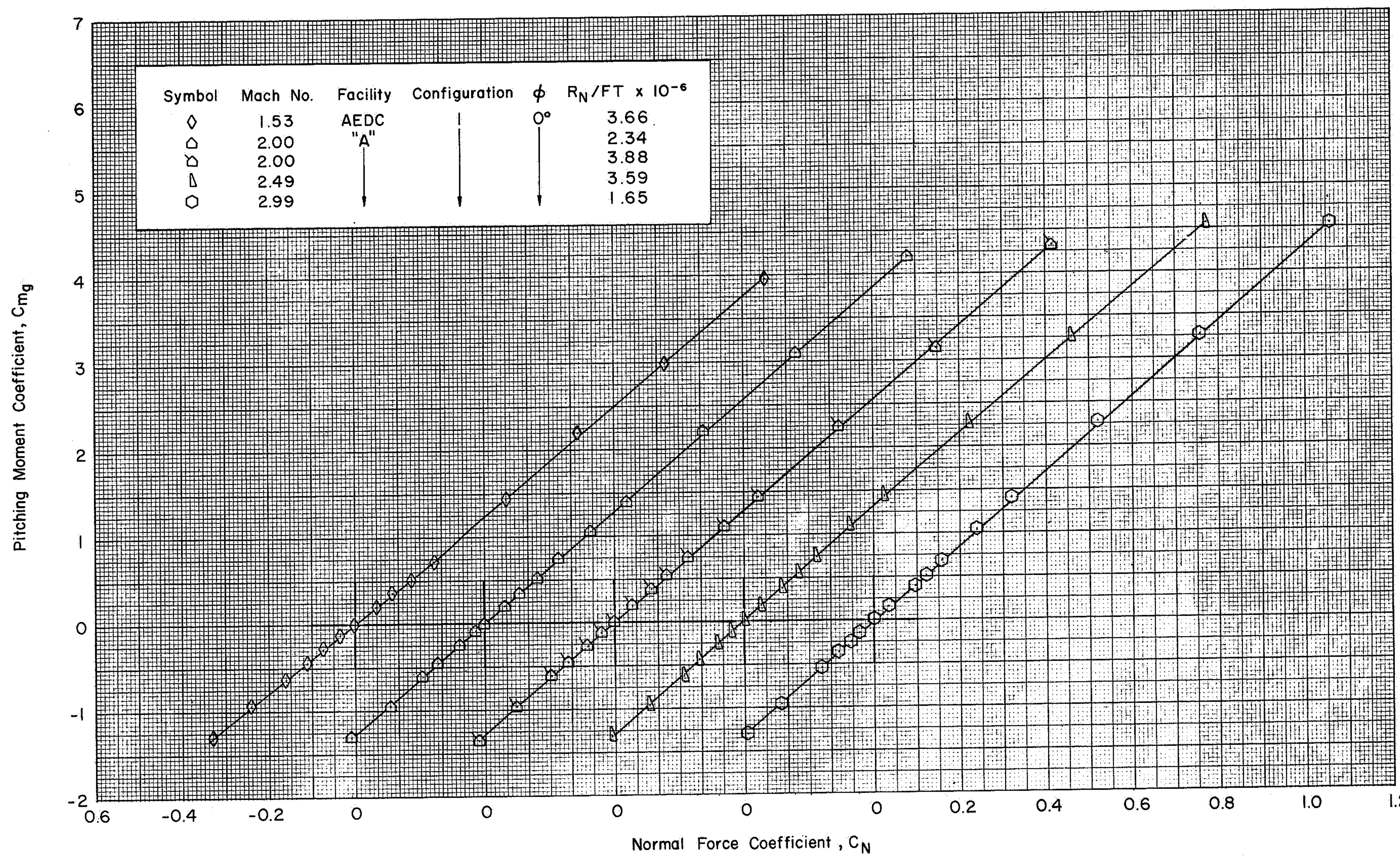

(b) C_{m_g} vs. C_N : $\phi = 0°$ (M=1.53-2.99)

Figure 11 Continued

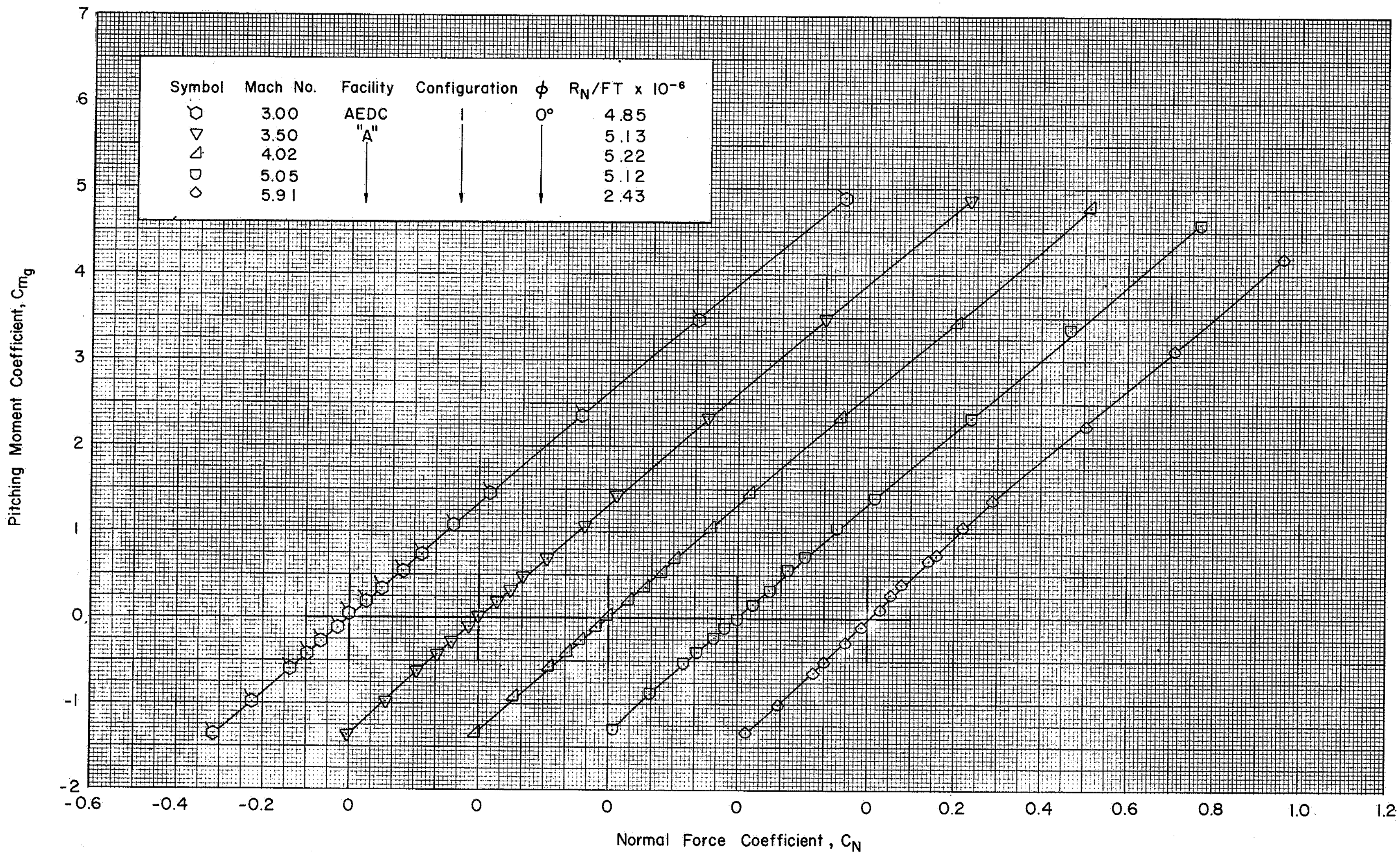

(b) Concluded : $\phi = 0°$ (M=3.00–5.91)

Figure 11 Concluded

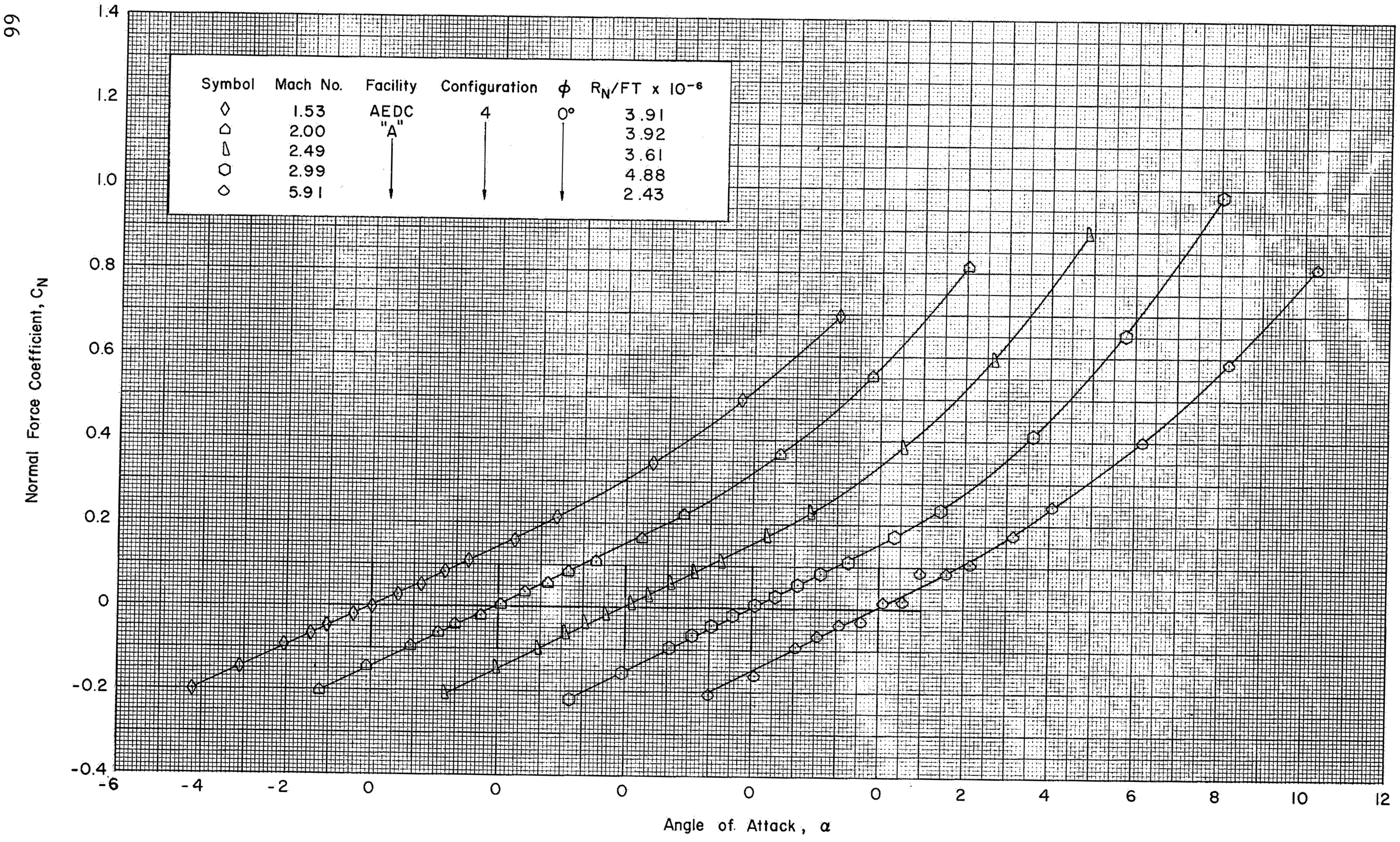

(a) C_N vs. α : $\phi = 0°$ (M=1.53–5.91)

Figure 12 Static Aerodynamic Characteristics of the APOLLO-SATURN V Launch Vehicle without Fins, Shrouds, and Base Flow Deflectors in the AEDC/VKF 40-Inch Supersonic Tunnel "A"

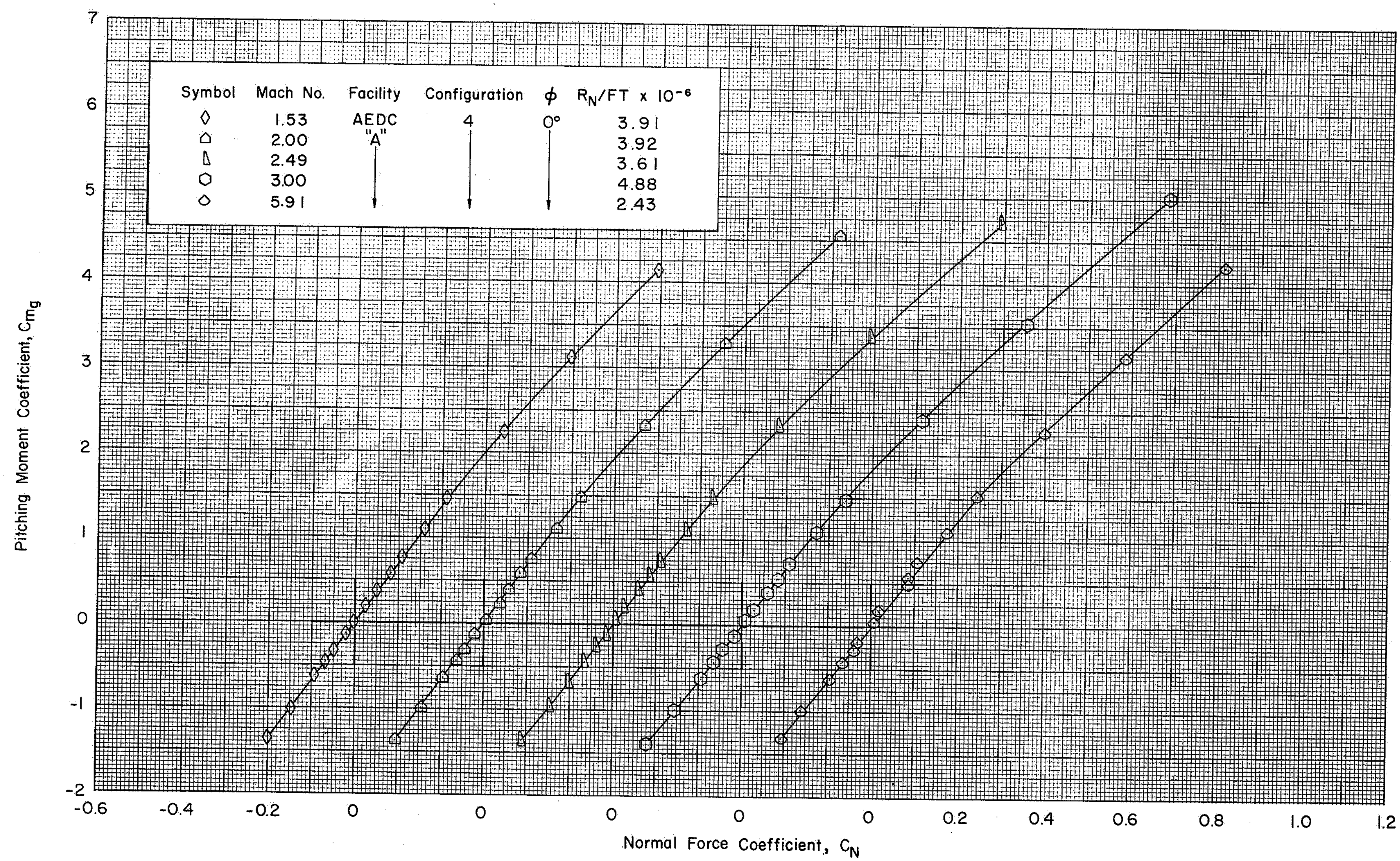

(b) C_{m_g} vs. C_N : ϕ=0° (M=1.53-5.91)

Figure 12 Concluded

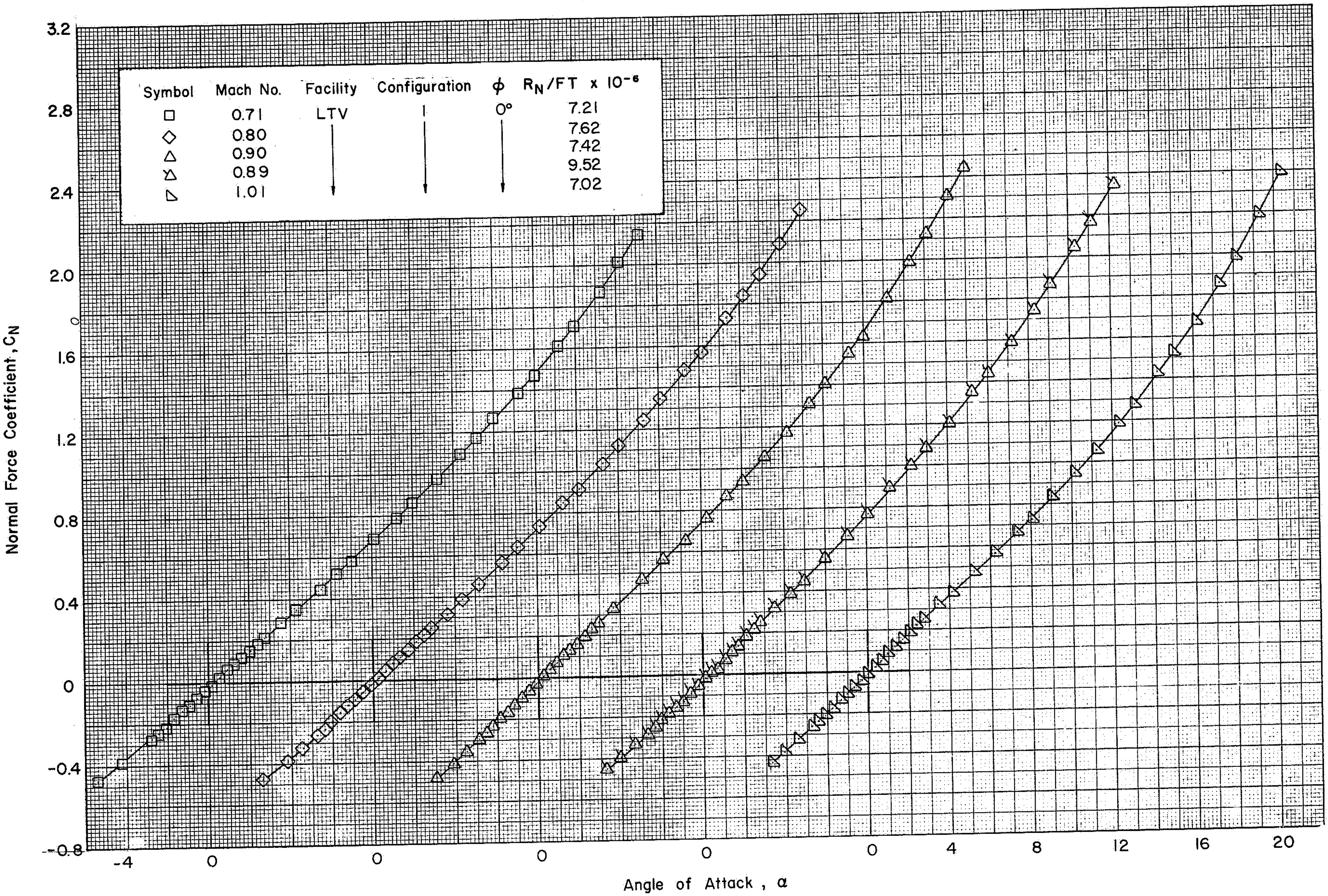

(a) C_N vs. α : $\phi = 0°$ (M=0.71 - 1.01)

Figure 13 Static Aerodynamic Characteristics of the APOLLO-SATURN V Launch Vehicle in the LTV 4-Foot High Speed Wind Tunnel

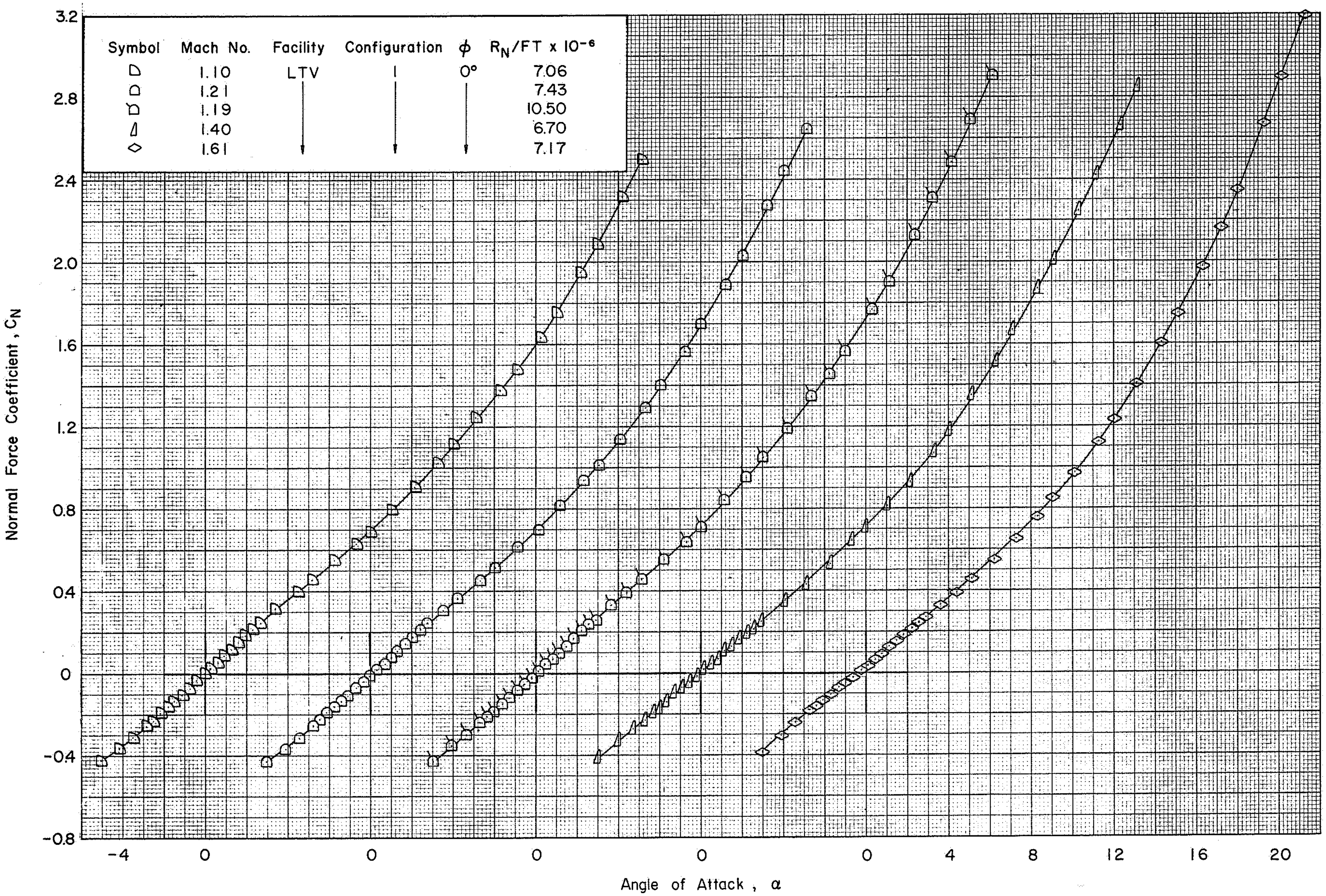

(a) Continued : $\phi = 0°$ (M=1.10 – 1.61)

Figure 13 Continued

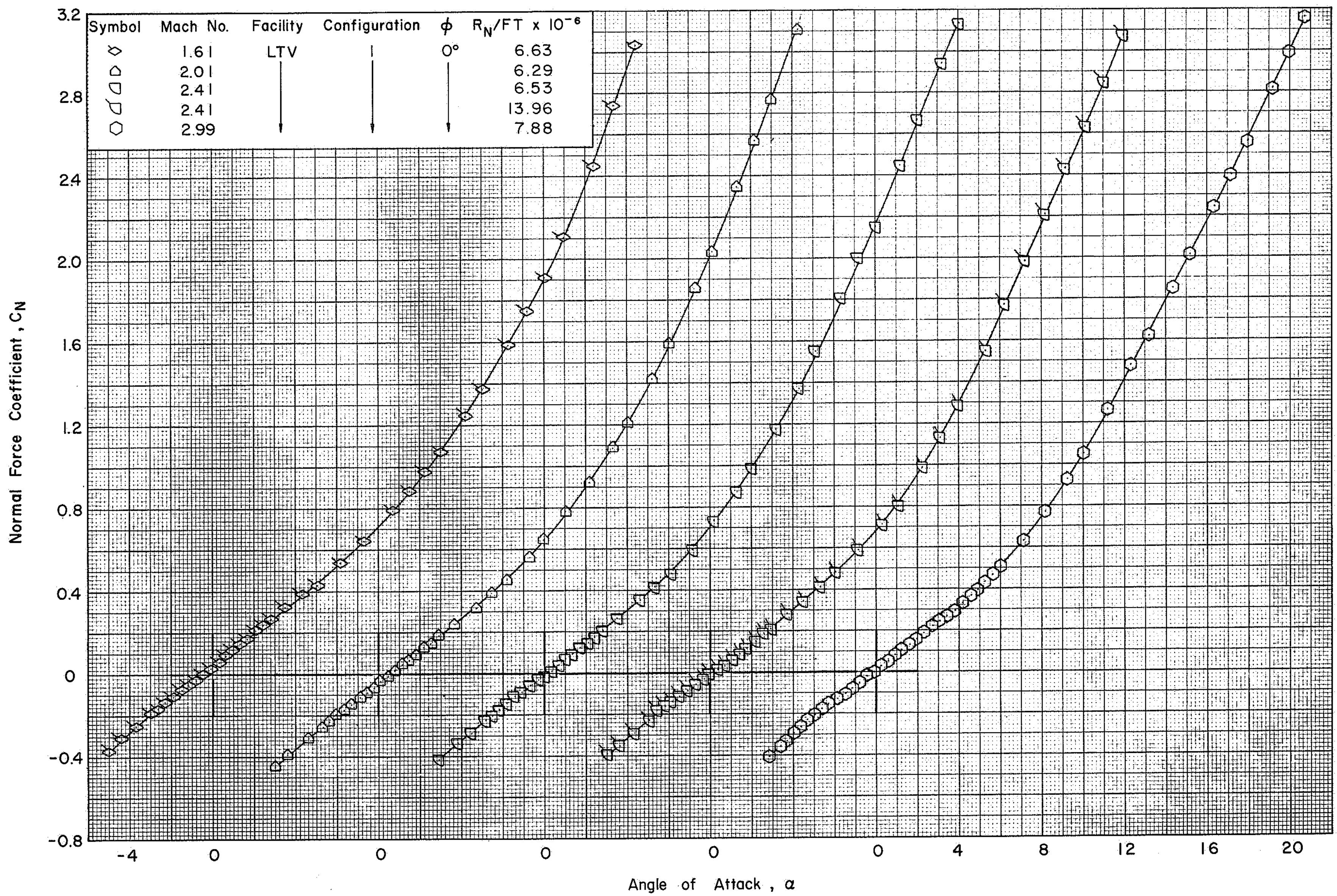

(a) Concluded : $\phi = 0°$ (M=1.61 - 2.99)

Figure 13 Continued

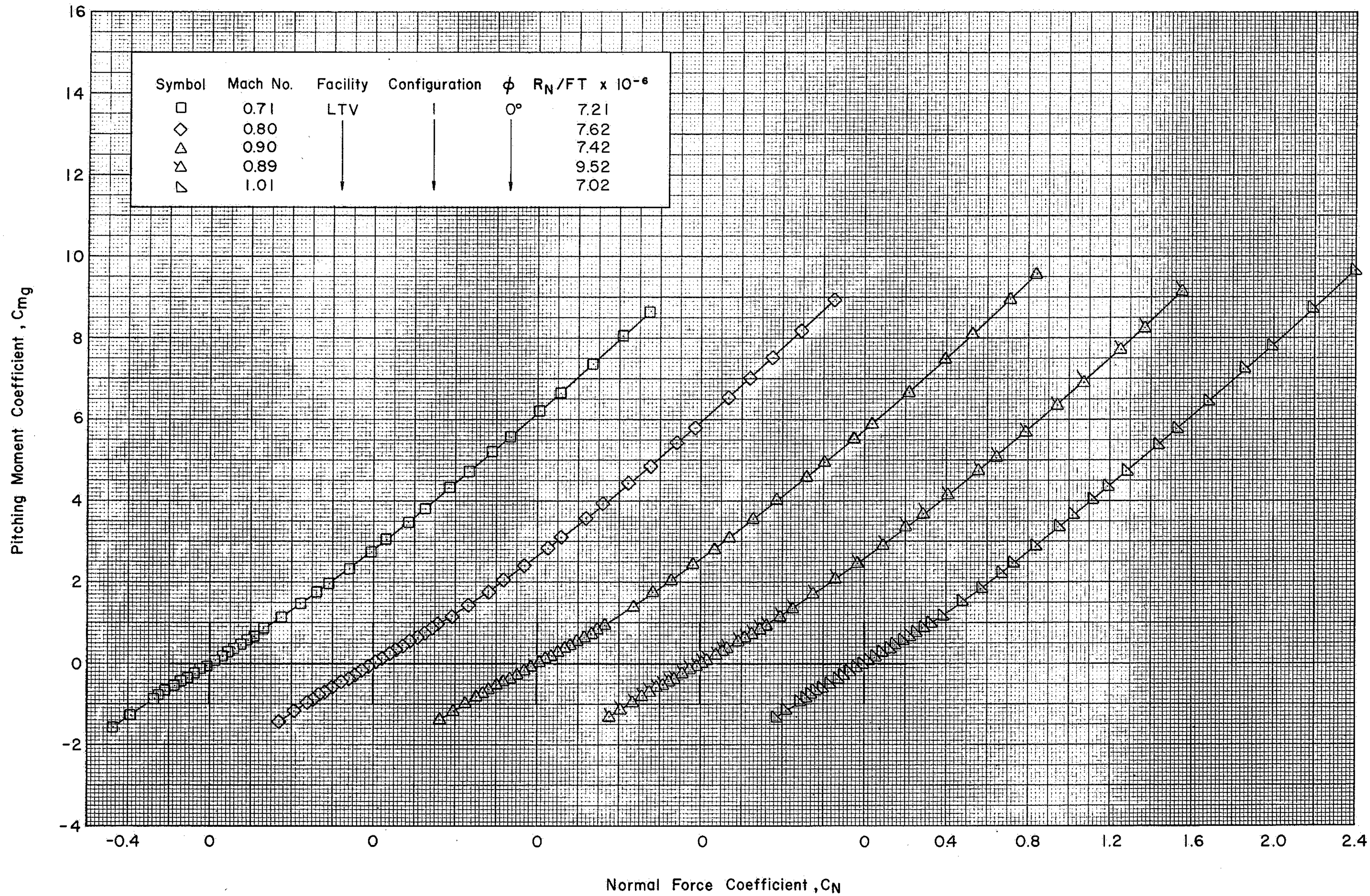

(b) C_{m_g} vs. C_N : $\phi=0°$ (M=0.71-1.01)

Figure 13 Continued

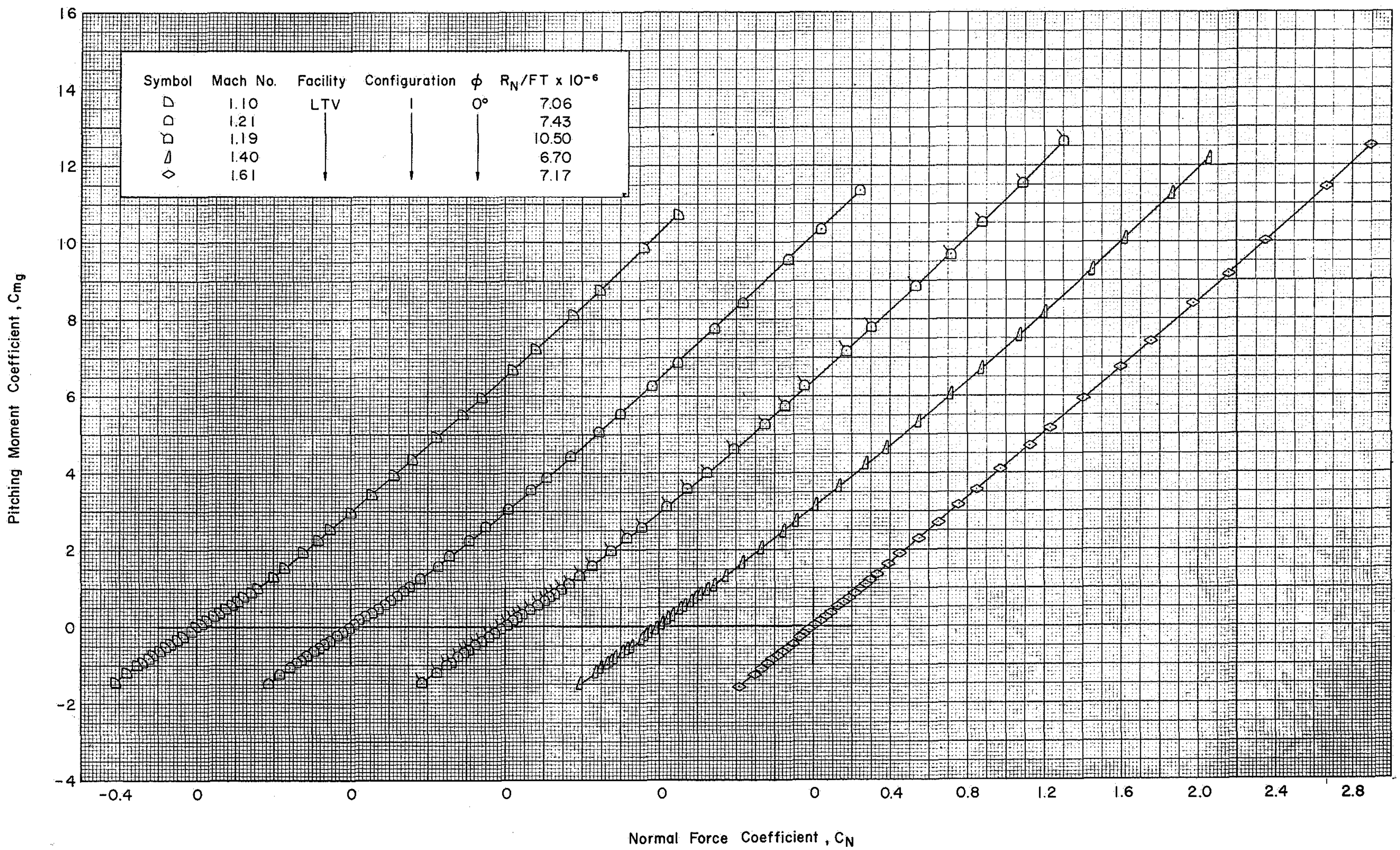

(b) Continued : ϕ=0° (M=1.10-1.61)

Figure 13 Continued

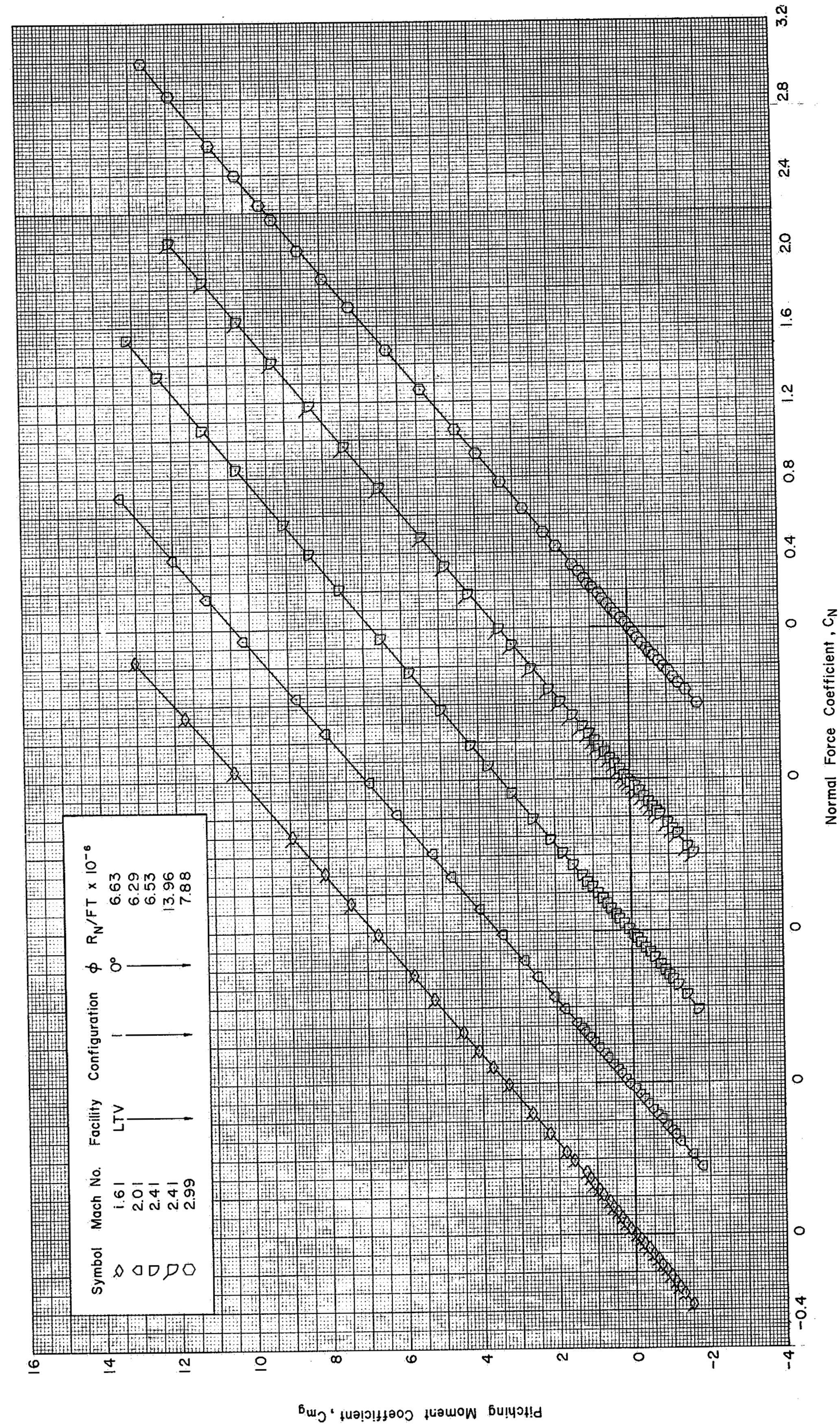

(b) Concluded : ϕ=0° (M=1.61 -2.99)

Figure 13 Continued

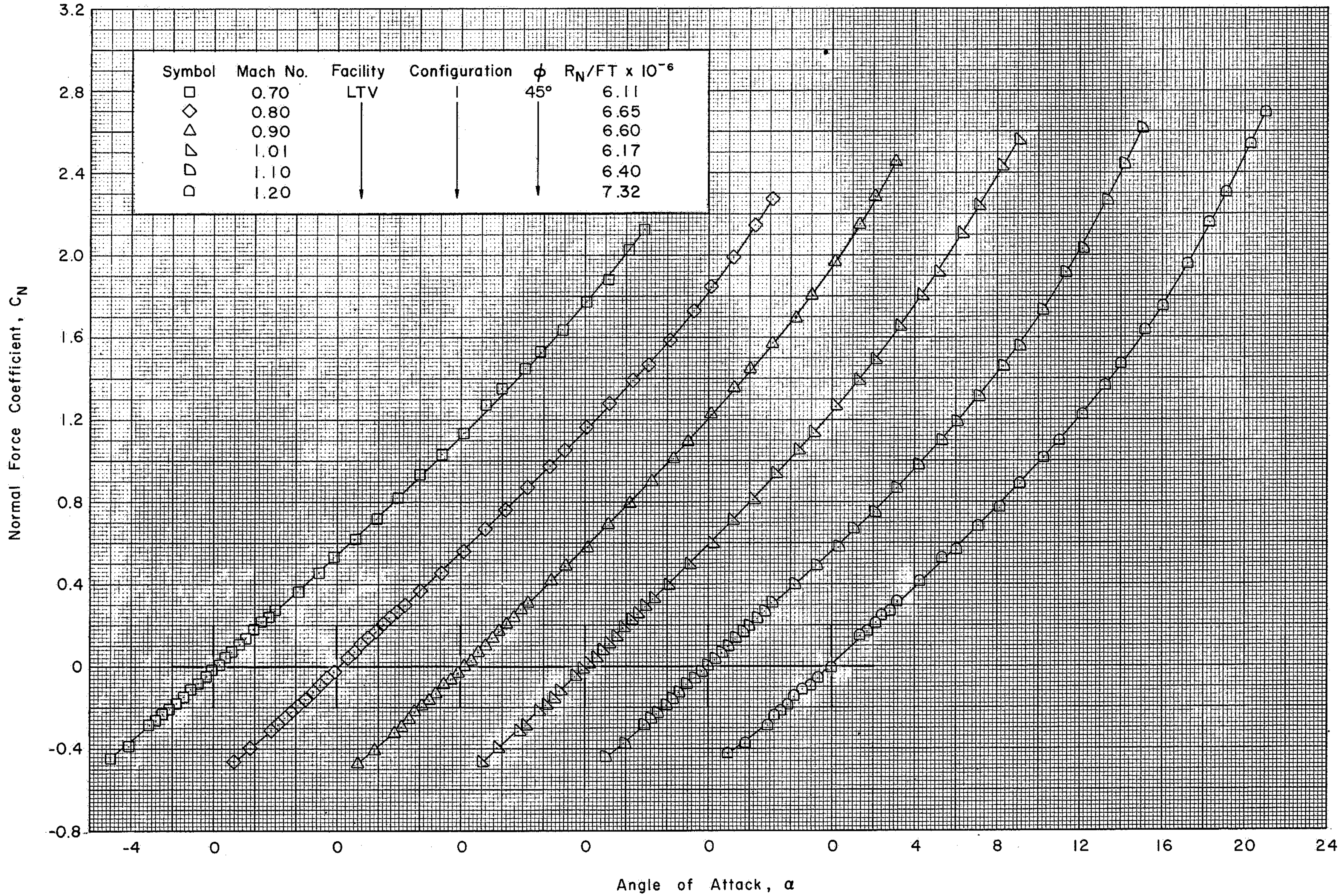

(c) C_N vs. α : $\phi = 45°$ (M=0.70-1.20)

Figure 13 Continued

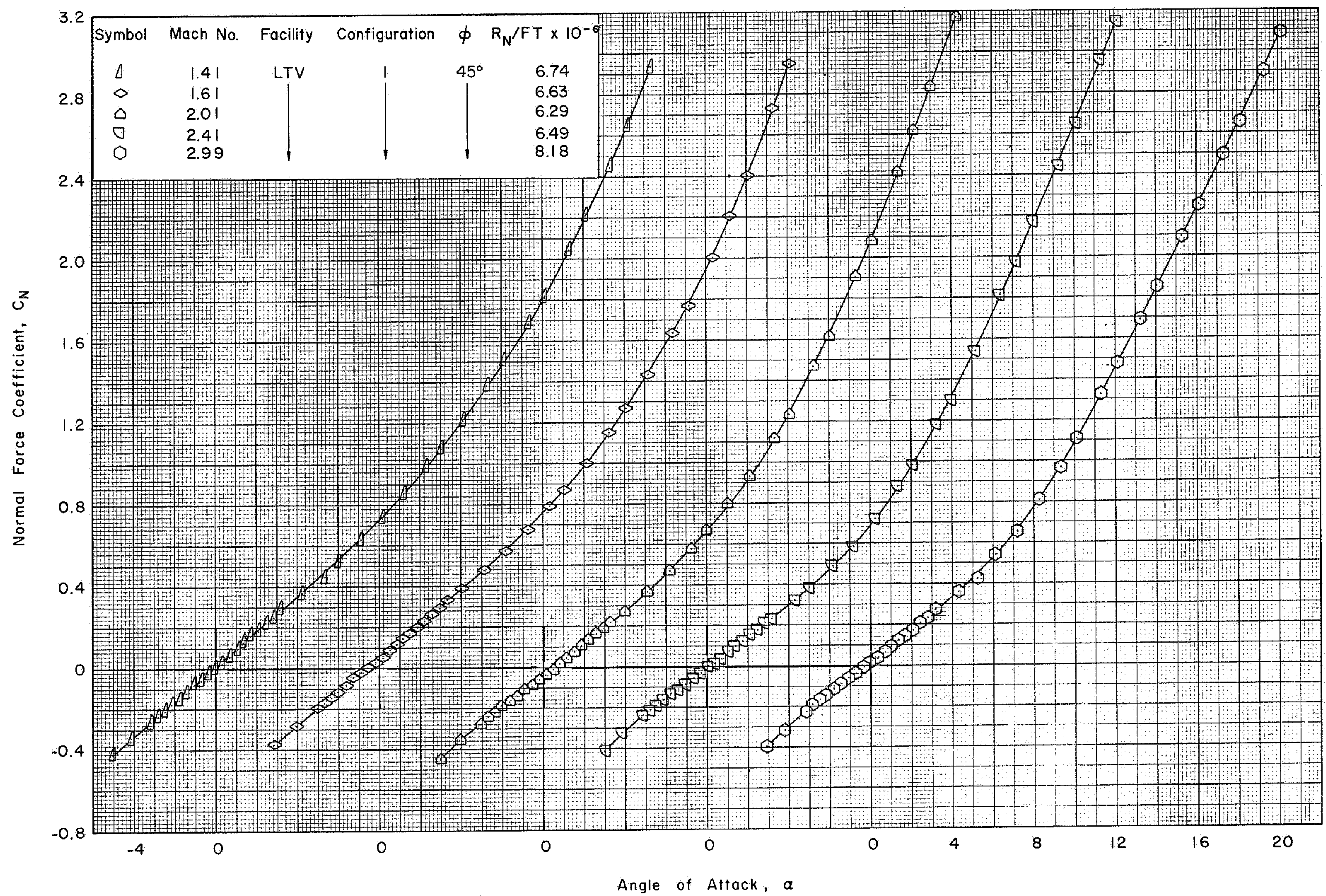

(c) Concluded : $\phi = 45°$ (M=1.41-2.99)

Figure 13 Continued

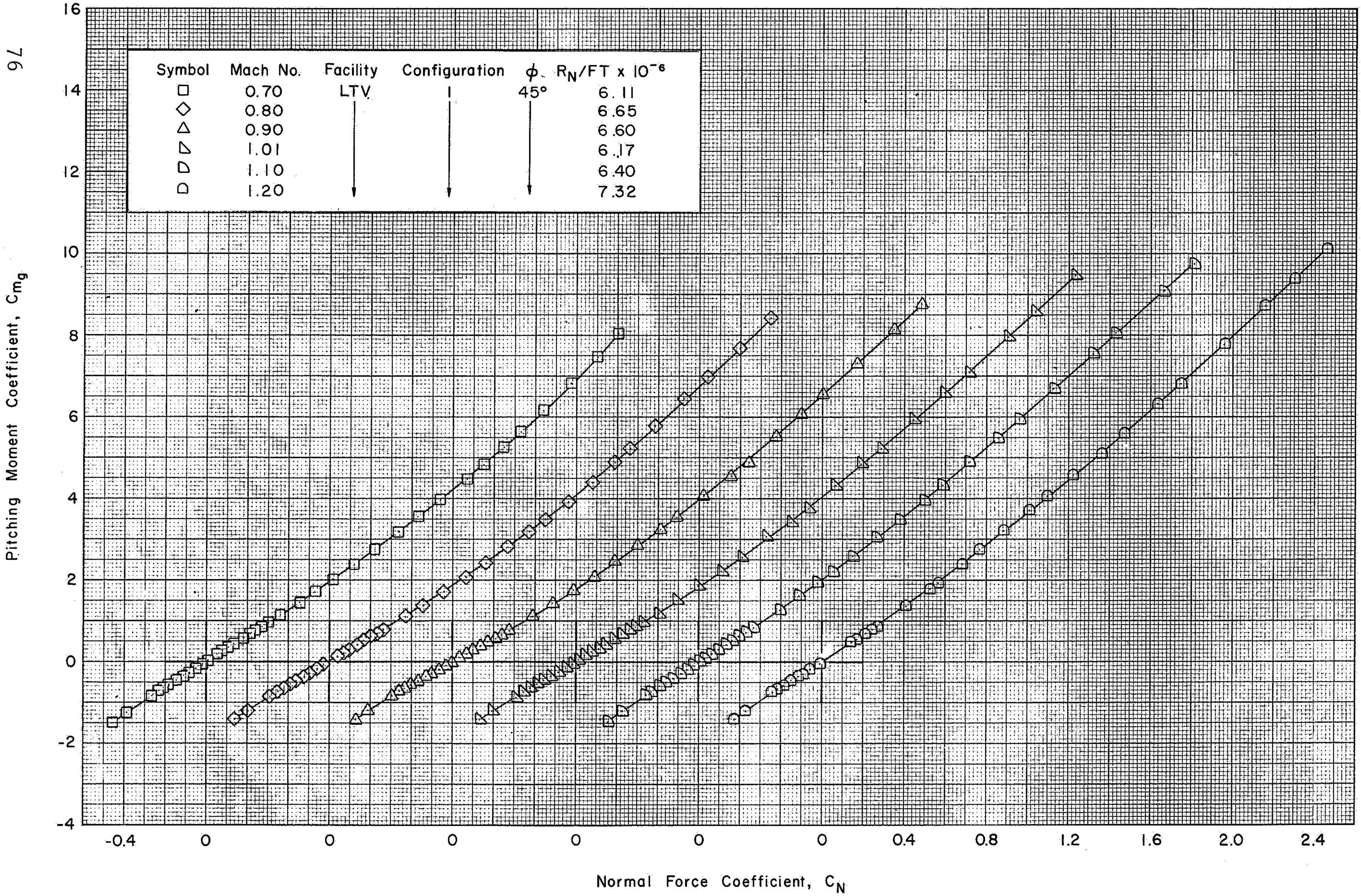

(d) C_{m_g} vs. C_N : $\phi = 45°$ (M=0.70-1.20)

Figure 13 Continued

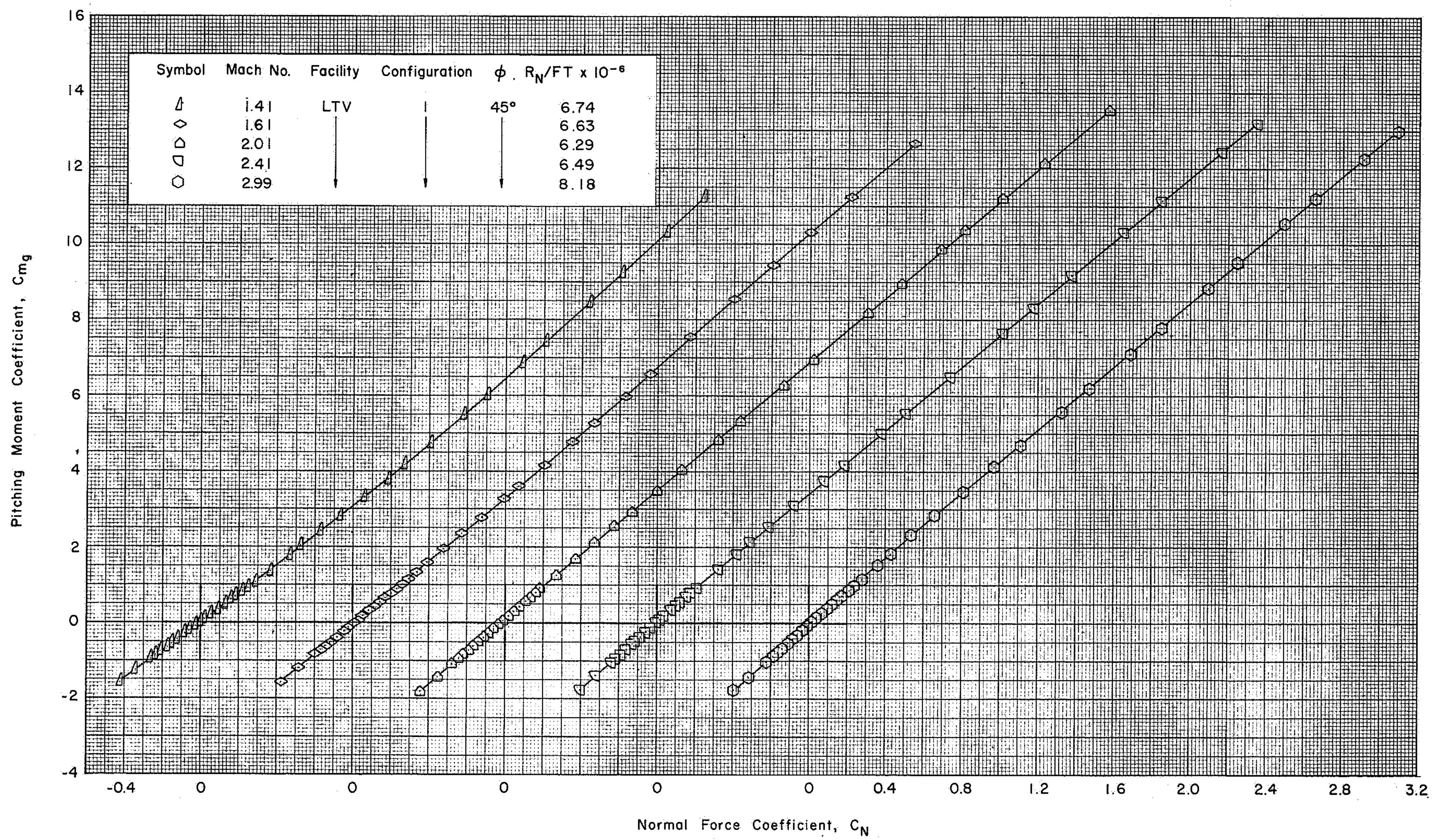

(d) Concluded : φ = 45° (M=1.41-2.99)

Figure 13 Continued

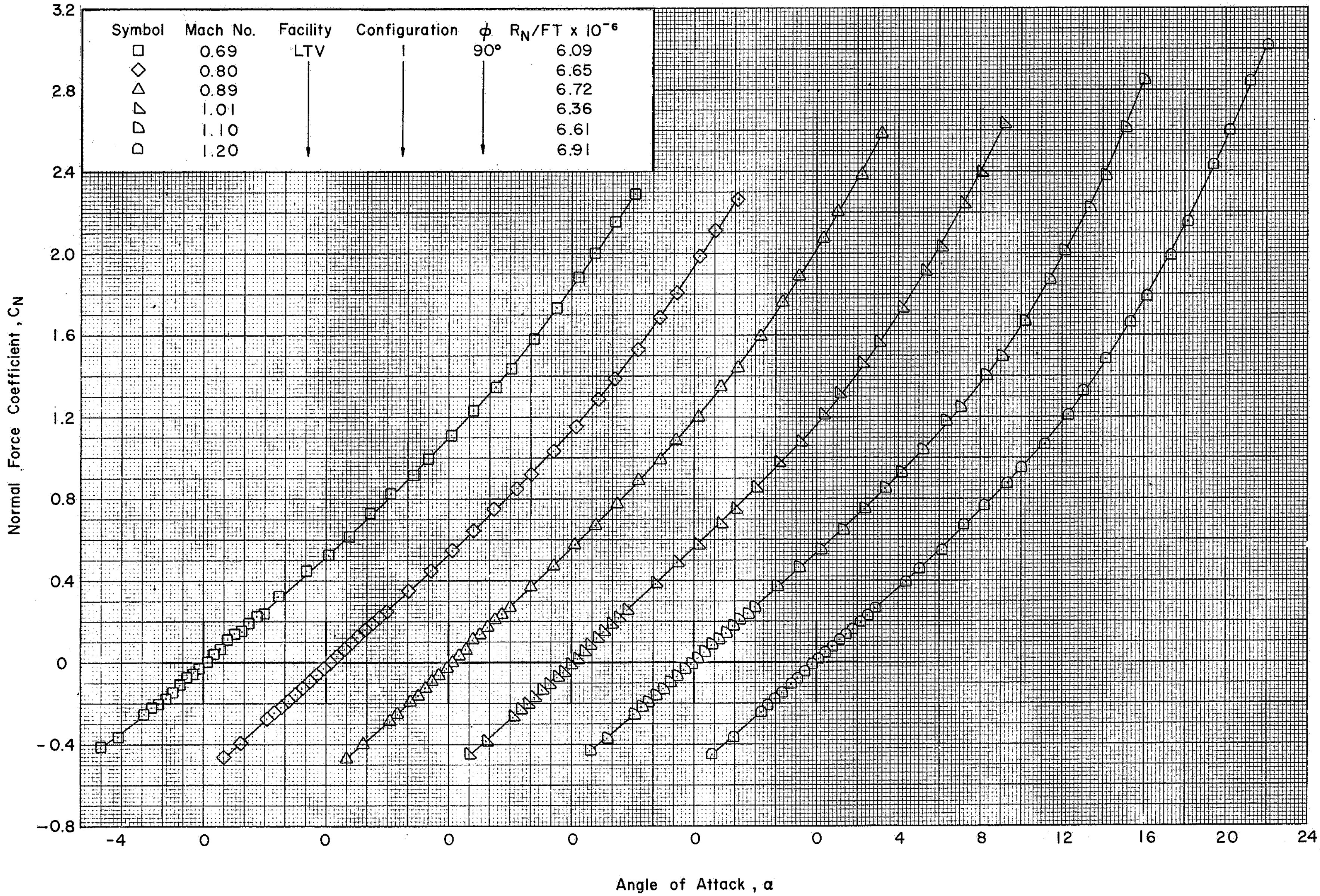

(e) C_N vs. α : $\phi = 90°$ (M=0.69-1.20)

Figure 13 Continued

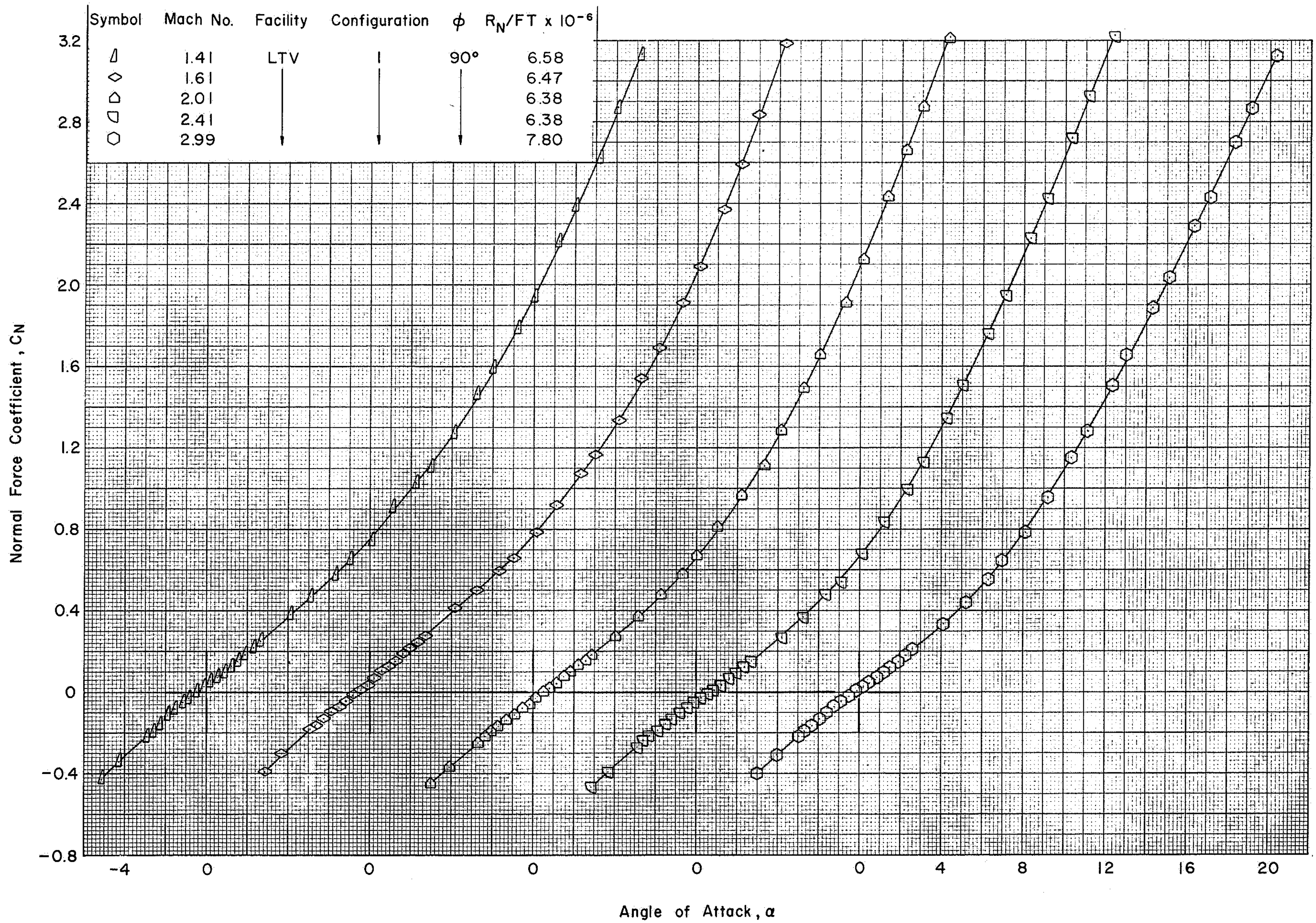

(e) Concluded : ϕ= 90° (M=1.41-2.99)

Figure 13 Continued

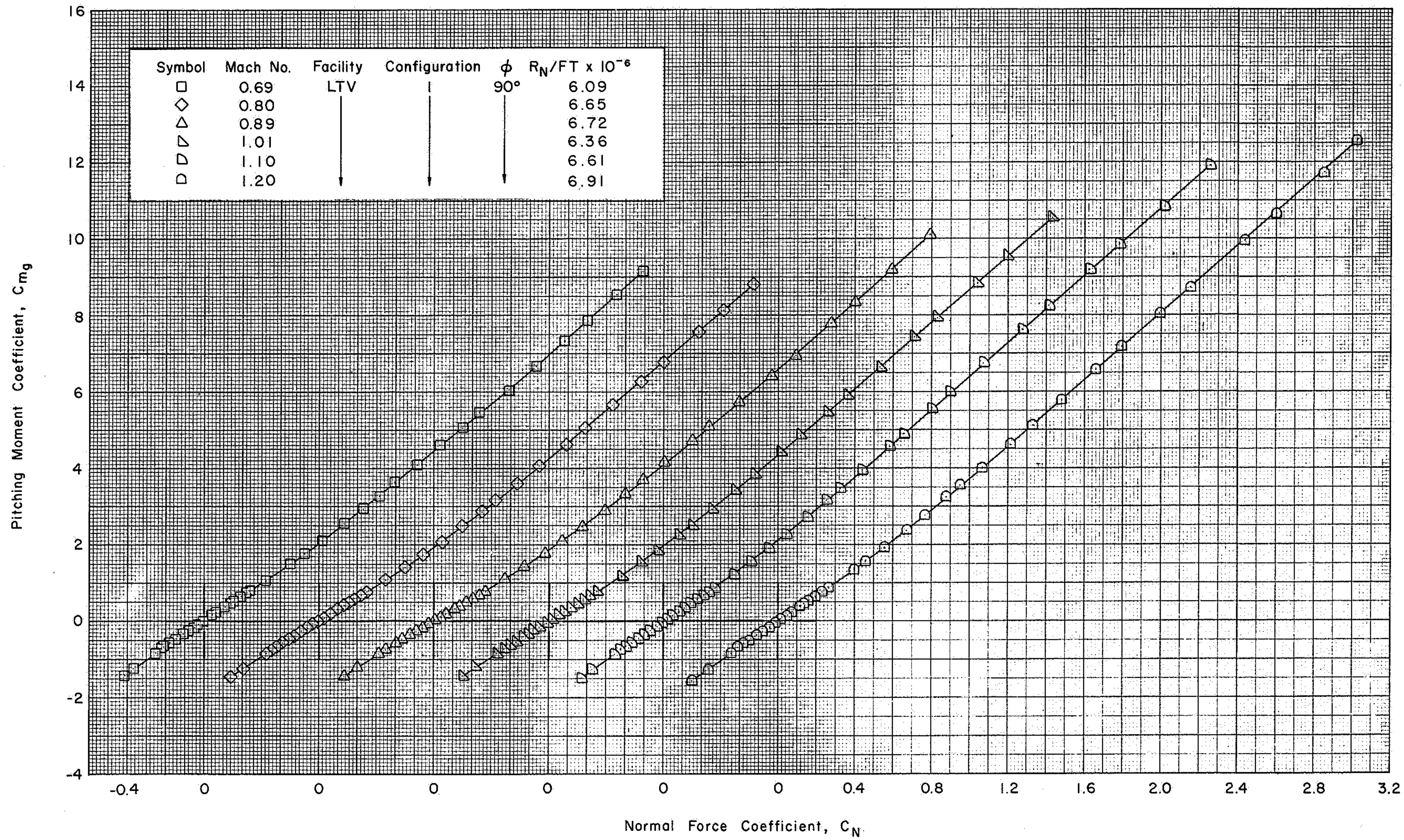

(f) C_{m_g} vs. C_N : ϕ=90° (M=0.69–1.20)

Figure 13 Continued

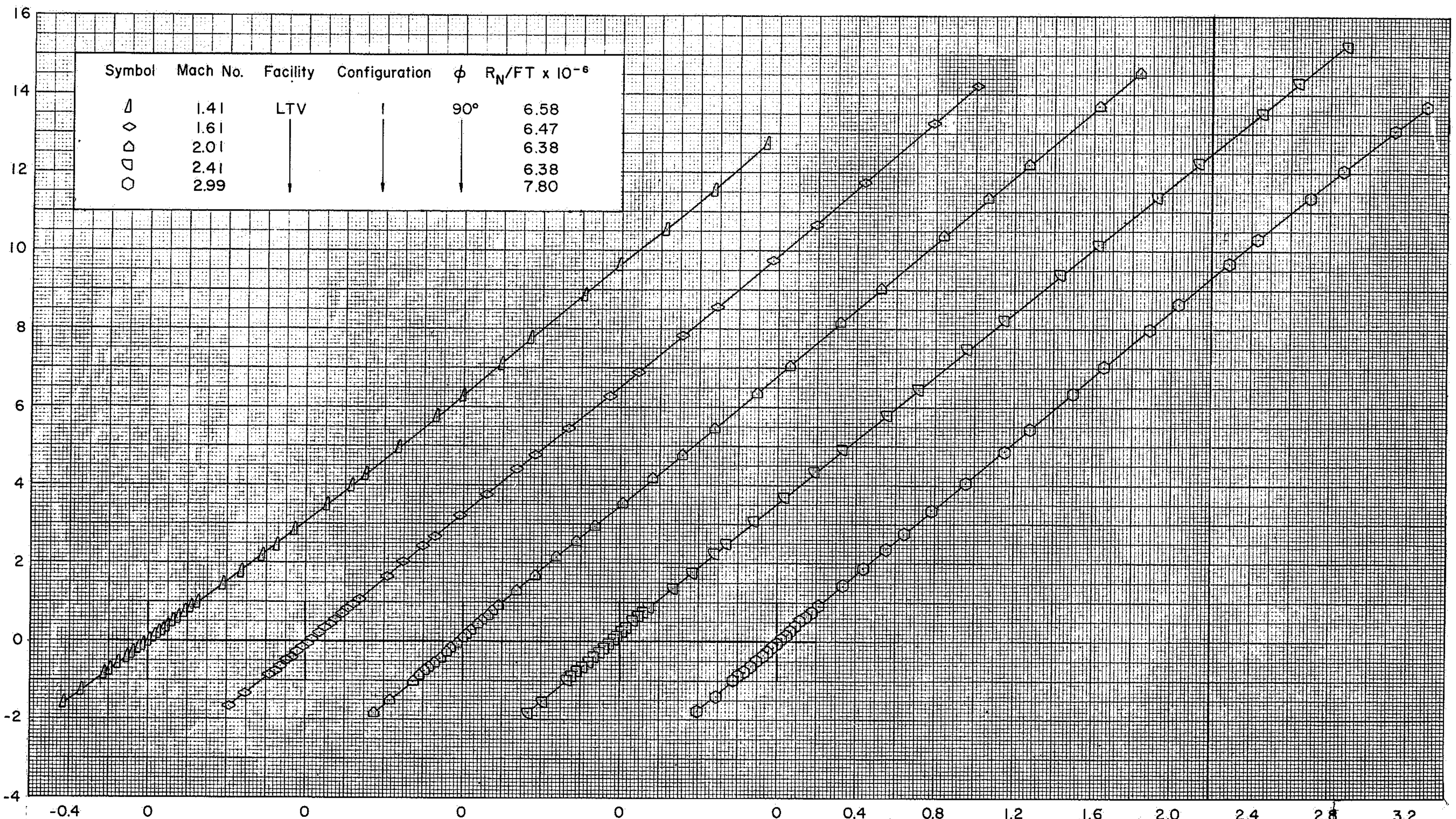

(f) Concluded : ϕ=90° (M=1.41−2.99)

Figure 13 Concluded

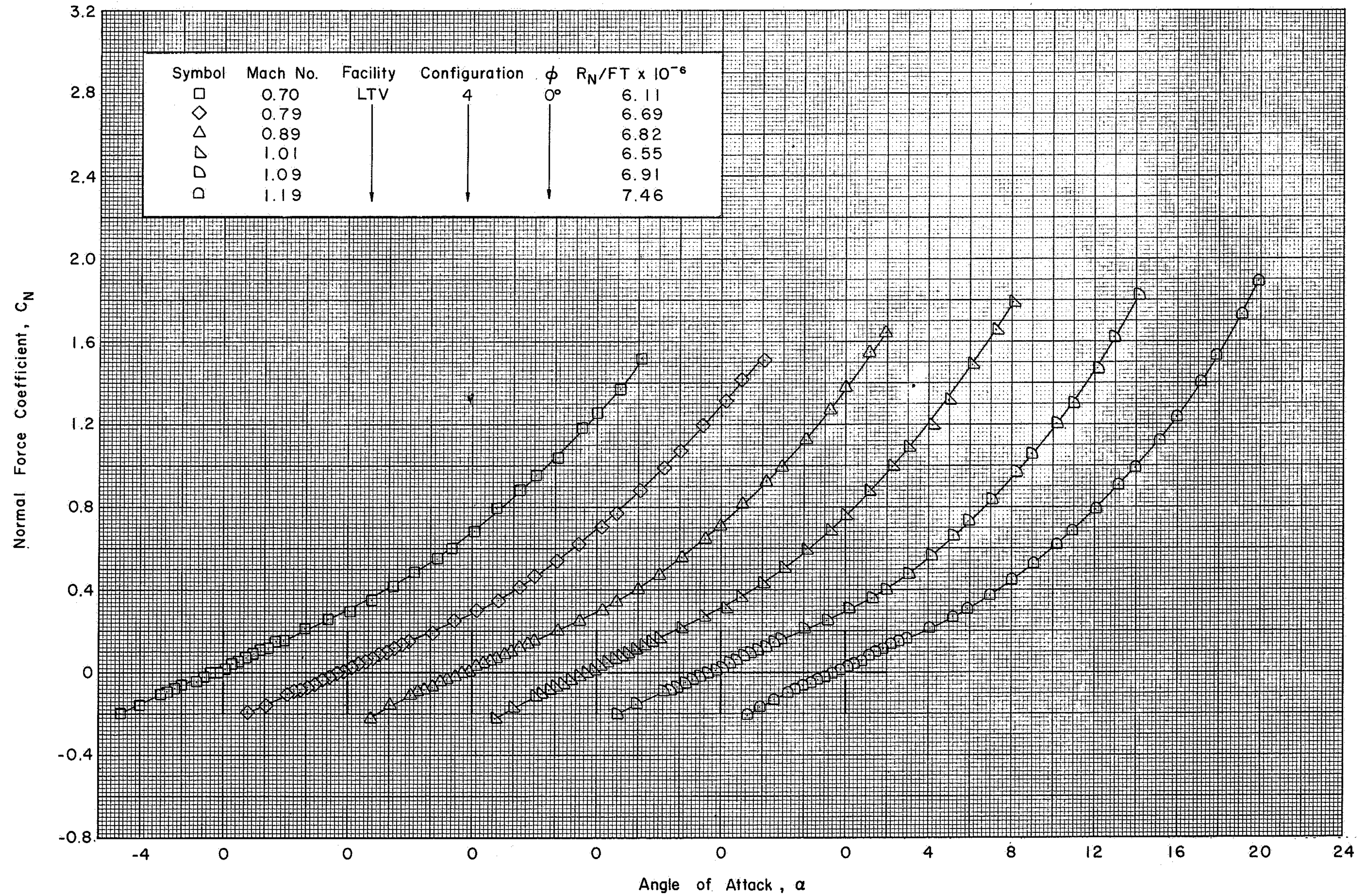

(a) C_N vs. α : $\phi = 0°$ (M=0.70-1.19)

Figure 14 Static Aerodynamic Characteristics of the APOLLO-SATURN V Launch Vehicle without Fins, Shrouds, and Base Flow Deflectors in the LTV 4-Foot High Speed Wind Tunnel

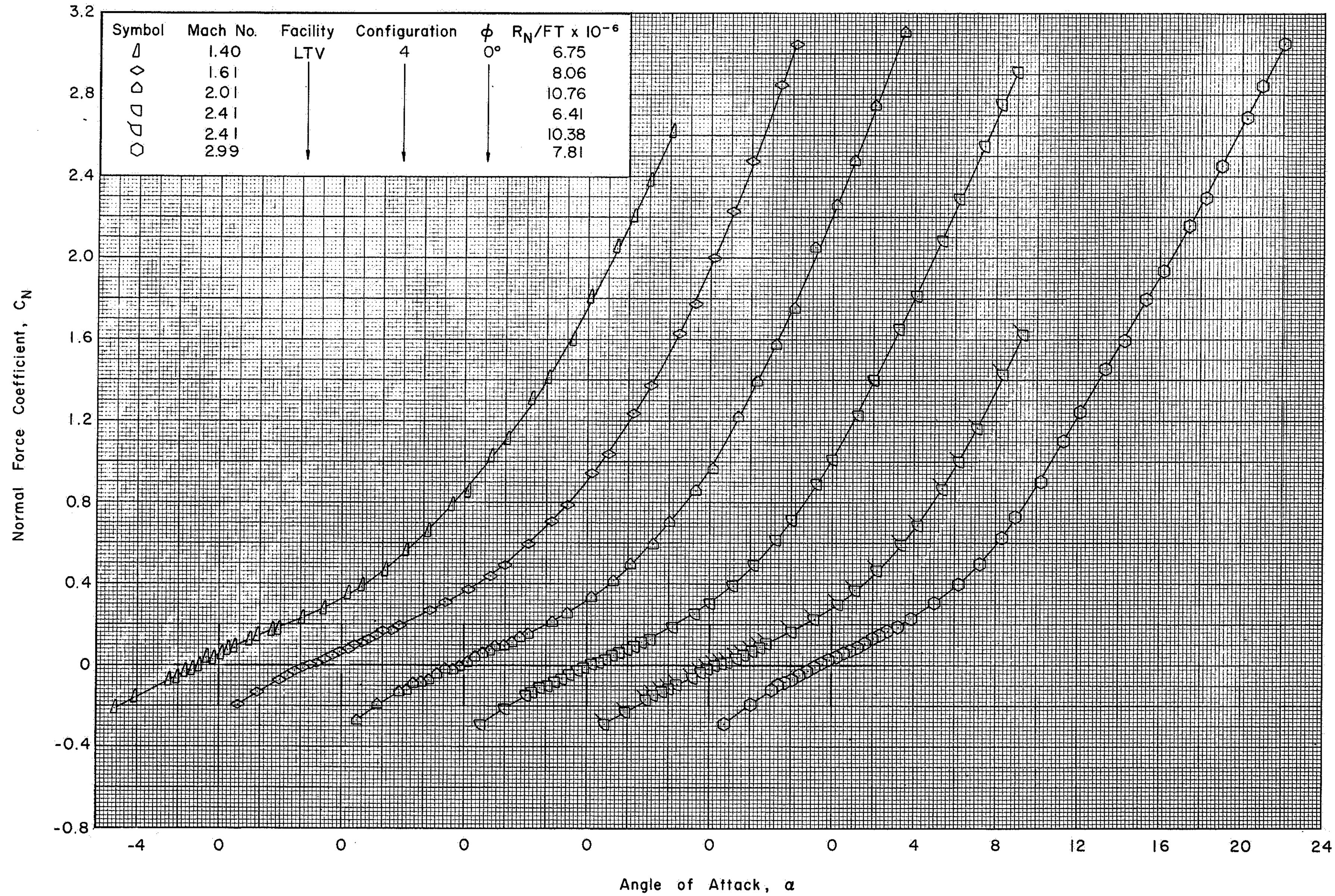

(a) Concluded : $\phi = 0°$ (M = 1.40-2.99)

Figure 14 Continued

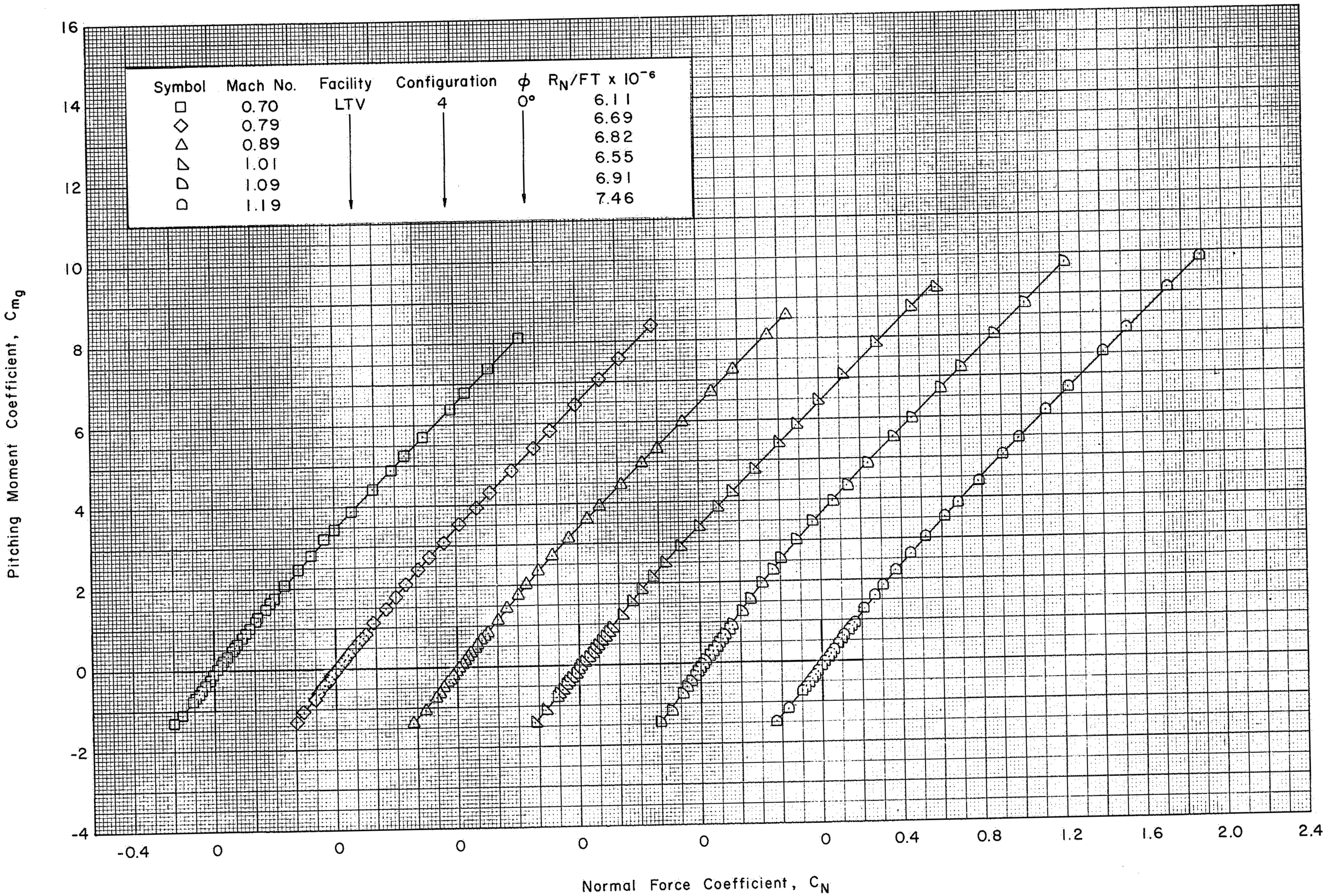

(b) C_{m_g} vs. C_N : $\phi = 0°$ (M=0.70-1.19)

Figure 14 Continued

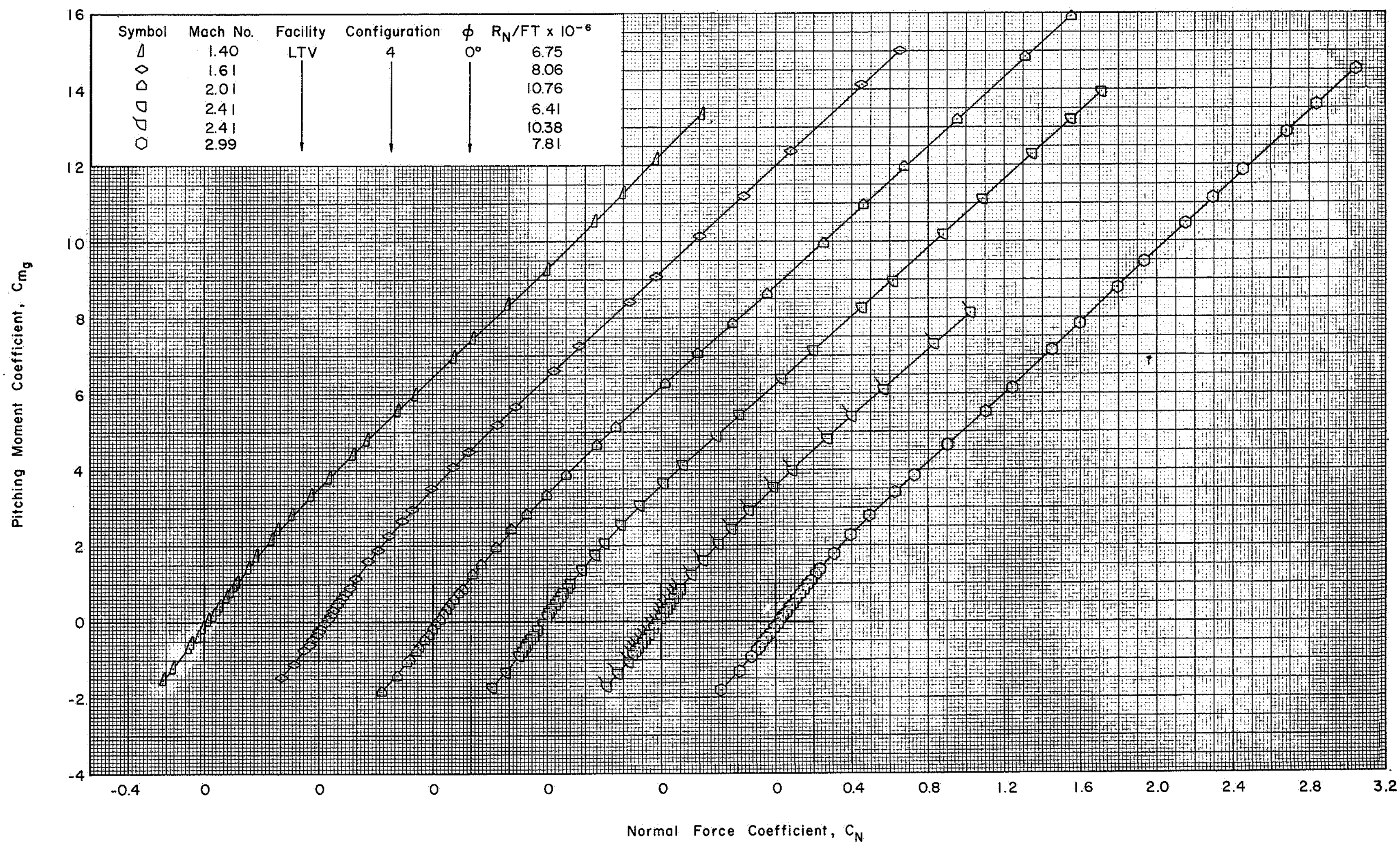

(b) Concluded : ϕ=0° (M=1.40–2.99)

Figure 14 Continued

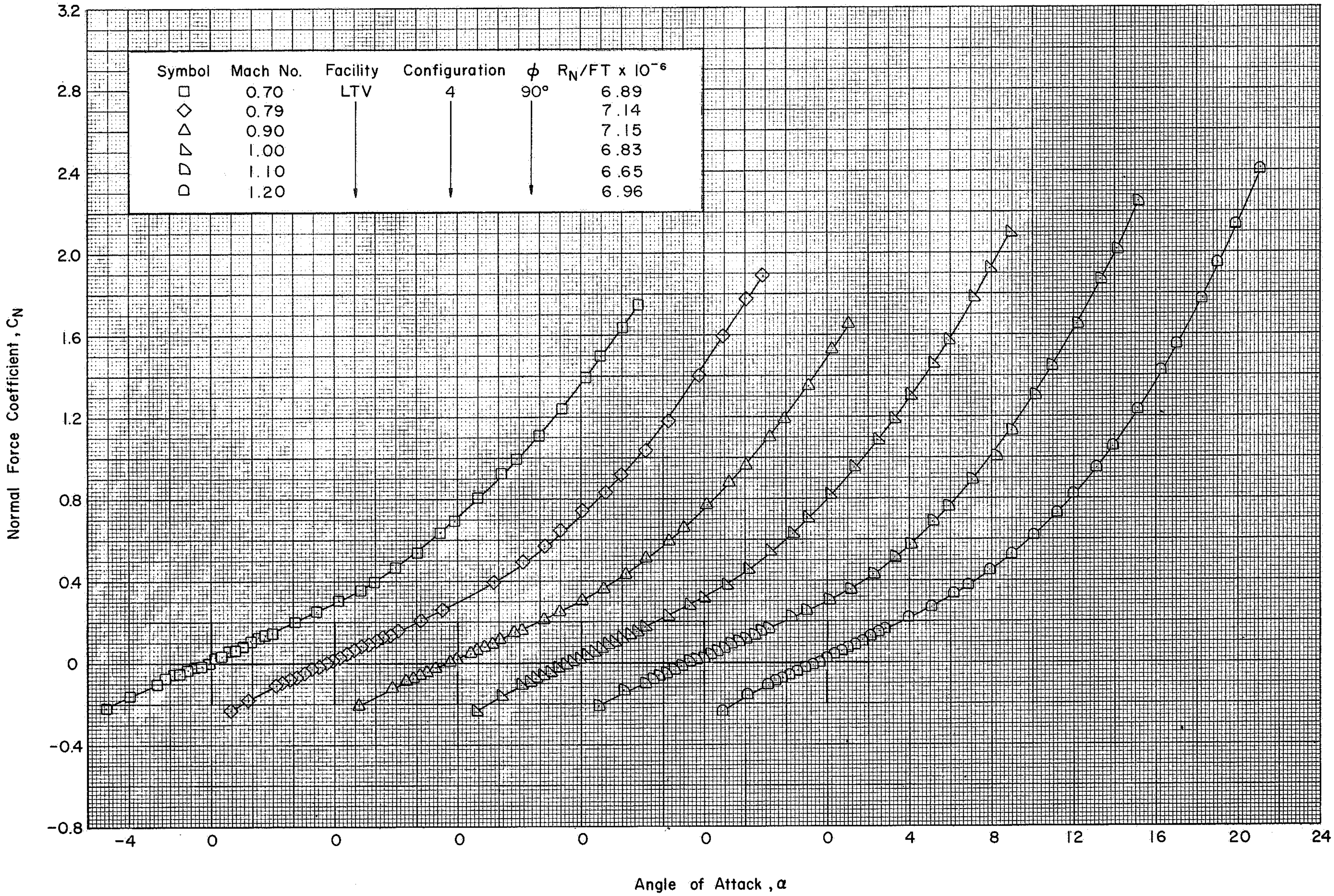

(c) C_N vs. α : ϕ=90° (M=0.70–1.20)

Figure 14 Continued

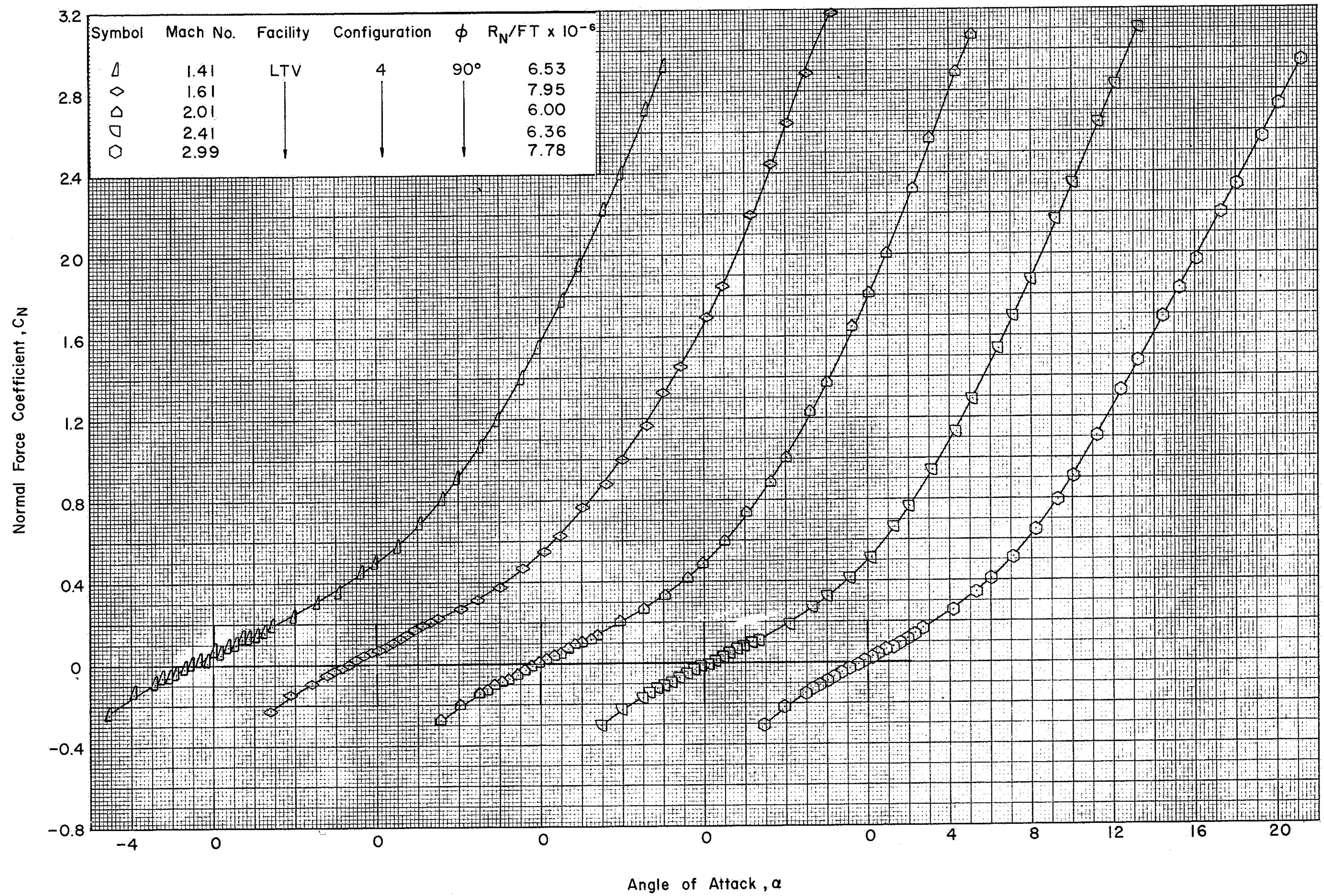

(c) Concluded : ϕ=90° (M=1.41 -2.99)

Figure 14 Continued

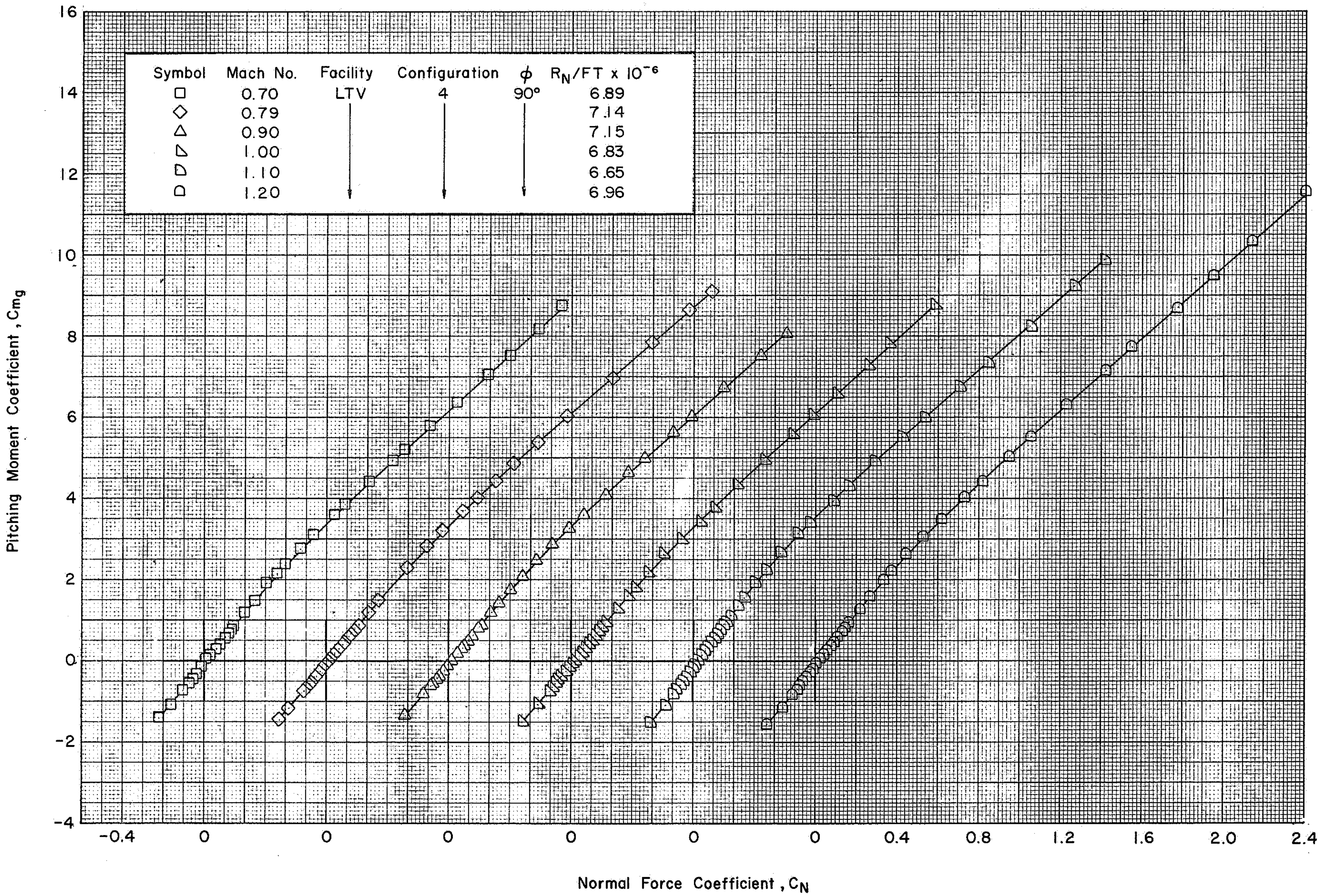

(d) C_{m_g} vs. C_N : ϕ=90° (M=0.70–1.20)

Figure 14 Continued

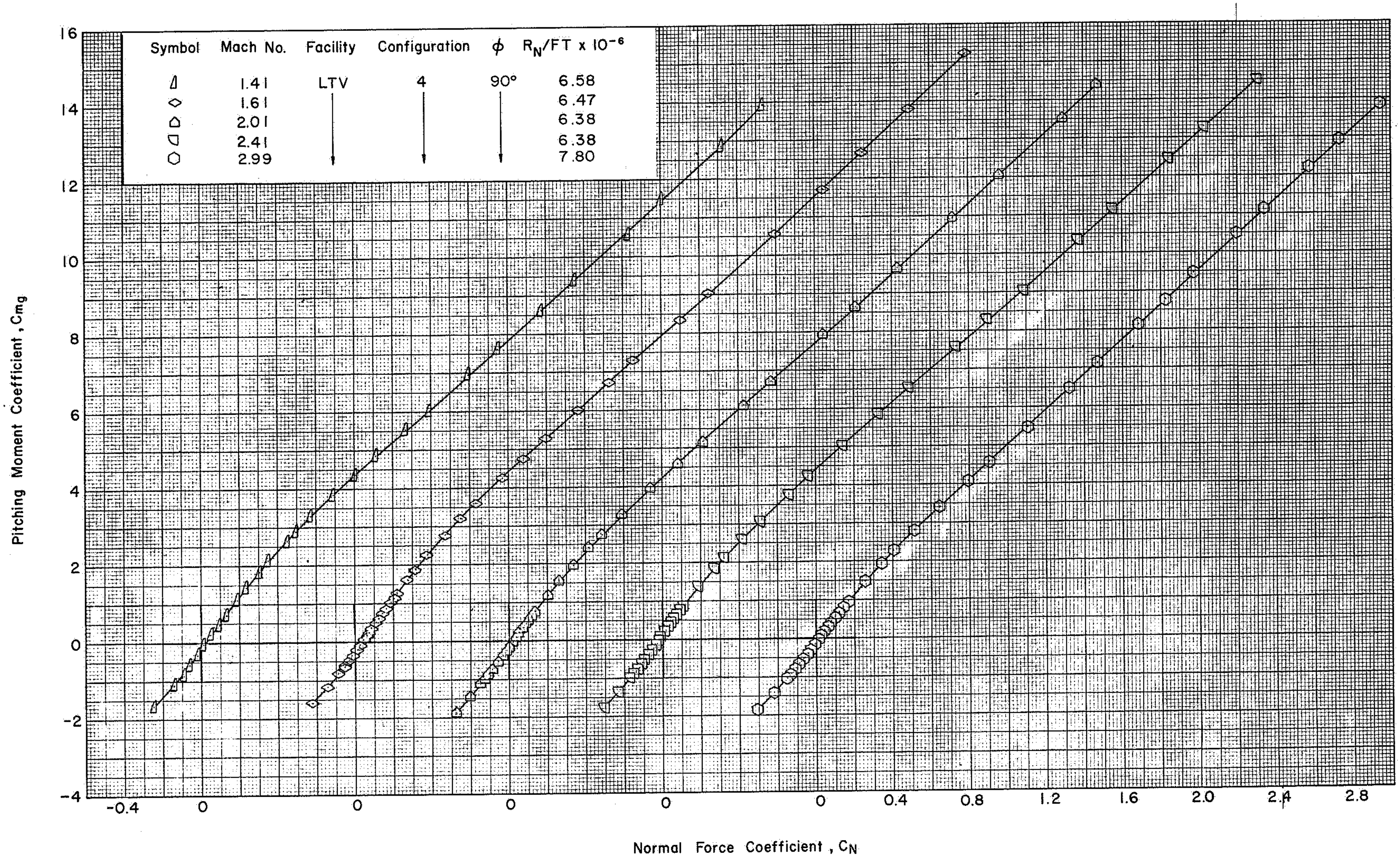

(d) Concluded : $\phi = 90°$ (M=1.41 - 2.99)

Figure 14 Concluded

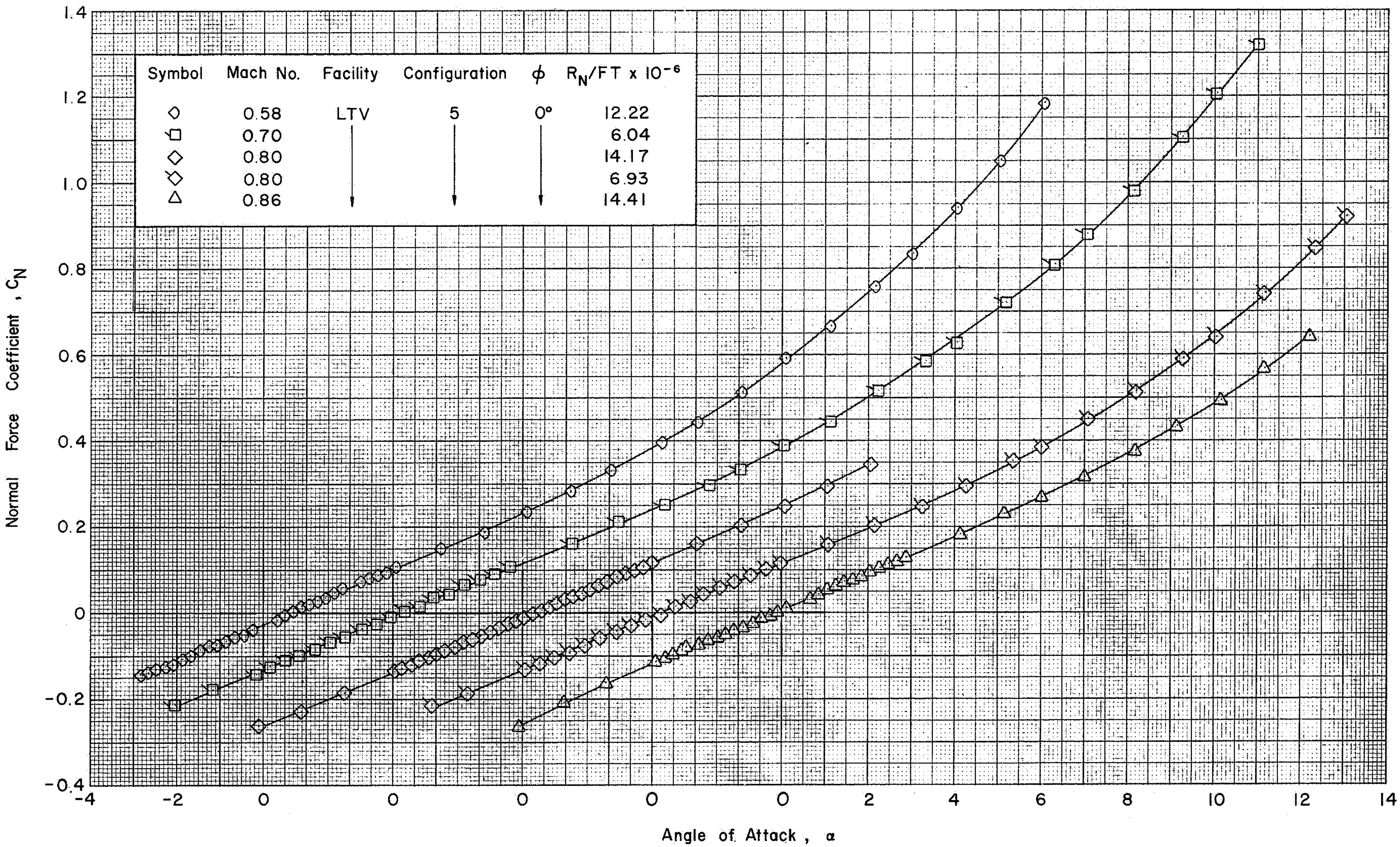

(a) C_N vs. α : $\phi = 0°$ (M=0.58-0.86)

Figure 15 Static Aerodynamic Characteristics of the APOLLO-SATURN V Launch Vehicle without Fins, Shrouds and Protuberances in the LTV 4-Foot High Speed Wind Tunnel

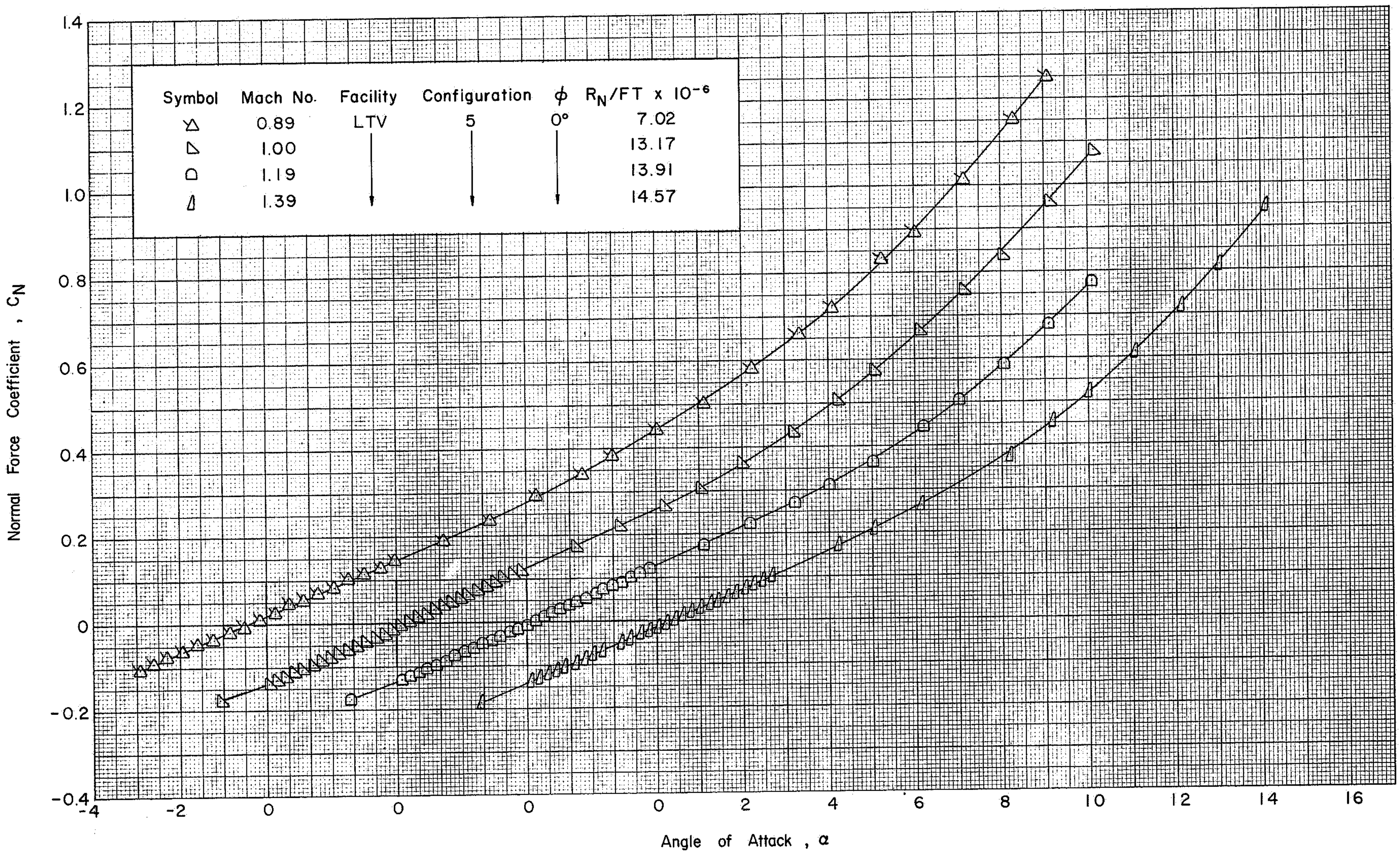

(a) Concluded : ϕ = 0° (M = 0.89-1.39)

Figure 15 Continued

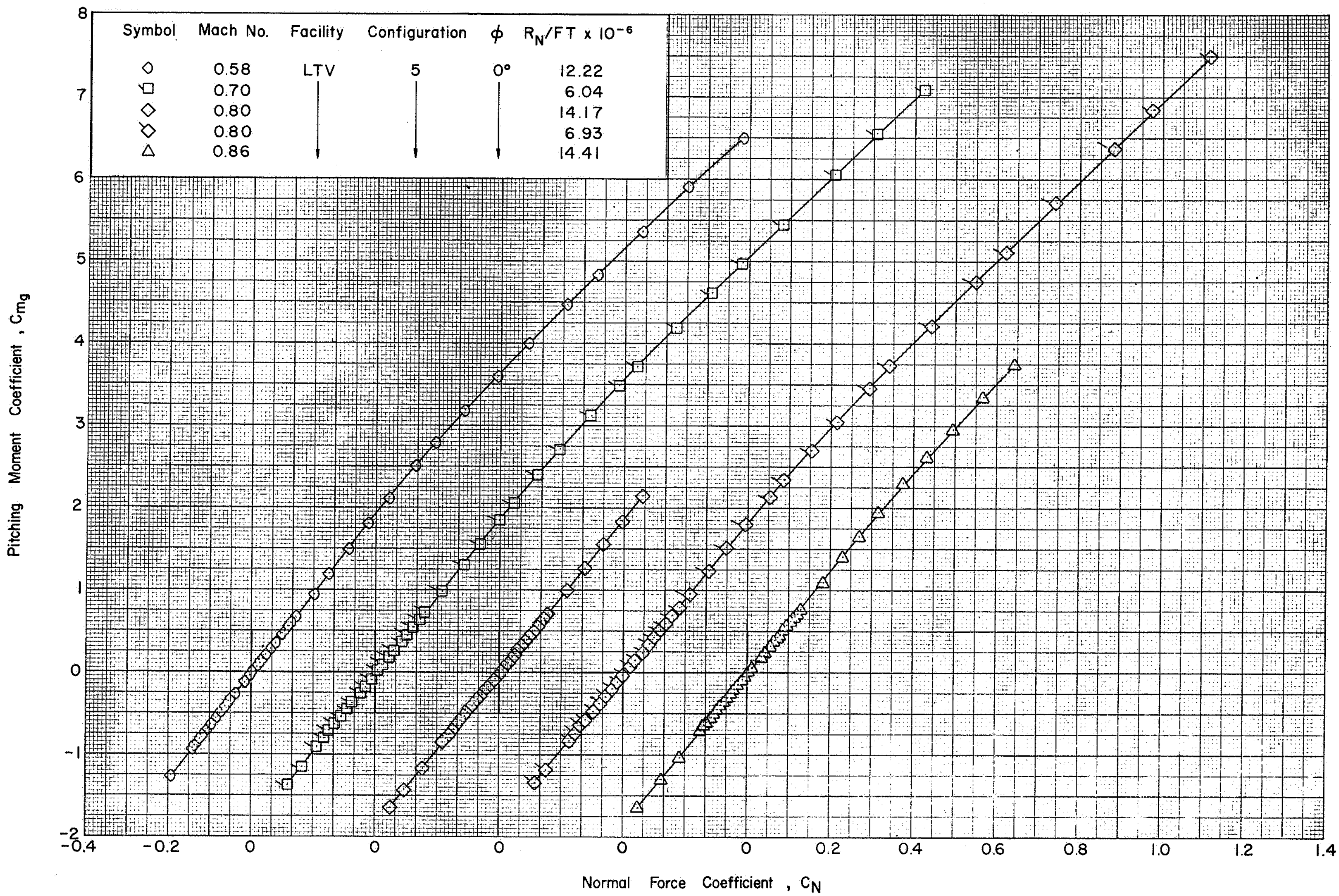

(b) C_{m_g} vs. C_N: $\phi = 0°$ (M=0.58-0.86)

Figure 15 Continued

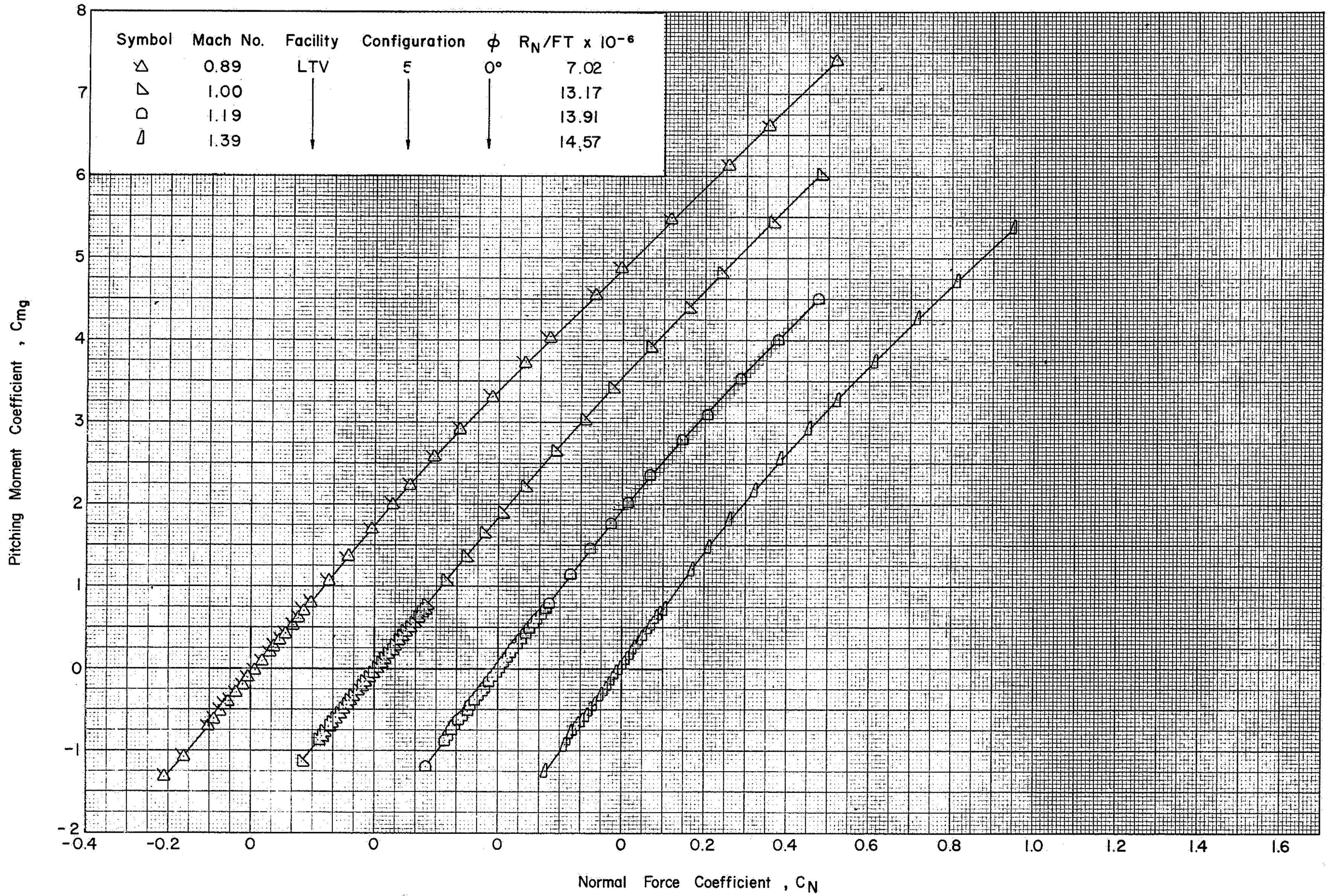

(b) Concluded: ϕ = 0°(M=0.89-1.39)

Figure 15 Concluded

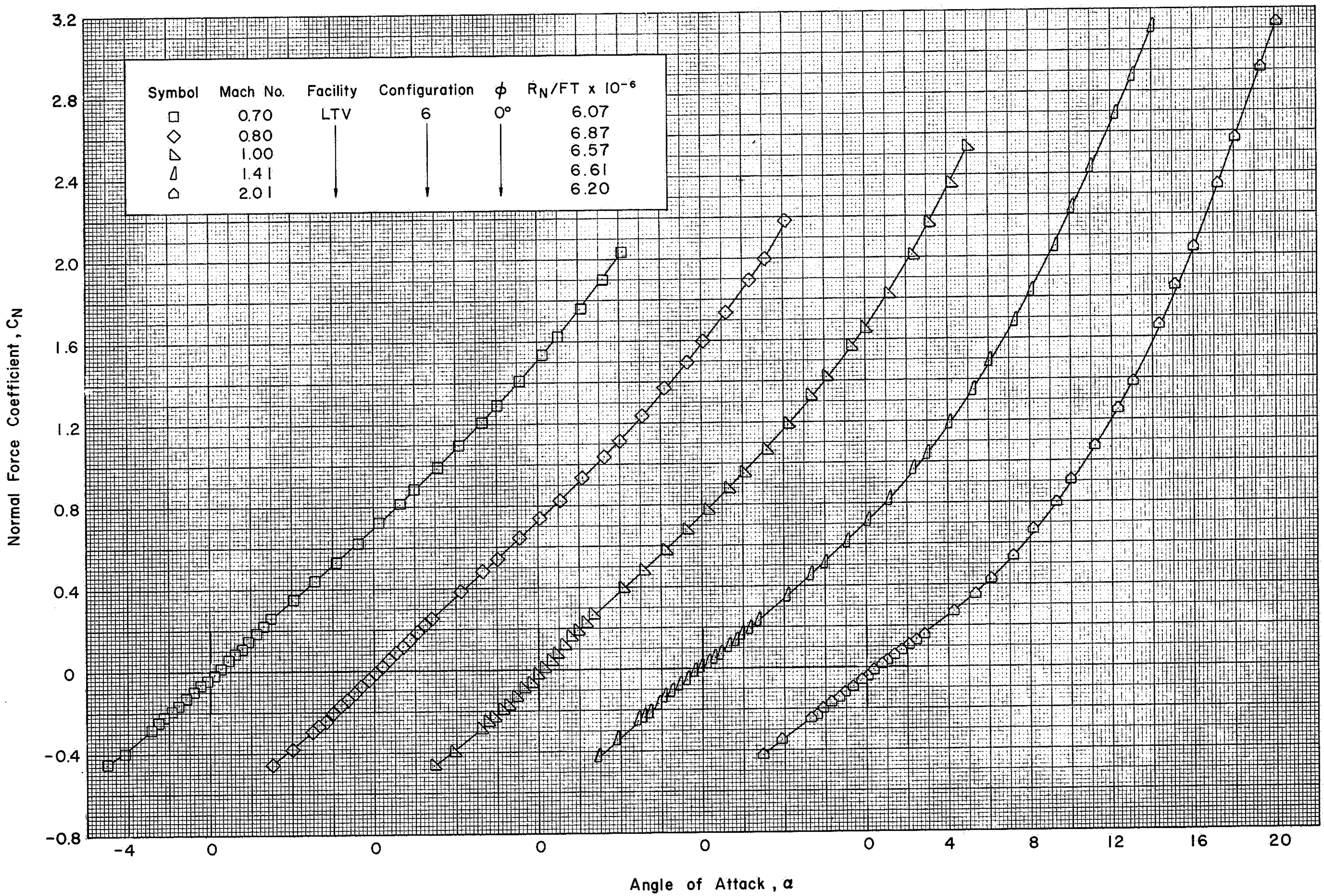

(a) C_N vs. α : $\phi = 0°$ (M=0.70–2.01)

Figure 16 Static Aerodynamic Characteristics of the APOLLO-SATURN V Launch Vehicle without LES and Command Module in the LTV 4-Foot High Speed Wind Tunnel

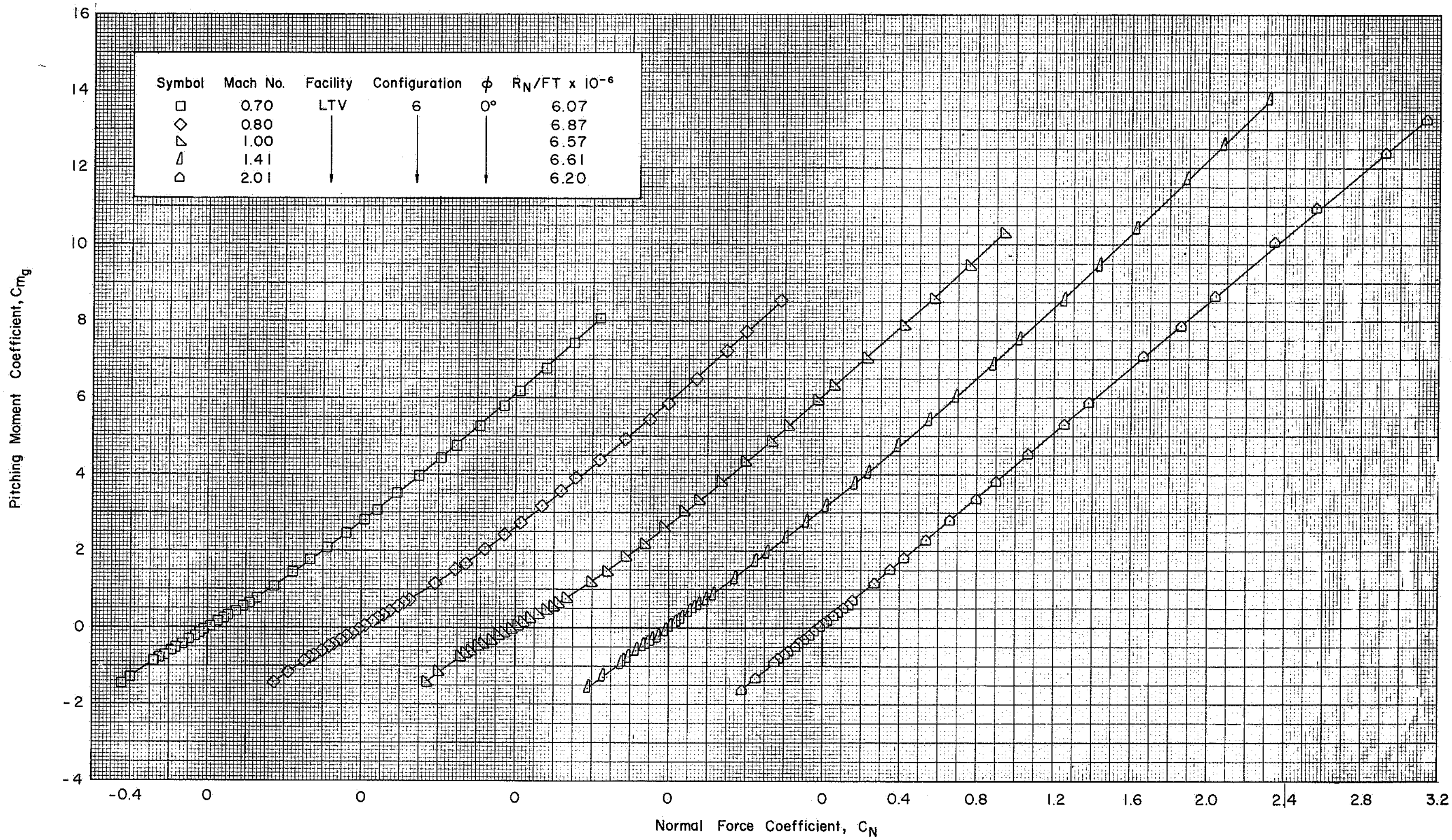

(b) C_{m_g} vs. C_N : $\phi = 0°$ (M=0.70-2.01)

Figure 16 Concluded

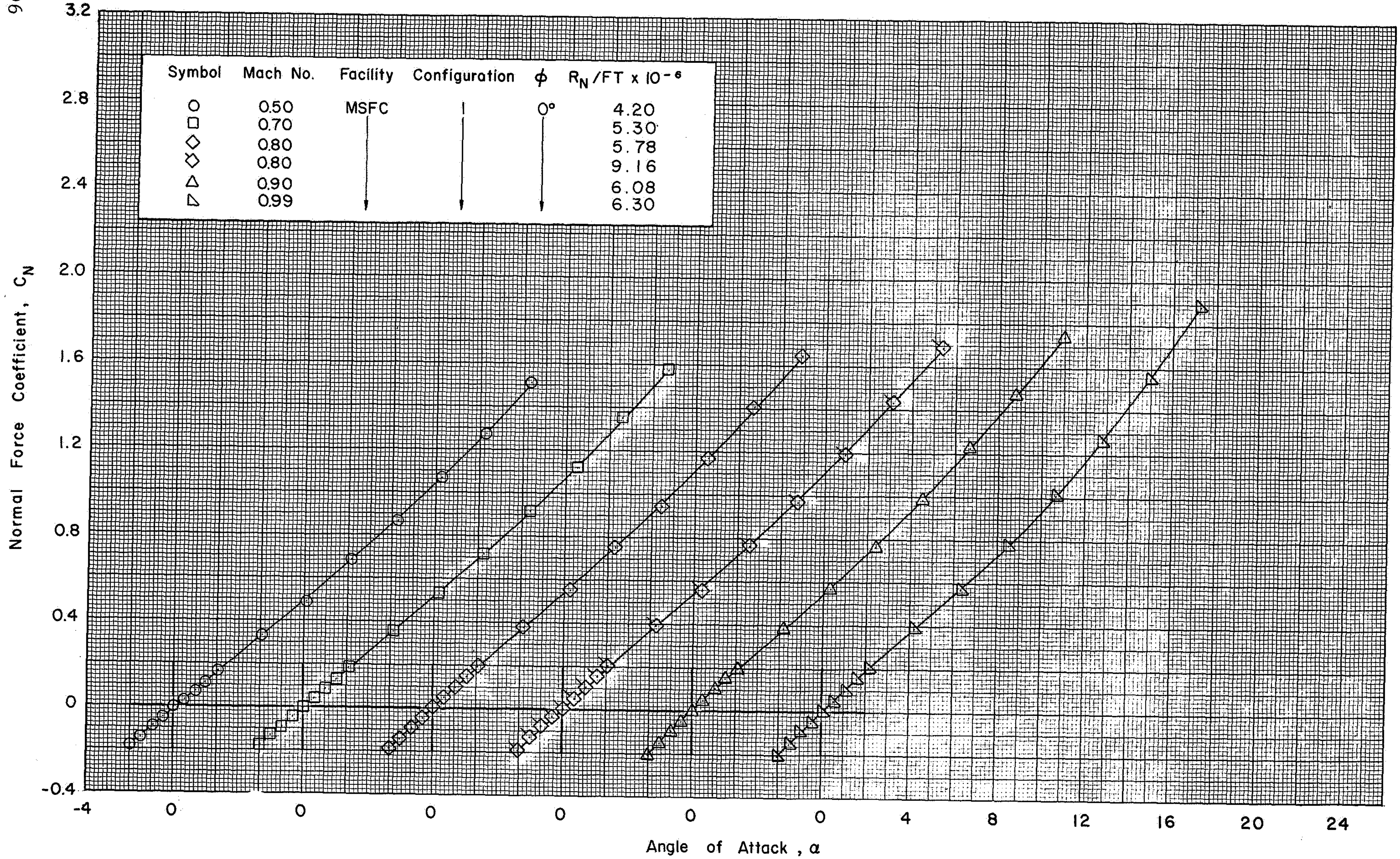

(a) C_N vs. α : $\phi = 0°$ (M=0.50-0.99)

Figure 17 Static Aerodynamic Characteristics of the APOLLO-SATURN V Launch Vehicle in the MSFC 14-Inch Trisonic Wind Tunnel

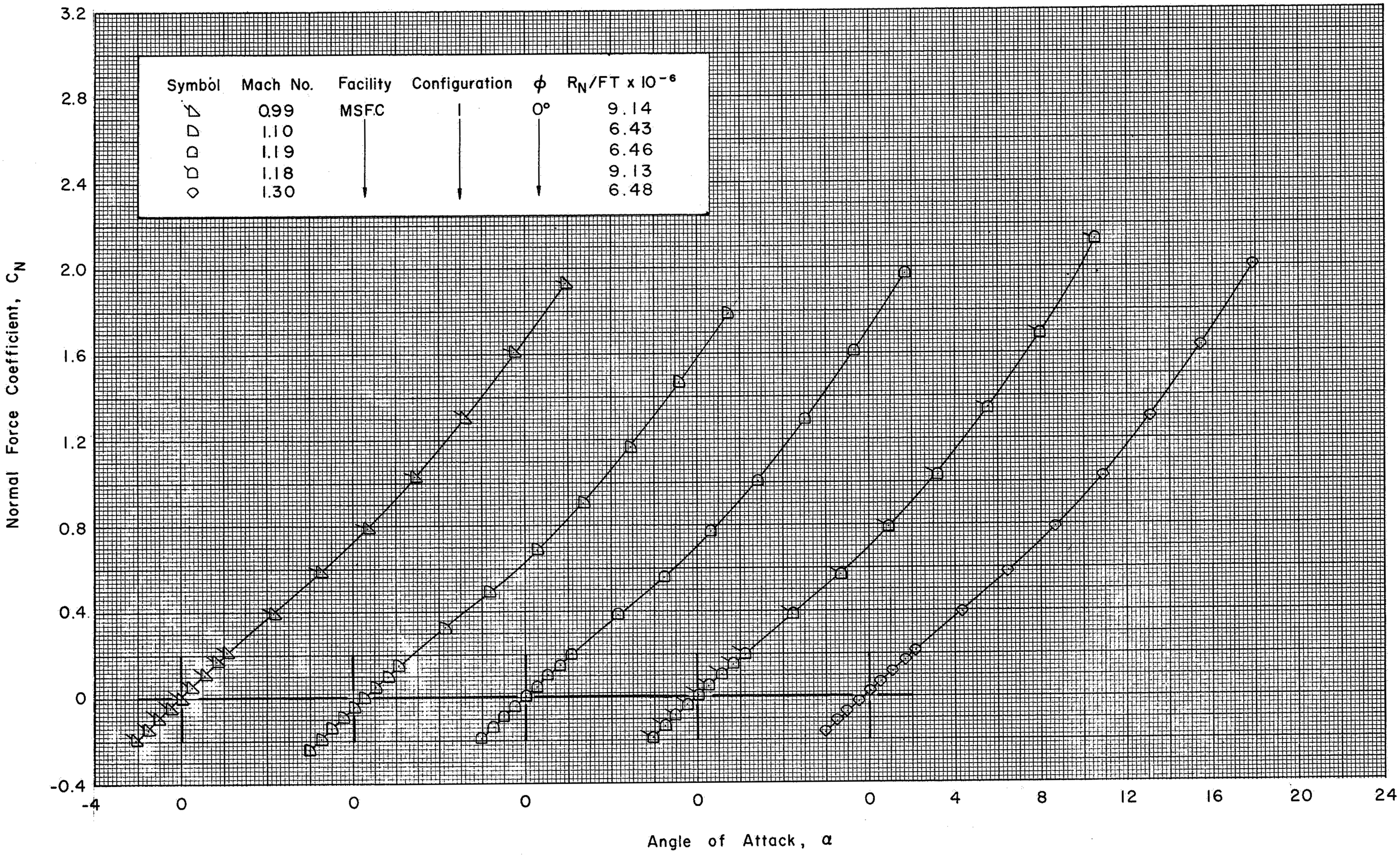

(a) Continued : $\phi = 0°$ (M=0.99-1.30)

Figure 17 Continued

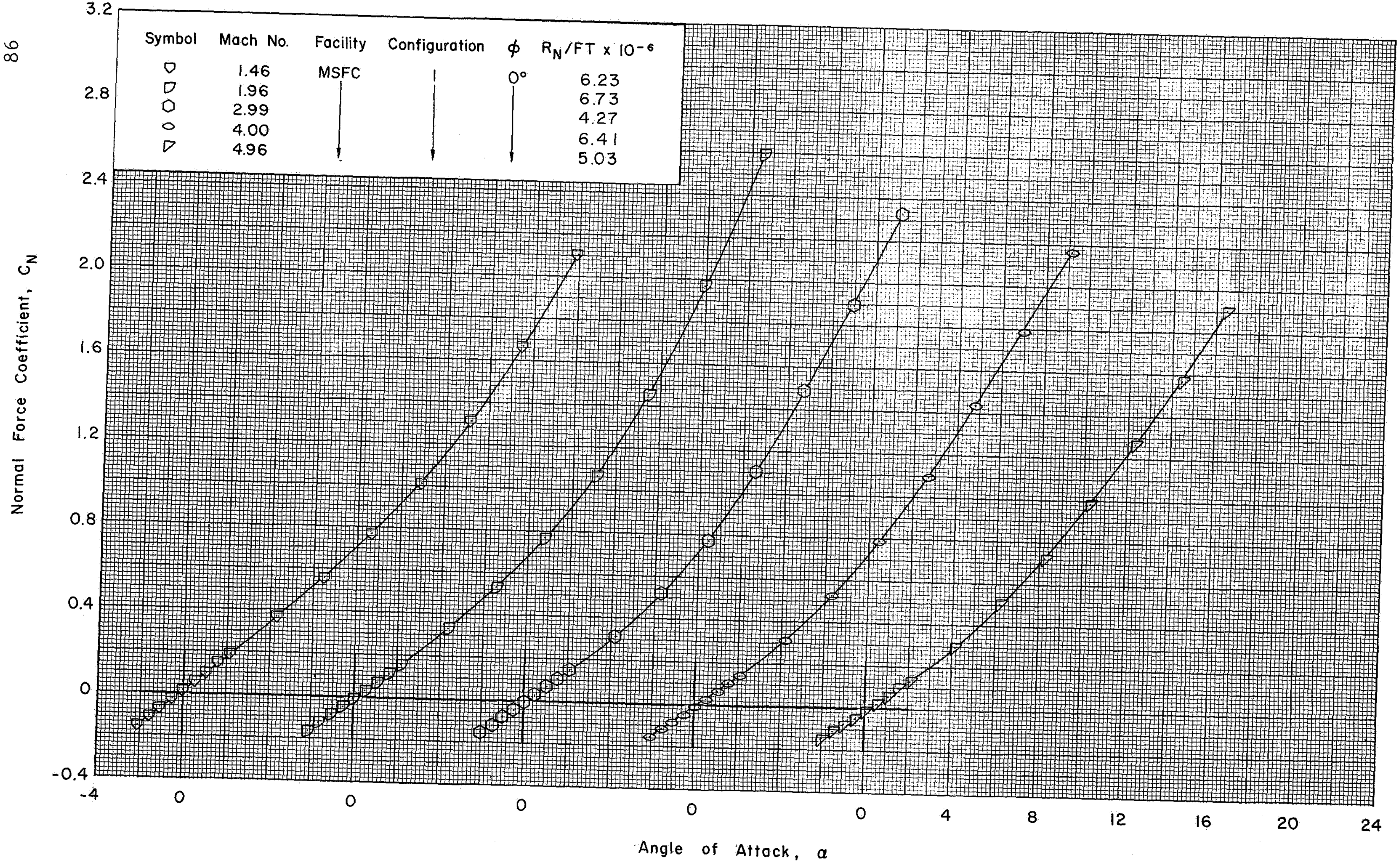

(a) Concluded: ϕ=0° (M=1.46–4.96)

Figure 17 Continued

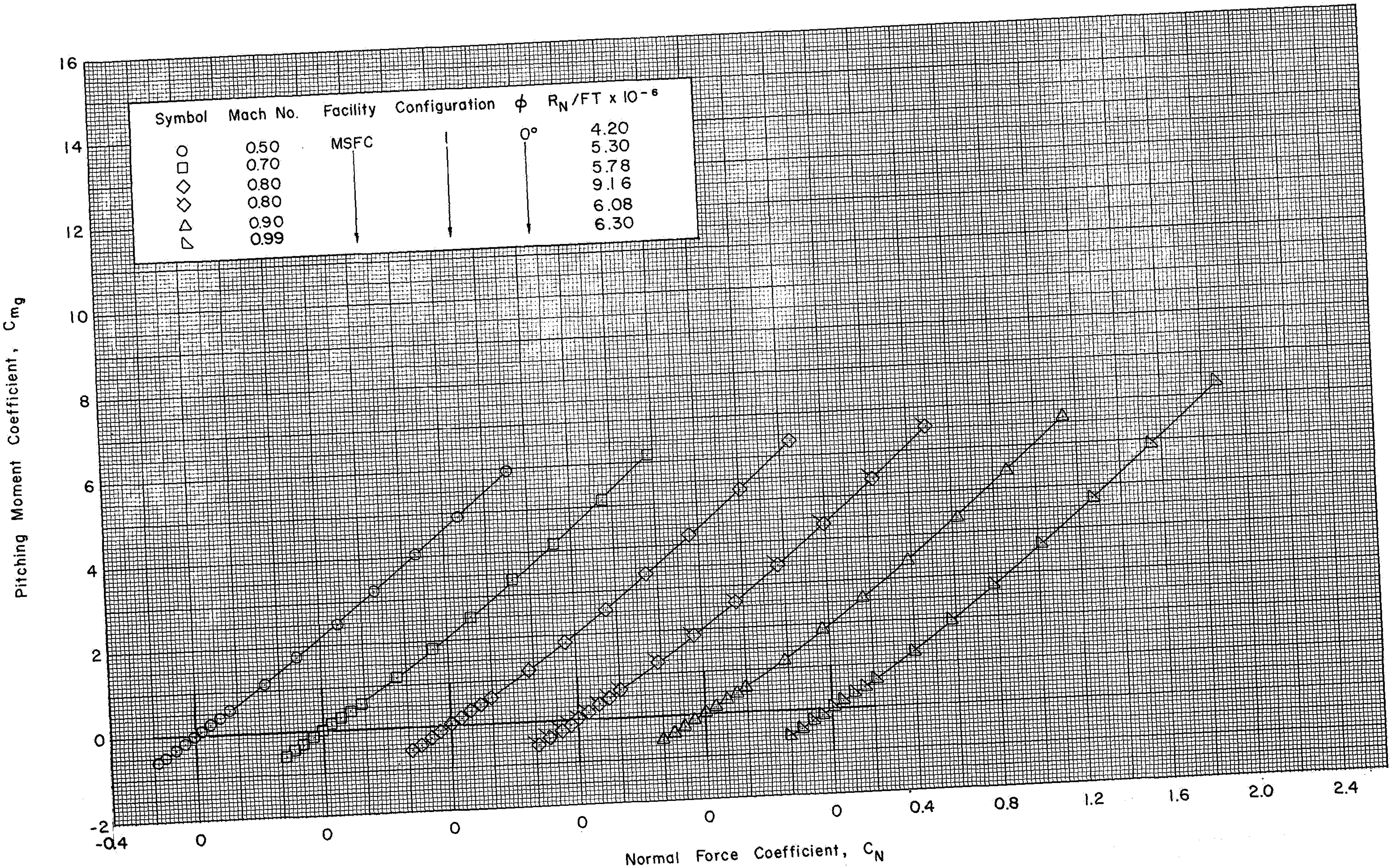

(b) C_{m_g} vs. C_N : $\phi = 0°$ (M=0.50-0.99)

Figure 17 Continued

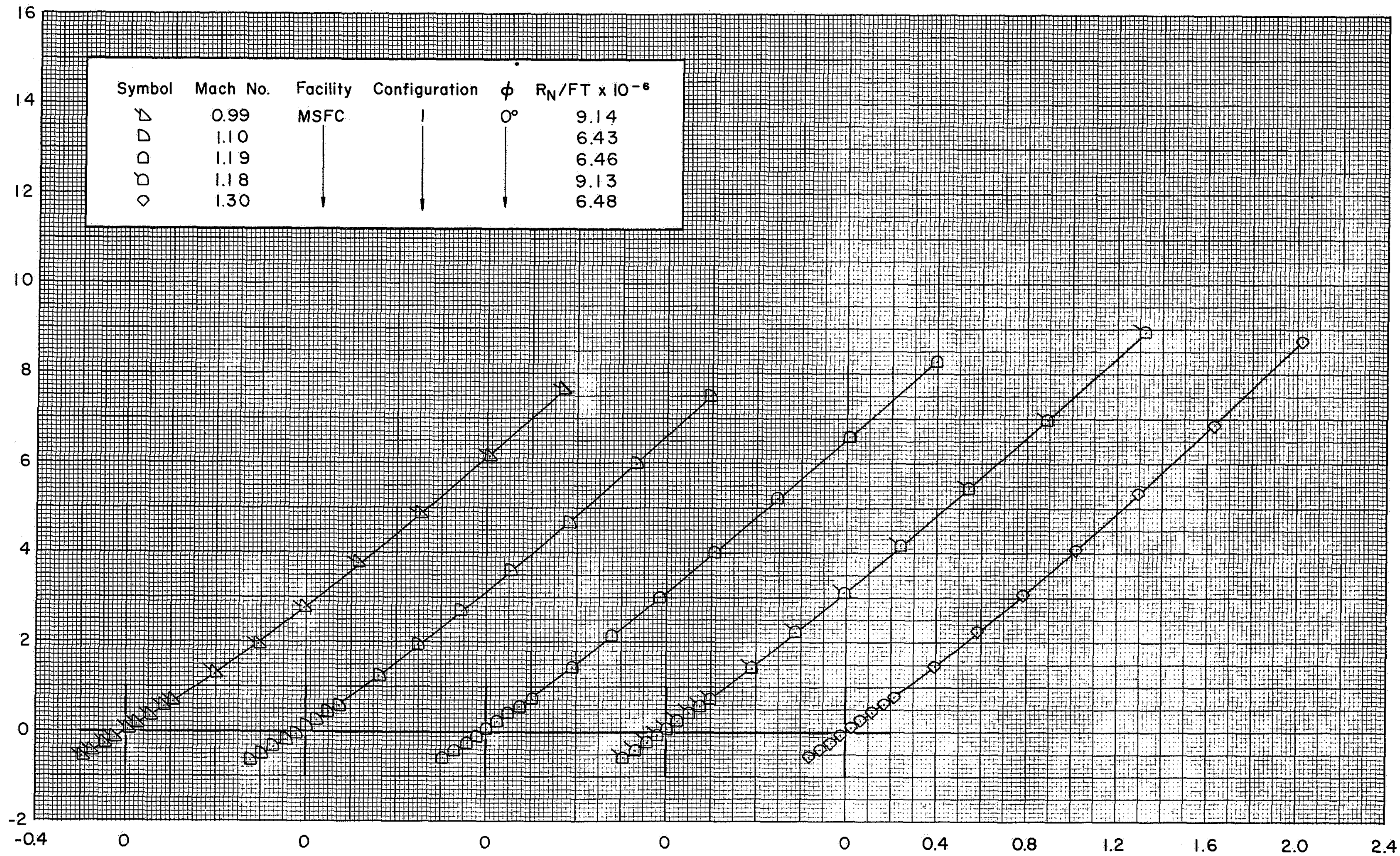

(b) Continued : $\phi = 0°$ (M=0.99-1.30)

Figure 17 Continued

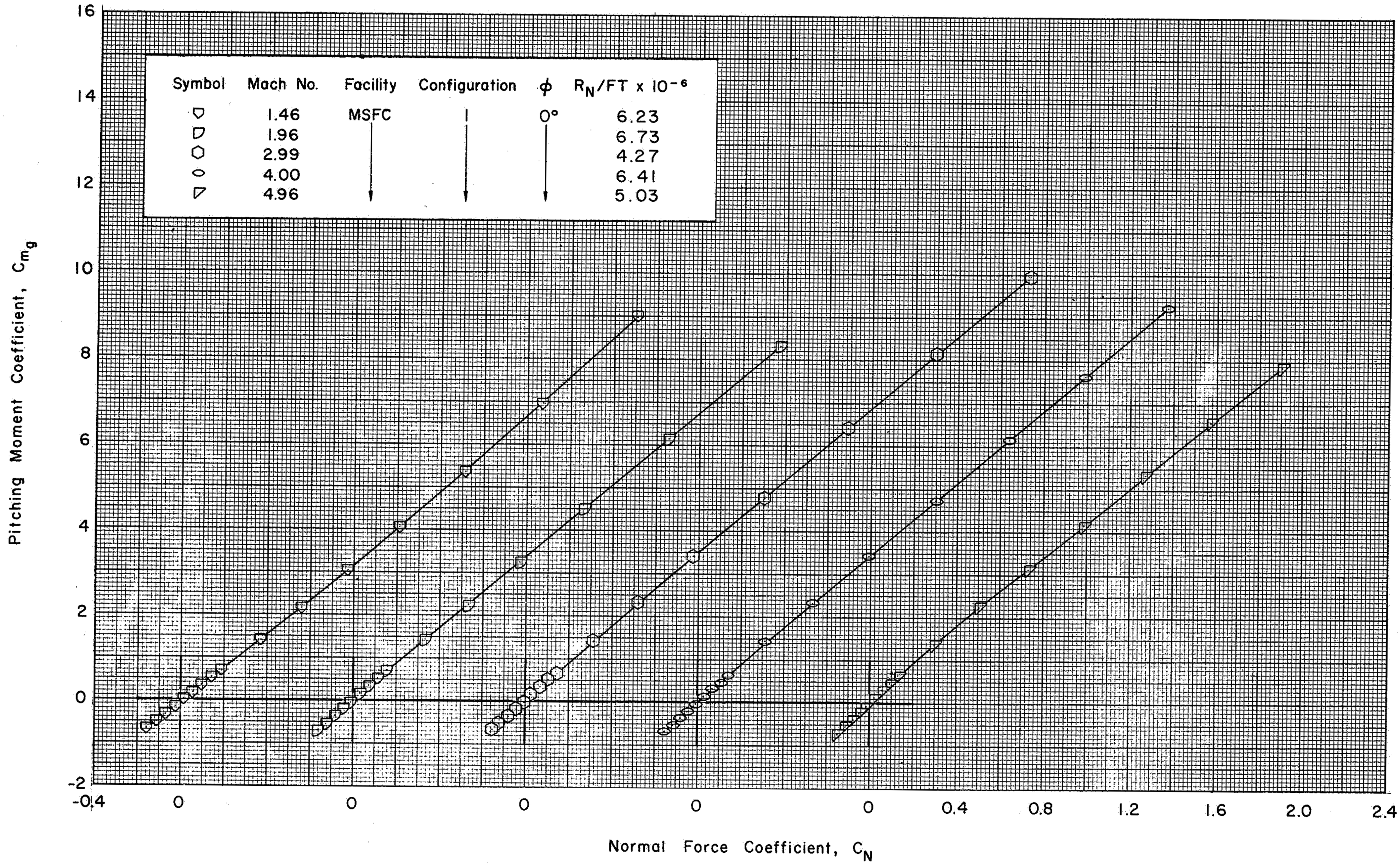

(b) Concluded : ϕ=0° (M=1.46–4.96)

Figure 17 Continued

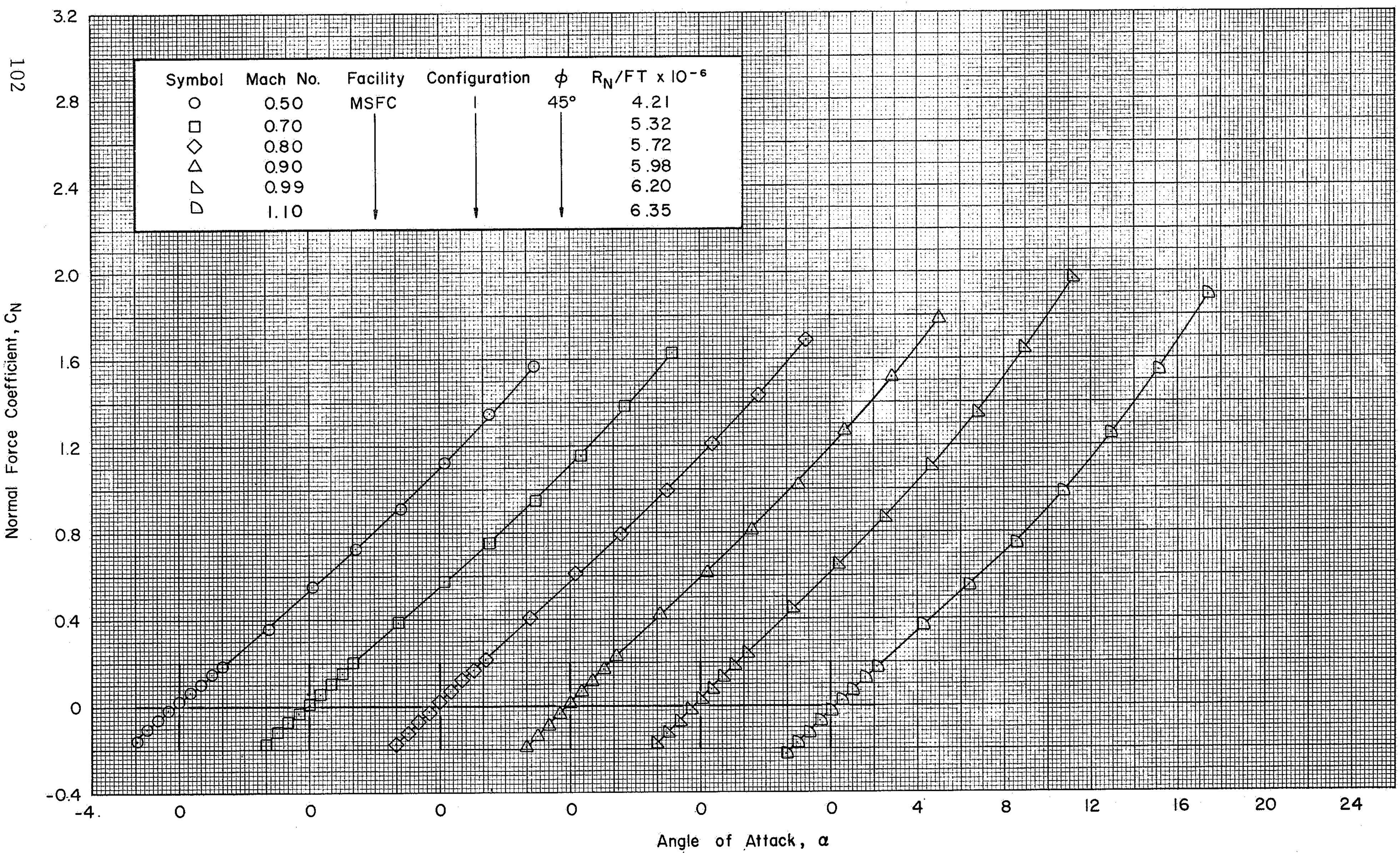

(c) C_N vs. α : $\phi = 45°$ (M=0.50-1.10)

Figure 17 Continued

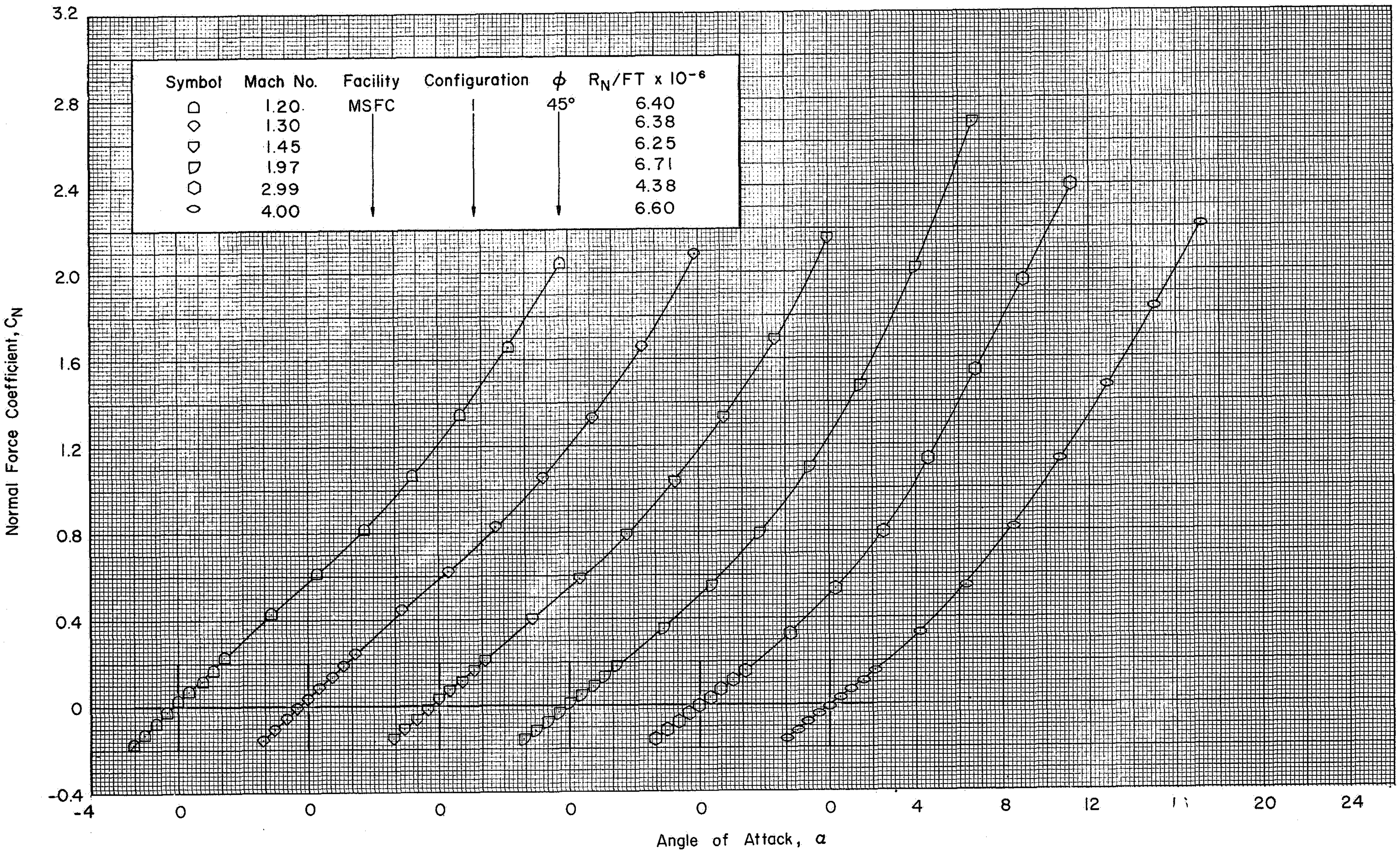

(c) Concluded : $\phi = 45°$ (M=1.20–4.00)

Figure 17 Continued

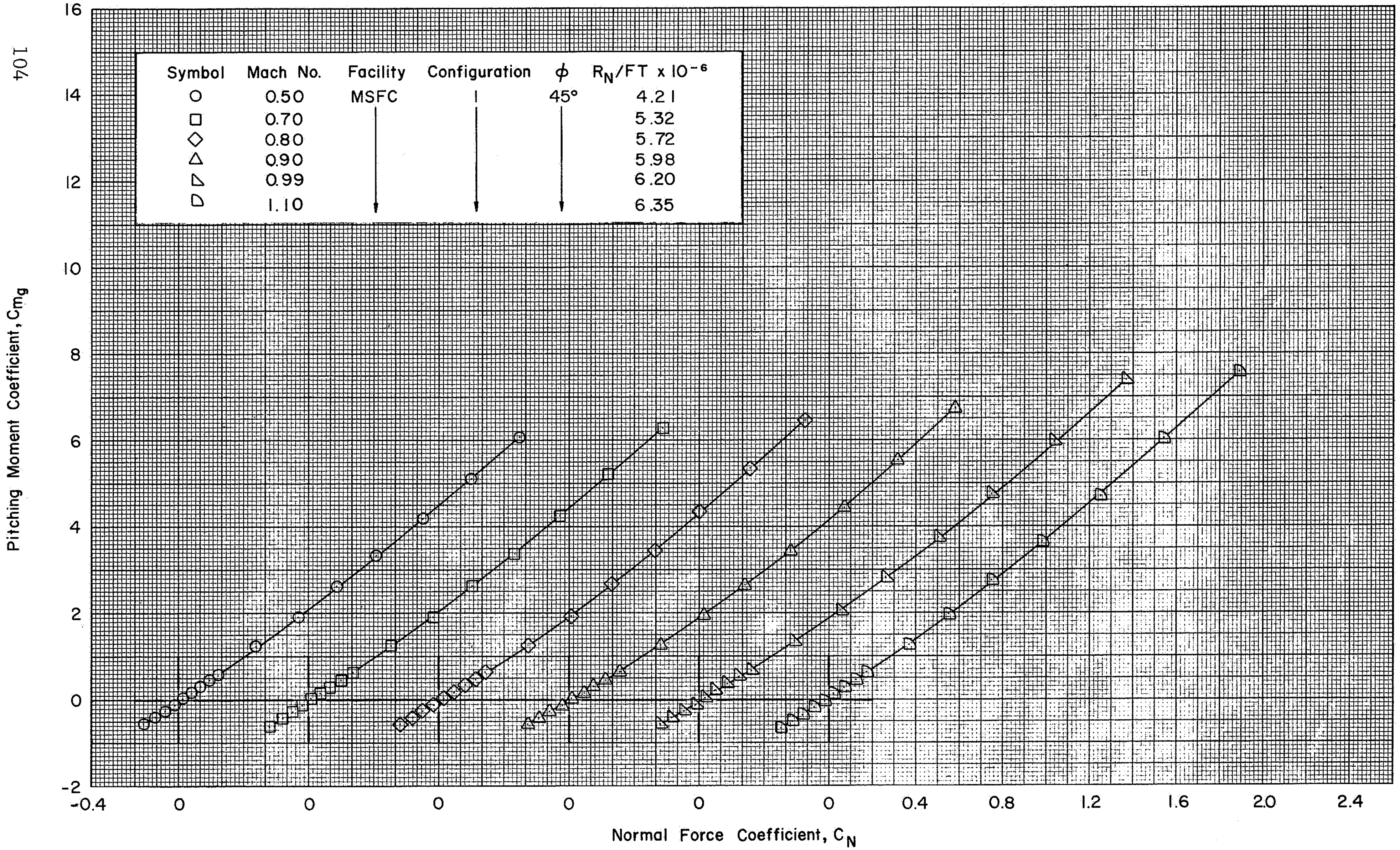

(d) C_{m_g} vs. C_N : $\phi = 45°$ (M=0.50-1.10)

Figure 17 Continued

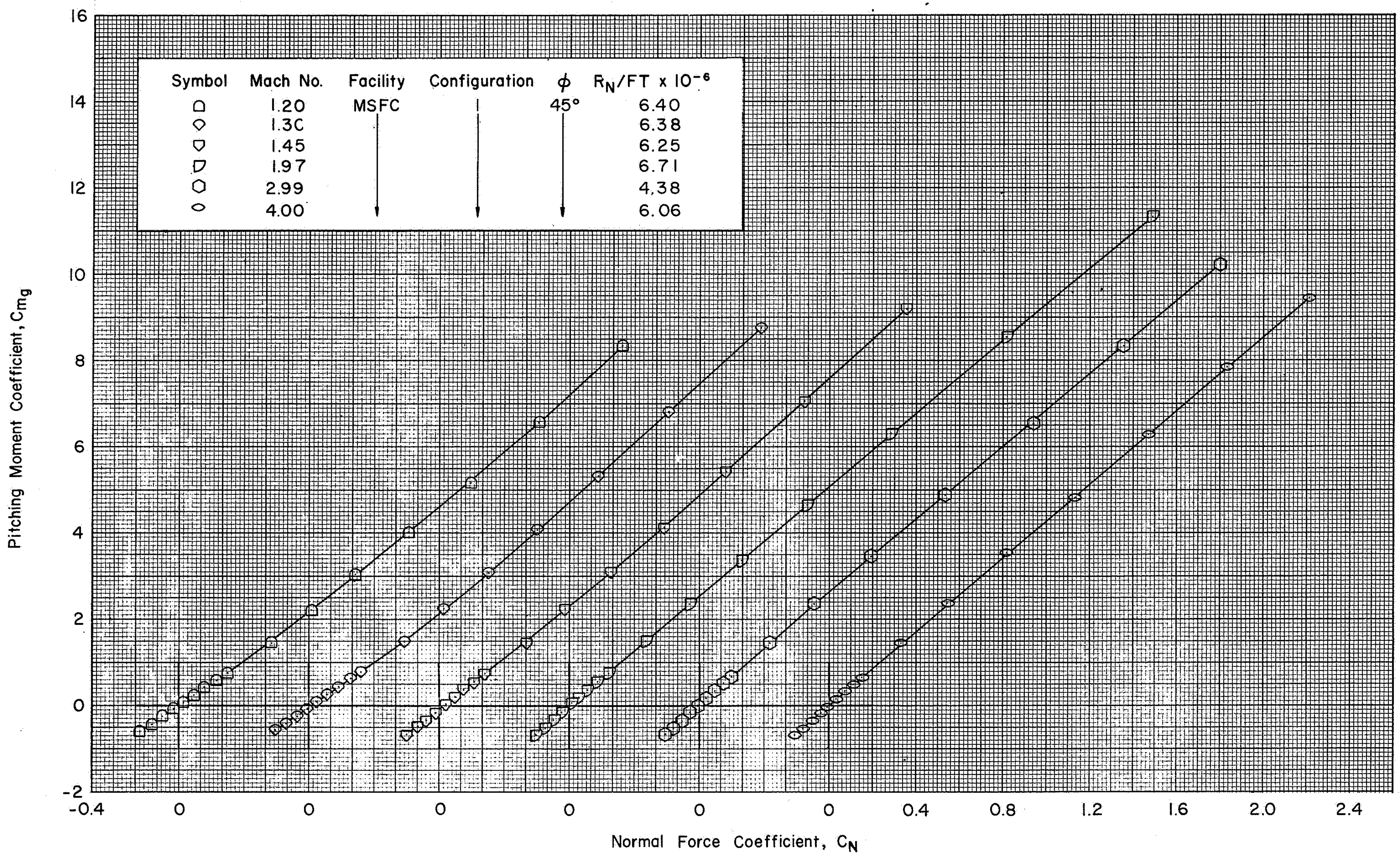

(d) Concluded : $\phi = 45°$ (M=1.20-4.00)

Figure 17 Continued

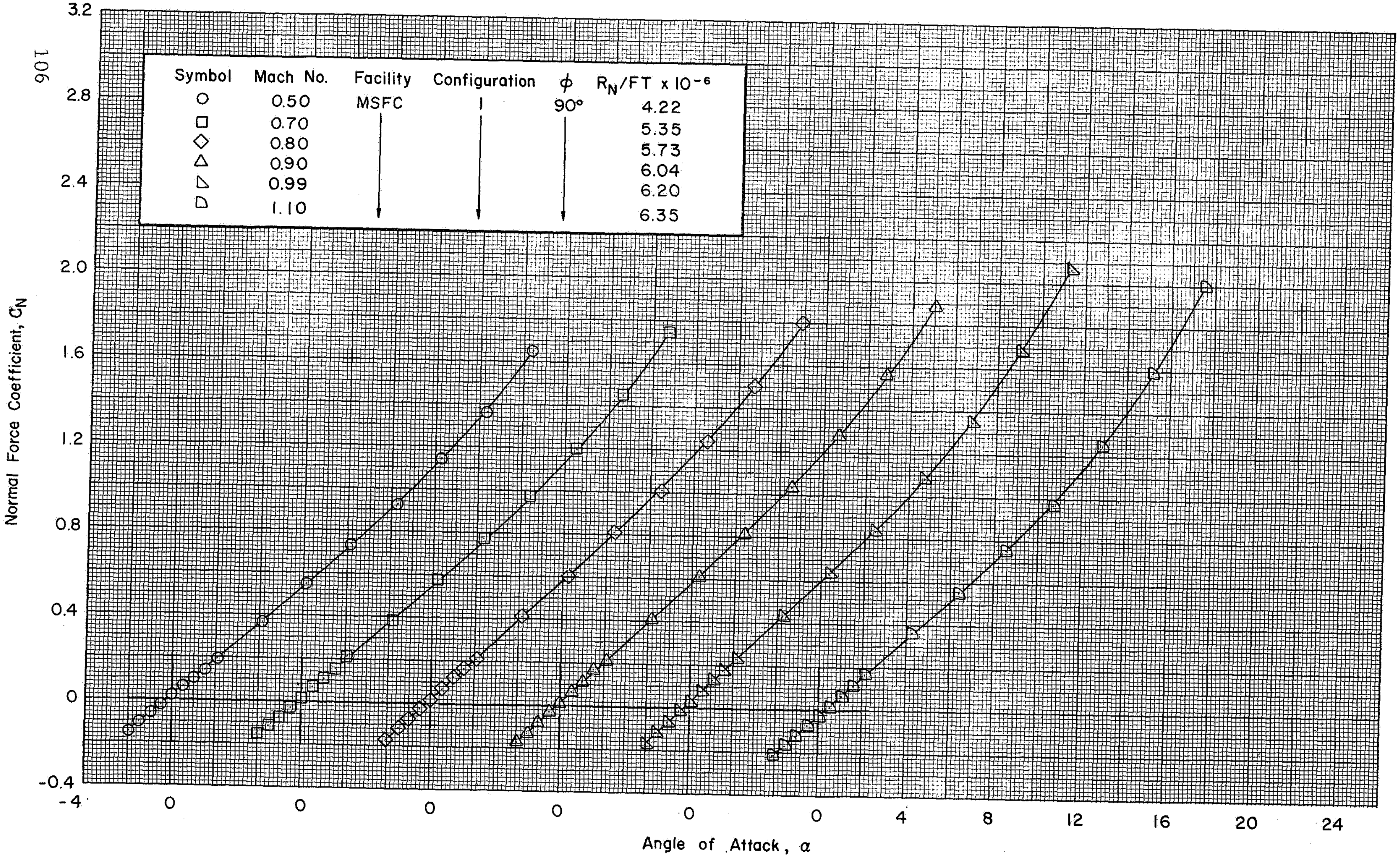

(e) C_N vs. α : ϕ=90° (M=0.50-1.10)

Figure 17 Continued

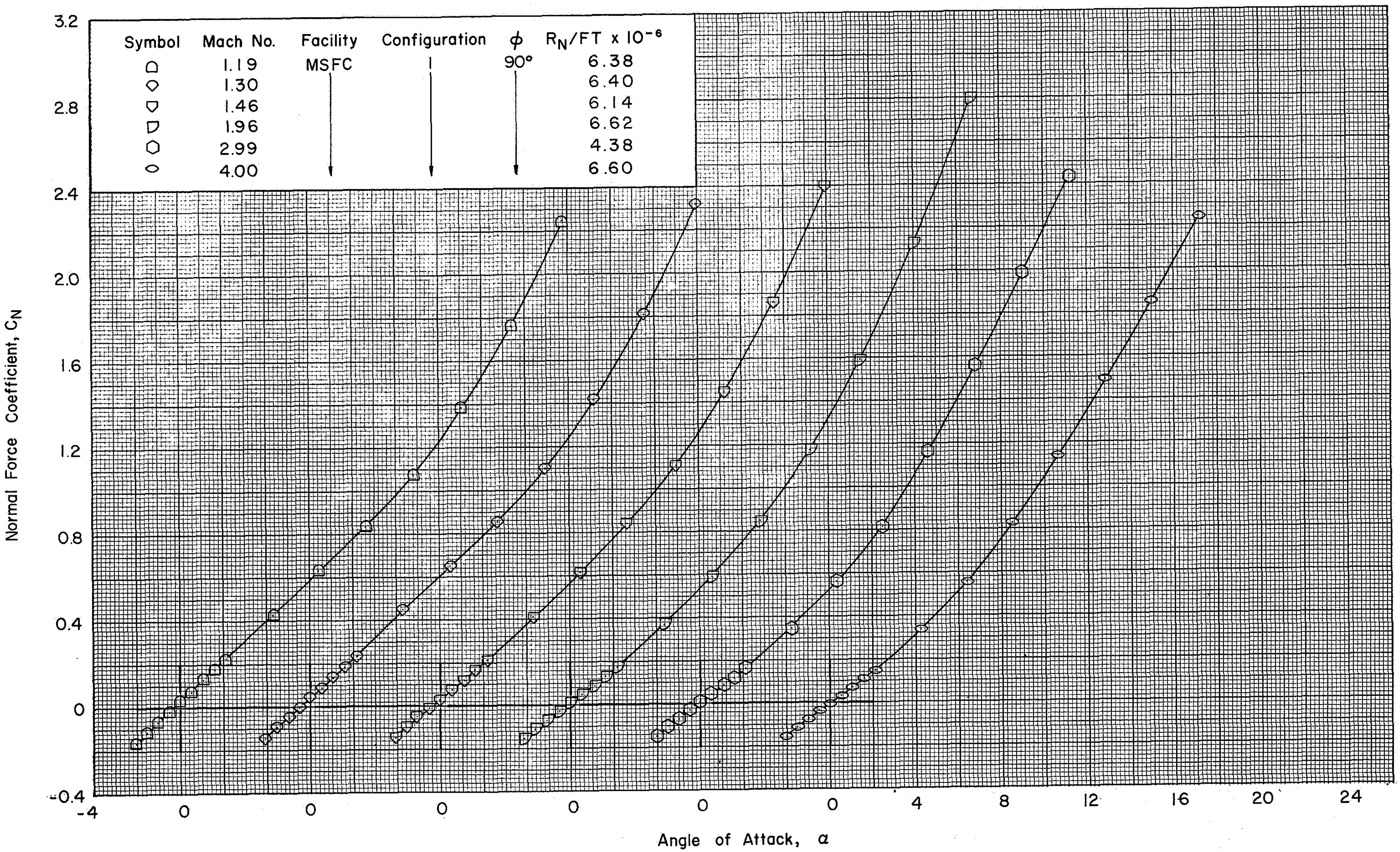

(e) Concluded : ϕ = 90° (M = 1.19 - 4.00)

Figure 17 Continued

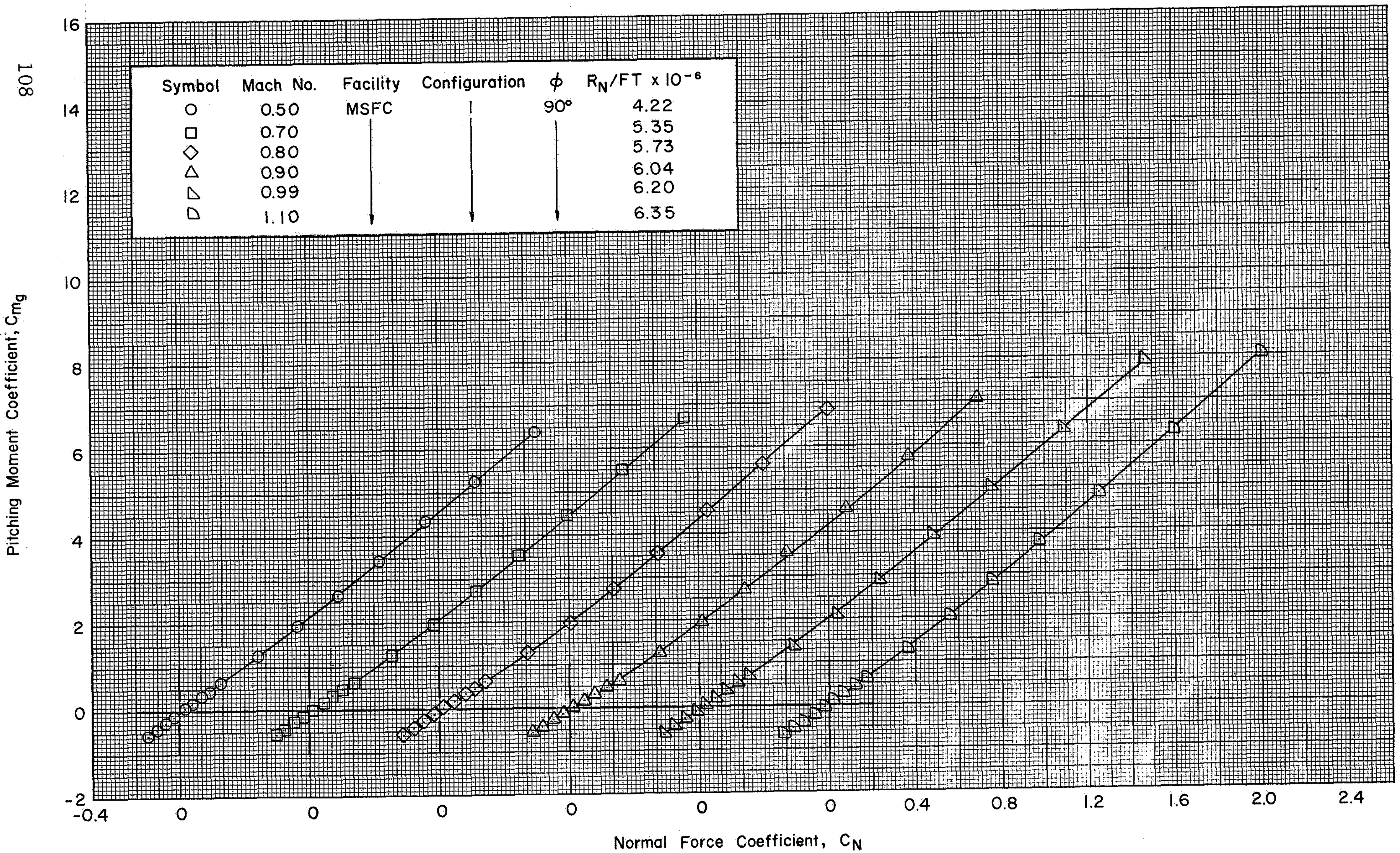

(f) C_{m_g} vs. C_N : $\phi = 90°$ (M=0.50–1.10)

Figure 17 Continued

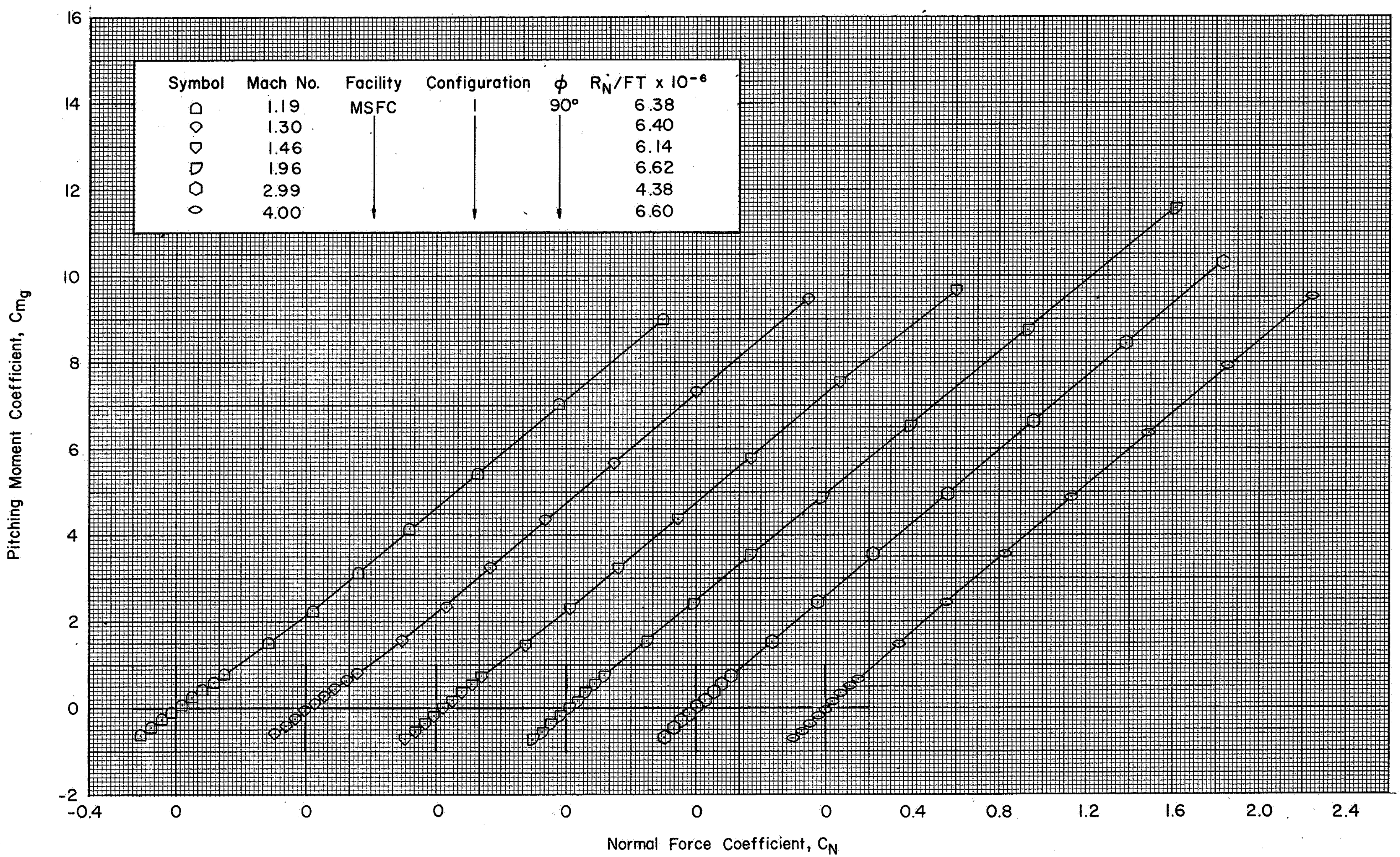

(f) Concluded : $\phi = 90°$ (M=1.19-4.00)

Figure 17 Concluded

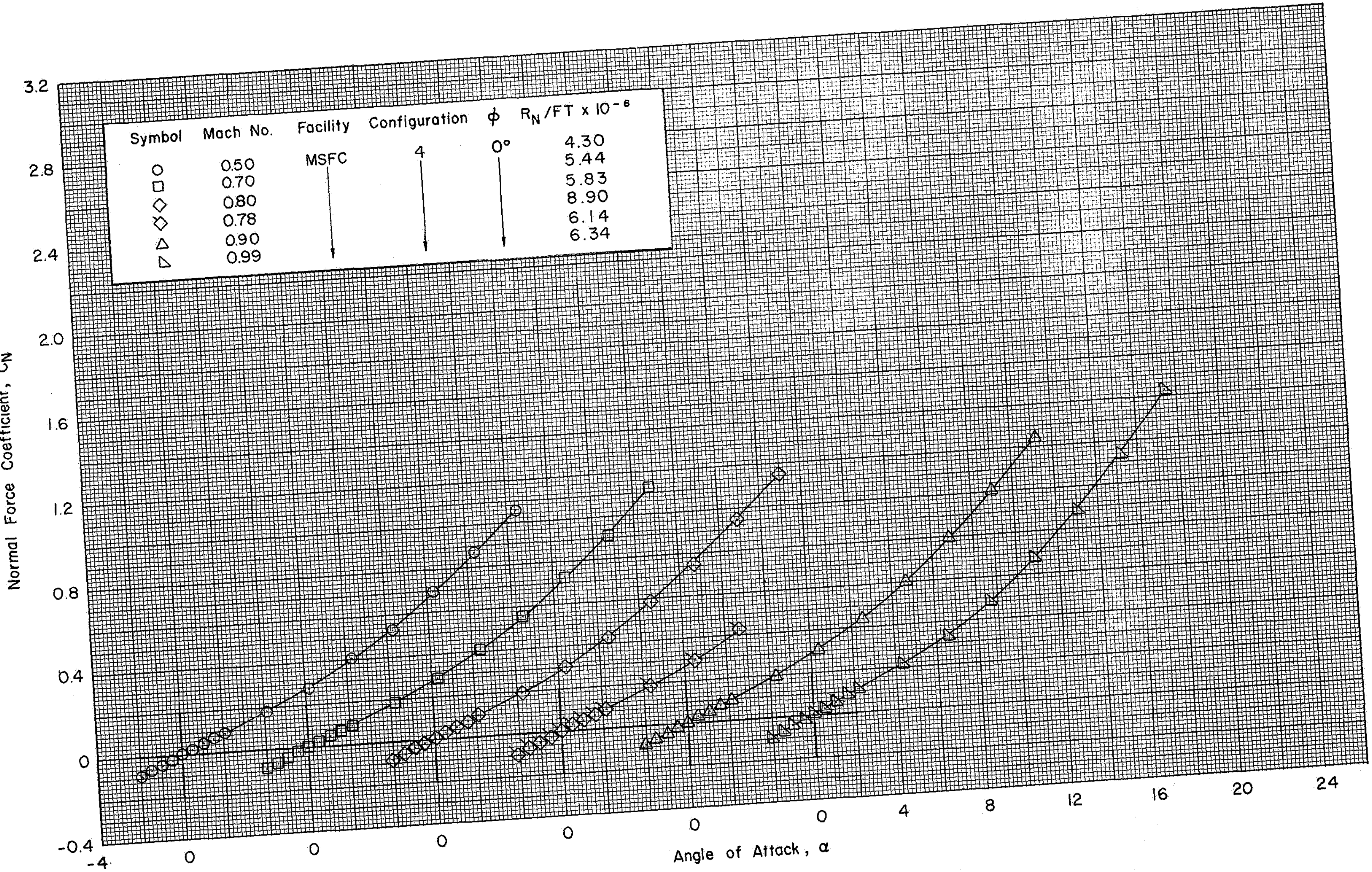

(a) C_N vs. α : $\phi = 0°$ (M=0.50-0.99)

Figure 18 Static Aerodynamic Characteristics of the APOLLO-SATURN V Launch Vehicle without Fins, Shrouds, and Base Flow Deflectors in the MSFC 14"-Inch Trisonic Wind Tunnel

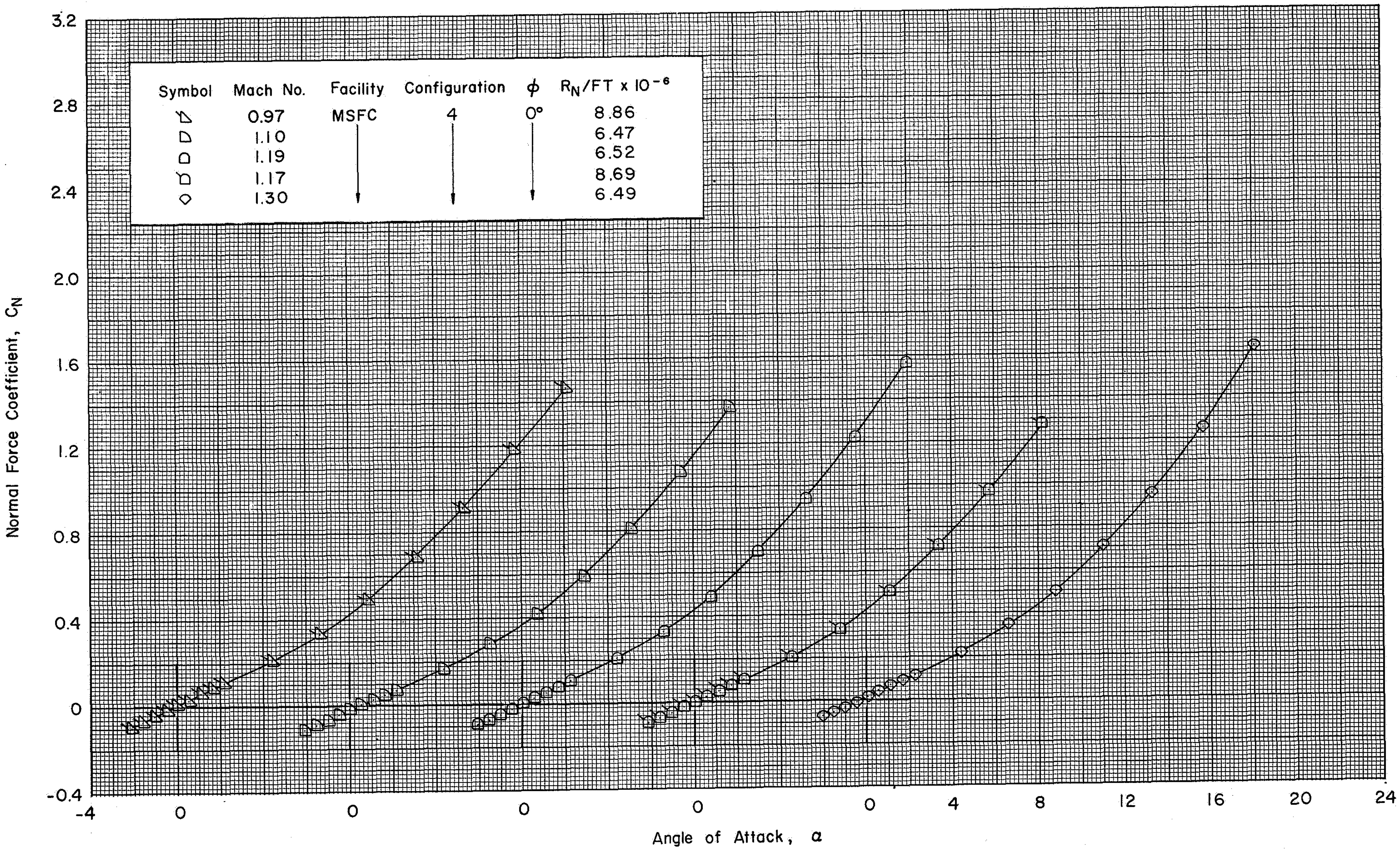

(a) Continued : $\phi = 0°$ (M=0.97–1.30)

Figure 18 Continued

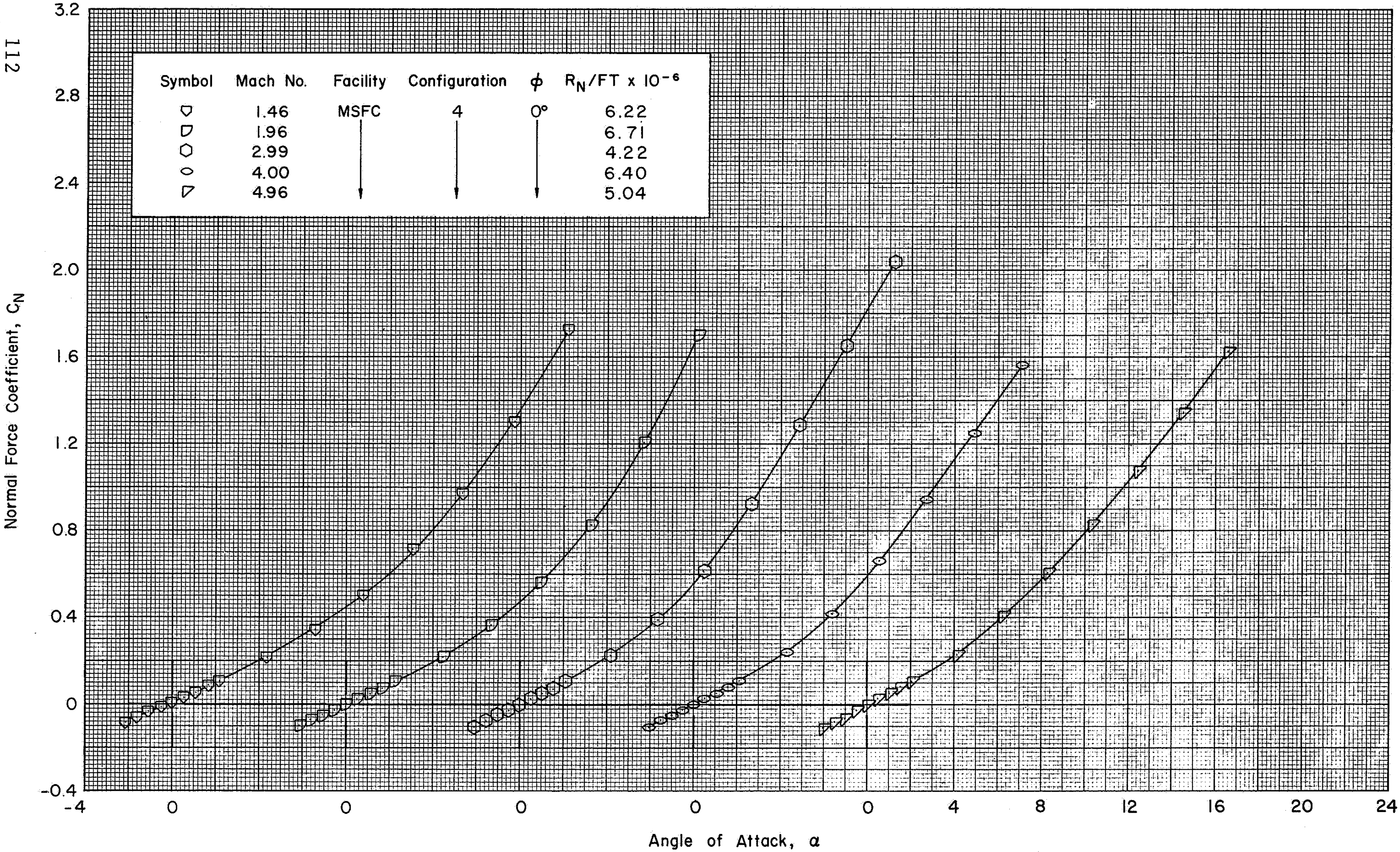

(a) Concluded: $\phi = 0°$ (M=1.46-4.96)

Figure 18 Continued

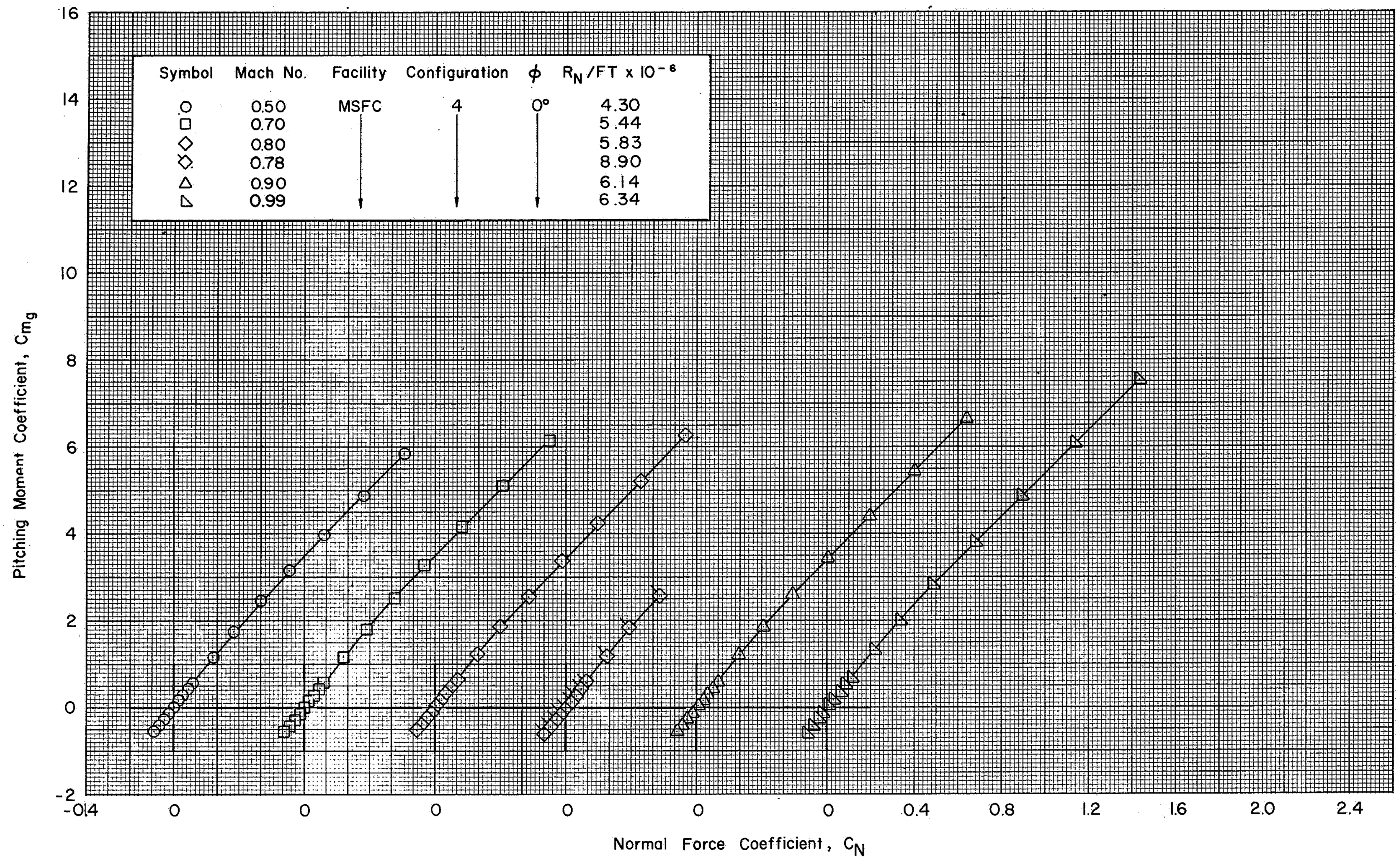

(b) C_{m_g} vs. C_N : $\phi = 0°$ (M=0.50-0.99)

Figure 18 Continued

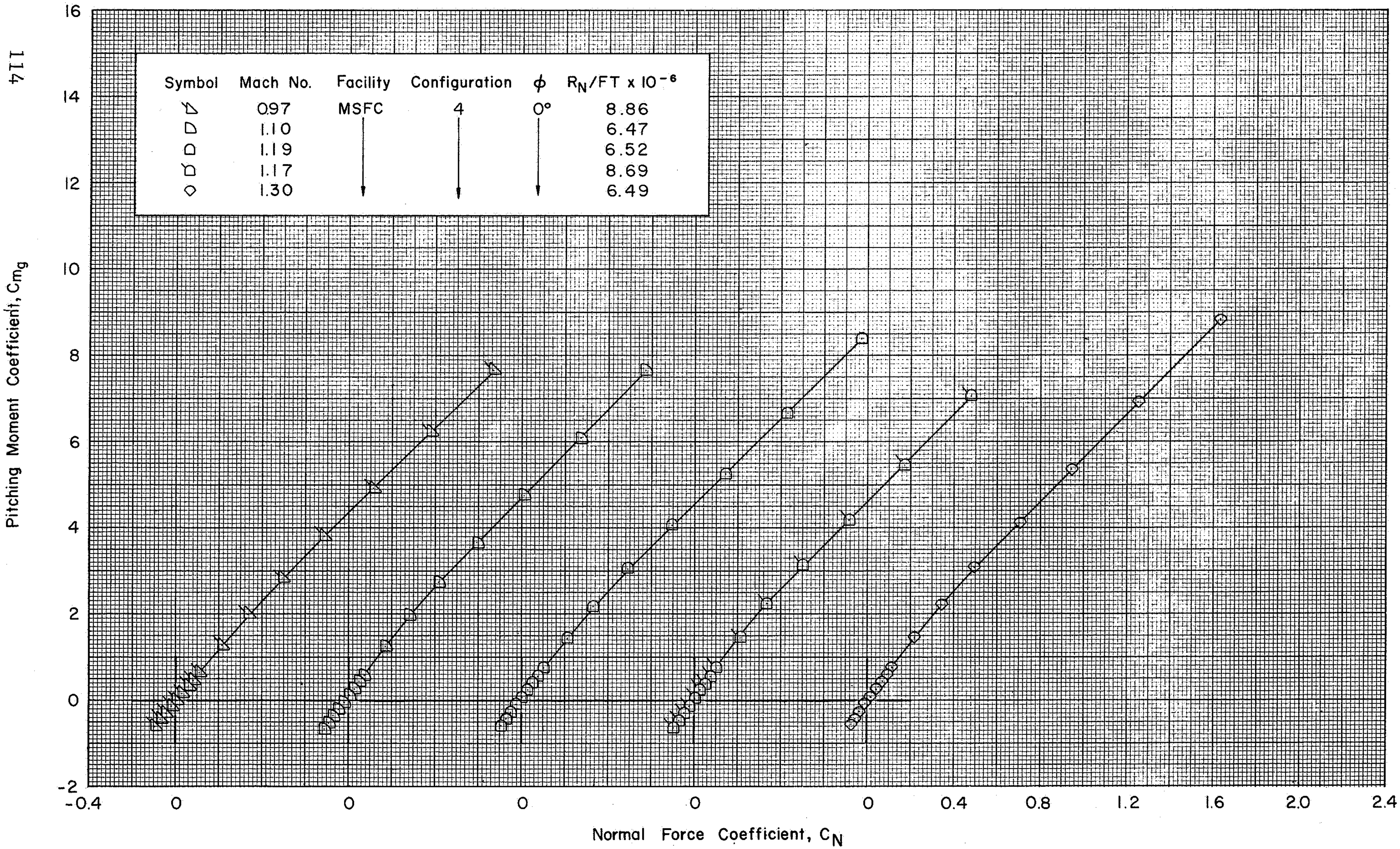

(b) Continued : $\phi = 0°$ (M=0.97-1.30)

Figure 18 Continued

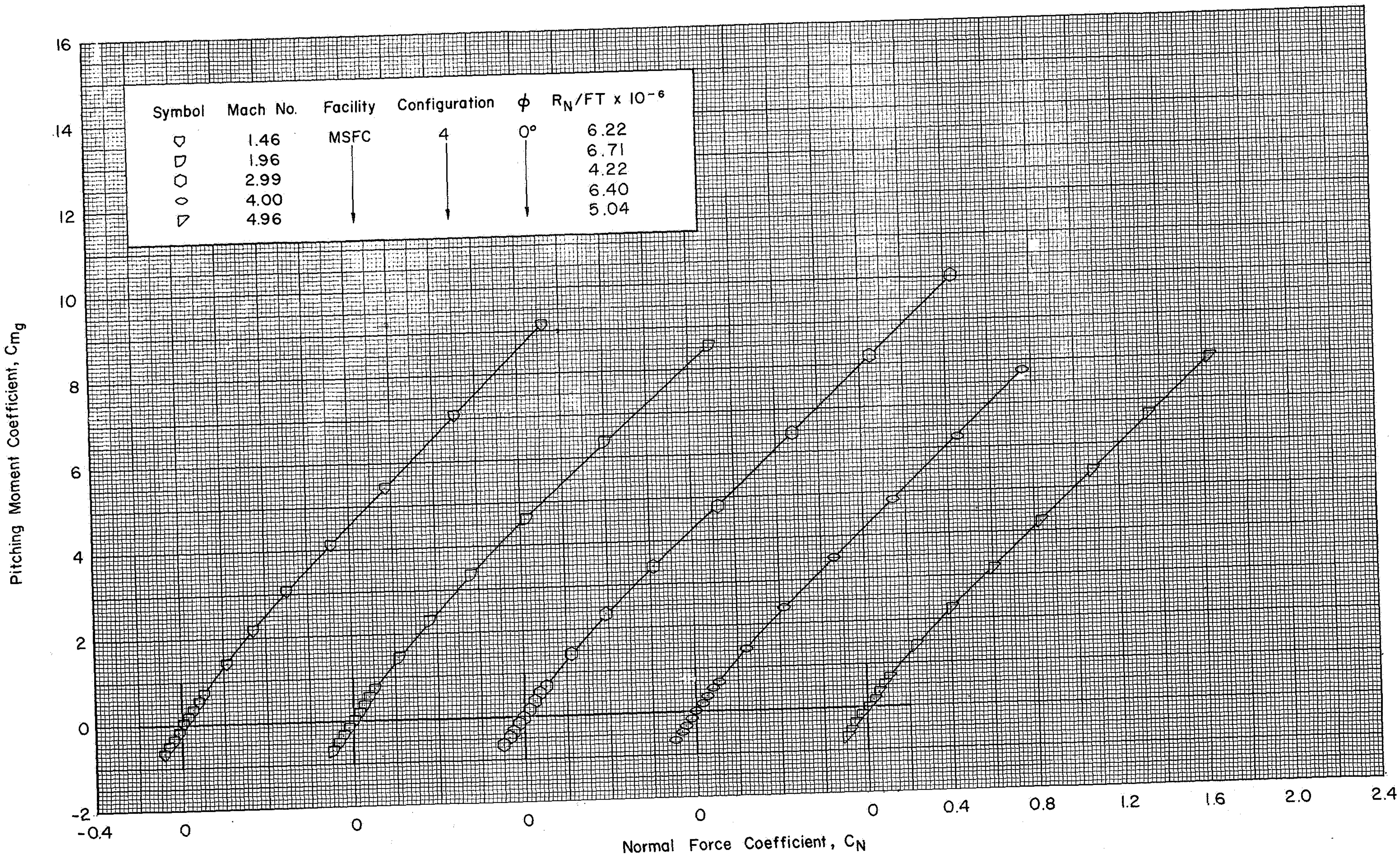

(b) Concluded : $\phi = 0°$ (M=1.46-4.96)

Figure 18 Continued

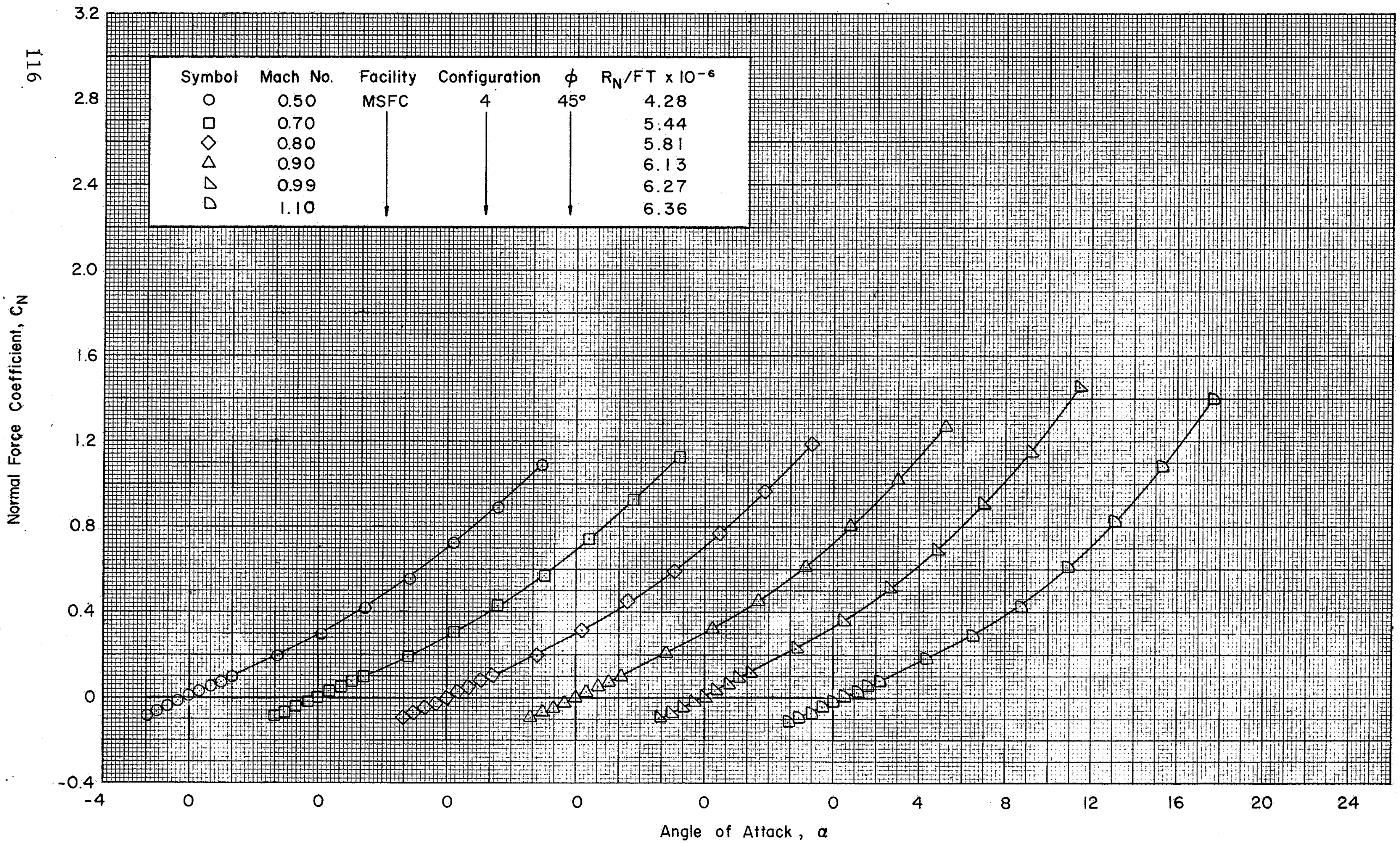

(c) C_N vs. α : ϕ=45°(M=0.50–1.10)

Figure 18 Continued

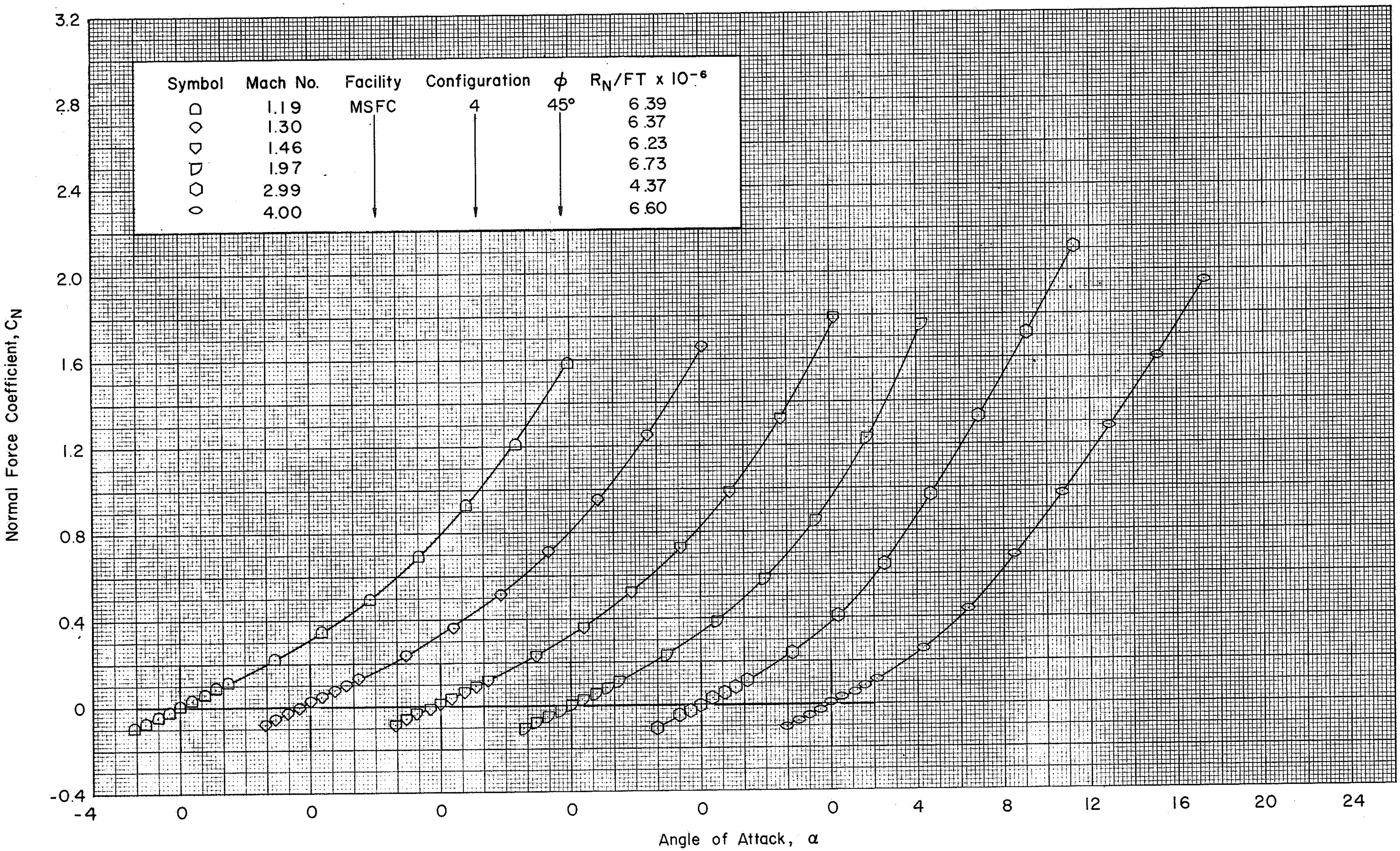

(c) Concluded: $\phi = 45°$ (M=1.19 - 4.00)

Figure 18 Continued

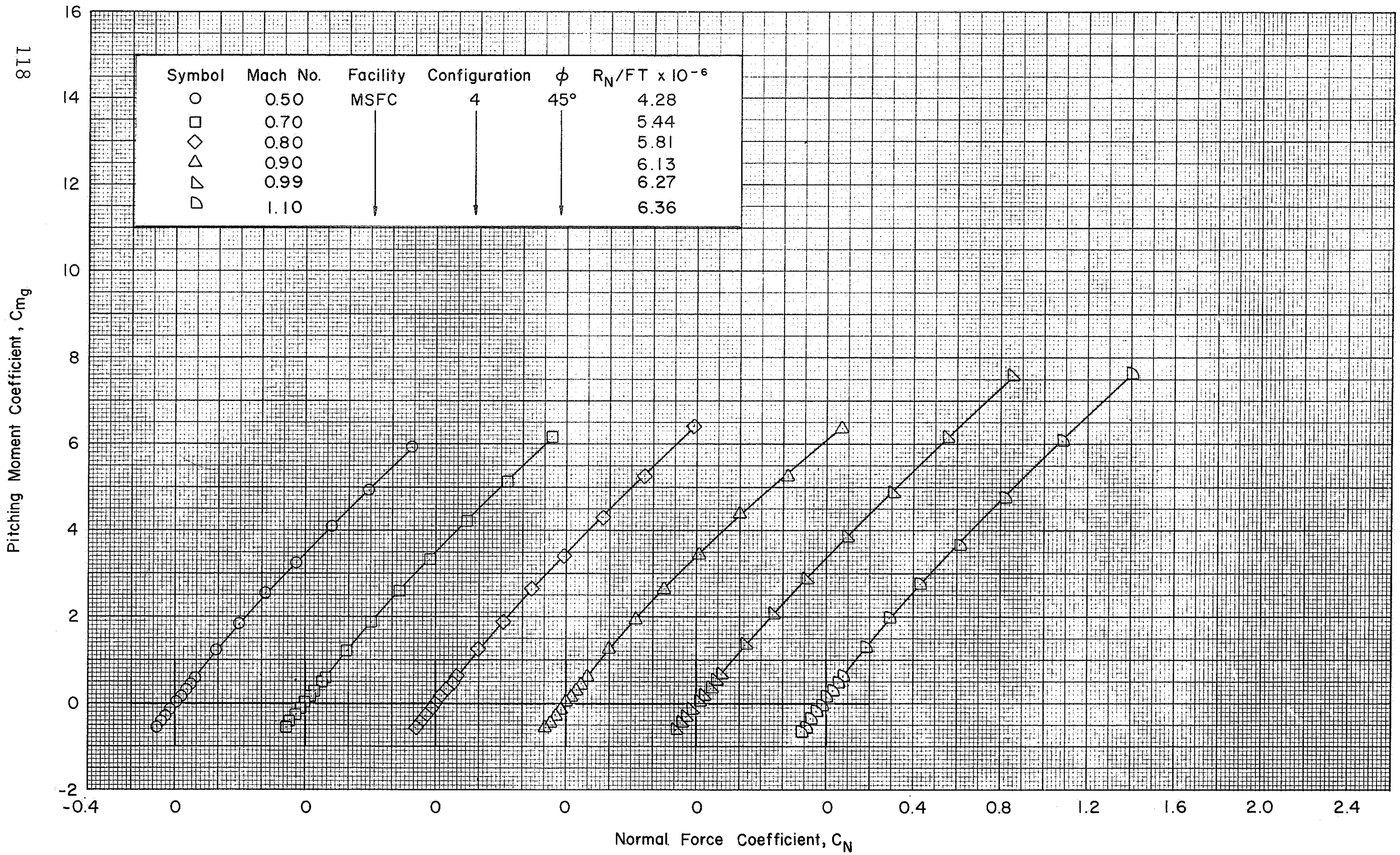

(d) C_{m_g} vs. C_N : $\phi = 45°$ (M=0.50-1.10)

Figure 18 Continued

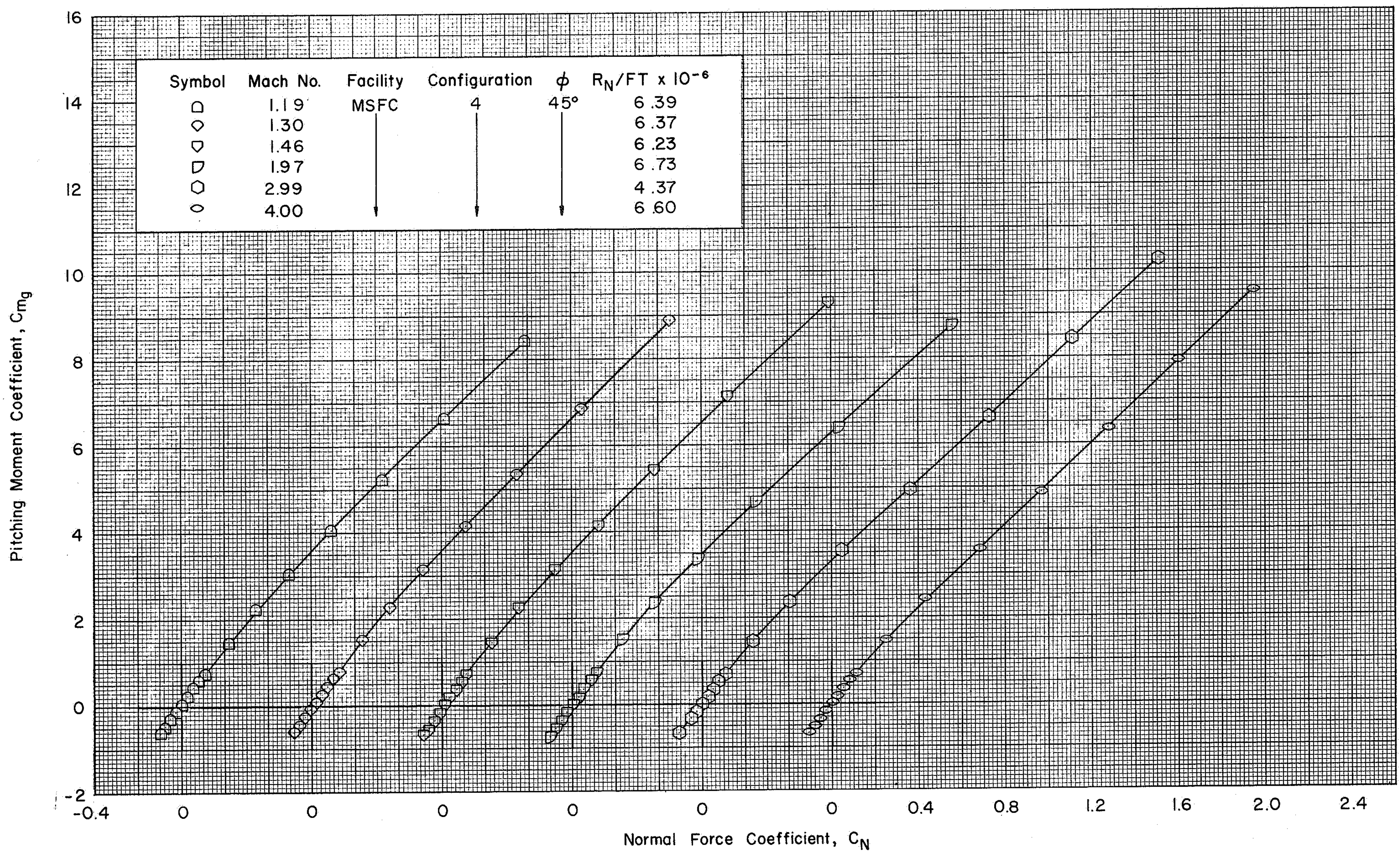

(d) Concluded : $\phi = 45°$ (M=1.19-4.00)

Figure 18 Continued

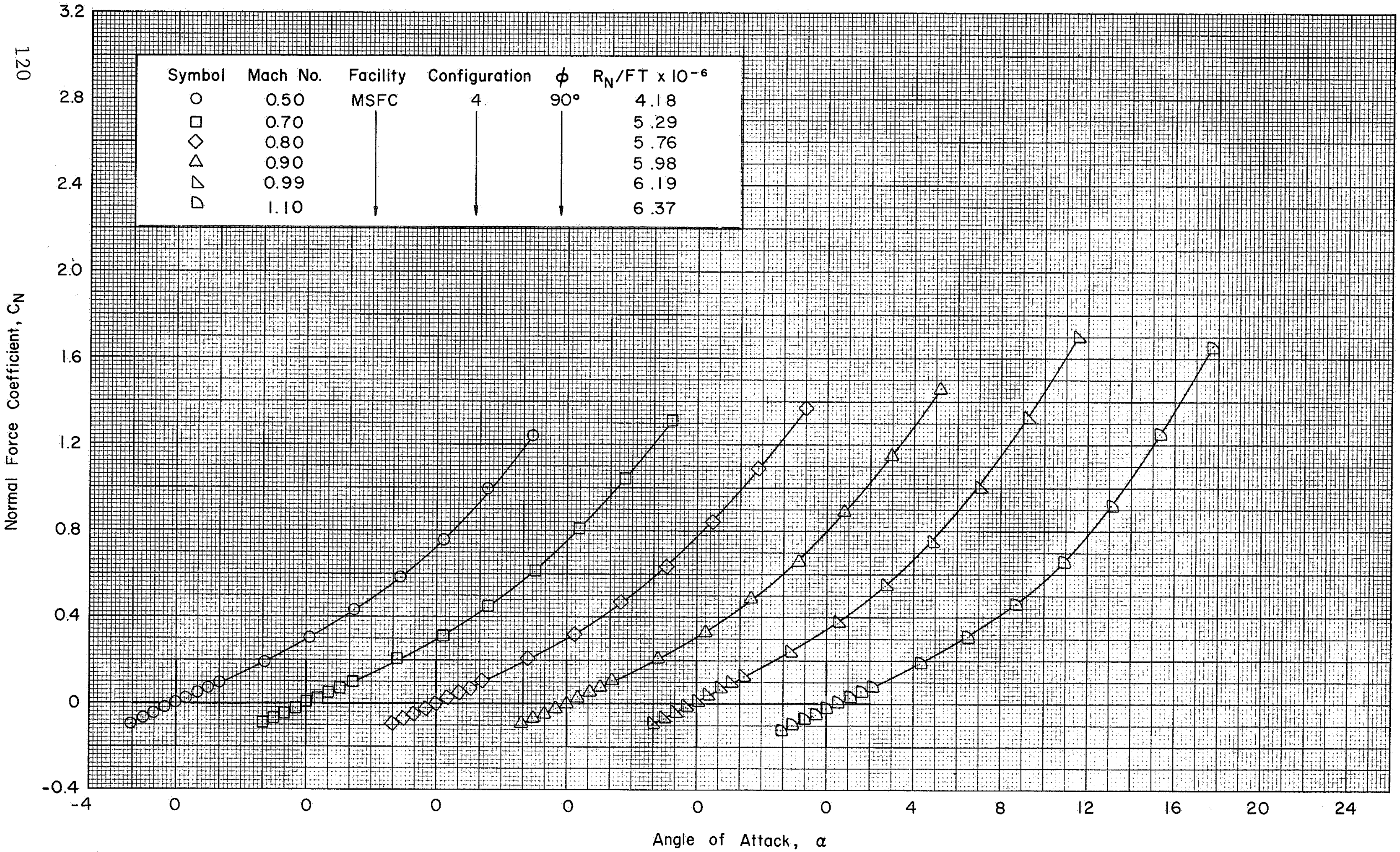

(e) C_N vs. α : ϕ =90° (M=0.50-1.10)

Figure 18 Continued

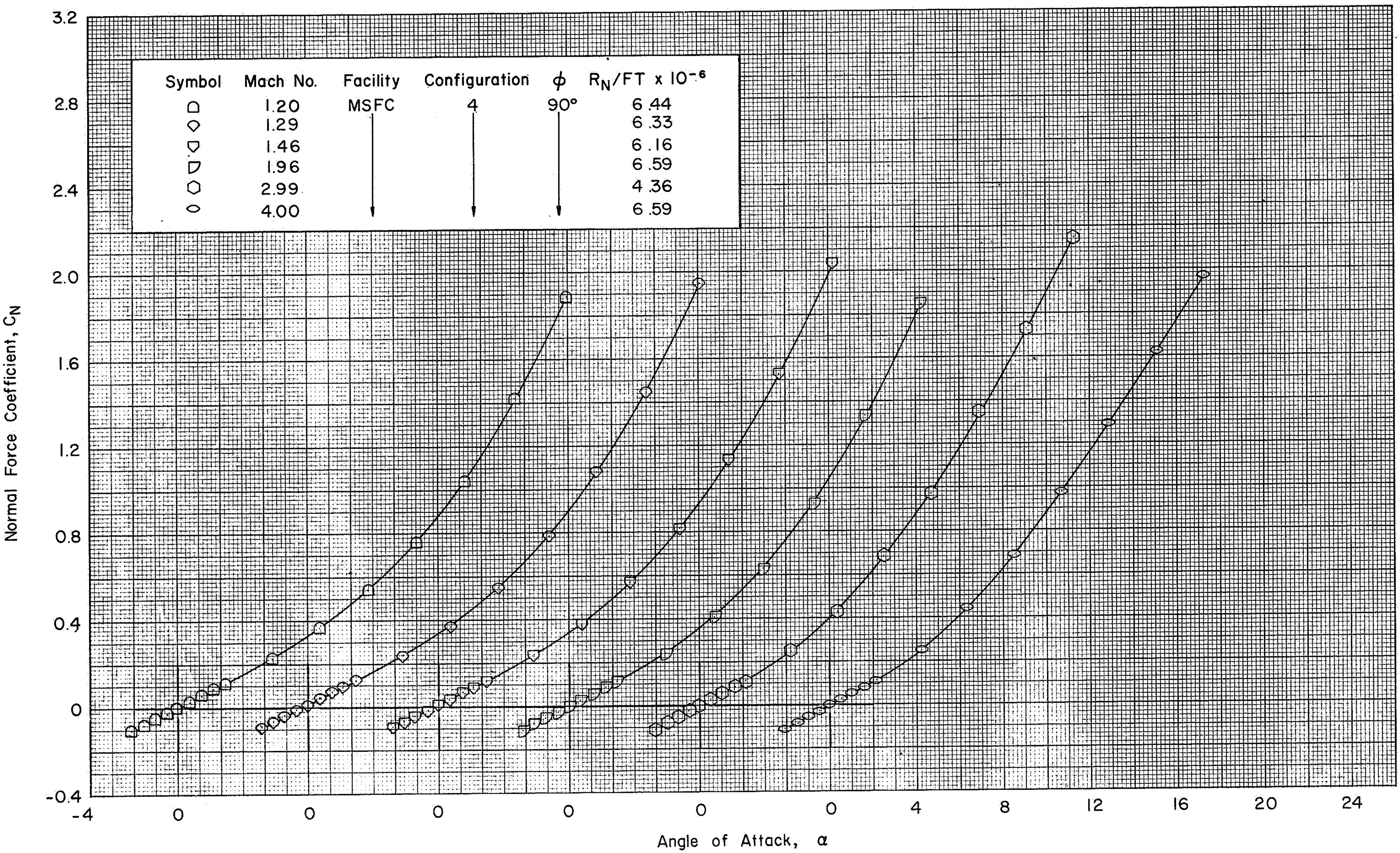

(e) Concluded : $\phi = 90°$ (M=1.20–4.00)

Figure 18 Continued

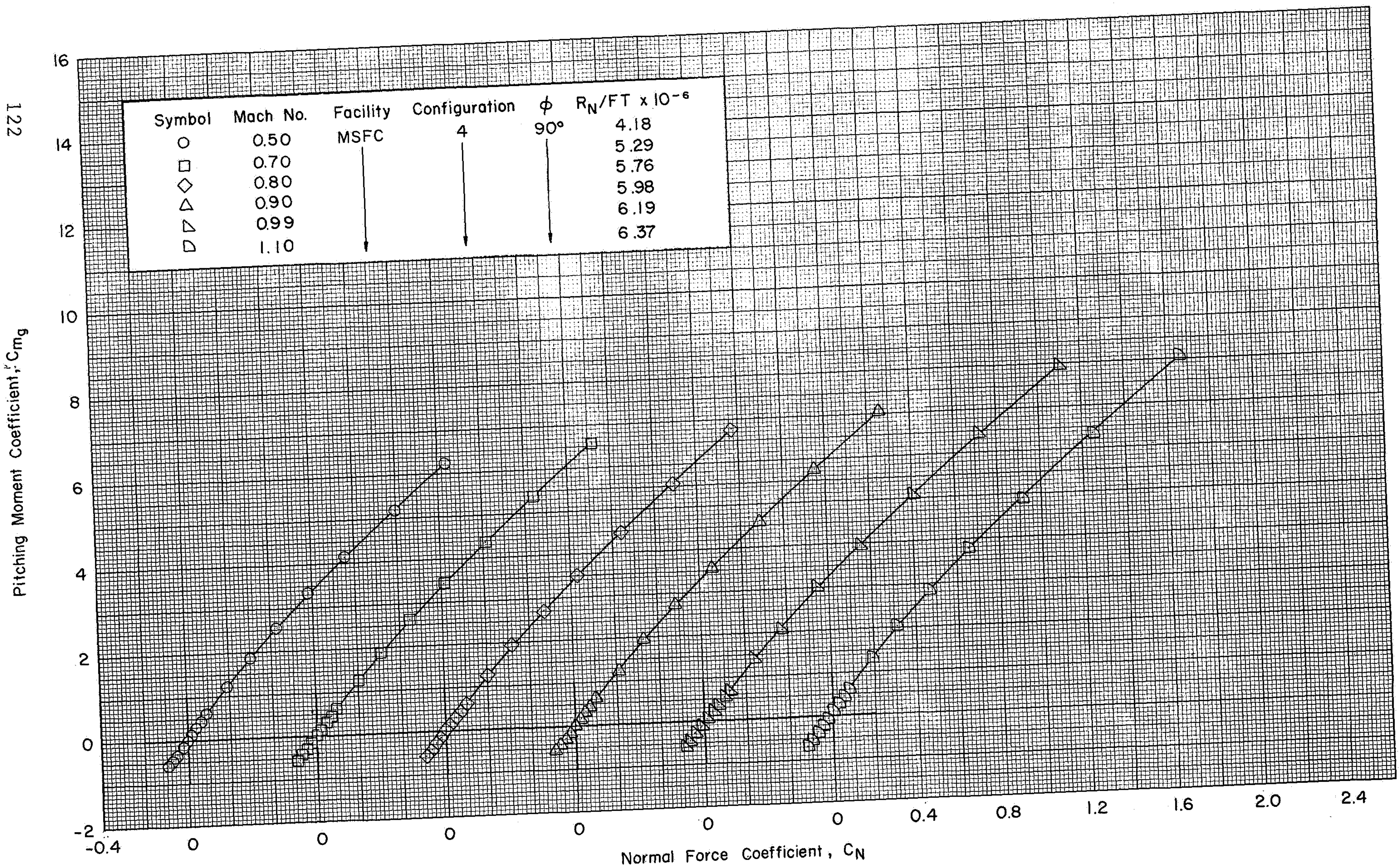

(f) C_{m_g} vs. C_N : ϕ=90° (M=0.50-1.10)

Figure 18 Continued

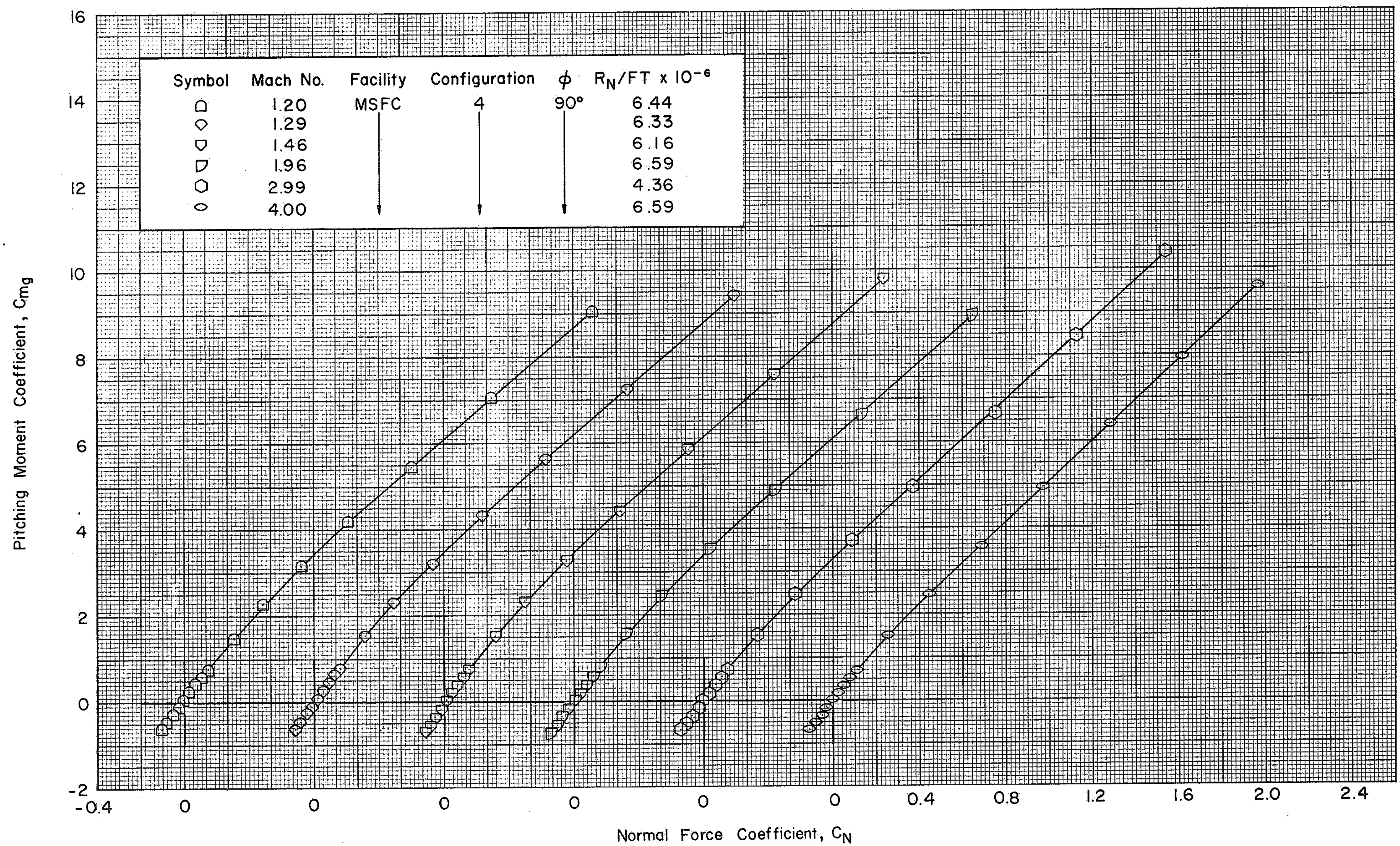

(f) Concluded : $\phi = 90°$ (M=1.20-4.00)

Figure 18 Concluded

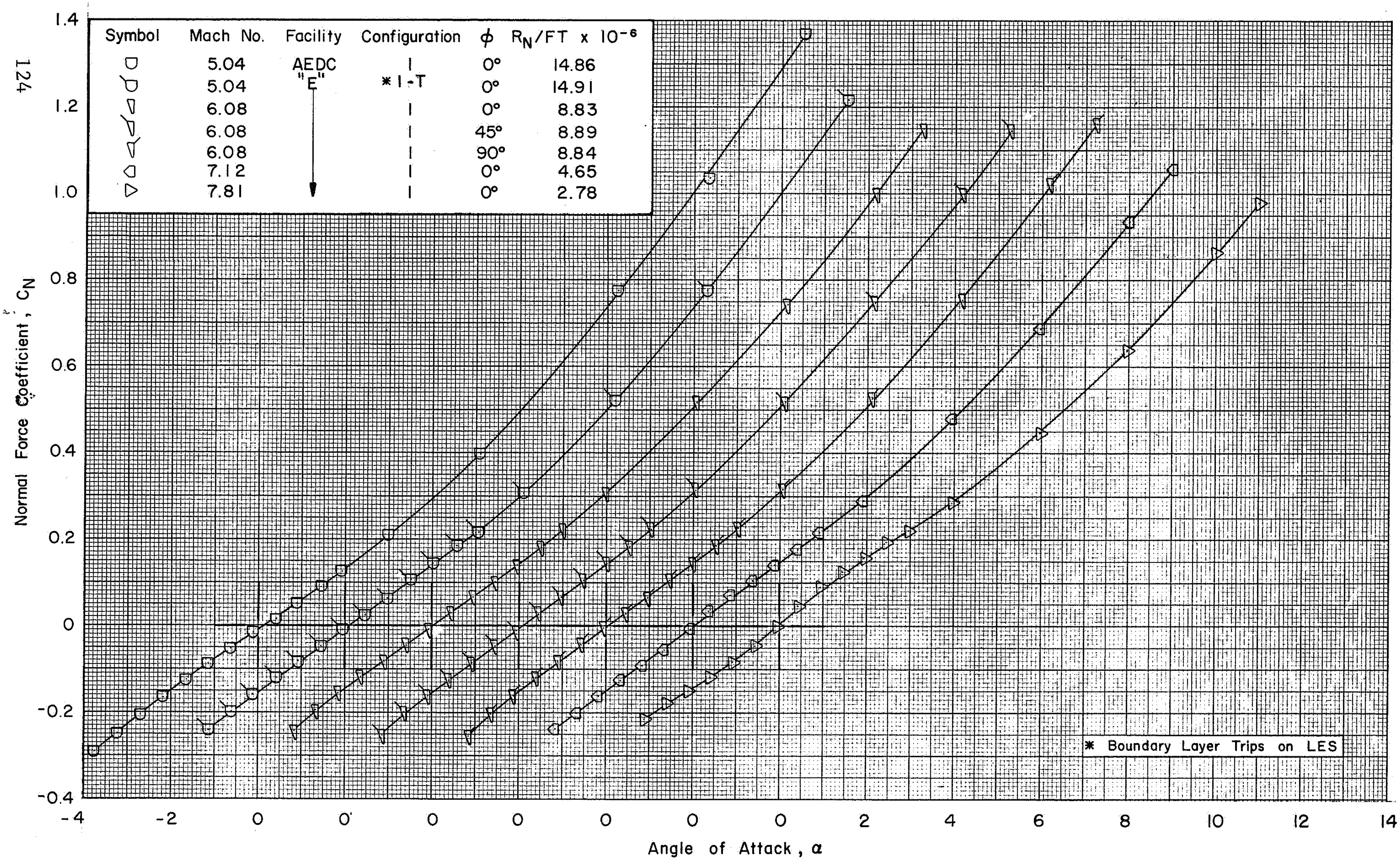

(a) C_N vs. α : $\phi = 0°$ (M= 5.04-7.81)

Figure 19 Static Aerodynamic Characteristics of the APOLLO-SATURN V Launch Vehicle in the AEDC/VKF 12' Inch Hypersonic Tunnel "E"

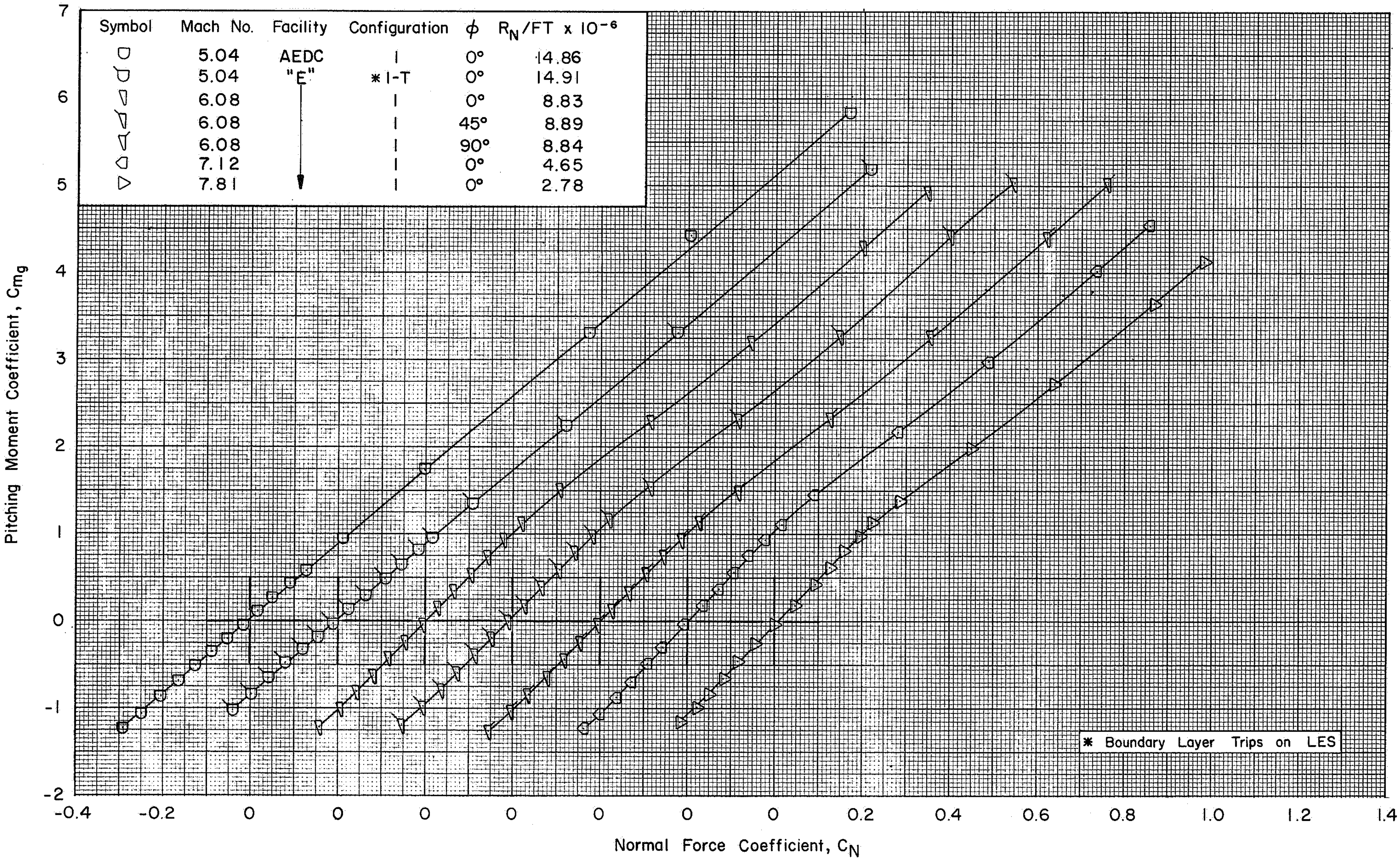

(b) C_{m_g} vs. C_N : $\phi = 0°$ (M = 5.04-7.81)

Figure 19 Concluded

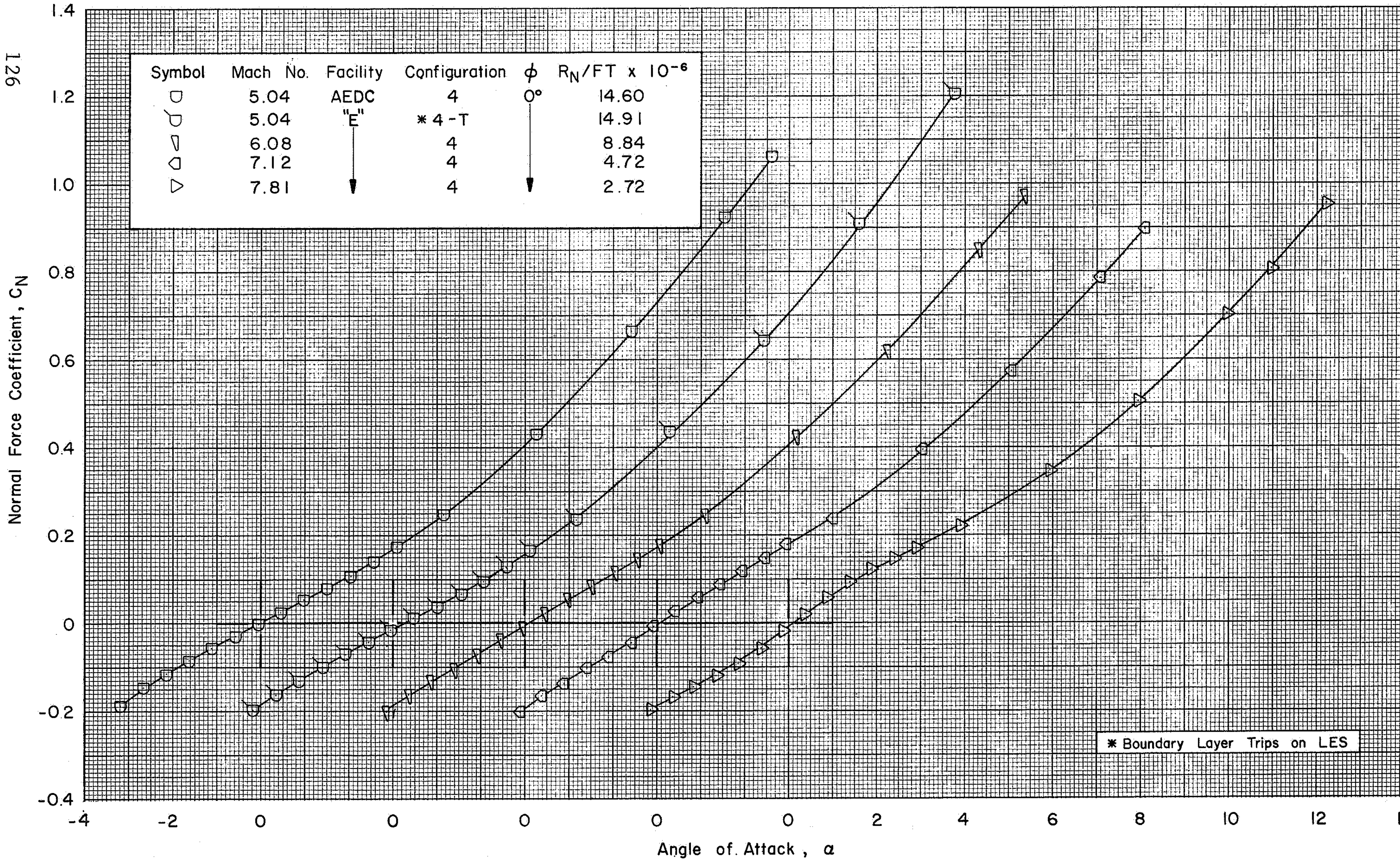

(a) C_N vs $\alpha : \phi = 0°$ (M=5.04–7.81)

Figure 20 Static Aerodynamic Characteristics of the APOLLO-SATURN V Launch Vehicle without Fins, Shrouds, and Base Flow Deflectors in the AEDC/VKF 12 Inch Hypersonic Tunnel "E"

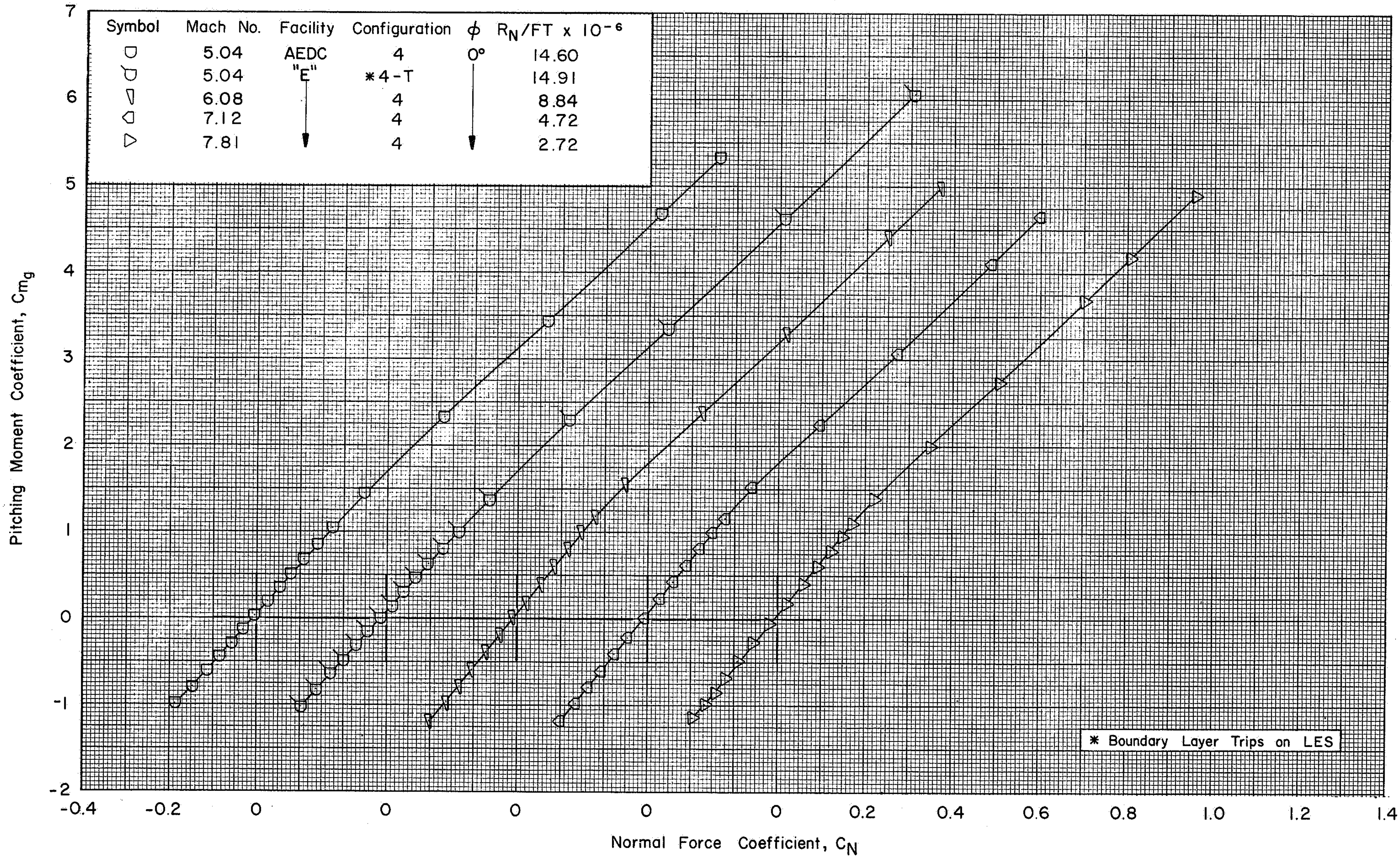

(b) Cm_g vs. C_N : $\phi = 0°$ (M= 5.04- 7.81)

Figure 20 Concluded

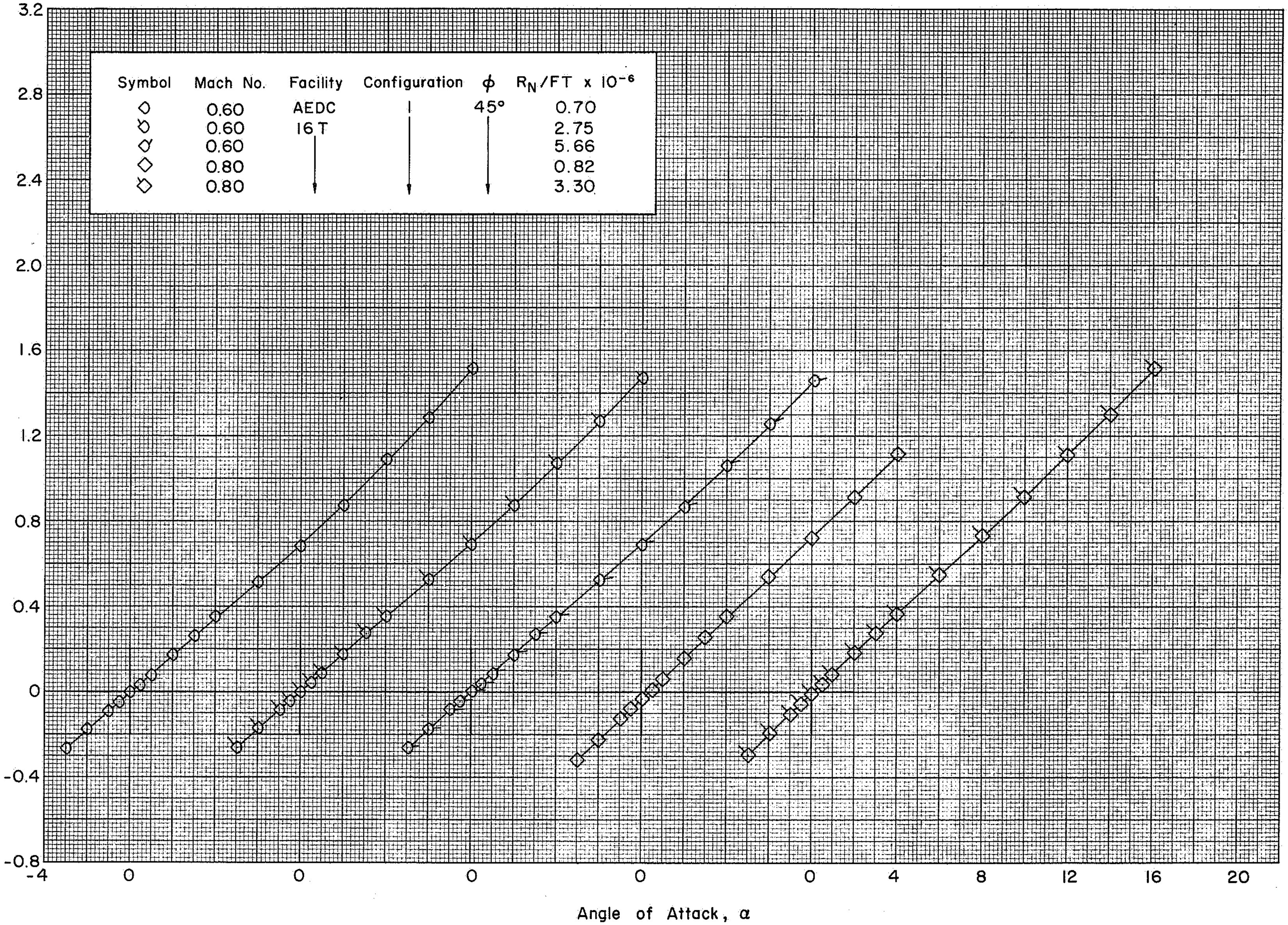

(a) C_N vs. α : ϕ=45° (M=0.60—0.80)

Figure 21 Static Aerodynamic Characteristics of the APOLLO-SATURN V Launch Vehicle in the AEDC / PWT 16-Foot Transonic Tunnel

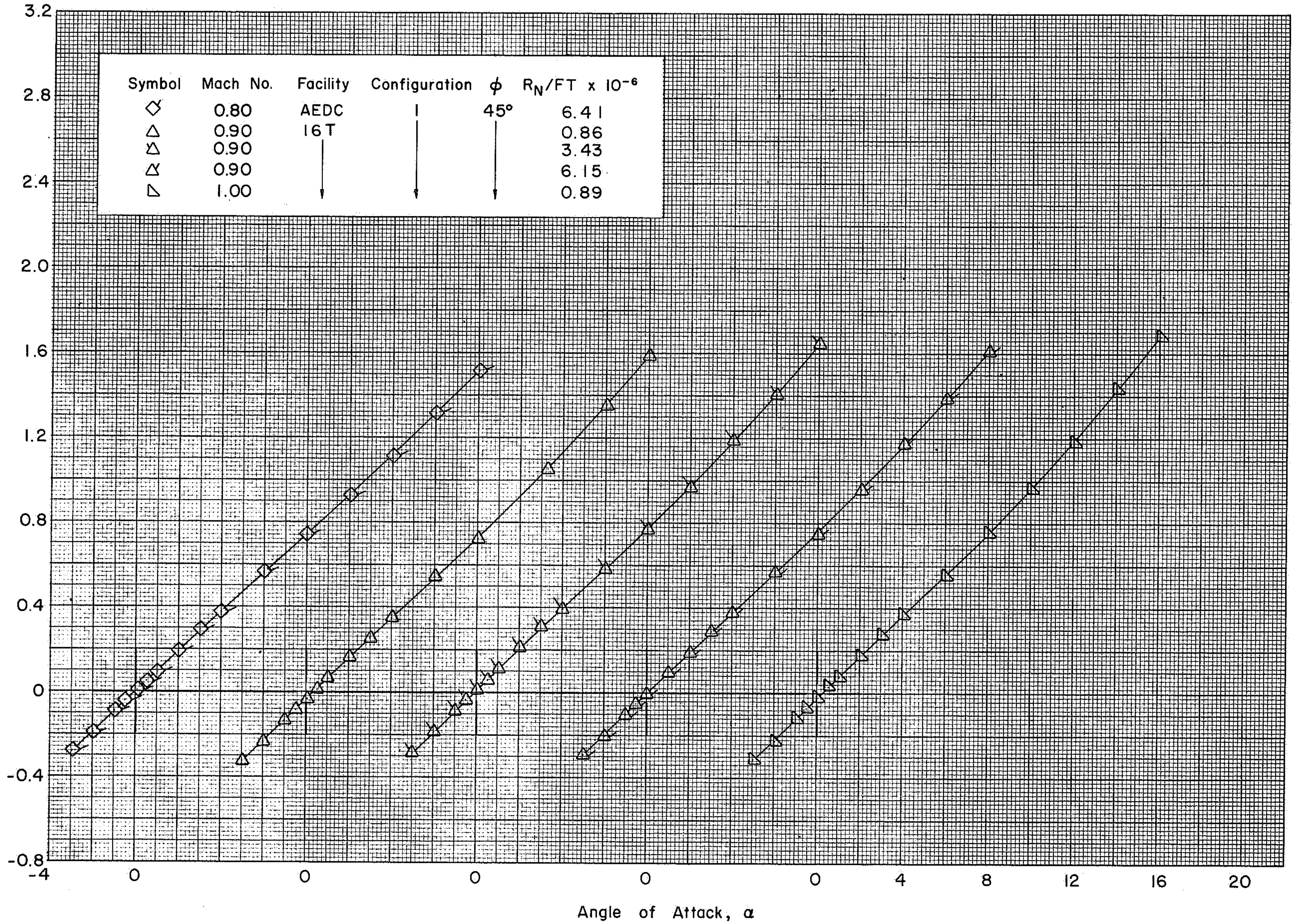

(a) Continued: $\phi = 45°$ (M=0.80−1.00)

Figure 21 Continued

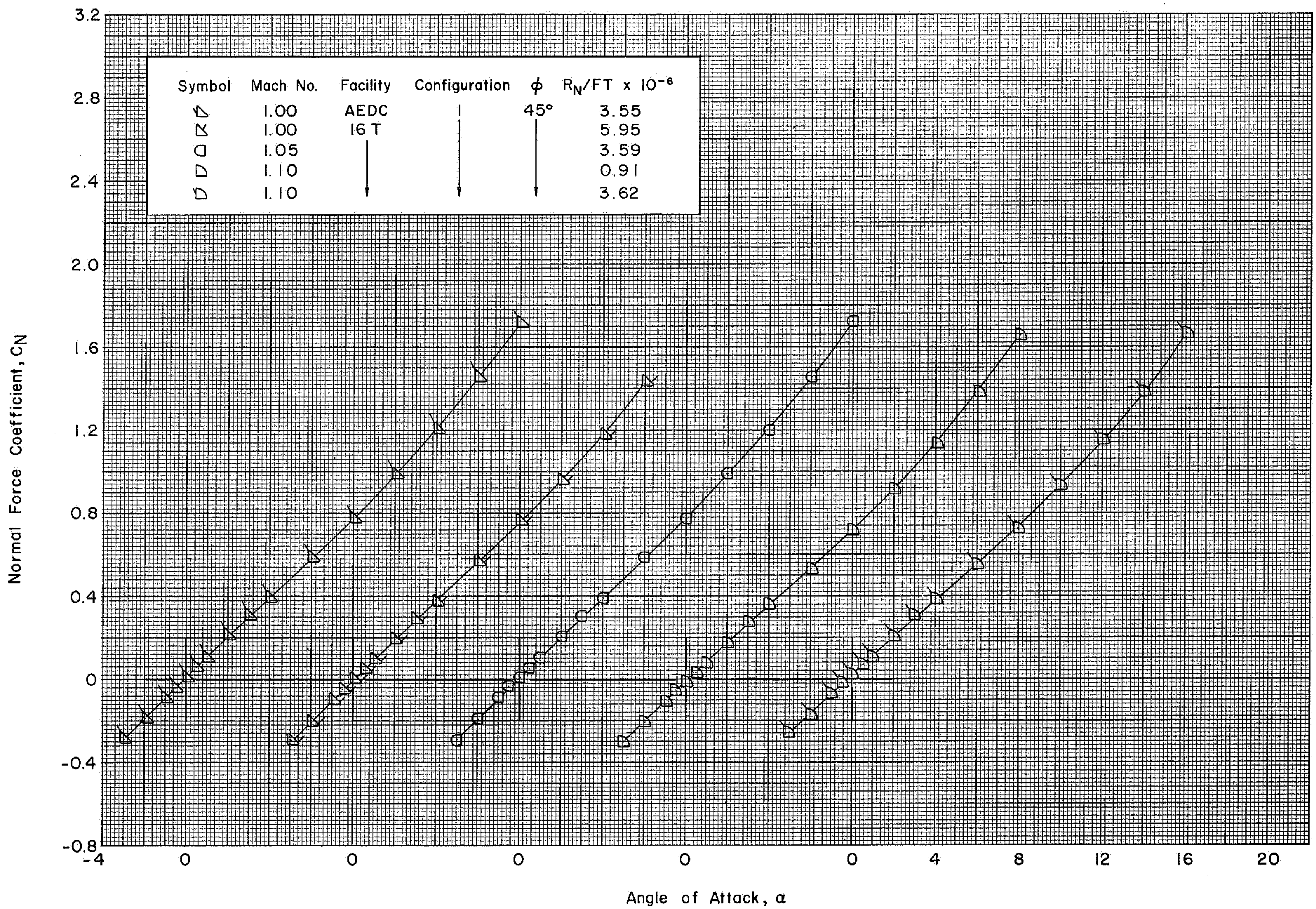

(a) Continued : $\phi = 45°$ (M = 1.00 − 1.10)

Figure 21 Continued

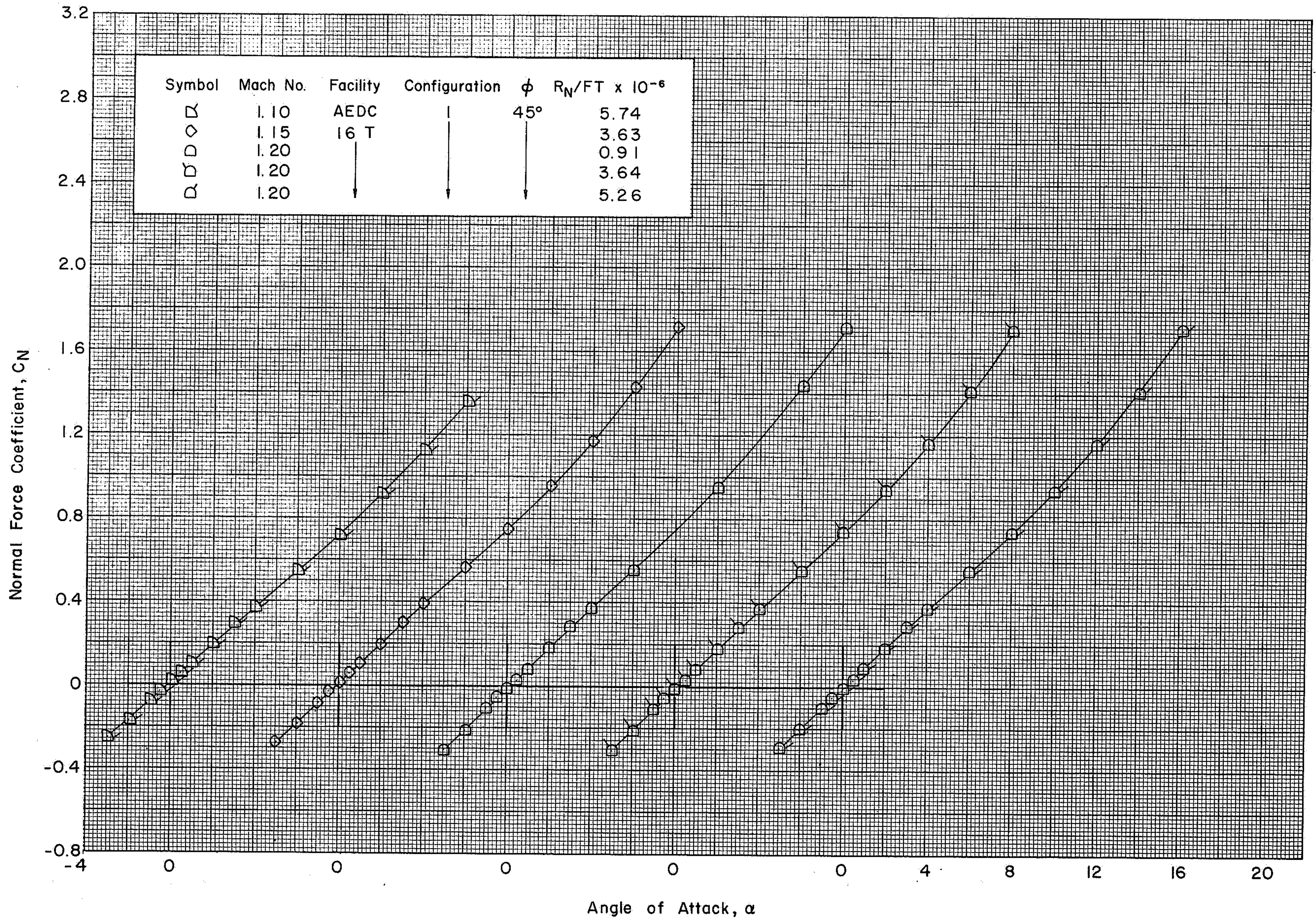

(a) Continued: $\phi = 45°$ (M=1.10–1.20)

Figure 21 Continued

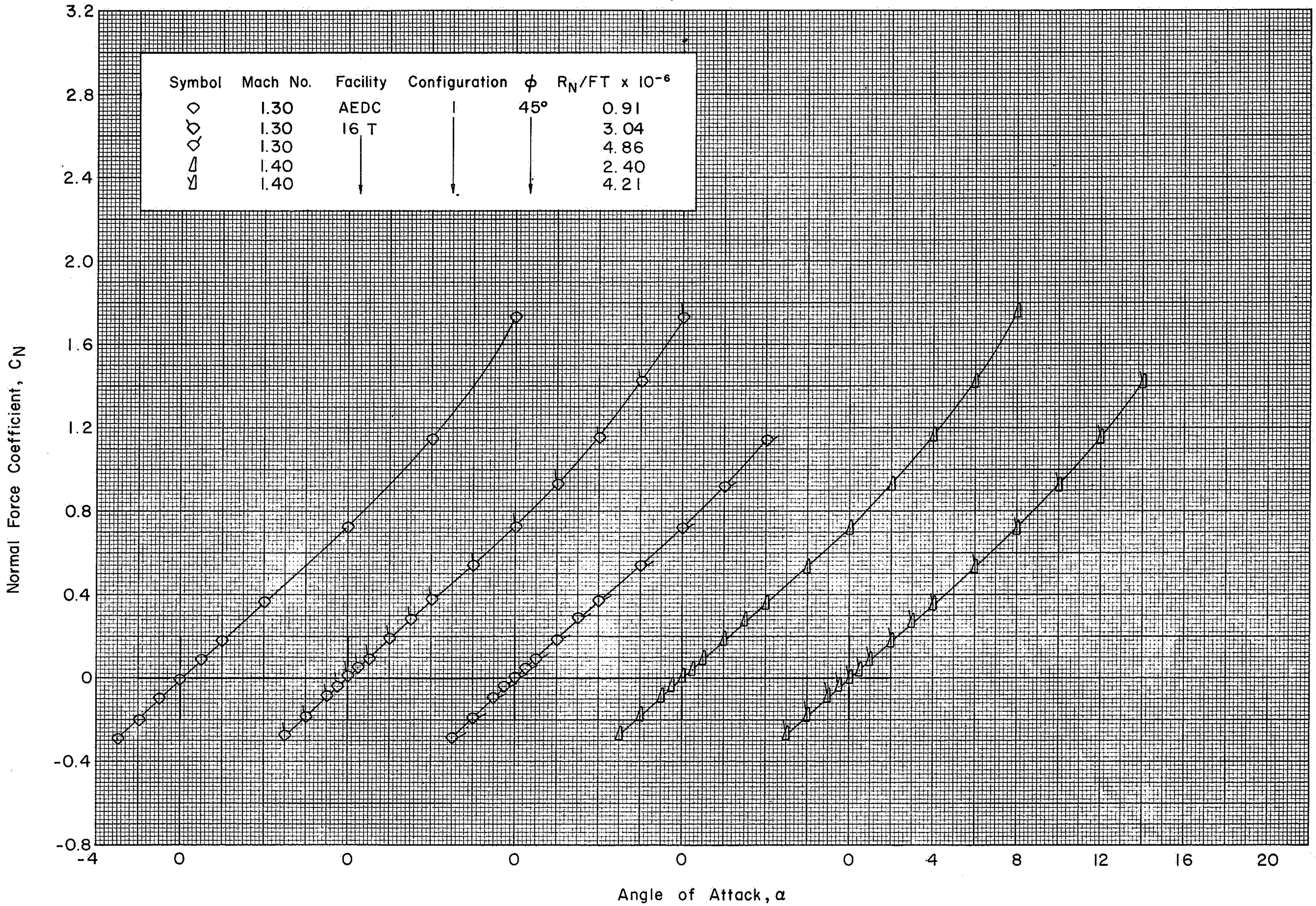

(a) Concluded: ϕ=45° (M=1.30-1.40)

Figure 21 Concluded

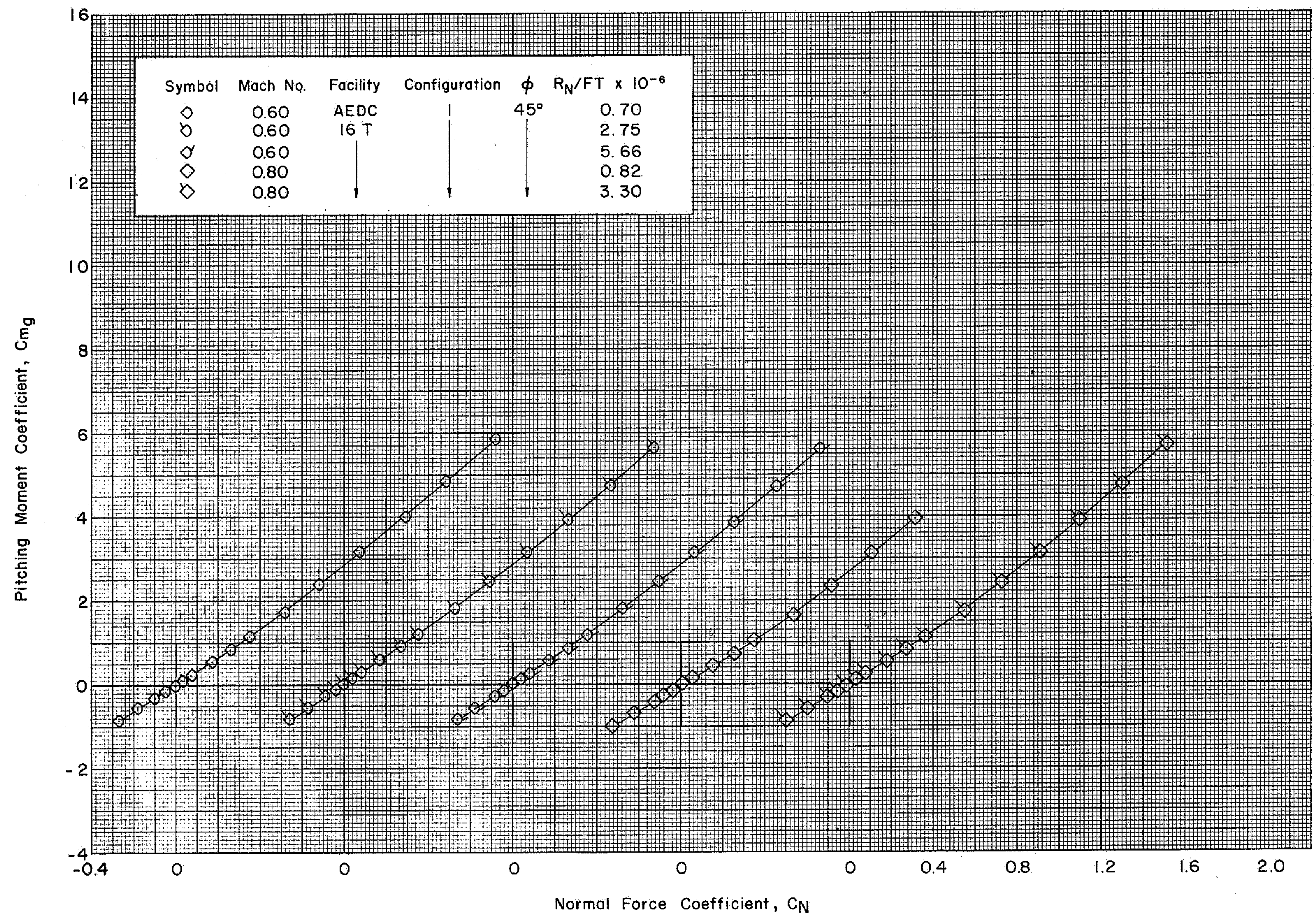

(b) C_{m_g} vs. C_N: $\phi = 45°$ (M = 0.60 – 0.80)

Figure 21 Continued

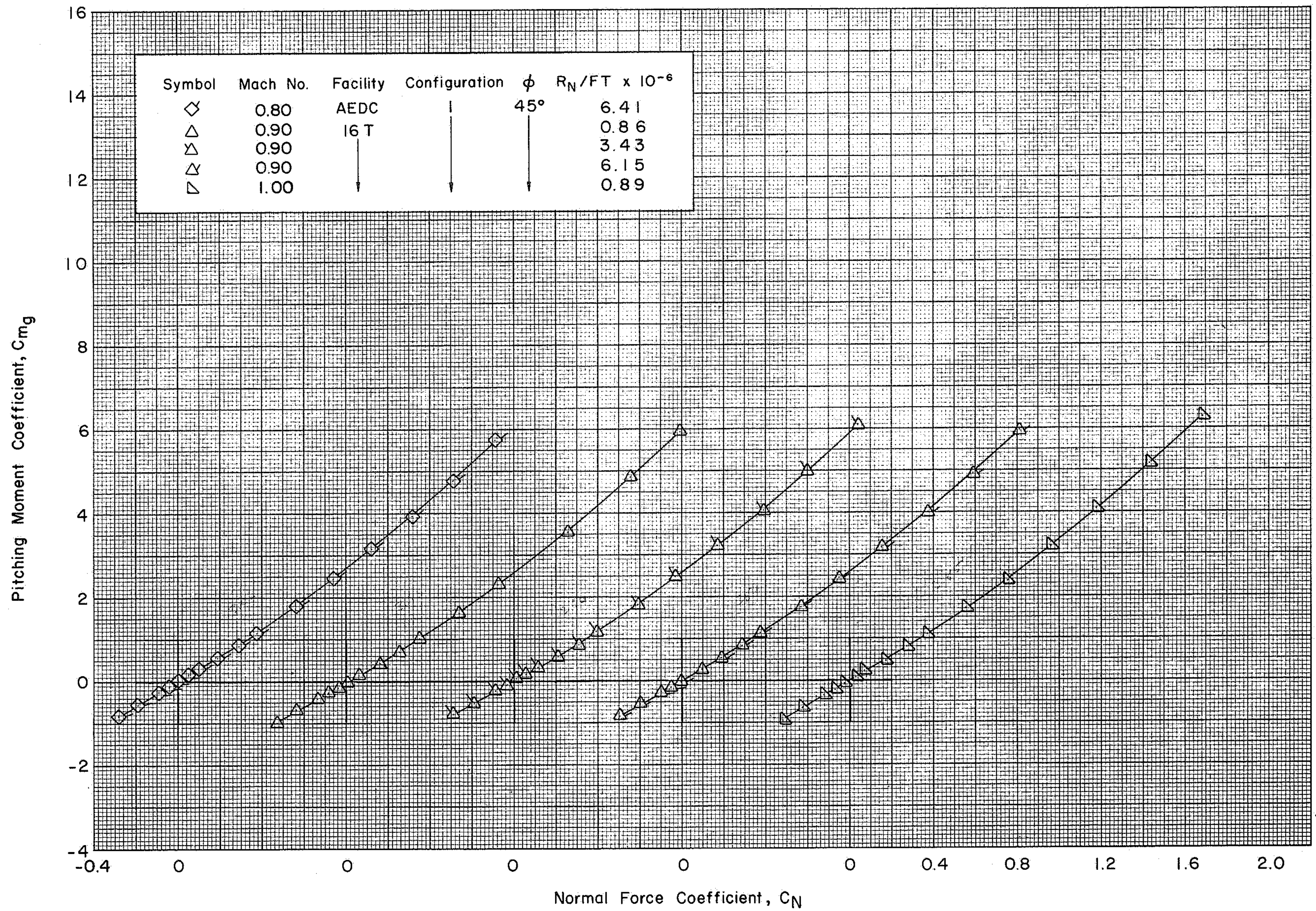

(b) Continued: ϕ=45° (M=0.80–1.00)

Figure 21 Continued

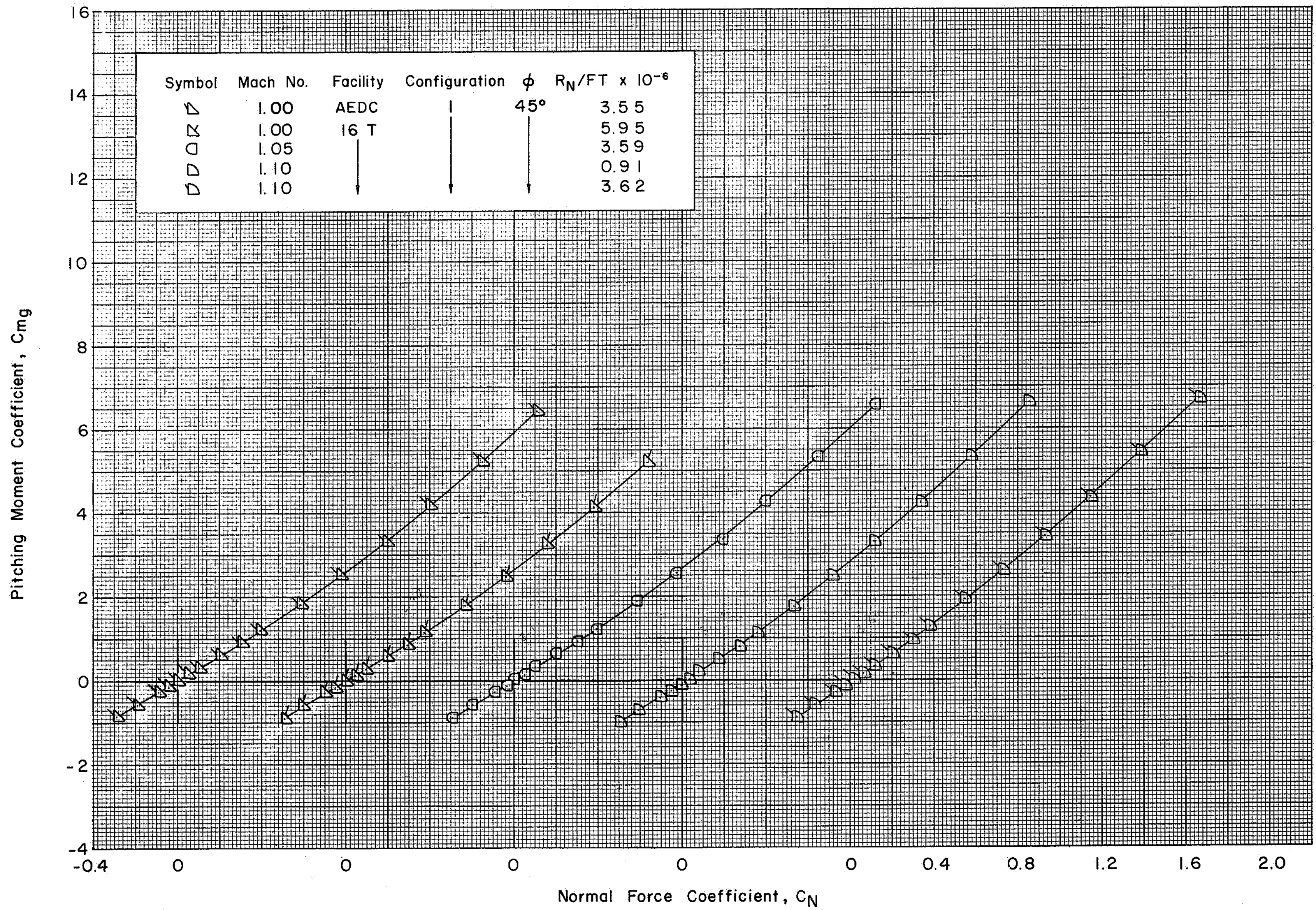

(b) Continued : $\phi = 45°$ (M=1.00 – 1.10)

Figure 21 Continued

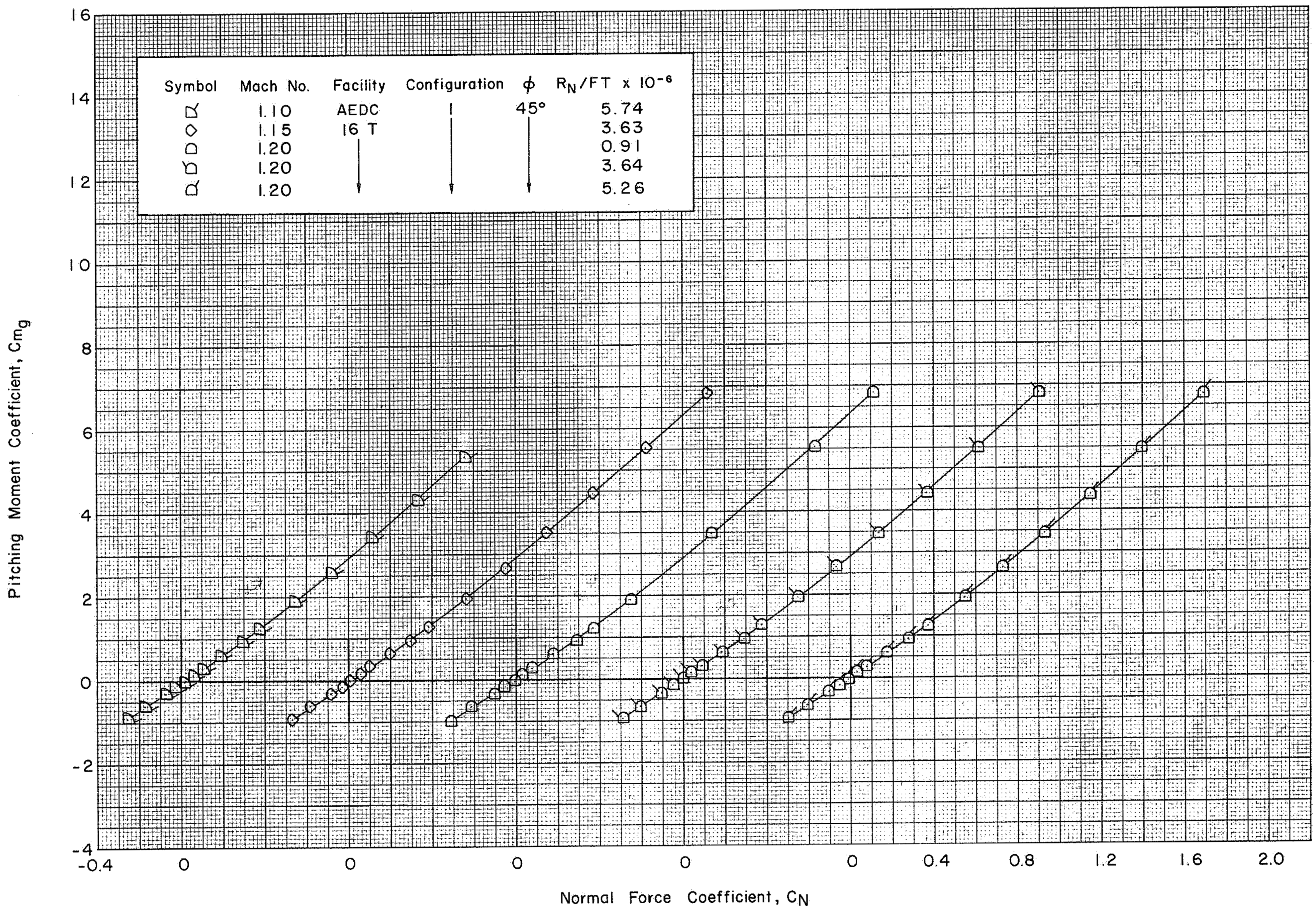

(b) Continued: ϕ=45° (M=1.10–1.20)

Figure 21 Continued

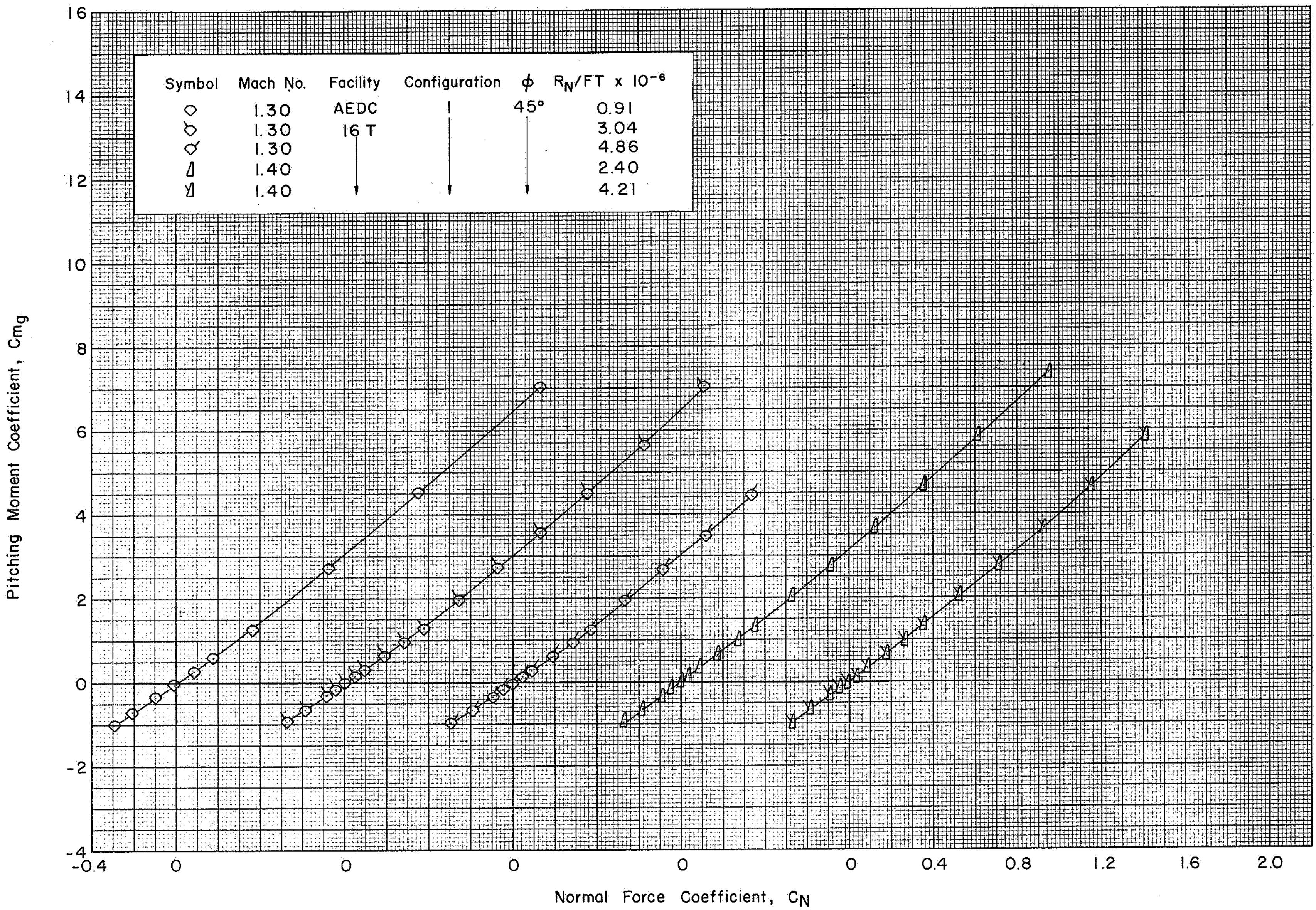

(b) Concluded : ϕ=45° (M = 1.30 – 1.40)

Figure 21 Concluded

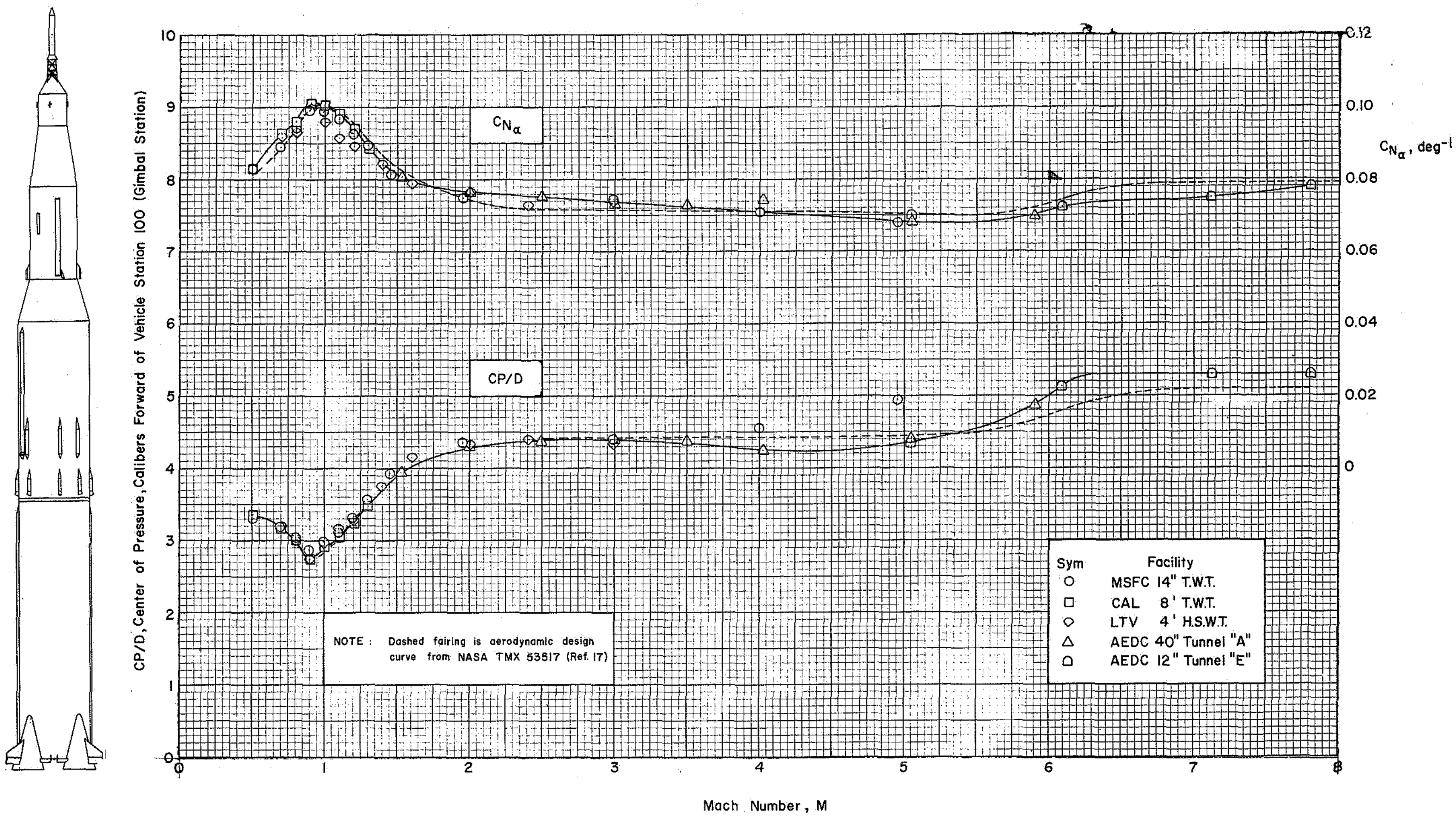

(a) $\phi = 0°$

Figure 22 Variation of Normal Force Coefficient Gradient and Center of Pressure with Mach Number for the APOLLO - SATURN V Launch Vehicle ($\alpha \approx 0°$)

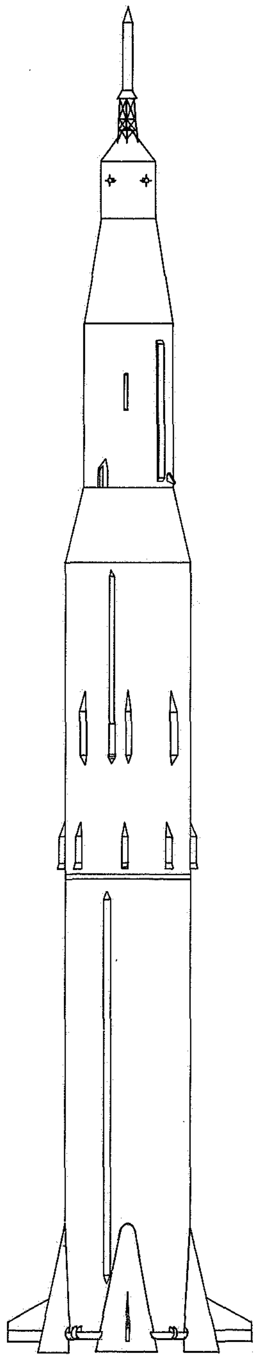

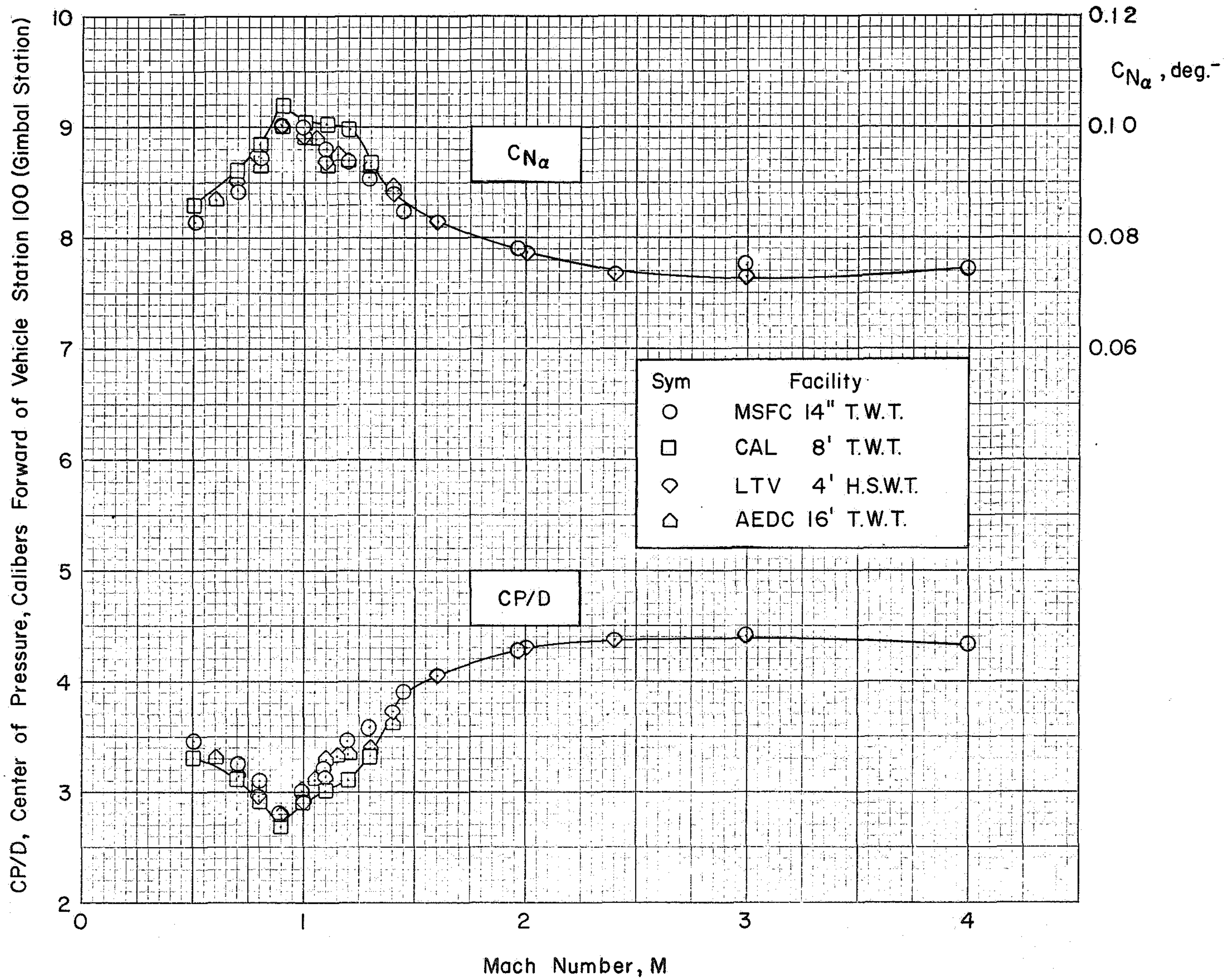

(b) $\phi = 45°$

Figure 22 Continued

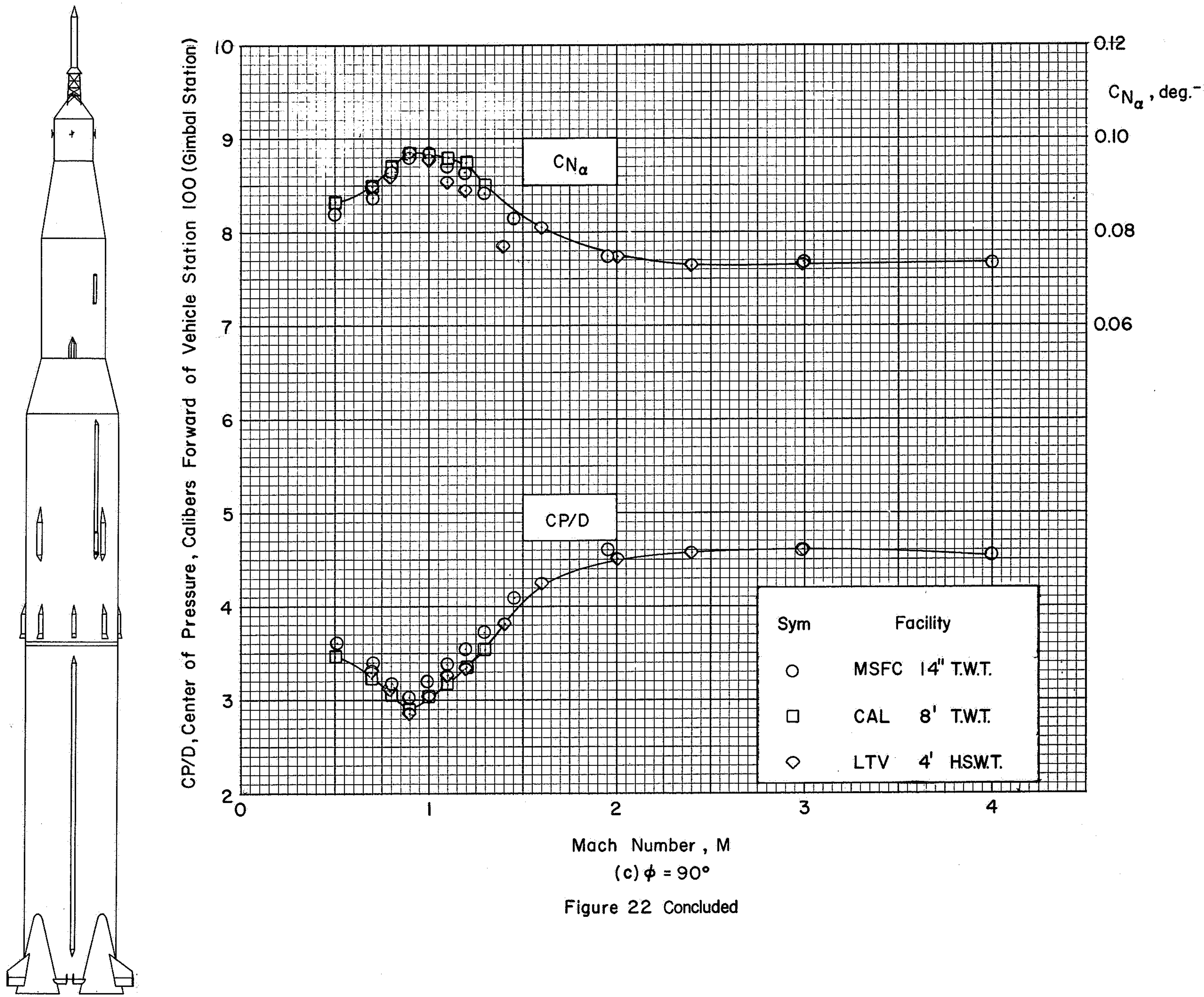

(c) $\phi = 90°$

Figure 22 Concluded

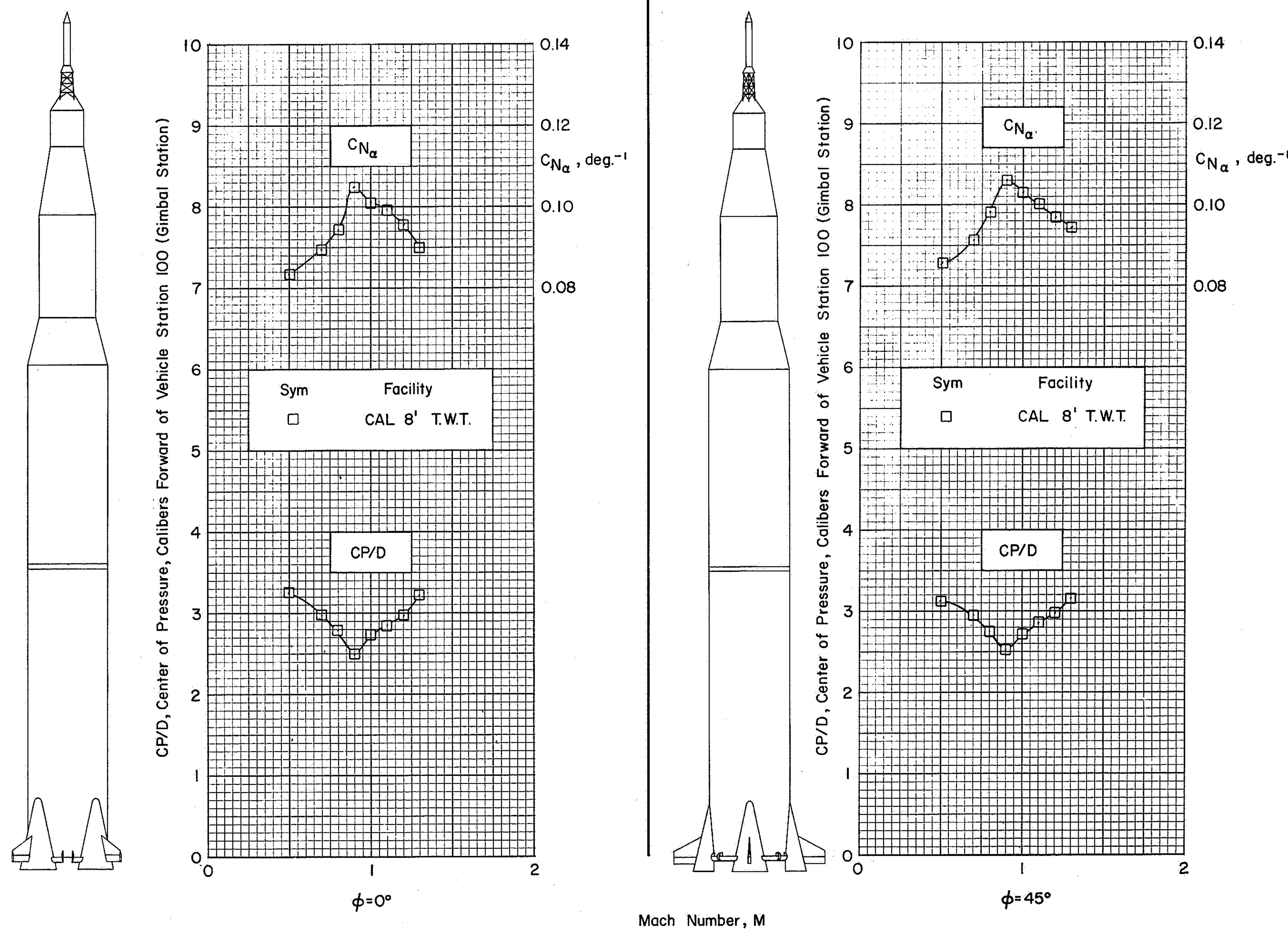

Figure 23 Variation of Normal Force Coefficient Gradient and Center of Pressure with Mach Number for the APOLLO-SATURN V Launch Vehicle without Protuberances ($\alpha \approx 0°$)

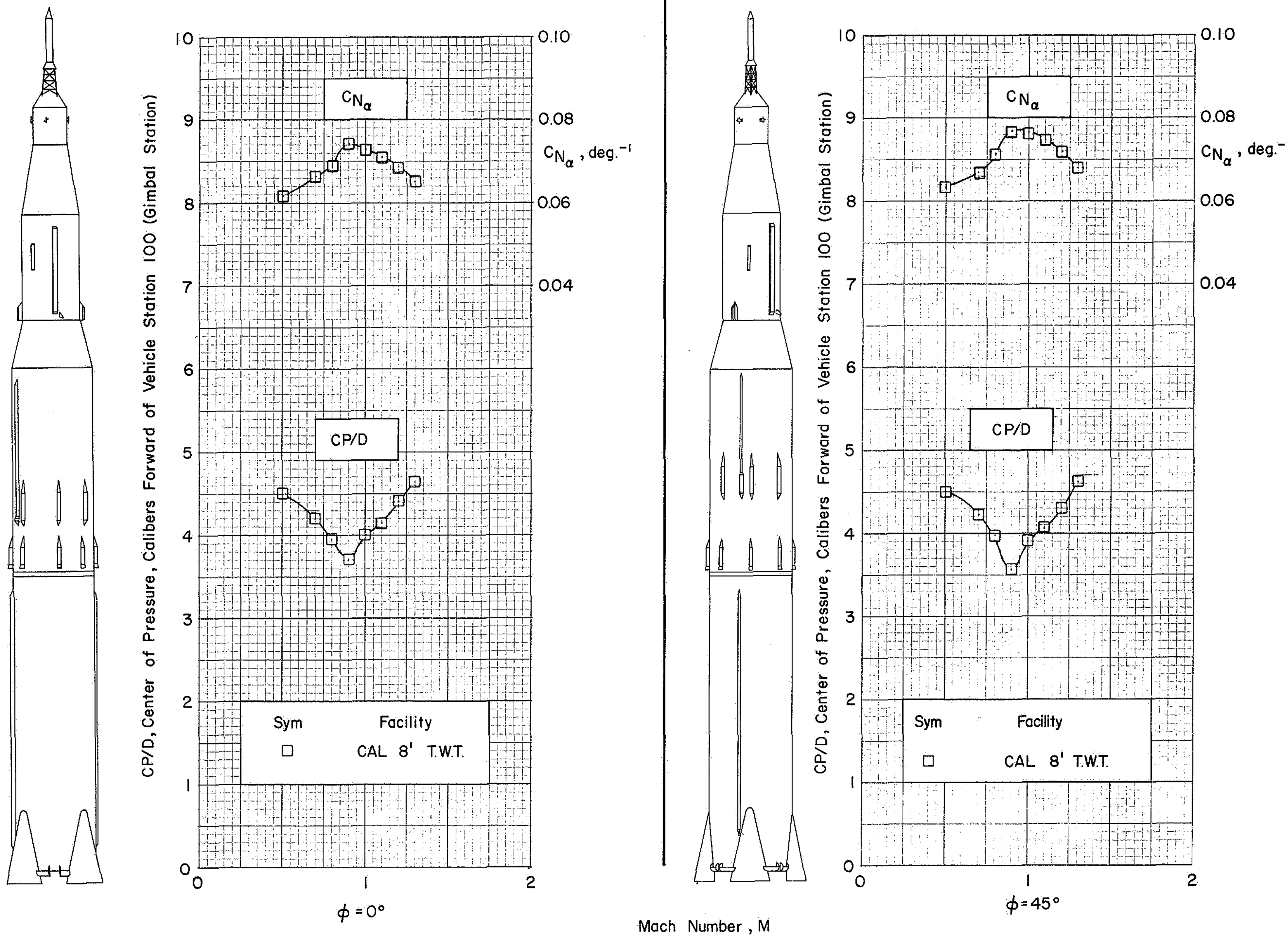

Figure 24 Variation of Normal Force Coefficient Gradient and Center of Pressure with Mach Number for the APOLLO-SATURN V Launch Vehicle without Fins ($\alpha \approx 0°$)

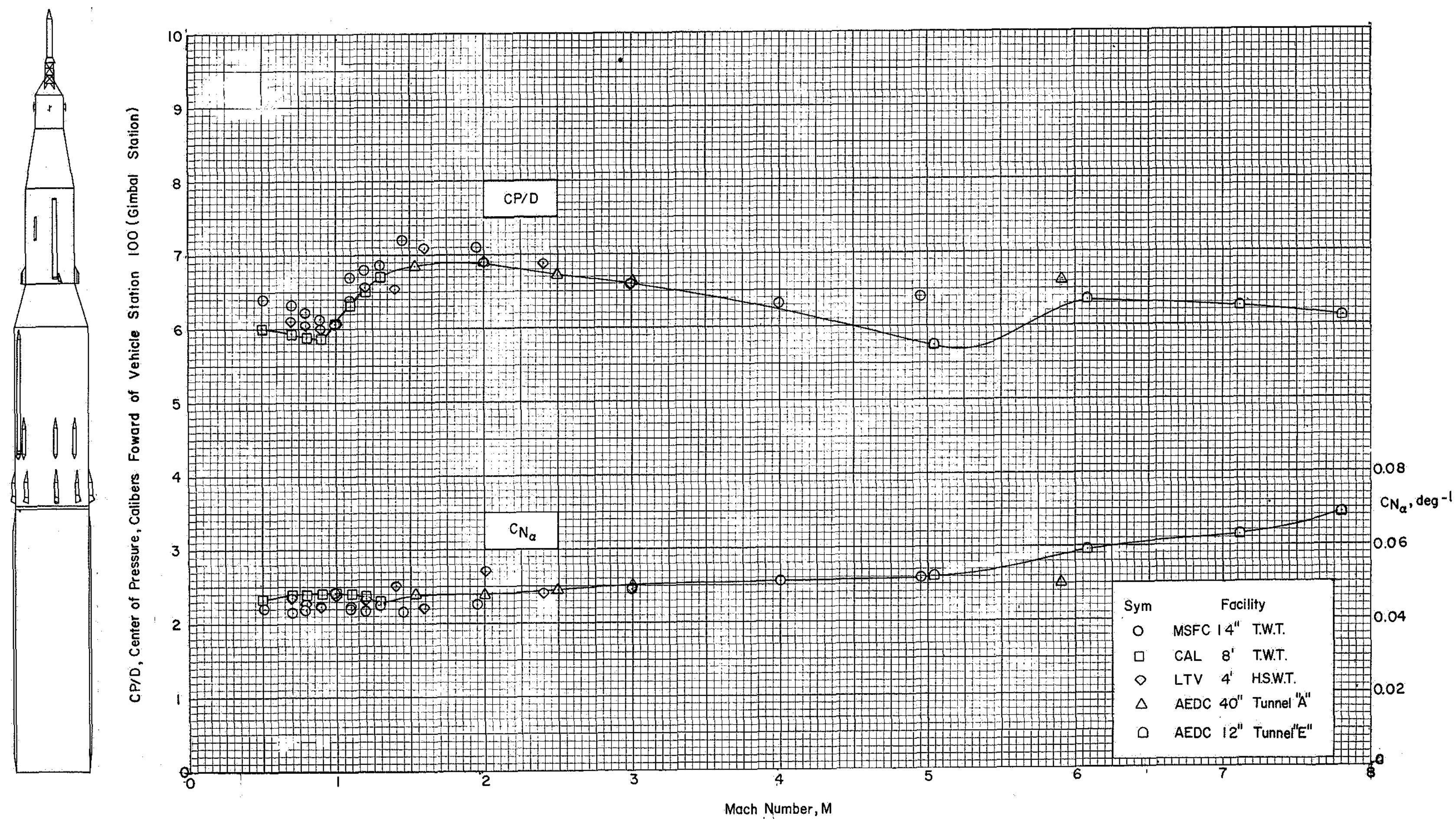

(a) $\phi = 0°$

Figure 25 Variation of Normal Force Coefficient Gradient and Center of Pressure with Mach Number for the APOLLO - SATURN V Launch Vehicle without Fins, Shrouds, and Base Flow Deflectors ($\alpha \approx 0°$)

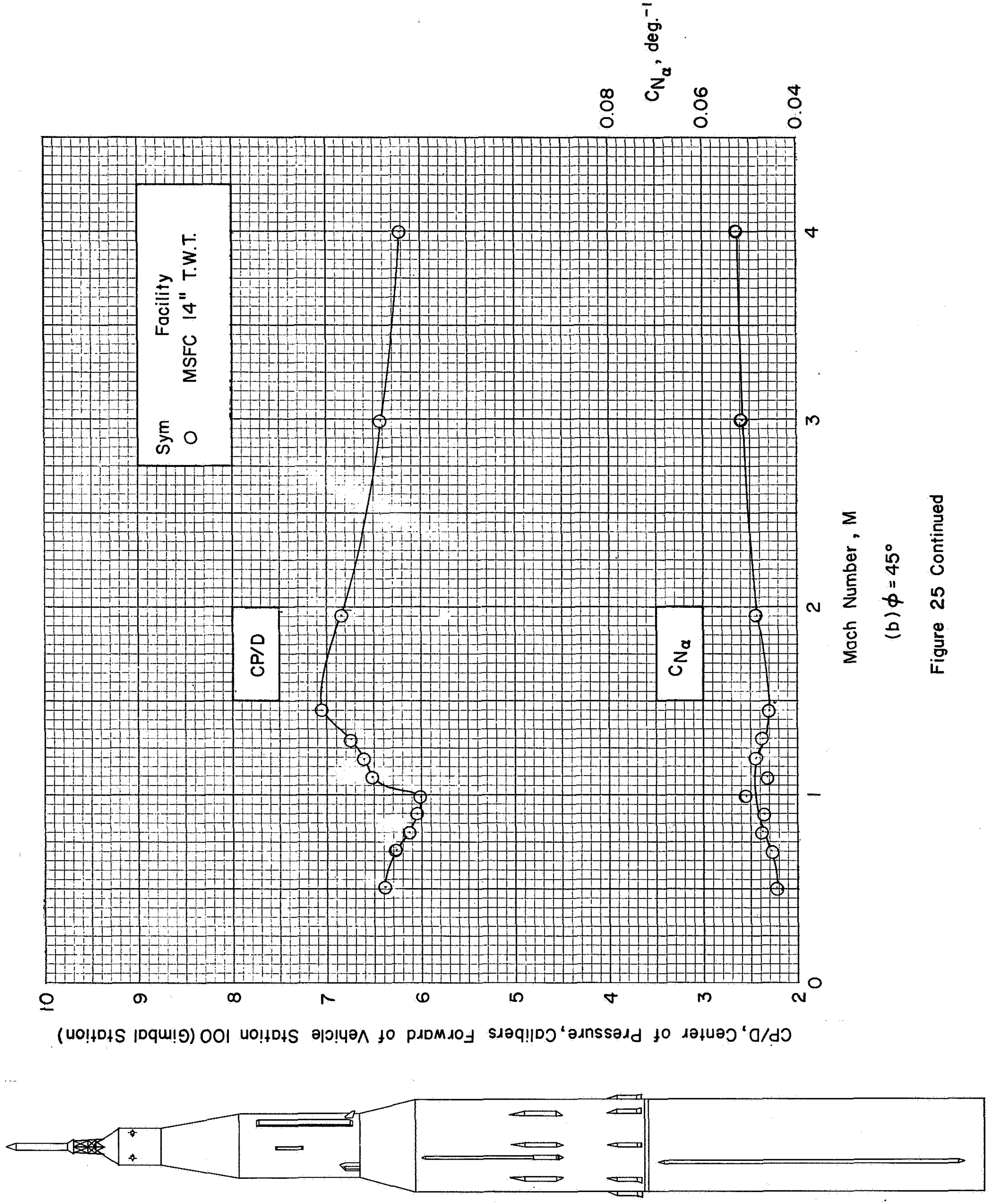

(b) $\phi = 45°$

Figure 25 Continued

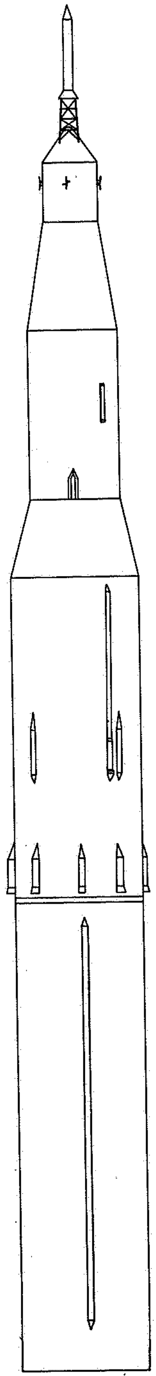

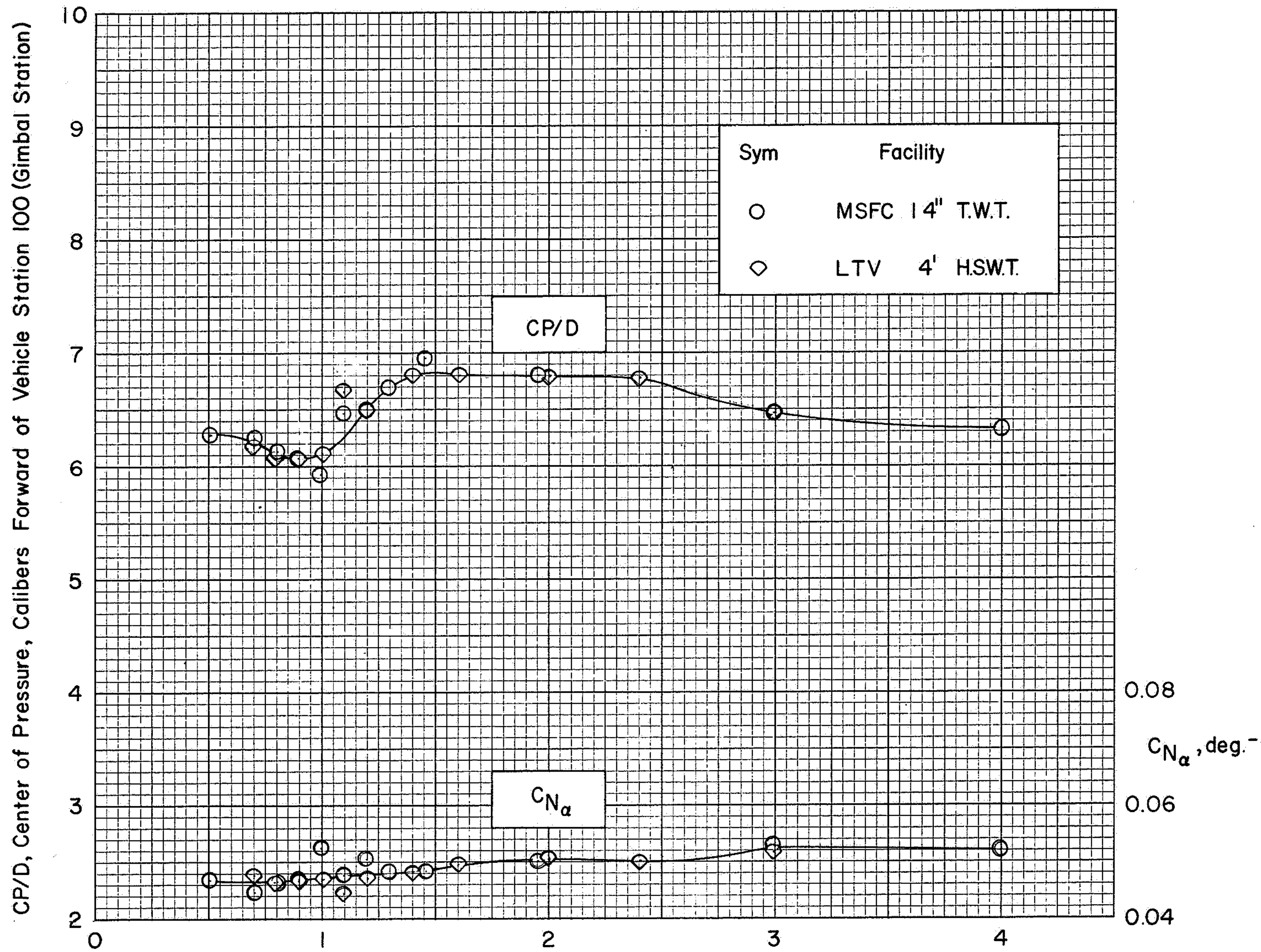

(c) $\phi = 90°$

Figure 25 Concluded

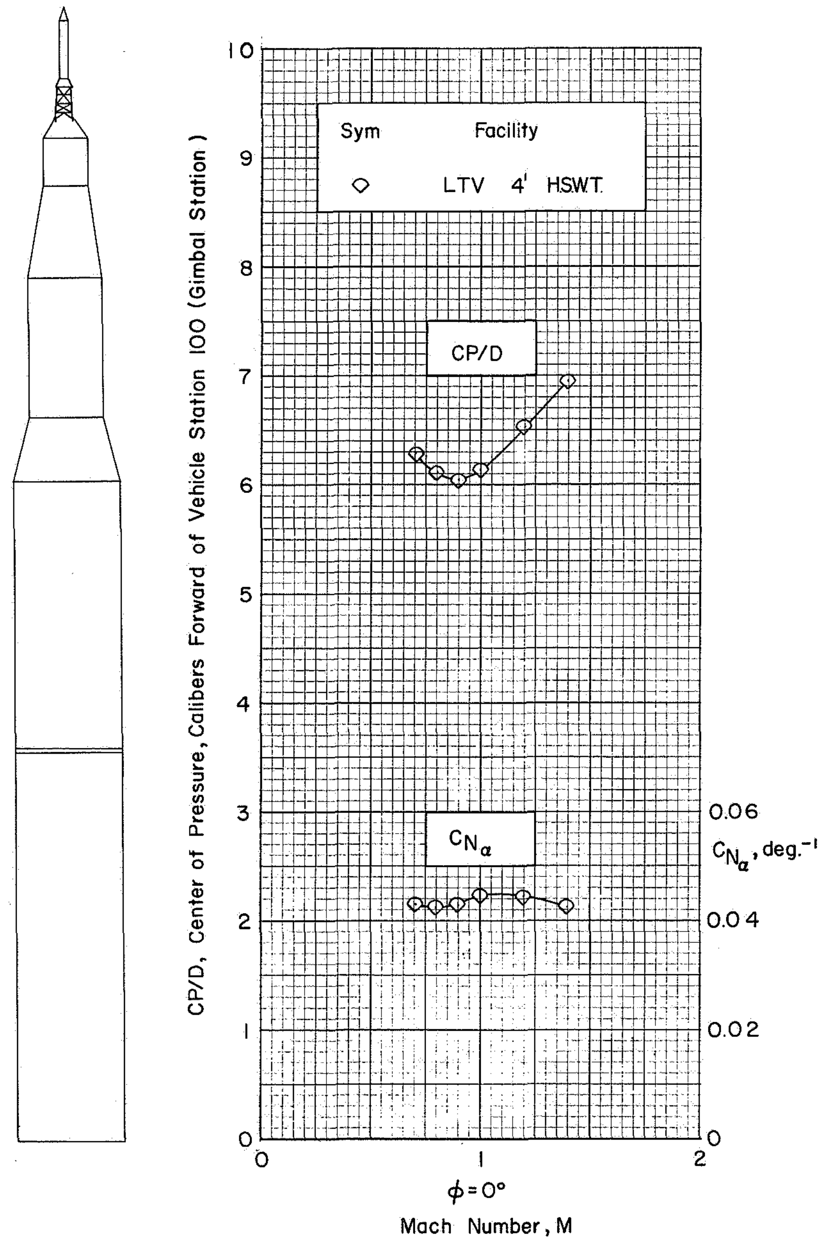

Figure 26 Variation of Normal Force Coefficient Gradient and Center of Pressure with Mach Number for the APOLLO-SATURN V Launch Vehicle without Fins, Shrouds, and Protuberances ($\alpha \approx 0°$)

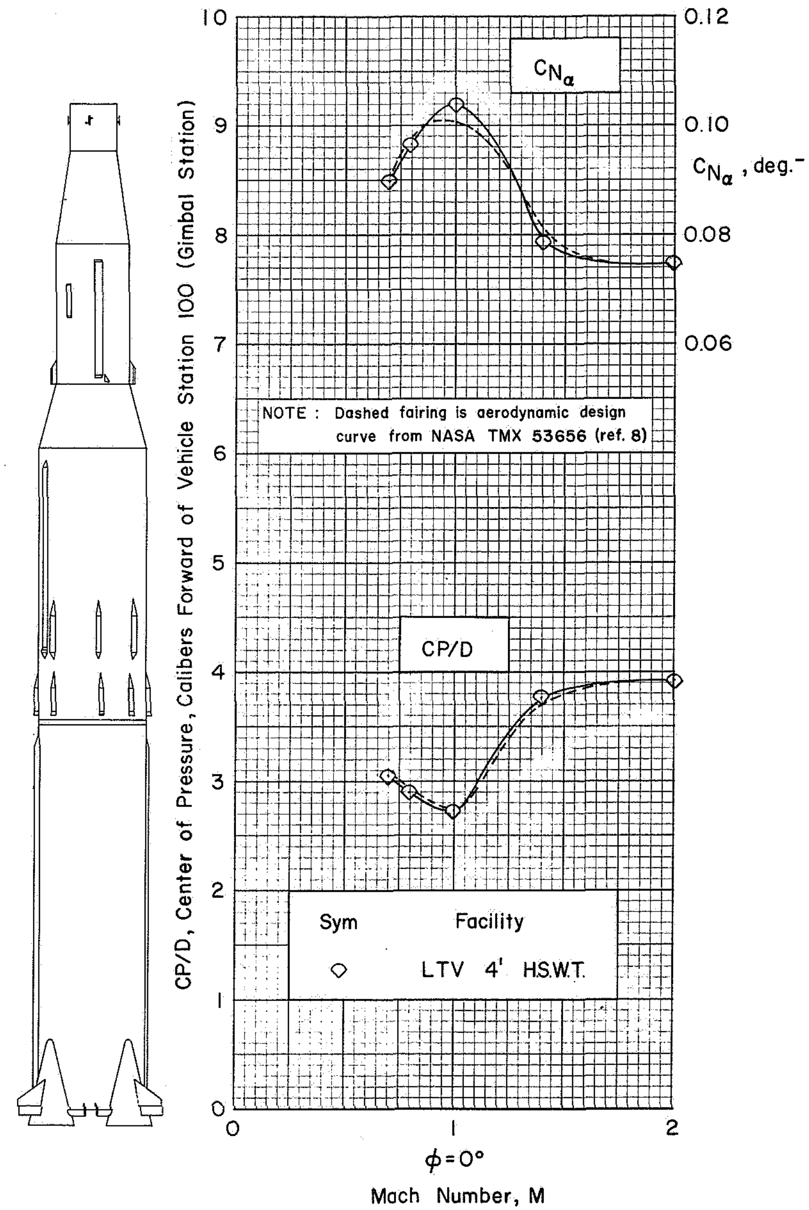

Figure 27 Variation of Normal Force Coefficient Gradient and Center of Pressure with Mach Number for the APOLLO-SATURN V Launch Vehicle without LES and Command Module ($\alpha \approx 0°$)

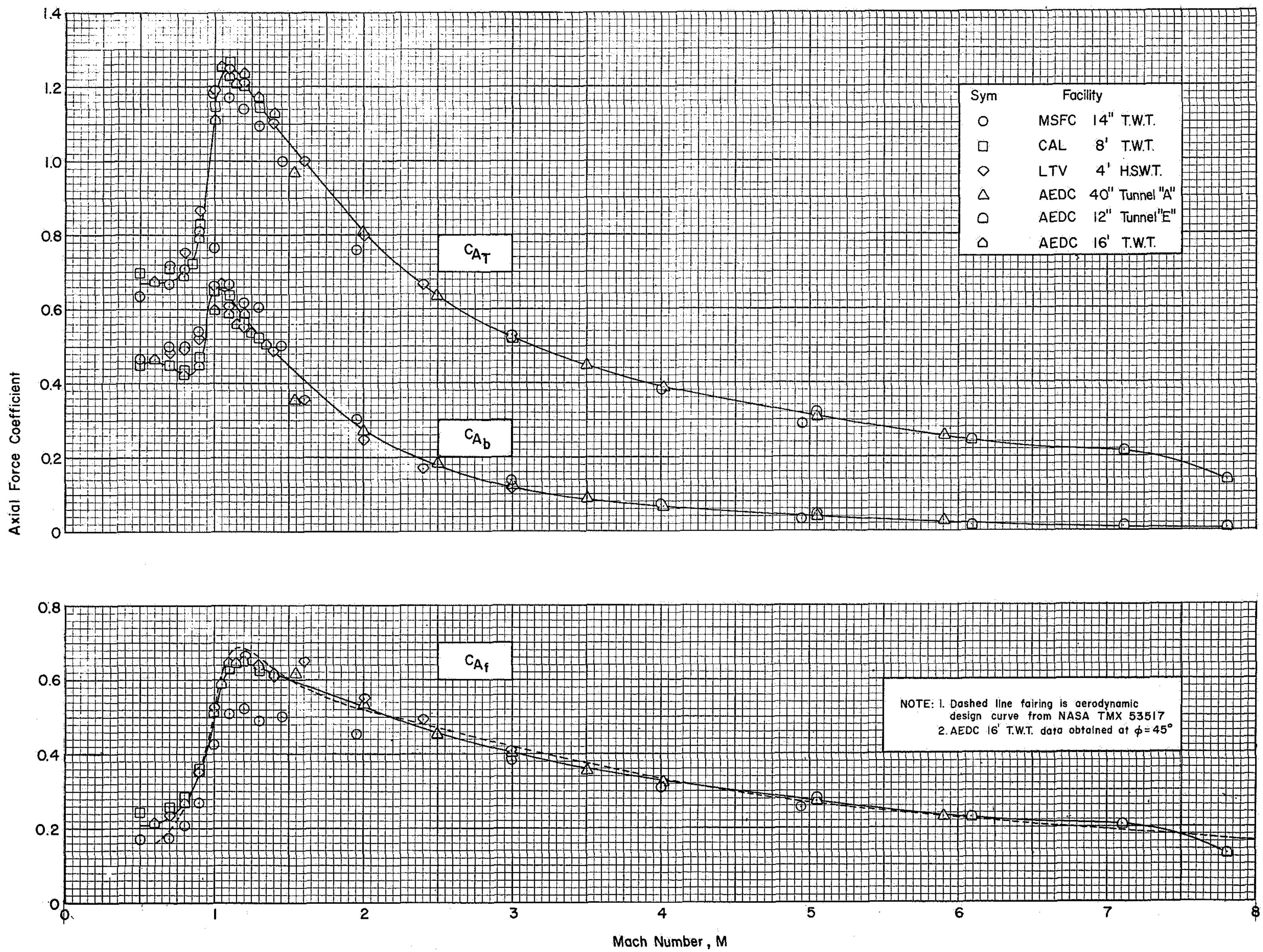

$\phi = 0°$

Figure 28 Variation of Axial Force Coefficient with Mach Number for the APOLLO - SATURN V Launch Vehicle ($\alpha \approx 0°$)

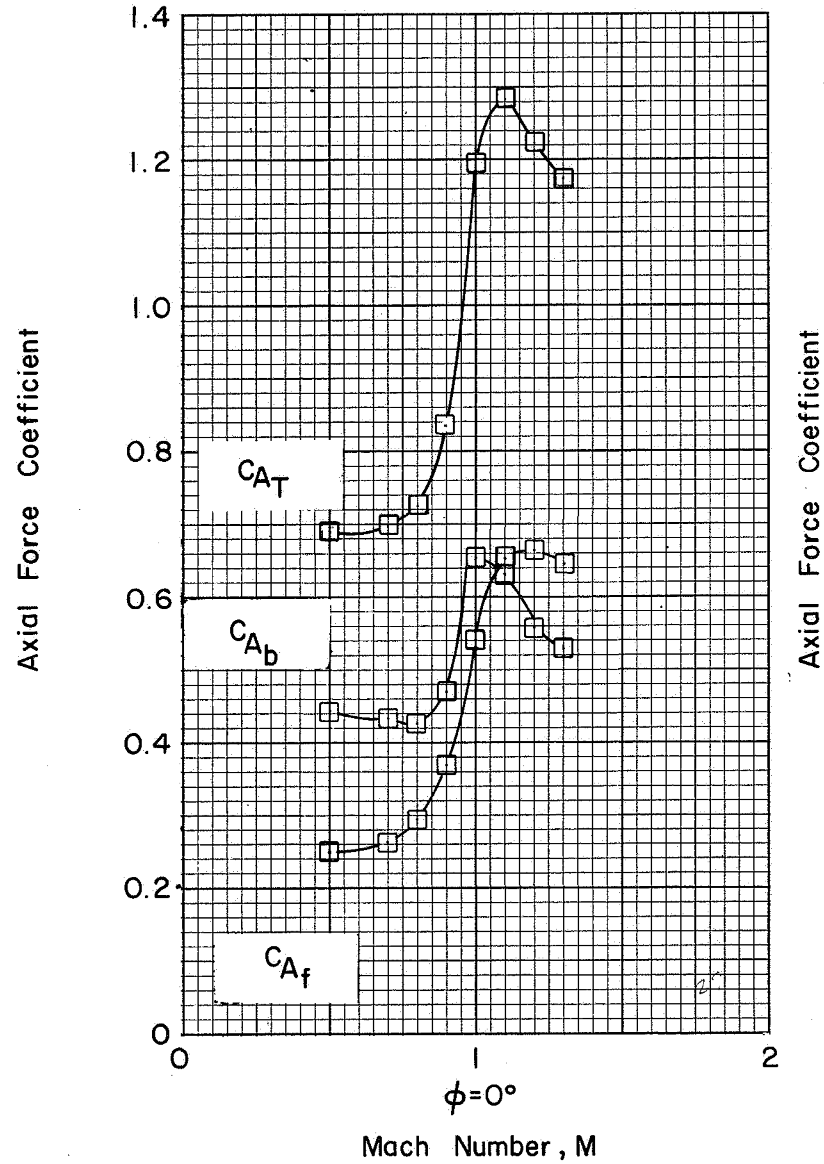

Figure 29 Variation of Axial Force Coefficient with Mach Number for the APOLLO-SATURN V Launch Vehicle without Protuberances ($\alpha \approx 0°$)

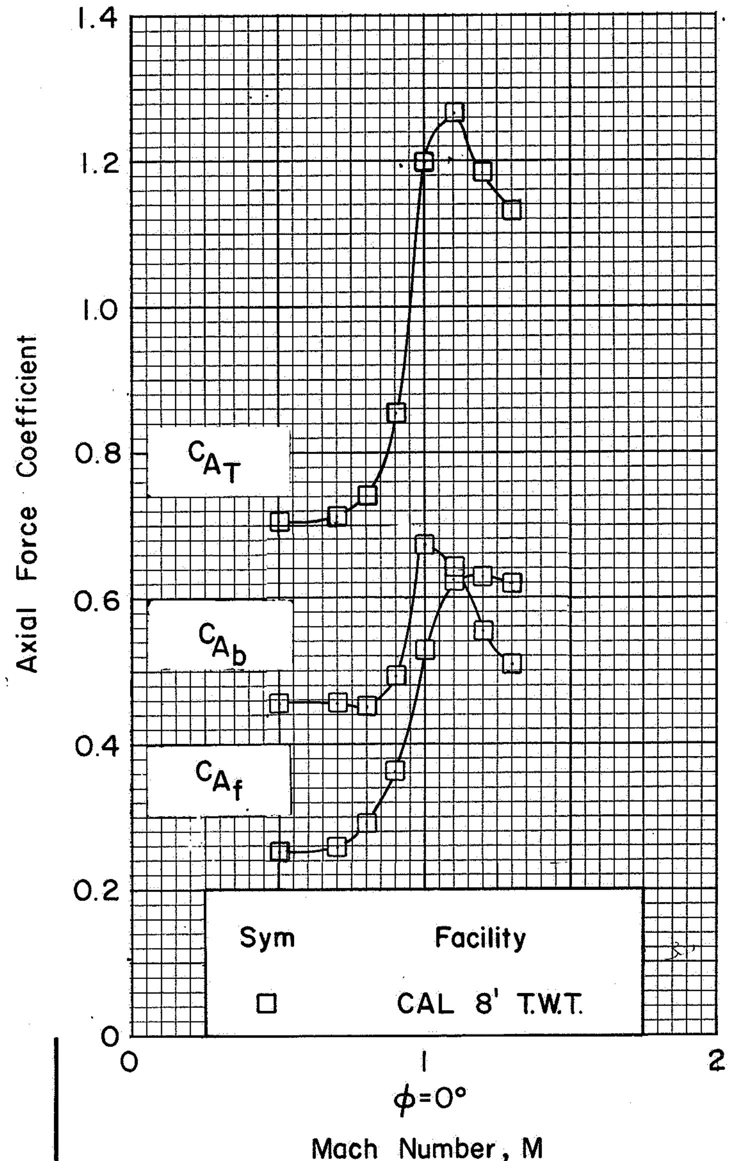

Figure 30 Variation of Axial Force Coefficient with Mach Number for the APOLLO-SATURN V Launch Vehicle without Fins ($\alpha \approx 0°$)

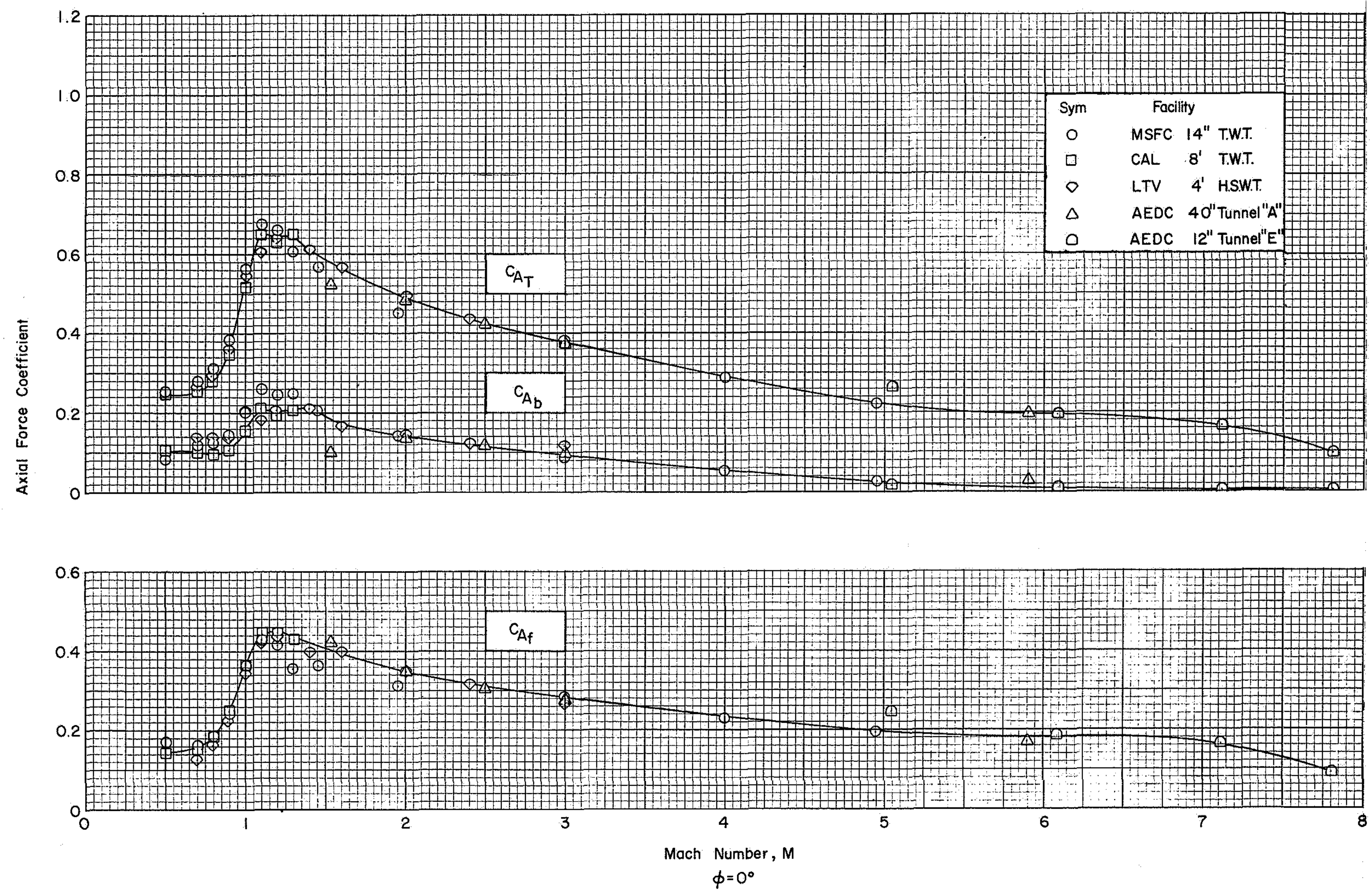

Figure 31 Variation of Axial Force Coefficient with Mach Number for the APOLLO-SATURN V Launch Vehicle without Fins, Shrouds, and Base Flow Deflectors ($\alpha \approx 0°$)

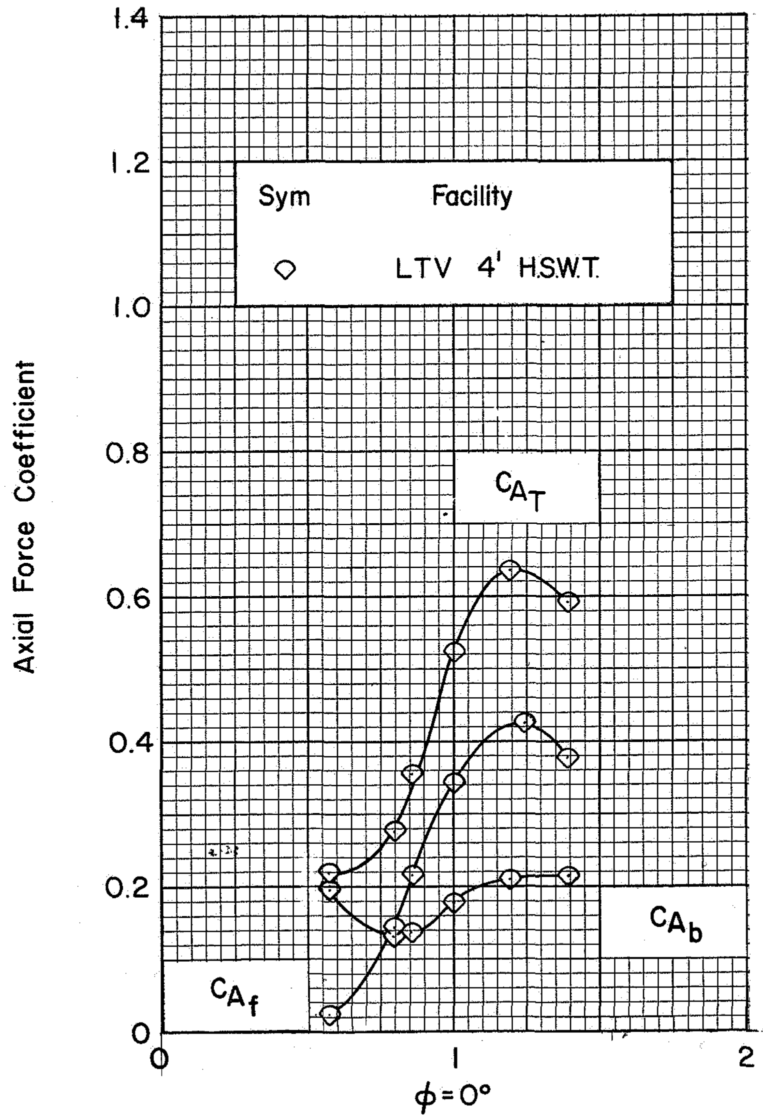

Figure 32 Variation of Axial Force Coefficient with Mach Number for the APOLLO-SATURN V Launch Vehicle without Fins, Shrouds, and Protuberances ($\alpha \approx 0°$)

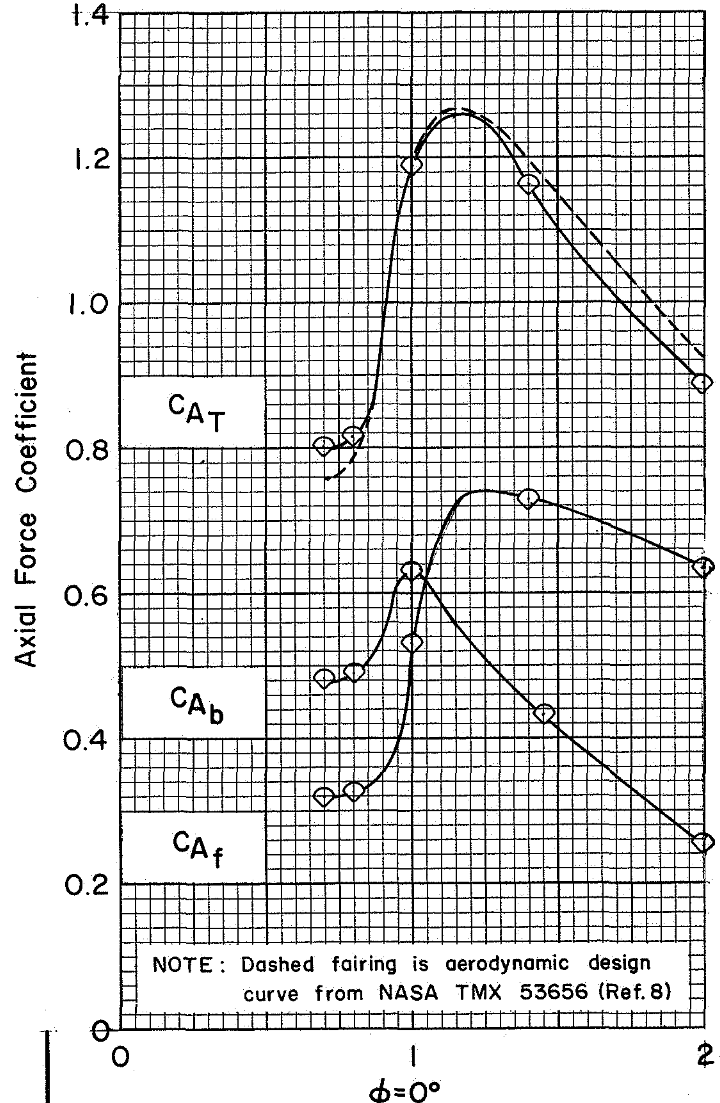

Figure 33 Variation of Axial Force Coefficient with Mach Number for the APOLLO-SATURN V Launch Vehicle without LES and Command Module ($\alpha \approx 0°$)

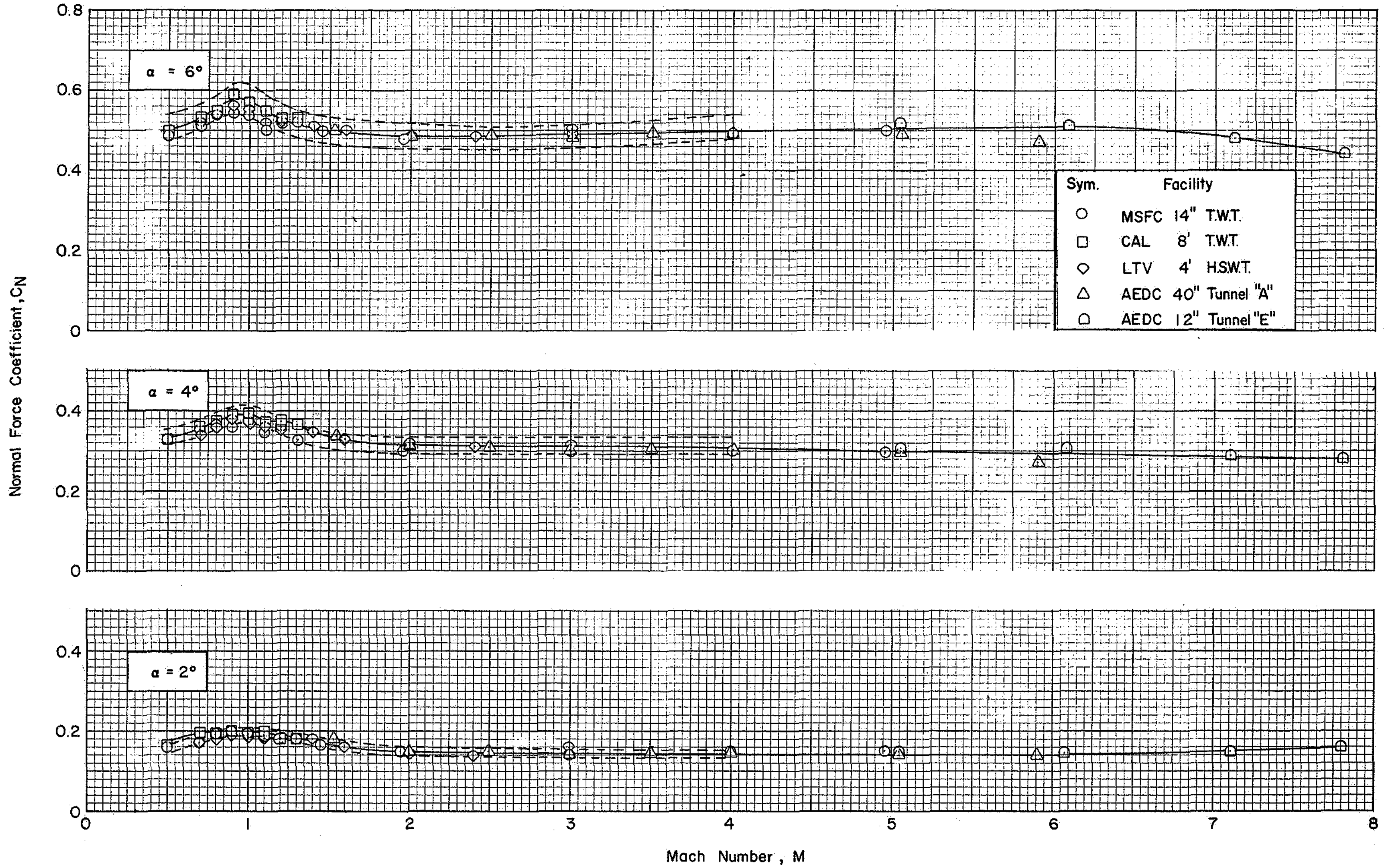

(a) C_N vs. M: $\phi = 0°$ ($\alpha = 2°, 4°, 6°$)

Figure 34 Variation of Normal Force Coefficient and Center of Pressure with Mach Number and Angle of Attack for the APOLLO-SATURN V Launch Vehicle

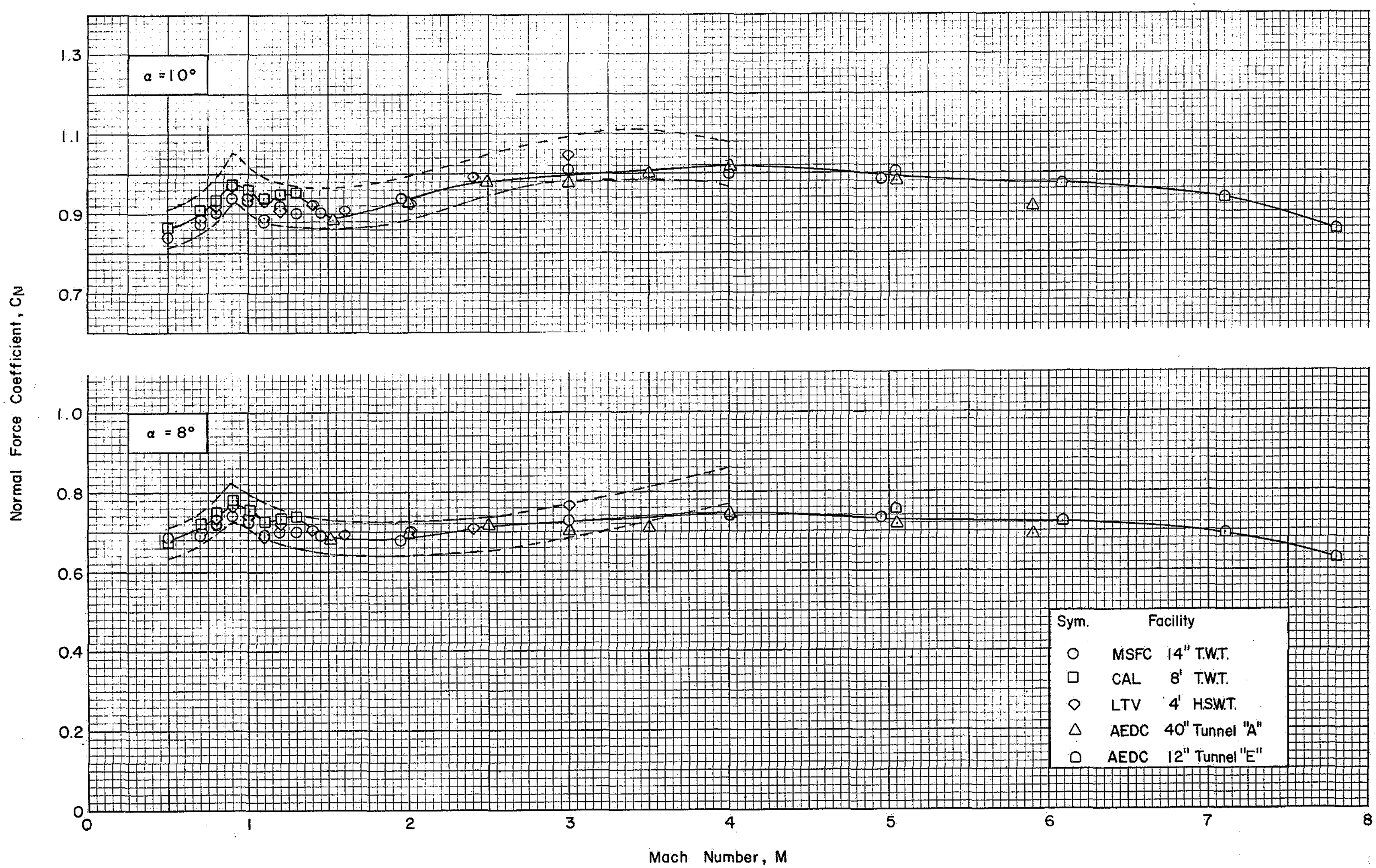

(a) Continued : $\phi=0°$ ($\alpha=8°$ & $10°$)

Figure 34 Continued

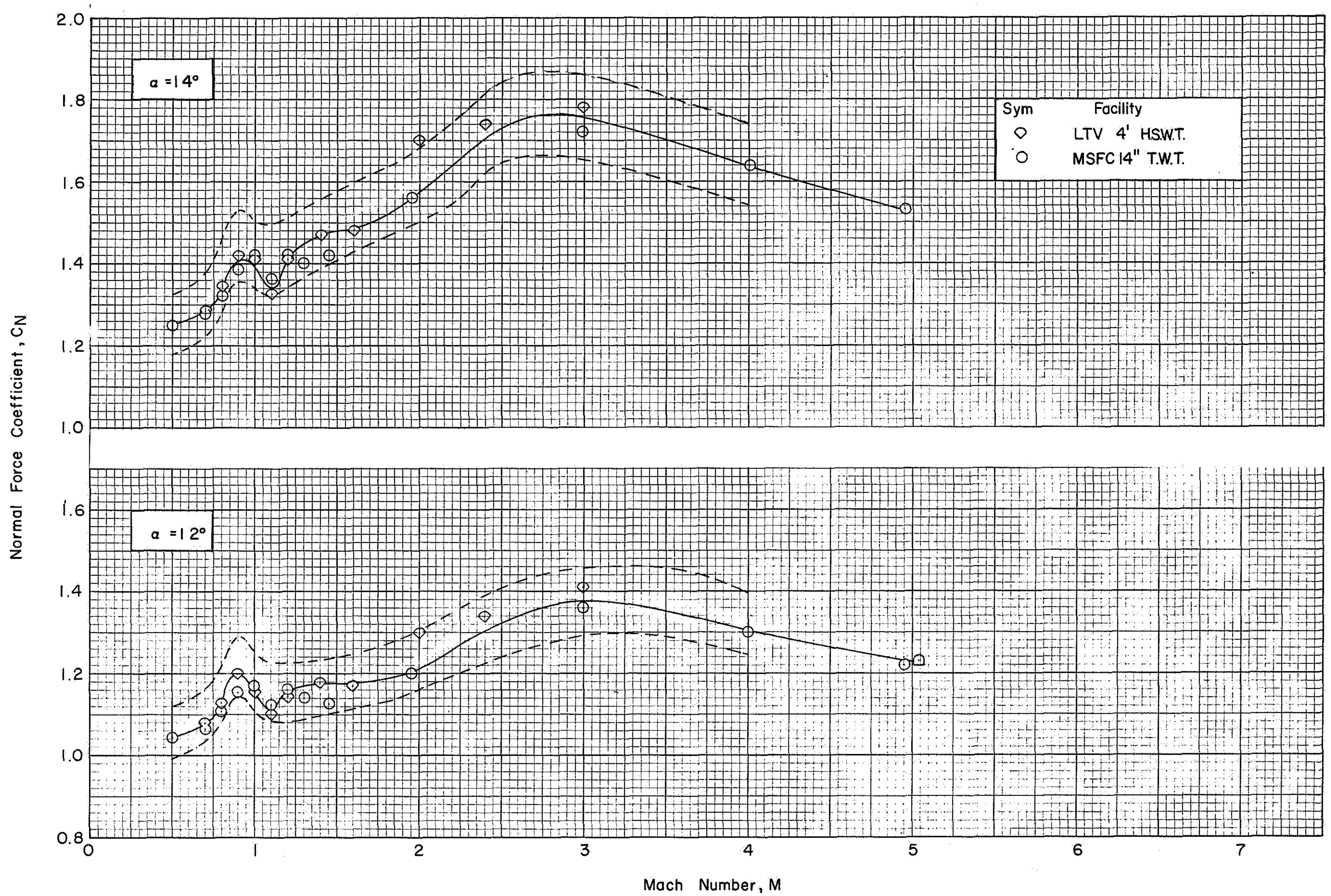

(a) Continued : $\phi = 0°$ ($\alpha = 12°$ & $14°$)

Figure 34 Continued

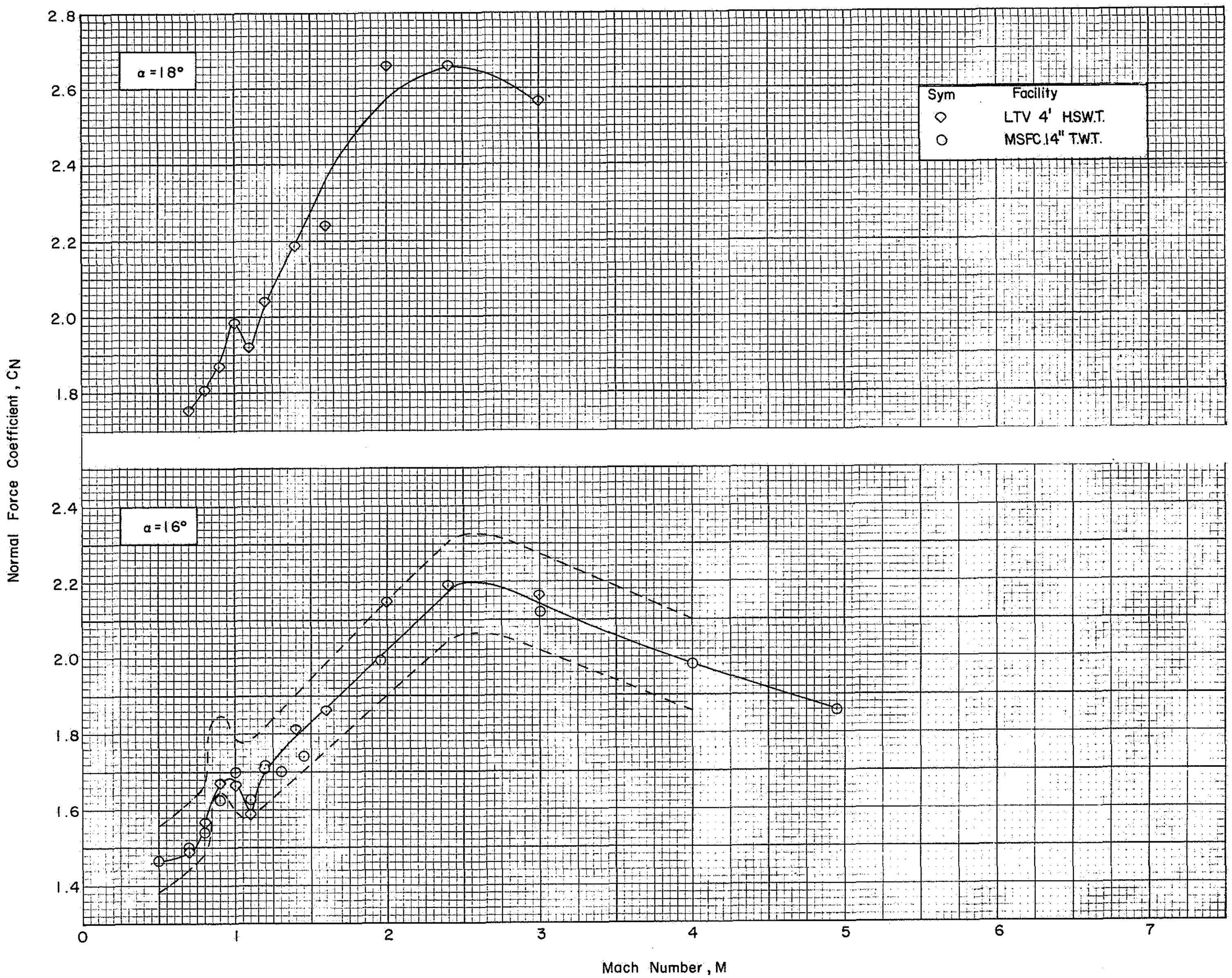

(a) Continued : $\phi = 0°$ ($\alpha = 16° \& 18°$)

Figure 34 Continued

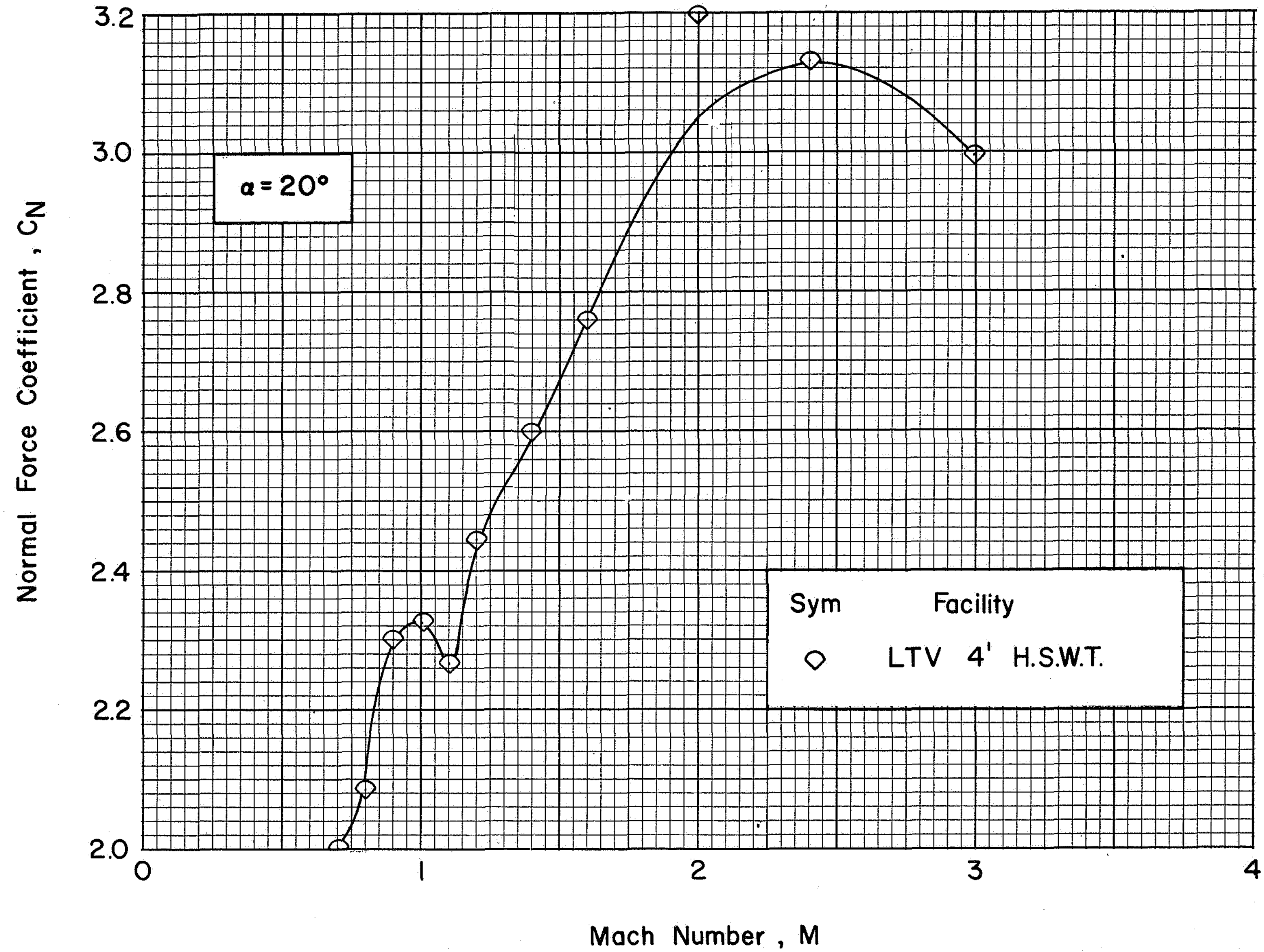

(a) Concluded: $\phi = 0° (\alpha = 20°)$

Figure 34 Continued

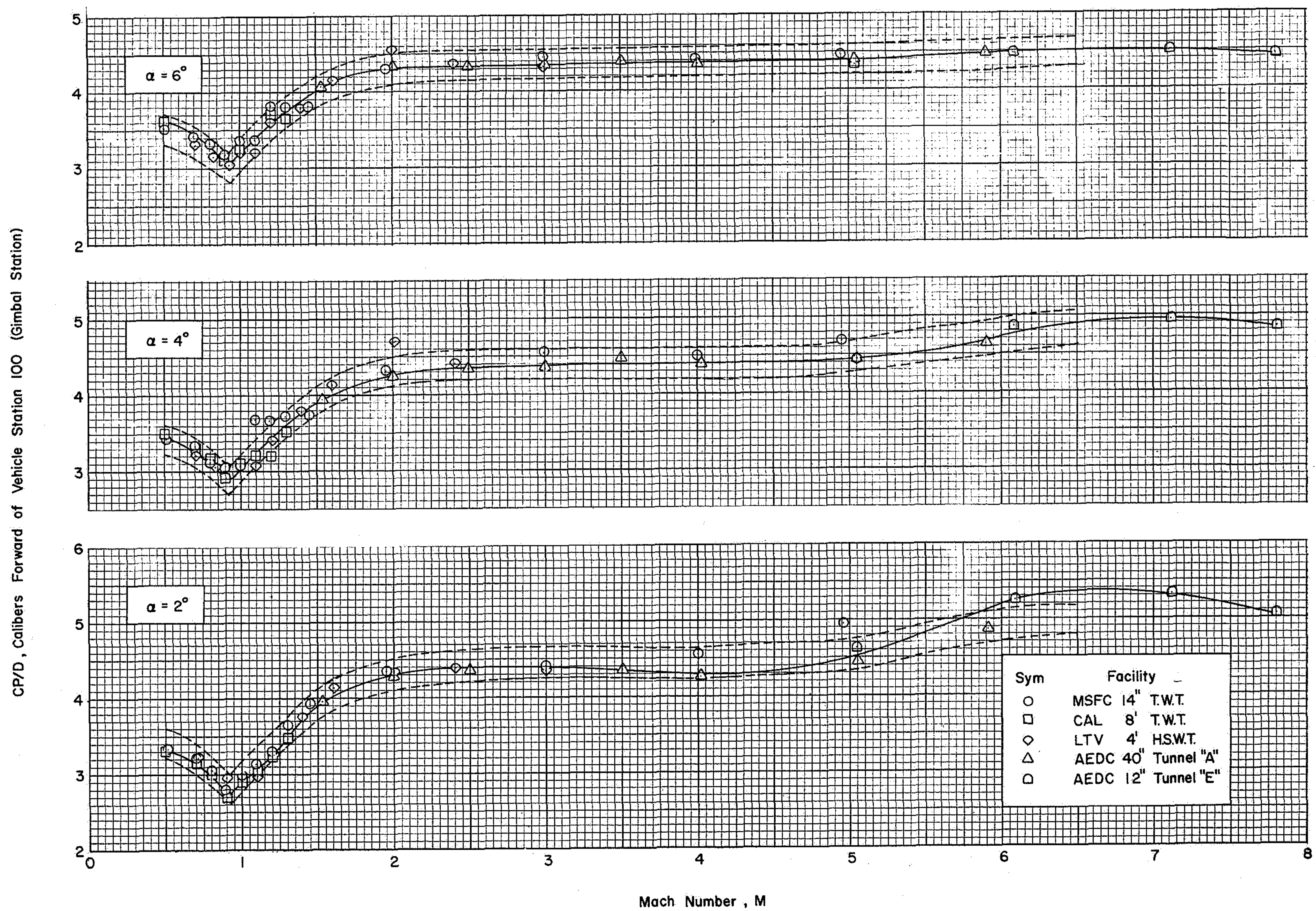

(b) CP/D vs. M: $\phi = 0°$ ($\alpha = 2°, 4°, 6°$)

Figure 34 Continued

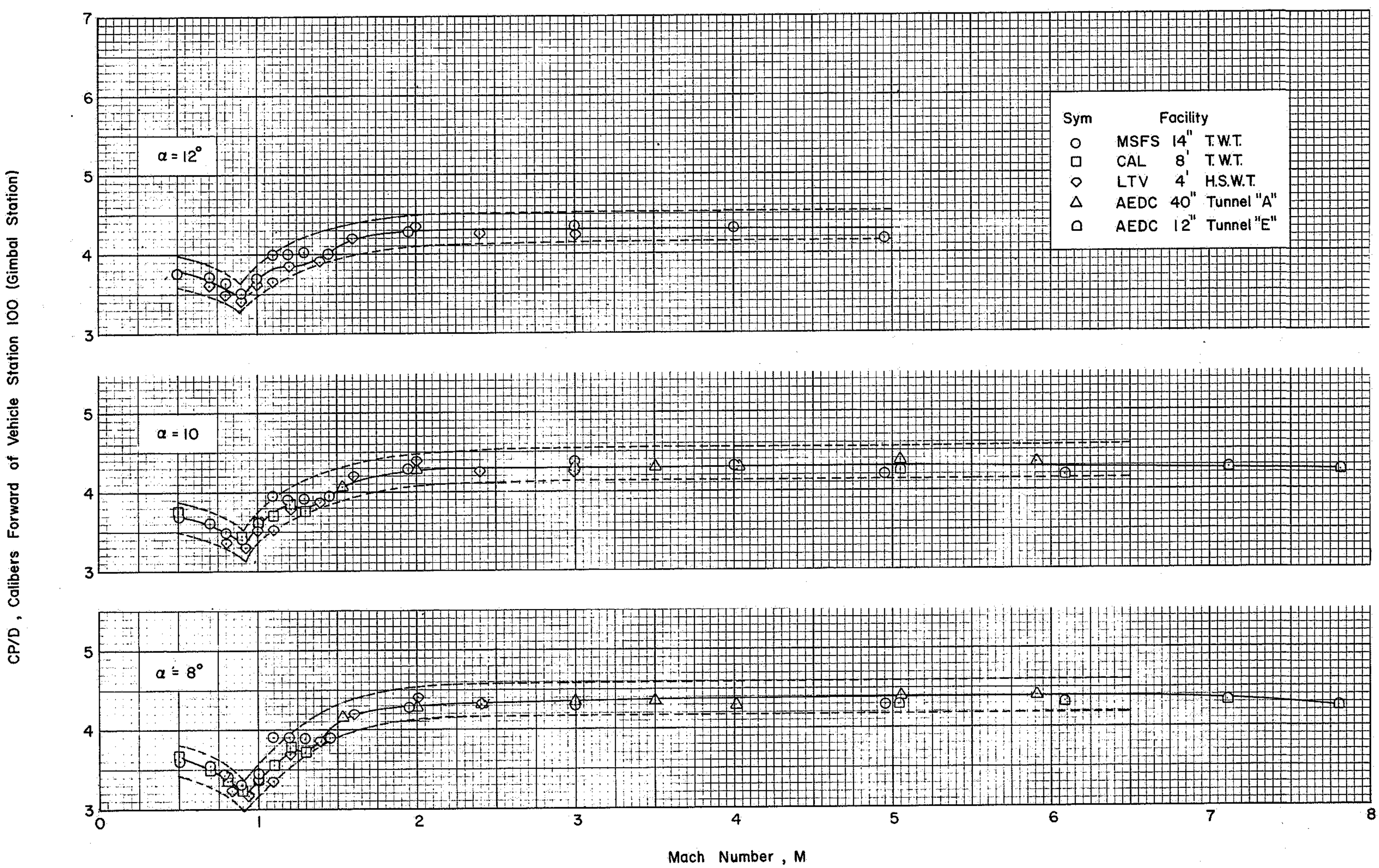

(b) Continued: $\phi = 0°$ ($\alpha = 8°, 10°, 12°$)

Figure 34 Continued

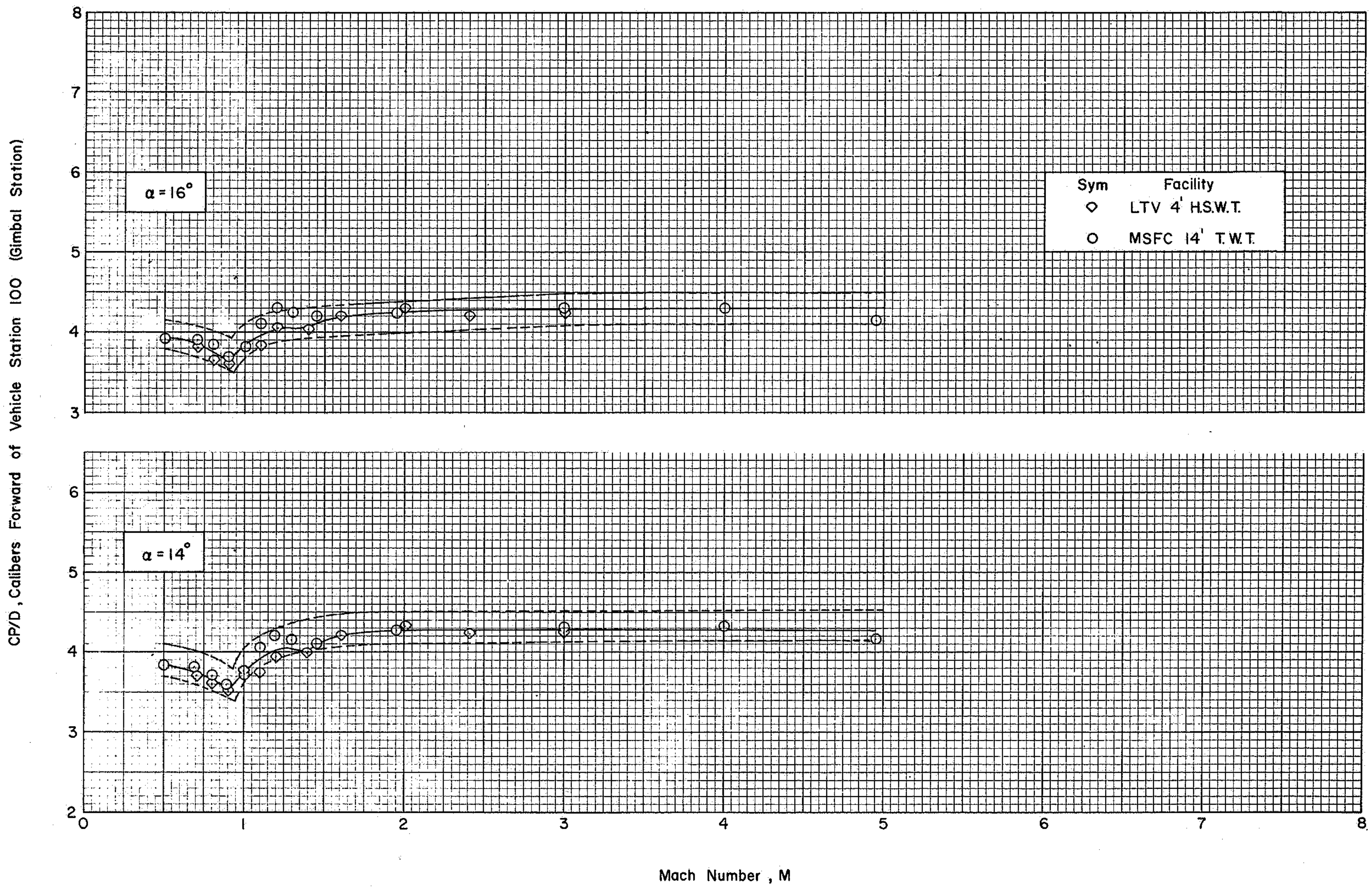

(b) Continued : $\phi = 0^{\circ}$ (α = 14 & 16)

Figure 34 Continued

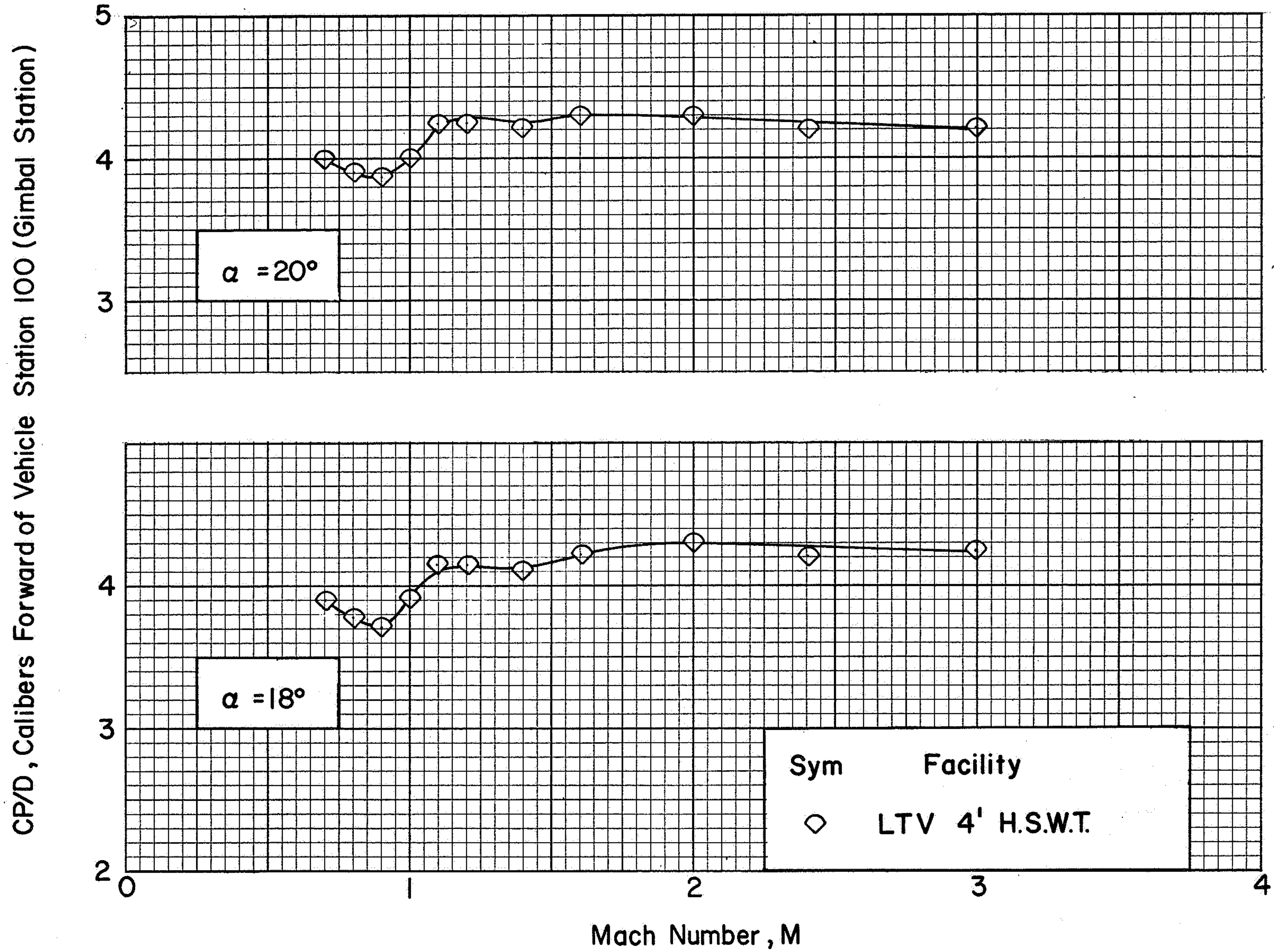

(b) Concluded : ϕ=0°(α=18° & 20°)

Figure 34 Concluded

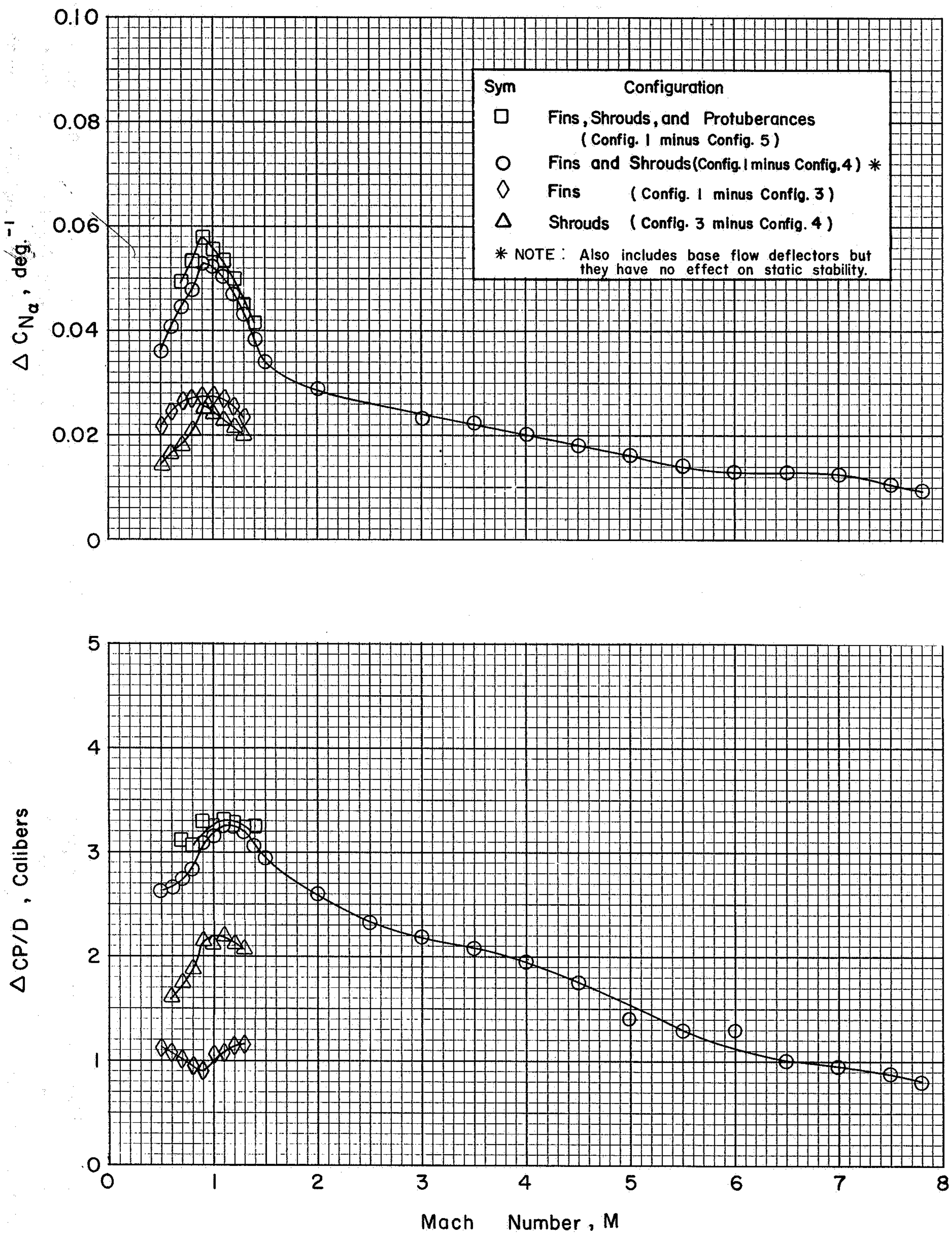

Figure 35 Effect of Fins, Shrouds and Protuberances on the Variation of Normal Force Coefficient and Center of Pressure with Mach Number for the APOLLO-SATURN V Launch Vehicle ($\alpha \approx 0°$, $\phi = 0°$)

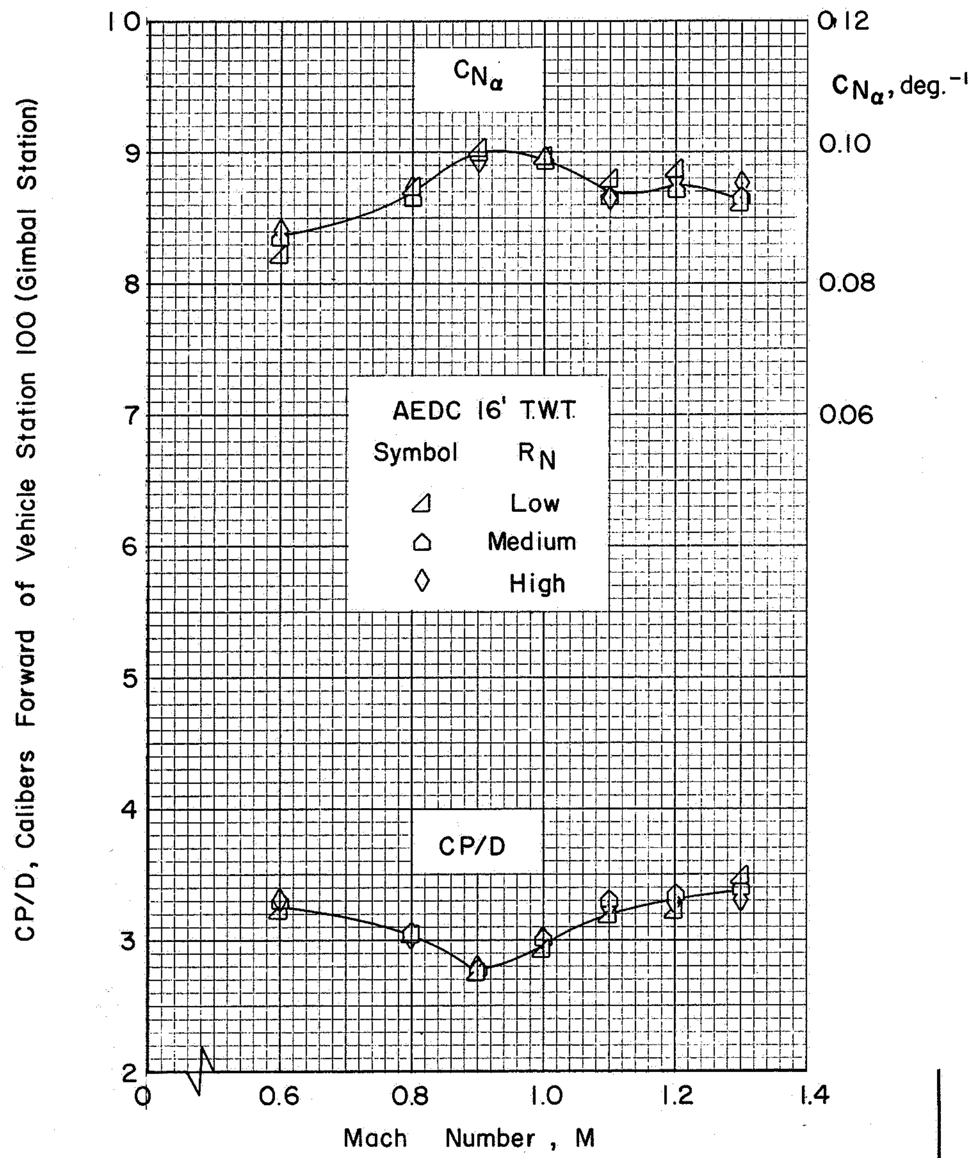

Figure 36 Effect of Reynolds Number on the Variation of Normal Force Coefficient Gradient and Center of Pressure with Mach Number for the APOLLO-SATURN V Launch Vehicle ($\alpha \approx 0°$, $\phi = 45°$)

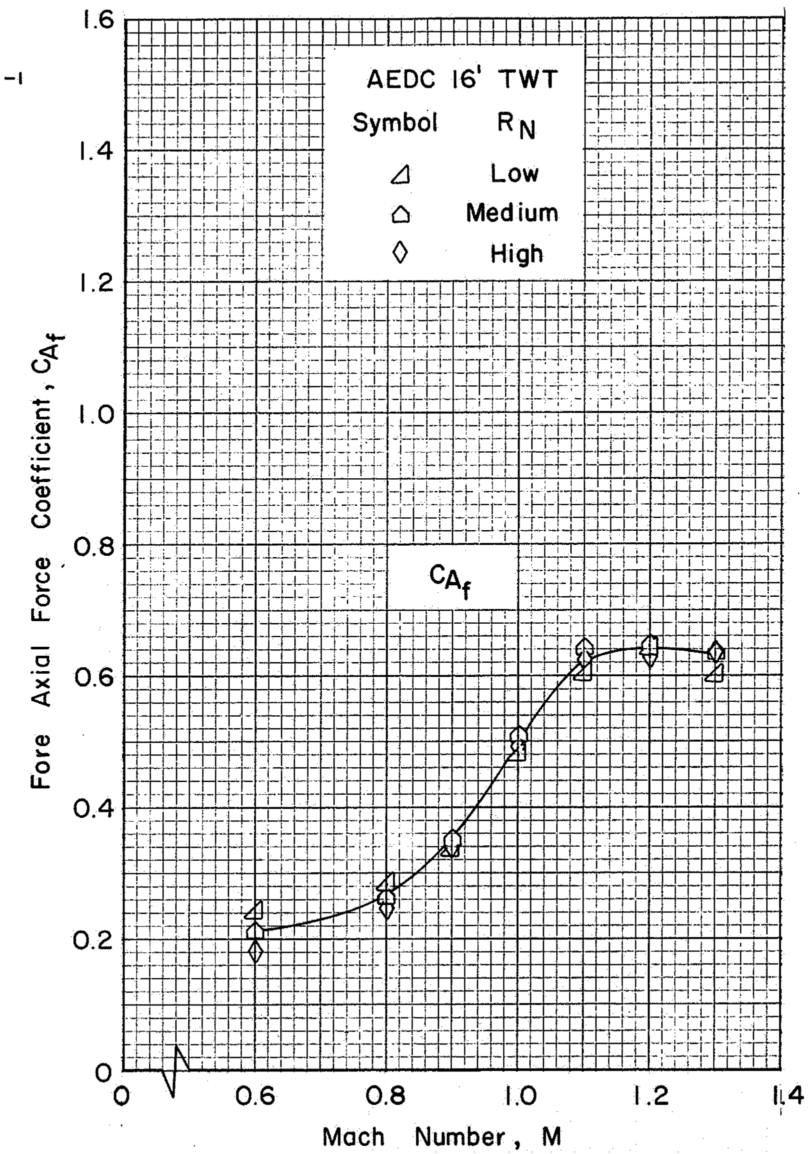

Figure 37 Effect of Reynolds Number on the Variation of Forebody Axial Force Coefficient with Mach Number for the APOLLO-SATURN V Launch Vehicle ($\alpha \approx 0°$, $\phi = 45°$)

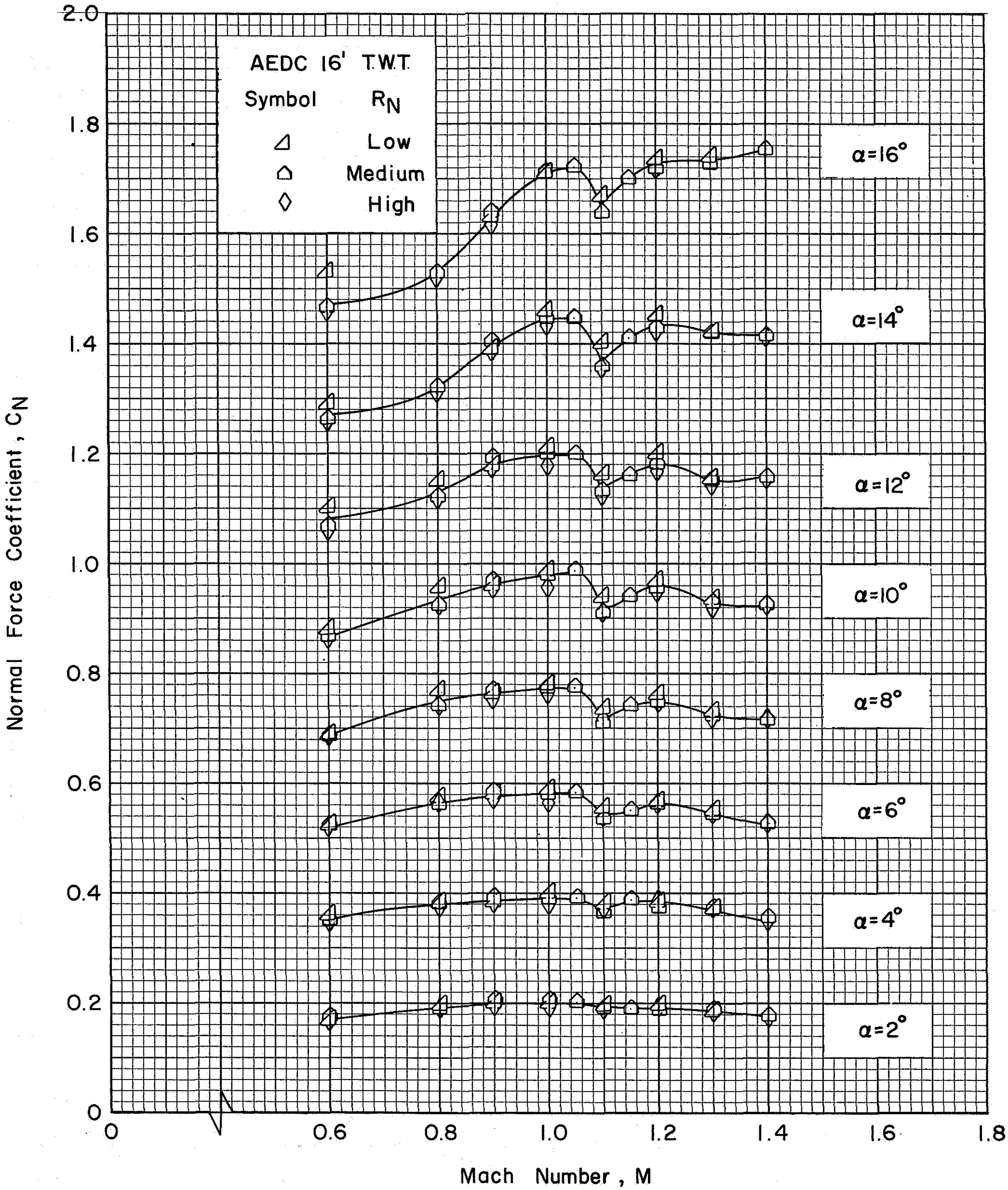

(a) C_N vs. M : ($\alpha = 2° - 16°$)

Figure 38 Effect of Reynolds Number on the Variation of Normal Force Coefficient and Center of Pressure with Mach Number and Angle of Attack for the APOLLO-SATURN V Launch Vehicle ($\phi = 45°$)

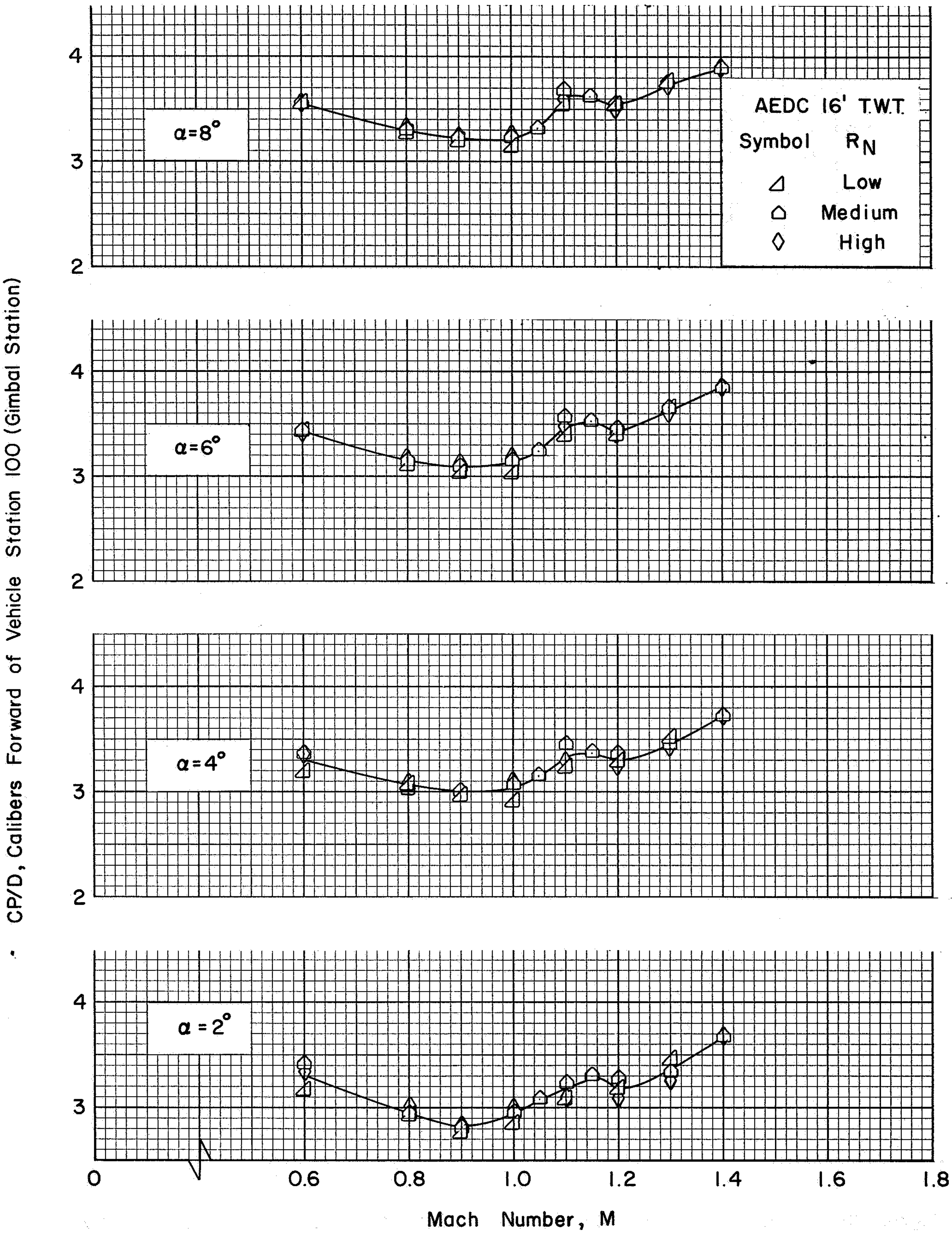

(b) CP/D vs. M: (α = 2°–8°)

Figure 38 Continued

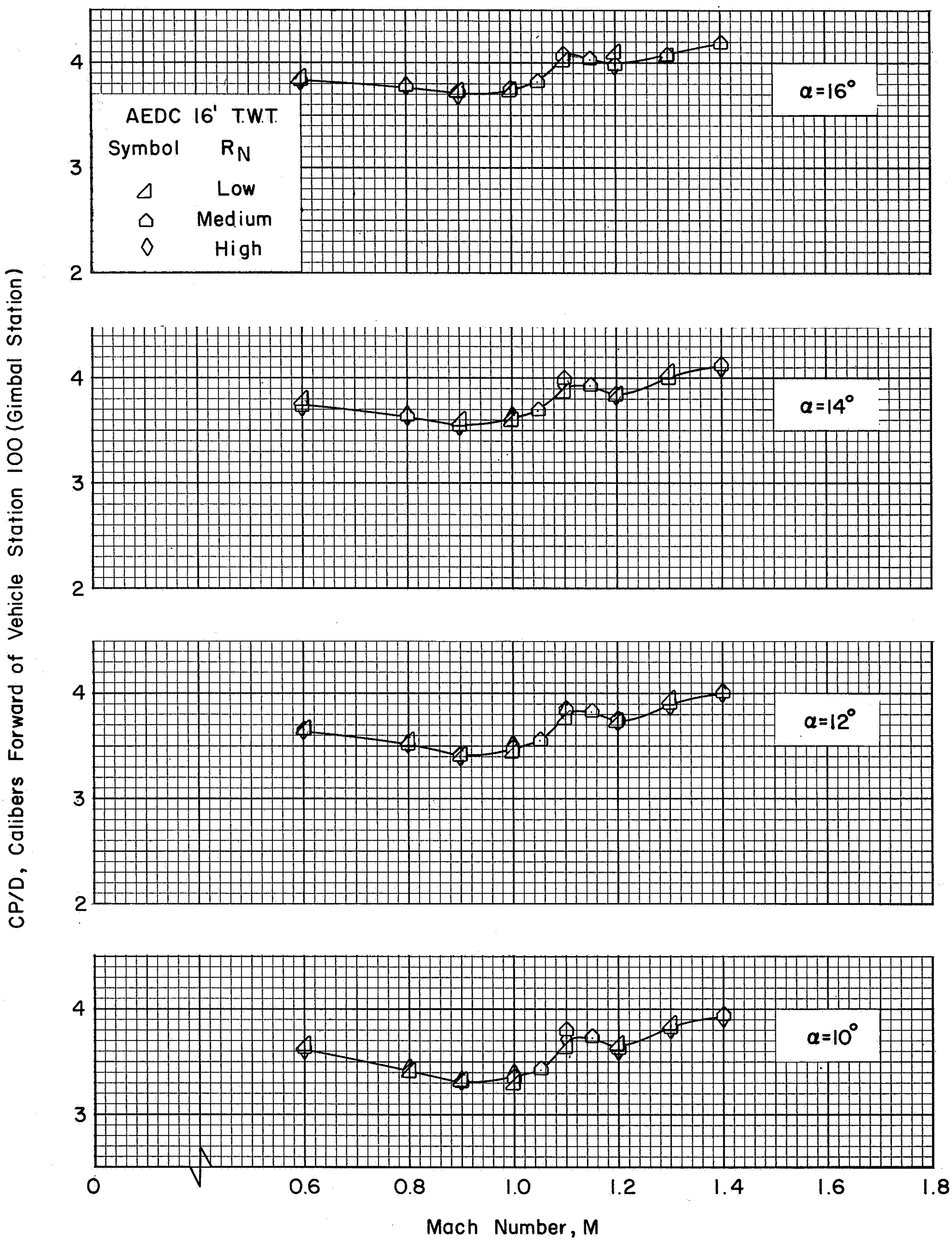

(c) Concluded: ($\alpha = 10° - 16°$)

Figure 38 Concluded

REFERENCES

1. Allen, H. H.; and E. W. Perkins, "Characteristics of Flow Over Inclined Bodies of Revolution," NACA RM A50L07, March 1961.

2. Anon., "8-Foot Transonic Wind Tunnel," CAL Report No. WTO-300, November 1964.

3. Anon., "Test Facilities Handbook (Sixth Edition)," Arnold Engineering Development Center, Unnumbered, November 1966.

4. Blackwell, K. L., "Static Aerodynamic Characteristics of the Apollo-Saturn V Configuration with Base Flow Scoops Removed," MSFC R-AERO-AD-68-31, May 1968.

5. Carlson, D. R.; and W. P. Walters, "A Supersonic/Hypersonic Aerodynamic Investigation of the Saturn IB/Apollo Upper Stage," NASA CR-362, January 1966.

6. Coats, J. D.; and L. J. Pfaff, "Flow Characteristics of AEDC/VKF 40-Inch Supersonic Wind Tunnel," AEDC TR-62-189, June 1962.

7. Gaines, M. F., "Effects of Roll Angle on the Static Longitudinal Stability and Axial Force Characteristics of the Apollo-Saturn V Launch Vehicle," R-AERO-AD-67-11, February 20, 1967.

8. Glasgow, Robert M., "Static Aerodynamic Characteristics of the Aborted Apollo/Saturn V Vehicle," NASA TM X-53656, September 22, 1967.

9. Gunn, J. A., "Check Calibration of the 16-Foot Transonic Tunnel," AEDC-TR-66-80, May 1966.

10. Henson, V. K., "Design Criteria: Apollo/Saturn V Aerodynamic Rolling Moment," R-AERO-AD-66-18, April 27, 1966.

11. Jenke, L. M., "Force Test of the Saturn V LOR and Saturn IB/AS-206 Configurations at Mach Numbers 1.5 through 8," AEDC-TR-66-263, February 1967.

12. Muhlhauser, C. H., "Static Longitudinal Stability and Axial Force Characteristics of the Apollo/Saturn V Launch Vehicle Without Base Flow Deflectors in the MSFC 14-Inch Trisonic Wind Tunnel," R-AERO-AD-68-32, June 1968.

13. Nieder, J. J., "Saturn V Induced Rolling Moment Data (Project AD-58)," TBC-FTS-H-162, November 1965.

14. Shadow, T. O; and T. R. Brice, "Static Stability and Pressure Test of a 0.04-Scale Model of the Apollo-Saturn V Vehicle at Mach Numbers from 0.60 through 1.40," AEDC-TR-68-21.

15. Simon, E. H., "The George C. Marshall Space Flight Center's 14 x 14-Inch Trisonic Wind Tunnel Technical Handbook," NASA TM X-53185, December 1964.

16. Simon, E. H., "Static Longitudinal Stability and Axial Force Investigation of the Saturn V LOR Vehicle for Mach Numbers 0.50 through 4.96 and Angles of Attack of -2 to +16 Degrees," MSFC 14-Inch TWT Report No. 350, January 1967.

17. Struzynski, N. A., "Transonic Wind Tunnel Test of 0.33, 0.55, and 0.90 Percent Scale Models of the NASA Saturn Vehicle," CAL Technical Report No. AA-2201-W-2, June 1966.

18. Vehicle Aerodynamic Section, "Static Aerodynamic Characteristics of the Apollo/Saturn V Vehicle," MSFC, Aero-Astrodynamics Laboratory, NASA TM X-53517, September 1966.

19. Waldrop, W. R.; and R. M. Glasgow, "Pretest Report for November 1967 Wind Tunnel Test in AEDC 16-Foot Transonic Wind Tunnel," Nortronics-Huntsville Memo No. 24, September 1967.

20. Waldrop, W. R., et al., "Static Transonic Aerodynamic Characteristics of a 4-Percent Model of the Apollo-Saturn V Vehicle," Nortronics-Huntsville Technical Report No. TR-792-8-273, April 1968.

21. Watkins, J. T., "First Stage Dispersion Analysis for Saturn V (SA-501-503 and 504-505)," R-AERO-DAP-44-65, May 1965.

22. Wolfe, J. A., "LTV High Speed Wind Tunnel," AER-ElR-13552-A, undated.

23. Ziegler, C. E., "Static Stability Tests on the 0.9 Percent Scale Saturn V Model in the Mach Number Range of 0.60 to 3.00," LTV Report No. HSWT Test 224, November 1966.

ABRIDGED BIBLIOGRAPHY OF SATURN V STATIC AERODYNAMIC REPORTS

This bibliography is not an extensive survey of the literature. It is a partial listing of previous experimental, static aerodynamic reports and associated analysis reports. Because of the nature of the material and the intended use of this bibliography, a chronological listing is used instead of the usual alphabetical listing. The listing is subdivided by source. Although most of the reports have limited distribution, they can be obtained if necessary from the Aerodynamic Design Branch (R-AERO-ADE), Aerophysics Division, Aero-Astrodynamics Laboratory of the George C. Marshall Space Flight Center.

NASA - MARSHALL SPACE FLIGHT CENTER

Sieber, A. T. and G. F. Romberg, "Static Longitudinal Stability and Drag Tests of Thirteen Preliminary Saturn C-5 Configurations," M-AERO-E-67-61, November 1961.

Romberg, G. F., "Static Longitudinal Stability at High Angles of Attack, Around Maximum Dynamic Pressure on Saturn C-5 Due to Pitching in a Plane 45-Degrees to the Horizontal," M-AERO-E-30-62, March 1962.

McAnnally, R. C. and C. D. Andrews, "Static Longitudinal Stability and Drag Characteristics of a Preliminary Saturn C-3 Tanking Mode - Second Launch Vehicle," M-AERO-E-82-62, June 1962.

Henderson, E. M. and C. D. Andrews, "Static Longitudinal Stability and Drag Characteristics of the Saturn C-5 Three-Stage-to-Escape Vehicles - Chemical and Nuclear," M-AERO-E-83-62, July 1962.

Dunn, B. G. and J. O. Windham, "Design Data: Wind Tunnel Results of Pressure Distributions Over the Conical Engine Shroud of a Saturn C-5 Launch Vehicle Model," M-AERO-E-161-62, October 1962.

Jump, R. A., "Conduit Covers Aerodynamic Loads for Saturn C-5, S-IC Stage," M-AERO-A-3-63, January 1963.

Morgan, J. R. and J. D. Johnson, "Presentation of Basic Data from TWT Investigation of Static Longitudinal Stability and Axial Force Characteristics of the Saturn V, Chemical, RIFT, and Nuclear Vehicles," M-AERO-E-86-63, February 1963.

Pitcock, R. E., "Experimental Static Longitudinal Stability and Drag Characteristics on Body Build-Up of the Saturn V LOR, Chemical, Three-Stage-to-Escape Vehicle," M-AERO-E-123-63, March 1963.

Romberg, G. F., "Evaluation of the Experimental Static Longitudinal Stability and Drag Characteristics of the Saturn I, Block II Vehicle for the Re-entry Mission of the Apollo Capsule," M-AERO-E-128-63, April 1963.

Morgan, J. R. and J. D. Johnson, "Presentation of Basic Data from Supersonic Wind Tunnel Investigation of Static Longitudinal Stability and Axial Force Characteristics of the Saturn V Chemical, RIFT, and Nuclear Vehicles (MSFC Project P34)," M-AERO-E-158-63, May 1963.

Johnson, B. H., "Preliminary Results of Wind Tunnel Investigation to Determine S-IC Engine Aerodynamic Gimbal Loads Without Engine Flow," M-AERO-E-204-63, July 1963.

Johnson, J. D., "Experimental Static Longitudinal Stability and Drag Characteristics of the Saturn V LOR, Chemical, Three-Stage-to-Escape Vehicle Without Fins and Engine Shrouds in the Transonic Mach Number Range," M-AERO-E-241-63, August 1963.

Sieber, A.T. and J. R. Morgan, "Experimental Static Longitudinal Stability and Axial Force Characteristics on the Saturn V-Chemical, RIFT, and Nuclear Vehicles," M-AERO-244-63, September 1963.

Henson, V. K., "Aerodynamic Design Criteria for the S-IC Stage Engine Shrouds of the Saturn V LOR Vehicle," MSFC Dwg. 10M04106, Rev. G., R-AERO-AD-64-12, March 1964.

Pitcock, R. E., "Experimental Basic Data Results of the Static Transonic Aerodynamic Characteristics of Preliminary Configurations of the Saturn V-LOR, Lunar Logistics, Nuclear, and RIFT Vehicles," R-AERO-AD-64-19, February 1964.

Johnson, B. H., "Experimentally Determined Power-On Pressure Distributions Over a Simulated F-1 Engine Attached to a Model Saturn V Launch Vehicle at Transonic Speeds," R-AERO-AD-64-12, March 1964.

Henson, V. K., "Design Criteria: Saturn V, LOR Vehicle, S-IC Stage Base Flow Deflectors and Shroud Scoop Aerodynamic Loads," R-AERO-AD-64-29, March 1964.

Bills, B. C., "Static Longitudinal Stability and Forebody Axial Force Characteristics of the Saturn V Lunar Logistics, Nuclear, and RIFT Vehicles in the AEDC's Hypersonic Tunnel E (M. 5.0 to 8.0) Basic Data Release," R-AERO-AD-64-31, March 1964.

Fortenberry, J. C., "Basic Data Release: Static Longitudinal Stability and Axial Force Characteristics of the Saturn V LOR, Lunar Logistics, Nuclear, and RIFT Configurations Obtained from Tests Conducted in BRL Supersonic Wind Tunnel (MSFC Project 68)," R-AERO-AD-64-49, May 1964.

Henson, V. K., "Design Criteria: Aerodynamic Loads and Pressure Distributions for the Saturn V LOR, S-IC Stage 75 Square-Foot Fins," R-AERO-AD-64-68, June 1964.

Lowery, T. J., "Gradient of the Normal Force Coefficient Due to Angular Misalignment of One Saturn V LOR Fin, Engine-Shroud Combination," R-AERO-AD-64-69, June 1964.

Pitcock, R. E., "Experimental Static Longitudinal Stability and Axial Force Characteristics of Several Preliminary Saturn V Configurations: Saturn V LOR, Lunar Logistics, Nuclear, and RIFT Vehicles," R-AERO-AD-64-74, July 1964.

Henson, V. K., "Design Criteria: Saturn V/S-IC Stage Base Flow Deflectors Configuration and Relationships with the Controlled Release Mechanisms," R-AERO-AD-64-93, October 1964.

Ramsey, P. E., "Results of the Q-Ball Pressure Distribution Investigation in the Cornell 8' TWT," R-AERO-AD-64-99, November 1964.

Henson, V. K., "Estimation of Aerodynamic Load Due to Ground Winds on the Saturn V/S-IVB Stage Service Lines," R-AERO-AD-64-100, November 1964.

Walker, C. E., "Experimental Investigation to Determine the Static Aerodynamic Characteristics of a Saturn V LOR Launch Vehicle Configuration with Simulated F-1 Engine Bells," R-AERO-AD-65-8, January 1965.

Lowery, T. J., "Design Criteria: Hypersonic Aerodynamic Characteristics of the Saturn V LOR Second Stage Flight Configuration," R-AERO-AD-65-18, March 1965.

Andrews, C. D. and D. R. Carlson, "Shadowgraph Study of the Upper Stage Flow Fields of Some Saturn V Study Configurations in the Transonic Mach Number Range," NASA TN D-2755, April 1965.

Johnson, B. H.,"Preliminary Data Release: Saturn V Booster Engine Aerodynamic Pressure and Load Distribution," R-AERO-AD-65-31, April 1965.

Henson, V. K., "Antennae Covers for the Instrument Units of the Saturn IB and Saturn V Vehicles," R-AERO-AD-65-22, April 1965.

Henson, V. K., "Design Criteria: Saturn V/S-IC Heat Shield Pressure Differential Resulting from Base Compartment Venting," R-AERO-AD-65-34, May 1965.

Lowery, T. J., "Design Criteria: Aerodynamics of the Apollo-Saturn V Vehicle During First Stage Separation," R-AERO-AD-65-56, September 1965.

Ramsey, P. E., "Experimental Investigation of the Effects of Booster Engine Shroud Length on the Static Longitudinal Stability and Axial Force Characteristics of the Saturn V LOR Launch Vehicle," R-AERO-AD-66-4, February 1966.

Henson, V. K., "Design Criteria: Protuberance Fairing Design and Aerodynamic Loads for the Saturn V Reflector for Orbital Tracking," R-AERO-AD-66-6, February 1966.

Henson, V. K., "Design Criteria: Static Aerodynamic Characteristics for the Apollo-Saturn V/S-IC Stage Protuberances," R-AERO-AD-66-22, May 1966.

Vehicle Aerodynamic Section, "Static Aerodynamic Characteristics of the Apollo-Saturn V Vehicle," NASA TM X-53517, September 1966.

Lowery, T. J., "Second Stage Axial Force Characteristics for the Apollo-Saturn V Vehicles," R-AERO-AD-66-41, September 1966.

Bacchus, D. L., "Summary of Input Design Criteria for Saturn V In-Flight Compartment Venting Studies," R-AERO-AD-66-50, November 1966.

Nunley, B. W., "Design Criteria: Apollo-Saturn V Vehicle Aerodynamic Load Distributions at Mach Numbers of 0, 0.5, 4.0, and 7.0," R-AERO-AD-66-52, November, 1966.

Ramsey, P. E., "Q-Ball Evolution Emergency Detection System Application and Error Analysis as Applied to the Apollo-Saturn," R-AERO-AD-66-40, September 1966.

Bacchus, D. L., "In-Flight Venting Analysis of the Saturn V Payload Compartment AS-504C Mission," R-AERO-AD-67-3, January 1967.

Gaines, M. F., "Effects of Roll Angle on the Static Longitudinal Stability and Axial Force Characteristics of the Apollo-Saturn V Launch Vehicle," R-AERO-AD-67-11, February 1967.

Henson, V. K., "Design Criteria: Aerodynamic Characteristics for Saturn V Lift-Off Analysis," R-AERO-AD-67-15, February 1967.

Glasgow, R. M., "Static Aerodynamic Characteristics of the Aborted Apollo-Saturn V Vehicle," NASA TM X-53587, March 1967.

Nunley, B. W., "Design Criteria: AS-501, AS-502 and AS-503 F-1 Engine Aerodynamic Hinge Moments," R-AERO-AD-67-39, April 1967.

Nunley, B. W., "Range Safety Aerodynamic Characteristics of the Apollo-Saturn V Vehicle," NASA TM X-53599, April 1967.

Henson, V. K., "Design Criteria: In-Flight Venting Analyses for the S-II/S-IVB Interstage of the Apollo-Saturn V Vehicle (Trajectories 503 and 504)," R-AERO-AD-67-58, June 1967.

Henson, V. K., "Design Criteria: Apollo-Saturn V/S-IC Compartment Internal Pressure Time Histories for the AS-504 Trajectory," R-AERO-AD-67-60, July 1967.

Henson, V. K., "Design Criteria: External Longitudinal Pressure Distributions Over the Apollo-Saturn V Spacecraft Compartment," R-AERO-68-12, March 1968.

Blackwell, K. L., "Static Aerodynamic Characteristics of the Apollo-Saturn V Configuration with Base Flow Scoops Removed," R-AERO-AD-68-31, May 1968.

Muhlhauser, C. H., "Static Longitudinal Stability and Axial Force Characteristics of the Apollo-Saturn V Launch Vehicle Without Base Flow Deflectors," R-AERO-AD-68-32, June 1968.

THE BOEING COMPANY

Nelson, Dennis E., "Wind Tunnel Test of MSFC Model 309 (AS-6771-1)," 5-7530-H-024, October 1962.

Emerson, T. S., "Cold Flow Studies of an F-1 Jet Impingement (P-36)," D%-11132, October 1962.

Alger, Dennis L., "C-5 Wind Tunnel Pressure Test No. P-43; Final Data Release," D5-11230, December 1962.

Nelson, Dennis E., "C-5 Fin-Shroud Combination, Wind Tunnel Force Test No. P-29; Final Data Release," D5-11231, Jaunary 1963.

Stain, W. C., "Results of Saturn V Fin-Shroud Wind Tunnel Force Test No. P-29," AERO-H-123, March 1963.

Asbjornsen, Terry R., "Saturn V Wind Tunnel Pressure Test No. P-41: Final Data Release," D5-11135, April 1963.

Wright, J. M., "Final Data Report: Saturn V RIFT, Wind Tunnel Pressure Test P-61," D5-11245, April 1963.

Keeney, F. J., "Radial Pressure Distribution Over the LEM Adapter and the S-II/S-IVB Interstage-Saturn V Configuration 4106," D5-11442, February 1964.

Nelson, D. E., "Final Data Release: Saturn V Upper Stages Pressure Distribution, Wind Tunnel Test AD-5-63," T5-6406, May 1964.

Wilson, E. K., "Aerodynamic Analysis of Saturn V LOR Chemical Vehicle Configuration 4106," D5-11281-2, September 1964.

Lentz, Paul S., "Final Data Release: Saturn V Induced Roll Test Wind Tunnel Test AD-33-64," T5-6407, October 1964.

Nelson, Dennis E. and E. K. Volk, "Data Report - Wind Tunnel Test P-58, Saturn V LOR Vehicle with Foreshortened Upper Stages," D5-11246, November 1964.

Nieder, J. J., "Hypersonic Static Longitudinal Stability and Axial Force Characteristics of the Saturn V Upper Stages," FTS-H-012, December 1964.

Stain, W. C., "Results of Induced Rolling Moment Test AD-33-64," FTS-H-019, January 1965.

Wright, J. M., "Final Data Release: Pressure and Normal Force Distribution on the S-IC/S-II Stages of the Saturn V LOR Wind Tunnel Test AD-43-64," T5-6601, January 1965.

Youngman, B. P., "Aerodynamic Analysis Normal Force Distribution on the S-IC/S-II Stages of the Saturn V LOR, Wind Tunnel Test AD-43-64," D5-15241, May 1965.

Nieder, J. J., "Hypersonic Static Longitudinal Stability and Axial Force Characteristics of the Saturn V Upper Stages AD-42-64," D5-15254, May 1965.

Nieder, J. J., "S-IC Tail Barrel Pressure Distribution," FTS-H-081, June 1965.

Wilson, E. K., "Fin Interference Due to the Shroud Scoops on Saturn V LOR Vehicle," FTS-H-113, August 1965.

Murakoshi, A. Y., "Final Data Release: Saturn V Cold Flow Nozzle Aerodynamic Hinge Moment Test AD-3-64," T5-6604, September 1965.

Cline, G. F., "Aerodynamic Characteristics of Saturn V/S-IC Stage Protuberances," FTS-H-156, October 1965.

Stain, W. C., "Analysis of Saturn V/S-IC Engine Aerodynamic Hinge Moments Obtained from Wind Tunnel Test AD-3-64," D5-15320, October 1965.

Nieder, J. J., "Saturn V Induced Rolling Moment Data (Project AD-58)," FTS-H-162, November 1965.

Watts, L. L., "Body Load Distributions in the Saturn V/S-IC Tail Barrel," FTS-H-165, November 1965.

Nieder, J. J., "Saturn V (LOR) Upper Stage Aerodynamic Characteristics (Project AD-58)," FTS-H-173, December 1965.

Watts, L. L.,"Fin and Shroud Loads for Saturn V/S-IC," FTS-H-181, January 1966.

Nieder, J. J., "Apollo/Saturn V Second Stage Flight Configuration Axial Force Characteristics," AT-H-056, April 1967.

Child, R. F., "Aerodynamic Analysis of Saturn V LOR Chemical Vehicle Configuration 0299," D5-11281-1, December 1967.

<u>MISCELLANEOUS</u>

Carlton, W. E., "An Investigation of the Aerodynamic Loads Acting on the Saturn C-5 Engine Shrouds with Three Fin Configurations at Transonic Speeds," AEDC-TDR-62-236, December 1962.

Knaupp, H. and C. F. Anderson, "Static Stability of Several Small Scale Models of the Saturn C-5 at Transonic Speeds," AEDC-TDR-63-225, October 1963.

Myers, J. R. and B. W. Roberts," Static Stability Tests of Several Saturn IB and Saturn V Configurations at Hypersonic Mach Numbers," AEDC-TM-64-8, March 1964.

Martin, P. W. and H. Kaupp, Jr., "Transonic Static Stability Test of Two 0.00333-Scale Models of the Saturn V LOR Configurations," AEDC-TDR-64-40, February 1964.

Myers, J. R. and C. J. Spurlin, "Static Stability of Six Saturn V LOR Upper Stage Configurations at Hypersonic Mach Numbers," AEDC-TR-65-17, January 1965.

Jenke, L. M., "Force Tests of the Saturn V LOR and Saturn IB/AS-206 Configurations at Mach Numbers 1.5 through 8.0," AEDC-TR-66-263, February 1967.

Shadow, T. O. and T. R. Brice, "Static Stability and Pressure Test of a 0.04-Scale Model of the Apollo-Saturn V Vehicle at Mach Numbers from 0.60 through 1.40," AEDC-TR-68-21, February 1968.

Struzynski, N. A., "Transonic Wind Tunnel Tests of .33, .55, and .90 Percent Scale Models of the NASA Saturn Vehicle," CAL No. AA-2201-W-2, October 1966.

Priebe, R. W., "Transonic Wind Tunnel Tests of a 0.90 Percent Scale Model of the NASA Saturn V Vehicle," CAL No. AA-2411-W-1, March 1968.

Melton, H. R., "Saturn V/S-IVB Auxiliary Propulsion System Fairing Wind Tunnel Test," DAC-SM-43624, April 1963.

Wilson, S. C.,"Saturn S-IVB General Protuberance Wind Tunnel Test Preliminary Report," DAC-SM-43625, April 1963.

Black, R. L., "A Report for Determining the Static Aerodynamic Characteristics of Scale Saturn V Launch Vehicles in the General Dynamics High Speed Wind Tunnel," GD-HST-TR-167-0, December 1965.

Waldrop, W. R., et al., "Static Transonic Aerodynamic Characteristics of a 4-Percent Model of the Apollo-Saturn V Vehicle," NSL-TR-792-8-273, April 1968.

Ziegler, C. E., "Static Stability Tests of the .9 Percent Scale Saturn V Model in the Mach Number Range of 0.60 to 3.00," LTV HSWT Test 224, November 1966.

APPROVAL NASA TM X-53770

RESULTS OF SEVERAL EXPERIMENTAL INVESTIGATIONS OF THE STATIC AERODYNAMIC CHARACTERISTICS FOR THE APOLLO/SATURN V LAUNCH VEHICLE

by Clyde E. Walker

The information in this report has been reviewed for security classification. Review of any information concerning Department of Defense or Atomic Energy Commission programs has been made by the MSFC Security Classification Officer. This report, in its entirety, has been determined to be unclassified.

This document has also been reviewed and approved for technical accuracy.

C. Dale Andrews
Chief, Experimental Aerodynamics Section

E. L. Linsley
Chief, Aerodynamic Design Branch

W. K. Dahm
Chief, Aerophysics Division

E. D. Geissler
Director, Aero-Astrodynamics Laboratory

DIR
Dr. von Braun

DEP-T
Dr. Rees

I-V-DIR
Col. James

R-DIR
Mr. Weidner

MS-IP
MS-IPL (8)
MS-H
HME-P
PAT
MS-T (6)

R-ASTR
Dr. Haeussermann
Mr. Moore
Mr. Hosenthien
Mr. Blackstone
Mr. Mink
Mr. Richard

R-P&VE
Mr. Heimburg
Mr. McCullough
Mr. Aberg
Mr. Glover
Mr. Goerner
Mr. Kroll
Mr. Furman
Mr. Showers (2)
Mr. Frederick
Mr. Blumrich
Mr. Stevens
Mr. Verble

Mr. E. A. Rawls
Chrysler Corp. Space Div.
Michoud Operations
Aerodynamics Group
P. O. Box 29200
New Orleans, La. 70129

R-AERO
Dr. Geissler
Mr. Jean
Mr. Hagood
Mr. Teague (12)
Mr. Horn
Mr. Ryan
Mr. Verderaime
Mr. Rheinfurth
Mr. Hall
Mr. Townsend
Mr. Lindberg
Mr. Hardage
Mr. Wittenstein
Mr. Ernstberger
Mr. Lovingood
Mr. Baker
Mr. Dahm
Mr. Holderer
Mr. Linsley
Mr. Wilson
Mr. Reed
Mr. Felix
Mr. Andrews (10)
Mr. Ramsey
Mr. Walker
Mr. Dunn
Mr. Nunley
Mr. Bacchus
Mr. Lowery
Mr. Henson
Mr. Harris

Tech. & Sci. Info. Facility (25)
Attn: NASA Rep. (S-AK/RKT)
Box 33
College Park, Md.

The Boeing Co.
Mail Stop AF-75
HIC Bldg.
Huntsville, Ala.
Attn: Mr. W. A. Smith
Mr. W. C. Stain (2)